# Tracing anthropogenic impacts on the eastern coast of South Africa

I n a u g u r a l d i s s e r t a t i o n

zur

Erlangung des akademischen Grades eines

Doktors der Naturwissenschaften (Dr. rer. nat.)

der

Mathematisch-Naturwissenschaftlichen Fakultät

der

Universität Greifswald

vorgelegt von

Paul Mehlhorn

Greifswald, 16. Mai 2022

| | |
|---|---|
| Dekan: | Prof. Dr. Gerald Kerth |
| 1. Gutachter: | Prof. Dr. Torsten Haberzettl |
| 2. Gutachter: | Prof. Dr. Trevor R. Hill |
| Tag der Promotion: | 30.09.2022 |

# Table of contents

# I Abstract

This thesis aims to investigate effects of anthropogenic environmental impact on the Richards Bay area. Located on the east coast of South Africa, Richards Bay Harbour evolved into the country's premier bulk cargo port. The Associated change in land-use and industrial as well as agricultural pollution pose environmental, ecological and human health risks. Here, sedimentological and geochemical investigations focus on the port as final sink for environmental and industrial pollutants, such as metal concentrations, organochlorine pesticides and microplastics.

The study is based on investigations of surface sediment samples from the water-sediment interface to identify spatial distribution patterns, as well as sediment cores to follow temporal changes. Endmember modelling of grainsize distributions, proved to be a viable parameter to distinguish different accumulation spaces and enabled the classification into six harbour sub-basins. Subsequent investigations on the content of microplastics, Polyethylene terephthalate (PET) and Low-density polyethylene (LDPE), showed that these different types of microplastics predominate in two different areas: PET appears to be directly tied to higher populated (tourism) beaches, while LDPE is deposited in low-current sub-basins.

Increased metal concentrations link to activities at the bulk cargo berths, where especially Cr and Cu concentrations exceeded the local sediment guideline thresholds. In the areas of high metal concentrations, bioindicators (ostracods, foraminiferas, diatoms) also indicate increased shares of malformed specimens. Multiple recovered sediment cores recorded changes in recent export practices, indicating ceased Cu handling and increased Cr handling over the past decade.

Noticing multiple possible influencing factors on elemental distributions, created by the surrounding geological and industrial impact, the usefulness of different normalisers (Al, Fe, Rb, Ti and silt fraction) for Cr, Cu, Co and Pb concentrations was compared and site specific baseline metal concentrations were defined. This identified Al and Rb to be effective normalisers in Richards Bay and Fe or Ti to be affected by local conditions.

Data of organochlorine pesticide pollution was gathered in the area of Richards Bay, Goedertrouw Dam and Umlalazi River. The two dominant groups of contaminants detected are dichlorodiphenyltrichloroethanes (∑DDT, 12 – 350 ng $g^{-1}$), linked to the use of malaria vector control, and hexachlorocyclohexanes (∑HCH 35 – 230 ng $g^{-1}$), an agricultural insecticide. Both indicate recent entry and exceed sediment quality guideline limits, raising

concern for local communities and estuarine environments.

Seismic data was used to investigate the preindustrial evolution of the incised valley system and bayhead delta at Richards Bay Harbour. A stratigraphically supported development model was created.

The thesis shows that harbour sediment is an important sink for inorganic and organic contaminants. Each investigation on environmental pollutants, such as metals, pesticides, microplastics or bioindicator analyses, indicates their deposition in distinct harbour sub-basins. Therefore, their effect can be spatially differentiated and related to plausible sources of pollution. Richards Bay thus represents a variously affected system along the South African coast, in which it is necessary to take environmental protection measures in terms of sustainable and environmentally friendly management.

# II Zusammenfassung

Der Hafen von Richards Bay liegt an der Ostküste Südafrikas und ist einer der größten und wichtigsten Umschlagspunkte für Massengüter des Landes. Der Fokus der vorliegenden Dissertation liegt auf dem Umwelteinfluss des Industriehafens sowie dessen Funktion als Senke für Umwelt- und Industrieschadstoffe (Metalle, chlororganische Pestizide, Mikroplastik). Anhand der Sedimentablagerungen innerhalb dieses Ökosystems werden die Auswirkungen sowie die räumliche und zeitliche Ausbreitung anthropogener Einflüsse untersucht.

Das Fundament dieser Arbeit bilden sedimentologische sowie geochemische Analysen des Oberflächensediments, welche die Belastungssituation des Ablagerungsraumes beschreiben und aus denen räumliche Zusammenhänge herausgearbeitet werden. Mittels Endmember-Modellierung der Korngrößenverteilungen konnten sechs Teilbecken bzw. Akkumulationsräume innerhalb des Hafens klassifiziert werden. Die Verteilungen einzelner Metallgehalte zeigen besonders deren Anreicherung in der Umgebung der Umschlagsterminals für Massengüter. Insbesondere Cr- und Cu-Gehalte übersteigen in dieser Region die Grenzwerte der nationalen Maßnahmenliste zur Untersuchung von Baggermaterial zur marinen Entsorgung. Gleichermaßen werden die innerhalb dieser Arbeit errechneten hafenspezifischen Hintergrundwerte überschritten. Al und Rb erwiesen sich als geeignet zur Normalisierung der Metallgehalte in Richards Bay. Lokale geochemische oder hydrodynamische Einflussfaktoren bedingen die Elementverteilung von Fe oder Ti, welche

somit nicht zur Normalisierung verwendet werden sollten. Multiproxy Analysen an Kurzkernen zeigen die Zunahme der Cr-Belastung sowie die Abnahme von Cu-Gehalten nach vorangehender Erhöhung. Damit korrelieren die Konzentrationsprofile in den Sedimentkernen mit dem Wechsel des Frachtgutes von Cu-haltiger Fracht hin zu der Verladung Cr-haltiger Fracht (Ferrochrom). Bioindikatoren (Ostrakoden, Foraminiferen, Diatomeen) zeigen an den Standorten hoher Metallkonzentrationen (insbesondere Cr, Cu und Co) eine erhöhte Tendenz zur Missbildung.

Die Verteilungen von Mikroplastik, Polyethylenterephthalat (PET) und Polyethylen niedriger Dichte (LDPE) sind durch zwei unterschiedliche Ablagerungsbereiche gekennzeichnet: die PET-Konzentration korreliert mit bevölkerungsreichen (touristischen) Gebieten, während LDPE in strömungsarmen Teilbecken abgelagert wird.

Die Belastung durch chlororganische Pestizide in Richards Bay kann auf zwei dominante Schadstoffgruppen zurückgeführt werden. Zum einen auf erhöhte Gehalte von Dichlordiphenyltrichlorethan (∑DDT, 12 – 350 ng $g^{-1}$) welches rezent zur Bekämpfung von Malaria eingesetzt wird. Zum anderen wurden erhöhte Konzentrationen von Hexachlorcyclohexan (∑HCH 35 – 230 ng $g^{-1}$), Bestandteile eines in der Landwirtschaft genutzten Insektizids, gemessen. Das Vorkommen dieser Verbindungen und ihre Metaboliten-Verhältnisse lassen auf deren rezenten Eintrag schließen. Des Weiteren wurde anhand seismischer Daten die präindustrielle Talentwicklung und die Deltabildung innerhalb des Hafenbeckens rekonstruiert.

Es konnte herausgestellt werden, dass die untersuchten Hafensedimente eine bedeutende Senke organischer und anorganischer Schadstoffe darstellen. Jede einzelne im Rahmen dieser Dissertation durchgeführte Untersuchung auf umweltrelevante Stoffe, wie Schwermetalle, Pestizide, Mikroplastik sowie die Analyse der Bioindikatoren zeigten eine Belastung des Untersuchungsgebietes durch den Industriehafen oder die damit verbundene Entwicklung des ländlichen Raumes. Zusätzlich konnten die jeweiligen Schadstoffe unterschiedlichen Teilbereichen des Hafens zugeordnet werden. Damit lassen sich die Verschmutzungen im Hafenbecken räumlich differenzieren und einer bestimmten Quelle zuordnen. Richards Bay stellt damit ein vielseitig belastetes und komplexes System dar. Zukünftig sollten zum Schutze von Umwelt und Bevölkerung zielgerichtete Maßnahmen ergriffen werden, um die Schadstoffbelastung zu verringern.

# Chapter 1
# Introduction

South Africa's rapidly rising population combined with the developing industrial sector results in multiple environmental pressures (Department of Environmental Affairs 2012), which can cause health risks and environmental changes, like the releases of heavy metals by industries (Khan et al. 2008; Lion and Olowoyo 2013) or pesticides in malaria vector control and agriculture (Humphries 2013; Buah-Kwofie and Humphries 2017). As the human population grows, especially in coastal regions, its continuous evolution determines the future of (global) marine environments and increases the need for sustainable management (Steinberg et al. 2016). In this sense, ports and port cities in particular, contribute to environmental pollution and detailed analyses of spatial and temporal anthropogenic impacts need to be carried out to understand the dynamics and potential adverse ecological and biological effects. The area of Richards Bay and the Mhlatuze catchment, as chosen in the project TRACES (Tracing Human and Climate impact in South Africa), offers a great setting to study multiple environmental stressors.

This thesis is part of the collaborative project TRACES (Tracing Human and Climate impact in South Africa – 01.06.2018-31.12.2021) within the SPACES II Program (Science Partnerships for the Assessment of Complex Earth System Processes) and funded by the German Federal Ministry of Education and Research (BMBF) [grant number: 03F0798C]. Within the selected ecosystem at the east coast of South Africa, the goal of Sub Project 1 (SP1; Sediment Transport and Pollutants I – Estuaries as Final Sinks) and hence of this thesis, was to establish high-resolution records of anthropogenic impact over the past 250 years. Correspondingly, two main questions were of particular interest for the project as well as this thesis:

- What are the effects of pollution by mining, industry and agriculture on the fluxes of heavy metals, persistent organic pollutants and microplastics in aquatic ecosystems?
- How does this affect the regional diversity of paleoecological indicators?

The regional sedimentological and geochemical characteristics of the surface sediment of Richards Bay Harbour e.g. elemental composition and heavy metals, the presence of organochlorine pesticides or microplastics distribution, give insight to the current state of the system and the effects of anthropogenic impact. Short sediment cores were analysed to reconstruct (sub-)recent system changes. To reach the second aim, close collaboration with associated investigations of marine biodiversity (e.g. Foraminifera, Ostracoda) of Sub Project 4 (SP4; Biodiversity and Bioindicators I - Brackish-Marine Systems) was necessary. Bioindicators provide further information on the impacts of pollutants by focussing on morphological reactions (malformations) or shell chemistry deterioration and help to reconstruct system changes or identify pre-industrial reference conditions.

## Motivation

Multiple environmental stressors are to be expected in the Richards Bay region. These may be created by the effects of the industrialised port, the use of organochlorine pesticides (OCPs) in agriculture or malaria vector control, or an enhanced entry of microplastics by the increasing population.

Only few data on metal concentrations in sediment exists from the industrialised Richards Bay Harbour (Wepener and Vermeulen 2005) despite an observed increase in metals above normal background levels (Henry and Moldan 1983; Hennig 1985; Henry et al. 1989; Wepener and Vermeulen 2005). Since their survey in 1999, Wepener and Vermeulen (2005) were the last to address and measure metal concentrations in sediments of Richards Bay Harbour, leaving a large temporal data gap to date. New investigations of metals within the port will give critical information on the current state of the system and are urgently needed to distinguish between natural background concentrations and anthropogenically induced metals in the harbour. Further, information about the harbours subsurface sediment is publically not available or virtually non-existent. The former estuary was significantly altered to develop an industrial deep-water harbour. The transition from the deposits of the original Mhlatuze Estuary to the anthropogenically overprinted harbour has hitherto been unexplored. The impact of maintenance dredging and its interference with surface sediment samples or sediment cores must be evaluated for a meaningful understanding of the sedimentary dynamics of the basin.

The immanent threat posed by organochlorine pesticides that are persistent, with potential to bioaccumulate in the environment, has received strong recognition in South Africa's globally important conservation areas (Buah-Kwofie and Humphries 2017). Significant levels of OCPs have been detected in Kruger National park (Gerber et al. 2015, 2016) and iSimangaliso Wetland Park (Humphries 2013; Buah-Kwofie and Humphries 2017; Buah-Kwofie et al. 2018, 2019). Human health and environmental challenges are associated with the use of these compounds, which are banned or restricted in use since South Africa's participation to the Stockholm Convention on Persistent Organic Pollutants (Fischer et al. 2011). However, since Richards Bay is considered a malaria endemic area (Weiss et al. 2019), the use of DDT in malaria vector control is legitimate and to be expected. Investigations on pesticides in sediments of the study area (including Richards Bay, Lake Mzingazi, Goedertrouw Dam, as well as the southern Umlalazi Nature Reserve) are urgently needed to evaluate threats of pesticide remobilisation and hence accumulation in food webs.

Oceanic pollution by microplastics is of ever-growing global concern (Thompson et al. 2004; Shim and Thomposon 2015; Hale et al. 2020). Previous studies along the South African coastal shelf and beaches have found that estuarine outlets, coastal tourism sites and ports discharge significant amounts of plastics into the ocean (Nel et al. 2017; Naidoo and Glassom 2019; Vetrimurugan et al. 2020). However, despite recognising harbours as source of pollution, publications have focussed on microplastics collected from offshore oceanic surface waters or beach sediment. It is thus needed to exactly identify source and sink relationships to obtain relevant information for a sustainable management. Investigations on the potential sources of pollution within the harbour itself, as well as potential sinks within the harbour are still lacking and will be focussed on using a microplastics detection method for bulk sediment (Hahn et al. 2019).

## Research area

Richards Bay is located in the province of KwaZulu-Natal, on the subtropical northeast coast of South Africa (Fig. 1.1). The region became of great scientific interest, especially in the 1970s by the upcoming plans to build a deep water harbour (Begg 1978). The concept was to divide the Mhlatuze Estuary by an artificial berm, and artificially relocating the river mouth to the south. Thus creating a sanctuary next to an industrial harbour. At the time, this led to the implementation of pre-harbour and post-harbour development reviews (Begg 1978) established in the South African marine pollution survey reports 1974 – 75 (Cloete and Oliff 1976) and 1976 – 79 (Gardner et al. 1983).

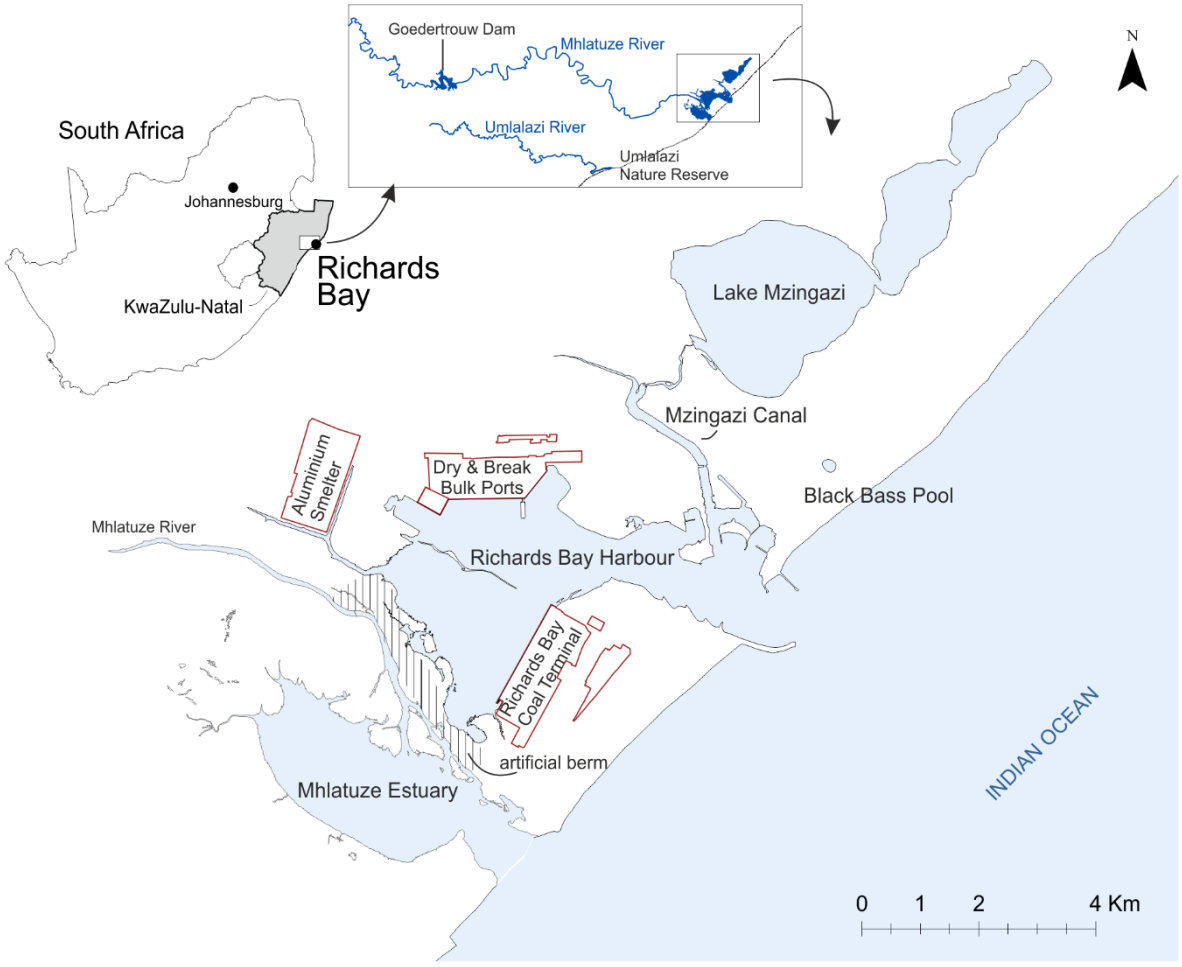


Fig. 1.1: Richards Bay in continental (top left) and regional context. Indicated are the different research sites of Richards Bay Harbour, Lake Mzingazi, Black Bass Pool, Goedertrouw Dam and the Umlalazi Nature Reserve.

Since its establishment in 1976, Richards Bay Harbour has grown into South Africa's premier bulk cargo port (Greenfield et al. 2011). Because the river Mhlatuze is canalised and diverted into the new Mhlatuze Estuary (Fig. 1.1), siltation in the port is minimized and the main

freshwater input comes from Lake Mzingazi via the Mzingazi Canal. The ports primary purpose was to facilitate the large-scale coal export through the Richards Bay Coal Terminal. Additionally, taking advantage of the newly constructed port, multiple industries settled at Richards Bay, of which an aluminium smelter and the bulk port terminals are in direct vicinity of the port basin (Fig. 1.1). Whilst industrial development proceeded, the site maintained its mangrove forests and represents the largest (Mhlatuze Estuary) and third largest (Richards Bay Harbour) colonies in KwaZulu-Natal and the Eastern Cape (Naidoo 2016).

The adjacent sampling site Lake Mzingazi is a coastal lake in the municipal area of Richards Bay. It is used as one of the most important water supplies in the area (Tonder 1986). The sampling site at Black Bass Pool represents a small freshwater lake between the suburban Meer En See and coastal dune forest. Goedertrouw Dam is the main water reserve in the Mhlatuze catchment and used by irrigators downstream of the dam, whilst also supplying water to the urban and industrial users in Richards Bay (Mallory 2000). Most parts of this thesis are based on surface sediment samples and short sediment cores directly taken from within Richards Bay Harbour.

## Thesis outline

This thesis aims to explore the impact of anthropogenic influence, including effects of industrial development, marine port operations, tourism and surrounding agricultural use of the Richards Bay region. Examined factors that lead to anthropogenic environmental stresses include fluxes of metals in surface and subsurface sediment, the distribution of persistent organic pollutants, the assessment of microplastics as well as the presence and response of micropaleontological marine taxa.

The preceding Chapter 1 introduces the reader to the research area and explains the motivation for this thesis. The following four Chapters 2-5 consist of four papers, published in (or submitted to) peer-reviewed journals (Chapter 2, 4, 5) and peer-reviewed book series (Chapter 3). The final Chapter 6 synthesises results of the individual publications of this work.

### Chapter 2

### Spatial distribution and consequences of contaminants in harbour sediments – A case study from Richards Bay Harbour, South Africa

*(Mehlhorn et al. 2021, Marine Pollution Bulletin)*

To understand system dynamics in Richards Bay Harbour, bathymetric data is compared to results of grainsize end-member modelling. Geochemical investigations, as well as possible source and sink relationships, are discussed with special consideration of the harbour sub-basins. Types of microplastics are characterised and regions of potential negatively affected bioindicators identified. The work is compared to previous field studies, adjacent regional ports and sediment quality guidelines of the National Action List on dredged sediment in South African ports.

### Chapter 3

### Comparison of different normalisers for identifying metal enrichment of sediment – a case study from Richards Bay Harbour, South Africa

*(Mehlhorn et al., accepted, In: von Maltitz, G., Midgley, G., Veitch, J., Brümmer, C., Viehberg, F., Rötter, R., Veste, M. (Eds). Sustainability of southern African ecosystems under global change: Science for management and policy interventions.)*

The sediment of Richards Bay Harbour is under the influence of different industrial and port operational processes that potentially alter its sedimentological and geochemical composition, such as possible effluents or spillage while loading operations of break bulk cargo

such as ferroalloys. Focussing on the assessment of potential environmental pollution factors and intensities, the use of Al, Fe, Rb, Ti and the silt fraction as normalisers for Cr, Cu, Co and Pb is compared. Baseline metal concentration models and Enrichment Factors are calculated and compared visually in order to ascertain if they provide the same or a different understanding on metal enrichment. Further, the results are compared to actual sediment guidelines.

### Chapter 4

### Bayhead delta evolution in the context of late Quaternary and Holocene sea-level change, Richards Bay, South Africa *(Dladla et al. 2021, Marine Geology)*

The establishment of the port of Richards Bay remarkably reconstructed the original estuary system (former Mhlatuze Estuary) towards serving international capsize port operations. The stratigraphic evolution of the underlying incised valley system and Bayhead delta are focussed on in this chapter. Seven seismic units (Unit 1 – 7) are reconstructed, based on seismic reflection data. Additional sediment cores also document composition and possible effects of dredging in the uppermost unit.

### Chapter 5

### Organochlorine pesticide contamination in sediments from Richards Bay, South Africa: spatial trends and ecotoxicological risks *(Mehlhorn et al., submitted)*

Additional samples from Richards Bay Harbour, Lake Mzingazi, Black Bass Pool, Goedertrouw Dam and the Umlalazi Nature Reserve were analysed for organochlorine pesticides. Successfully identified pesticides (dominant groups: hexachlorocyclohexanes ΣHCH and dichlorodiphenyltrichloroethanes ΣDDT) are investigated for their source and sink relationships within the harbour and the lakes. Finally, this dataset is compared to regional data on organochlorine pesticides.

### Chapter 6

### Synthesis

This final chapter synthesises Chapters 2-5 regarding chronological challenges in the sediment of Richards Bay and similarities or differences regarding source and sink relationships of the investigated pollutants. This Chapter summarizes the thesis results and provides an outlook on further studies.

## Statement of own contribution to the manuscripts

1 **Mehlhorn, P.**, Viehberg, F., Kirsten, K., Newman, B., Frenzel, P., Gildeeva, O., Green, A., Hahn, A., Haberzettl, T. 2021. Spatial distribution and consequences of contaminants in harbour sediments – A case study from Richards Bay Harbour, South Africa. *Marine Pollution Bulletin*, 172, 112764. https://doi.org/10.1016/j.marpolbul.2021.112764.

The first author wrote the manuscript, analysed and interpreted bathymetric, granulometric and geochemical data and prepared all figures and tables. Finn Viehberg and Torsten Haberzettll supported the author throughout the manuscript creation process with valuable comments and discussions. Kelly Kirsten (Bioindicators/Bioindication), Brent Newman (2012 Richards Bay dataset, baseline model, enrichment factor), Peter Frenzel (Bioindicators/Bioindication), Olga Gildeeva (Bioindicators/Bioindication), Andrew Green (Multibeam echosounder image) and Annette Hahn (Microplastics) shared data and text modules for methods or interpretation. All co-authors contributed to questions and discussions and commented on a draft of the manuscript.

| *Authors* | *Concept of the research approach* | *Analyses design* | *Data collection* | *Data analysis and interpretation* | *Writing the manuscript* | *Suggested publication equivalent* |
|---|---|---|---|---|---|---|
| Mehlhorn | x | x | x | x | x | 1.0 |
| Viehberg | x | x | | x | | n.a. |
| Kirsten | | | x | x | | n.a. |
| Newman | | | x | x | | n.a. |
| Frenzel | x | | x | x | | n.a. |
| Gildeeva | | | x | | | n.a. |
| Green | | | x | x | | n.a. |
| Hahn | | | x | | | n.a. |
| Haberzettl | x | x | x | x | | n.a. |

(Paul Mehlhorn) (Prof. Dr. Torsten Haberzettl)

2 **Mehlhorn, P.**, Newman, B., Haberzettl, T. [accepted]: Comparison of different normalisers for identifying metal enrichment of sediment – a case study from Richards Bay Harbour, South Africa. In: von Maltitz, G., Midgley, G., Veitch, J., Brümmer, C., Viehberg, F., Rötter, R., Veste, M. (Eds). *Sustainability of southern African ecosystems under global change: Science for management and policy interventions.* Springer, Heidelberg.

The first author wrote the manuscript, defined the structure and finalised the manuscript. He performed spatial interpretations and prepared the figures. Brent Newman and Torsten Haberzettl supported the author throughout the manuscript creation process with valuable comments and discussions. All co-authors contributed to questions and discussions and commented on a draft of the manuscript.

| *Authors* | *Concept of the research approach* | *Analyses design* | *Data collection* | *Data analysis and interpretation* | *Writing the manuscript* | *Suggested publication equivalent* |
|---|---|---|---|---|---|---|
| Mehlhorn | x | x | x | x | x | 1.0 |
| Newman | x | | | x | | n.a. |
| Haberzettl | x | | x | x | | n.a. |

State of publication: Accepted (8 February 2022) and soon to be published (2022). In: von Maltitz, G., Midgley, G., Veitch, J., Brümmer, C., Viehberg, F., Rötter, R., Veste, M. (Eds). *Sustainability of southern African ecosystems under global change: Science for management and policy interventions*. Springer, Heidelberg (This citation may be subject to change).

(Paul Mehlhorn) (Prof. Dr. Torsten Haberzettl)

3 Dladla, N. N., Green, A., Cooper, J. A. G., **Mehlhorn, P.**, Haberzettl, T. (2021). Bayhead delta evolution in the context of late Quaternary and Holocene sea-level change, Richards Bay, South Africa. *Marine Geology*, 441, 106608. https://doi.org/10.1016/j.margeo.2021.106608.

Paul Mehlhorn collected and shared data on core lithology, as seen in Fig. 12, used for description and interpretation in various sections. The first author wrote the manuscript. All co-authors contributed to questions and discussions and commented on a draft of the manuscript.

| *Authors* | *Concept of the research approach* | *Analyses design* | *Data collection* | *Data analysis and interpretation* | *Writing the manuscript* | *Suggested publication equivalent* |
|---|---|---|---|---|---|---|
| Dladla | x | x | x | x | x | n.a. |
| Green | x | | x | x | | n.a. |
| Cooper | | | | x | | n.a. |
| Mehlhorn | | | x | x | | 0.5 |
| Haberzettl | | | x | x | | n.a. |

(Paul Mehlhorn) (Prof. Dr. Torsten Haberzettl)

4 **Mehlhorn, P.**, Humphries, M., Gensel, J., Buah-Kwofie, A., Tyohemba, R. L., Haberzettl, T. [subm.]: Organochlorine pesticide contamination in sediments from Richards Bay, South Africa: spatial trends and ecotoxicological risks. *Environmental Science and Pollution Research*.

The first author wrote the manuscript, prepared tables and figures. Marc Humphries and Torsten Haberzettl supported the author throughout the manuscript creation process with valuable comments and discussions. Julia Gensel, Archibold Buah-Kwofie and Raymond Tyohemba contributed to the analyses design and interpretation. All co-authors contributed to questions and discussions and commented on a draft of the manuscript.

| *Authors* | *Concept of the research approach* | *Analyses design* | *Data collection* | *Data analysis and interpretation* | *Writing the manuscript* | *Suggested publication equivalent* |
|---|---|---|---|---|---|---|
| Mehlhorn | x | x | x | x | x | 1.0 |
| Humphries | x | x | x | x | | n.a. |
| Gensel | | x | x | x | | n.a. |
| Buah-Kwofie | | x | x | | | n.a. |
| Tyohemba | | x | x | | | n.a. |
| Haberzettl | x | | x | | | n.a. |

Submitted to: Environmental Science and Pollution Research

Publisher: Springer Nature

Date of submission: 25 December 2021

Manuscript ID: ESPR-D-21-18646

(Paul Mehlhorn) (Prof. Dr. Torsten Haberzettl)

## References

Begg, G. 1978: The estuaries of Natal: a resource inventory report to the Natal Town and Regional Planning Commission conducted under the auspices of the Oceanographic Research Institute. Natal Town and Regional Planning Report (41), 1–657, Durban, South Africa.

Buah-Kwofie, A., Humphries, M. S. 2017: The distribution of organochlorine pesticides in sediments from iSimangaliso Wetland Park: Ecological risks and implications for conservation in a biodiversity hotspot. *Environmental Pollution* 229, 715–723. DOI: 10.1016/j.envpol.2017.07.031.

Buah-Kwofie, A., Humphries, M. S., Pillay, L. 2018: Bioaccumulation and risk assessment of organochlorine pesticides in fish from a global biodiversity hotspot: iSimangaliso Wetland Park, South Africa. *The Science of the Total Environment* 621, 273–281. DOI: 10.1016/j.scitotenv.2017.11.212.

Buah-Kwofie, A., Humphries, M. S., Pillay, L. 2019: Dietary exposure and risk assessment of organochlorine pesticide residues in rural communities living within catchment areas of iSimangaliso World Heritage Site, South Africa. *Environmental Science and Pollution Research International* 26 (17), 17774–17786. DOI: 10.1007/s11356-019-05046-9.

Cloete, C. E., Oliff, W. D. 1976: South African Marine Pollution Survey Report 1974-1975. South African National Scientific Programmes Report 8, 60 pp., Pretoria, South Africa.

Department of Environmental Affairs 2012: 2nd South Africa Environment Outlook. A report on the state of the environment. Executive summary. Department of Environmental Affairs, 60 pp., Pretoria, South Africa.

Fischer, D., Costley, S., Moloi, M., Jila, X., Khauoe, G. 2011: South Africa National Implementation Plan for the Stockholm Convention on Persistent Organic Pollutants.

Gardner, B. D., Connell, A. D., Eagle, g. A., Moldan, A. G. S., Oliff, W. D., Orren, M. J., Watling, R. J. 1983: South African Marine Pollution Survey Report 1974-1975. South African National Scientific Programmes Report 73, 105 pp., Pretoria, South Africa.

Gerber, R., Smit, N. J., van Vuren, J. H. J., Nakayama, S. M. M., Yohannes, Y. B., Ikenaka, Y., Ishizuka, M., Wepener, V. 2015: Application of a Sediment Quality Index for the assessment and monitoring of metals and organochlorines in a premier conservation area. *Environmental Science and Pollution Research International* 22 (24), 19971–19989. DOI: 10.1007/s11356-015-5206-z.

Gerber, R., Smit, N. J., van Vuren, J. H. J., Nakayama, S. M. M., Yohannes, Y. B., Ikenaka, Y., Ishizuka, M., Wepener, V. 2016: Bioaccumulation and human health risk assessment of DDT and other organochlorine pesticides in an apex aquatic predator from a premier conservation area. *The Science of the Total Environment* 550, 522–533. DOI: 10.1016/j.scitotenv.2016.01.129.

Greenfield, R., Wepener, V., Degger, N., Brink, K. 2011: Richards Bay Harbour: metal exposure monitoring over the last 34 years. *Marine Pollution Bulletin* 62 (8), 1926–1931. DOI: 10.1016/j.marpolbul.2011.04.026.

Hahn, A., Gerdts, G., Völker, C., Niebühr, V. 2019: Using FTIRS as pre-screening method for detection of microplastic in bulk sediment samples. *The Science of the Total Environment* 689, 341–346. DOI: 10.1016/j.scitotenv.2019.06.227.

Hale, R. C., Seeley, M. E., La Guardia, M. J., Mai, L., Zeng, E. Y. 2020: A Global Perspective on Microplastics. *Journal of Geophysical Research: Oceans,* 125 (1). DOI: 10.1029/2018JC014719.

Hennig, H. F.-K. O. 1985: Review of metal concentrations in southern African coastal waters, sediments and organisms. *South African National Scientific Programmes Report No. 108.* CSIR, Pretoria.

Henry, J. L., McGibbon, S., Davis, G., MacKay, R. M., Moldan, A. G.S. 1989: Heavy metals, carbon and hydrocarbons in the sediments of Table Bay Harbour. *Special Report Sea Fisheries Research Institute South Africa* 4, 26 pp., Cape Town, South Africa.

Henry, J. L., Moldan, A. G. S. 1983: Metal concentrations in surface sediments from five South African harbours. *Internal Report, Sea Fisheries Research Institute*, 8 pp., Cape Town, South Africa.

Humphries, M. S. 2013: DDT residue contamination in sediments from Lake Sibaya in northern KwaZulu-Natal, South Africa: implications for conservation in a World Heritage Site. *Chemosphere* 93 (8), 1494–1499. DOI: 10.1016/j.chemosphere.2013.07.047.

Khan, S., Cao, Q., Zheng, Y. M., Huang, Y. Z., Zhu, Y. G. 2008: Health risks of heavy metals in contaminated soils and food crops irrigated with wastewater in Beijing, China. *Environmental Pollution* 152 (3), 686–692. DOI: 10.1016/j.envpol.2007.06.056.

Lion, G. N., Olowoyo, J. O. 2013: Population health risk due to dietary intake of toxic heavy metals from Spinacia oleracea harvested from soils collected in and around Tshwane, South Africa. *South African Journal of Botany* 88, 178–182. DOI: 10.1016/j.sajb.2013.07.014.

Mallory, S. J.L. 2000: Strategic Environmental Assessment for Water use Mhlatuze Catchment. Water Resources Assessment. Available online at https://www.dws.gov.za/sfra/SEA/Mhlathuze%20Final%20Report/AppendixB_Water%20Resources.pdf, accessed 21 March 2022.

Naidoo, G. 2016: The mangroves of South Africa: An ecophysiological review. *South African Journal of Botany* 107, 101–113. DOI: 10.1016/j.sajb.2016.04.014.

Naidoo, T., Glassom, D. 2019: Sea-surface microplastic concentrations along the coastal shelf of KwaZulu-Natal, South Africa. *Marine Pollution Bulletin* 149, 110514. DOI: 10.1016/j.marpolbul.2019.110514.

Nel, H. A., Hean, J. W., Noundou, X. S., Froneman, P. W. 2017: Do microplastic loads reflect the population demographics along the southern African coastline? *Marine Pollution Bulletin* 115 (1-2), 115–119. DOI: 10.1016/j.marpolbul.2016.11.056.

Steinberg, P. D., Airoldi, L., Banks, J., Leung, K. M.Y. 2016: Introduction to the special issue on the World Harbour Project. *Regional Studies in Marine Science* 8, 217–219. DOI: 10.1016/j.rsma.2016.10.001.

van Tonder, G. J., Botha J. F., Müller, J.L. 1986 The problems of sea water intrusions near Lake Mzingazi at Richards Bay. *Water SA* 12, 83-88.

Vetrimurugan, E., Jonathan, M. P., Sarkar, S. K., Rodríguez-González, F., Roy, P. D., Velumani, S., Sakthi, J. S. 2020: Occurrence, distribution and provenance of micro plastics: A large scale quantitative analysis of beach sediments from southeastern coast of South Africa. *The Science of the Total Environment* 746, 141103. DOI: 10.1016/j.scitotenv.2020.141103.

Weiss, D. J., Lucas, T. C. D., Nguyen, M., Nandi, A. K., Bisanzio, D., Battle, K. E., Cameron, E., Twohig, K. A., Pfeffer, D. A., Rozier, J. A., Gibson, H. S., Rao, P. C., Casey, D., Bertozzi-Villa, A., Collins, E. L., Dalrymple, U., Gray, N., Harris, J. R., Howes, R. E., Kang, S. Y., Keddie, S. H., May, D., Rumisha, S., Thorn, M. P., Barber, R., Fullman, N., Huynh, C. K., Kulikoff, X., Kutz, M. J., Lopez, A. D., Mokdad, A. H., Naghavi, M., Nguyen, G., Shackelford, K. A., Vos, T., Wang, H., Smith, D. L., Lim, S. S., Murray, C. J. L., Bhatt, S., Hay, S. I., Gething, P. W. 2019: Mapping the global prevalence, incidence, and mortality of Plasmodium falciparum, 2000–17: a spatial and temporal modelling study. *The Lancet* 394 (10195), 322–331. DOI: 10.1016/S0140-6736(19)31097-9.

Wepener, V., Vermeulen, L. A. 2005: A note on the concentrations and bioavailability of selected metals in sediments of Richards Bay Harbour, South Africa. *Water SA* 31 (4), 589–596. DOI: 10.4314/wsa.v31i4.5149.

Shim, W. J., Thomposon, R. C. 2015: Microplastics in the Ocean. *Archives of Environmental Contamination and Toxicology* 69 (3), 265–268. DOI: 10.1007/s00244-015-0216-x.

Thompson, R. C., Olsen, Y., Mitchell, R. P., Davis, A., Rowland, S. J., John, A. W. G., McGonigle, D., Russel, A. E. 2004: Lost at sea: where is all the plastic? *Science (New York)* 304 (5672), p. 838. DOI: 10.1126/science.1094559.

# Chapter 2

# Spatial distribution and consequences of contaminants in harbour sediments – A case study from Richards Bay Harbour, South Africa

Paul Mehlhorn[a,*], Finn Viehberg[a], Kelly Kirsten[b], Brent Newman[c,d], Peter Frenzel[e], Olga Gildeeva[e], Andrew Green[f,g], Annette Hahn[h], Torsten Haberzettl[a]

[a] University of Greifswald, Institute for Geography and Geology, F.L.-Jahn Str. 16, 17489 Greifswald, Germany

[b] University of Cape Town, Department of Geological Sciences, South Lane, Upper Campus, 7701 Rondebosch, South Africa

[c] Coastal Systems Research Group, CSIR, P.O. Box 59081, Umbilo, 4075 Durban, South Africa

[d] Nelson Mandela University, P.O. Box 77000, Port Elizabeth 6031, South Africa

[e] Friedrich-Schiller-University Jena, Institute of Geosciences, Burgweg 11, 07749 Jena, Germany

[f] Geological Sciences, University of KwaZulu-Natal, Private Bag X54001, Durban 4000, South Africa

[g] School of Geography and Environmental Sciences, Ulster University, Coleraine BT52 1SA, UK

[h] University of Bremen, MARUM – Center for Marine Environmental Sciences, Leobener Str. 8, 28359 Bremen, Germany

Published in: Marine Pollution Bulletin 172 (2021) 112764

Marine Pollution Bulletin 172 (2021) 112764

Contents lists available at ScienceDirect

Marine Pollution Bulletin

journal homepage: www.elsevier.com/locate/marpolbul

# Spatial distribution and consequences of contaminants in harbour sediments – A case study from Richards Bay Harbour, South Africa

Paul Mehlhorn [a,*], Finn Viehberg [a], Kelly Kirsten [b], Brent Newman [c,d], Peter Frenzel [e], Olga Gildeeva [e], Andrew Green [f,g], Annette Hahn [h], Torsten Haberzettl [a]

[a] University of Greifswald, Institute for Geography and Geology, F.L.-Jahn Str. 16, 17489 Greifswald, Germany
[b] University of Cape Town, Department of Geological Sciences, South Lane, Upper Campus, 7701 Rondebosch, South Africa
[c] Coastal Systems Research Group, CSIR, P.O. Box 59081, Umbilo, 4075 Durban, South Africa
[d] Nelson Mandela University, P.O. Box 77000, Port Elizabeth 6031, South Africa
[e] Friedrich-Schiller-University Jena, Institute of Geosciences, Burgweg 11, 07749 Jena, Germany
[f] Geological Sciences, University of KwaZulu-Natal, Private Bag X54001, Durban 4000, South Africa
[g] School of Geography and Environmental Sciences, Ulster University, Coleraine BT52 1SA, UK
[h] University of Bremen, MARUM – Center for Marine Environmental Sciences, Leobener Str. 8, 28359 Bremen, Germany

ARTICLE INFO

*Keywords:*
Metal contamination
Chromium
Magnetic susceptibility
Microplastics
Calcareous microfossils
Sediment

ABSTRACT

Richards Bay Harbour (RBH) is situated in the industrialized area on the northeast coast of South Africa. To decipher recent human activities and accompanying environmental degradation, surface sediment was collected across RBH and analysed for granulometric and elemental composition, microfaunal assemblages, and microplastics. Microplastics occur most abundantly near recreational areas, whereas metal contamination relates to activities at bulk goods terminals from which they are imported or exported. In particular, Cr and Cu concentrations in surface sediment near bulk goods terminals exceed South African sediment quality guidelines. In metal contaminated sediment, bioindicators reflected stress and were noticeably impacted. A transect of short sediment cores reflects spatial and historical metal contamination and allows quantification of the load of metals within the sediment column. The volume of metal (Cr) contaminated sediment was estimated at almost 2 million $m^3$.

## 1. Introduction

South Africa's northeast coast is becoming increasingly pressured by human activity. This anthropogenic impact, combined with effects of climate change, places stress on aquatic and terrestrial environments (Department of Environmental Affairs, 2012a). Richards Bay was one of the last remaining undisturbed large estuaries on the KwaZulu-Natal coast (Cloete and Oliff, 1976) until the establishment of Richards Bay Harbour (RBH) in the early 1970s.

The original estuary was a sheltered coastal waterbody open to the ocean (Whitfield, 1992). During harbour construction, the basin's topography and river connection were changed fundamentally, by placing a berm that divided the estuary (Fig. 1). This disconnected today's port from the Mhlatuze River, which now only feeds a natural sanctuary to the south of the berm (Figs. 1, 3). Thus, riverine water, sediment discharge, and agricultural nutrient input from the Mhlatuze catchment does not reach the harbour (Cloete and Oliff, 1976). Since construction, RBH has been under full marine influence apart from minor freshwater inflows via the Mzingazi and Bhizolo Canals (Begg, 1978). The Mzingazi Canal connects to Lake Mzingazi, which is a subordinate freshwater supply (Fig. 1).

RBH is a deep water port (permissible draught of 17.5–19.5 m) that was constructed to facilitate the export of coal, but also to serve the needs of two aluminium smelters, a granular fertilizer and sulphuric and phosphoric acid plant, and the export of heavy minerals mined nearby (Goodenough, 2003; Schwab and Becker, 2014). Additional industry, including wood chip processing and a ferrochrome smelter, has since established in the area. The contemporary industrial sector of the region makes RBH susceptible to pollution. The simultaneous accelerated growth of the city of Richards Bay increased its population density and proximity, and increased the threat of contemporary microplastic pollution as well.

* Corresponding author.
*E-mail address:* paul.mehlhorn@uni-greifswald.de (P. Mehlhorn).

https://doi.org/10.1016/j.marpolbul.2021.112764
Received 26 February 2021; Received in revised form 20 July 2021; Accepted 21 July 2021
Available online 20 August 2021

During the late 1990s, Vermeulen and Wepener (1999) pointed out data gaps in monitoring in RBH since construction of the port. Their subsequent studies analysed metal concentrations in surface sediments of RBH, revealing elevated concentrations of Cr, Cu and Zn in two sub basins (Wepener and Vermeulen, 2005). However, apart from periodic subsequent studies (e.g. Greenfield et al., 2011; Wepener and Degger, 2020), there is little published information on the pollution status of RBH.

The objective of this study was thus to investigate sediment dynamics and the spatial and temporal variation of various pollutants in sediment in RBH, with a focus on metal concentrations and microplastics and the impact of sedimentary metals on diatom, ostracod and foraminifer diversity. The study also makes use of short sediment cores to identify temporal changes in pollution.

## 2. Materials and methods

### 2.1. Field methods

In August/September 2018, 86 surface-sediment samples were collected using an *Ekman-Birge* bottom sampler (HYDROBIOS, Kiel, Germany). The topmost 1 cm of sediment was removed from the grab using a plastic spoon for metal analysis and a metal spoon for organic and microplastic analysis. Aliquots of sediment were transferred to 15 ml *Nasco* Whirl-Pak's and glass vials (microplastic analyses) and cooled until further processing.

Thirty sediment cores were retrieved using a UWITEC gravity corer (UWITEC, Mondsee, Austria) with 90 mm tube diameter (Fig. 2). The cores were stored at 4 °C in the laboratory until further processing.

During fieldwork, an echo sounder (Garmin echoMap CHIRP 42cv) constantly recorded water depth. These measurements were tide corrected via a tide table provided by the South African Navy Hydrographic Office (SANHO) (high and low stand phases interpolated by local regression). Practical salinity (electrical conductivity) and oxygen were measured using a WTW340i multiprobe (Xylem Inc., Rye Brook, NY, USA).

Multibeam bathymetric data were collected using a Norbit iWBMS 400 kHz narrow beam multibeam echosounder with an integrated inertial navigation system (Applanix WaveMaster II). Sound velocity variation in the water column was inspected using a Valeport sound velocity probe. Positioning and further vessel motion (including tidal variation) were modelled using a Real Time Kinematic GPS. Data were processed in BEAMWORX, where sound velocity casts and tidal variations were integrated into the soundings, spurious soundings were removed, and the final seafloor elevation data was exported as a 0.5 × 0.5 m grid for this study. The data resolved to approximately 10 cm in the vertical domain.

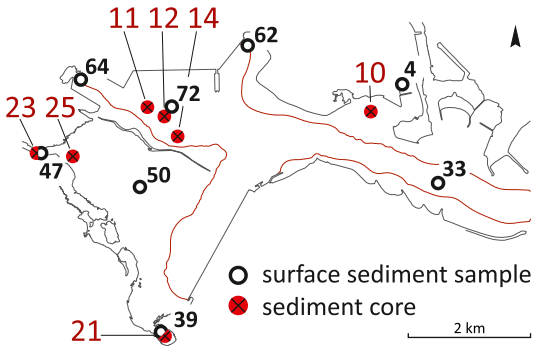


**Fig. 2.** Sediment short core locations (red dots) and micropaleontology samples (black cirlces).

### 2.2. Grain-size analysis and end member modelling

Aliquots of 0.5–2 g wet sediment were taken for grain-size analyses. The material was soaked in 2 ml hydrochloric acid (HCl, 10%) and 5 ml hydrogen peroxide ($H_2O_2$, 10%). Residues were dispersed overnight with 5 ml tetrasodium pyrophosphate ($Na_4P_2O_7$ 10 $H_2O$, 0.1 M) in an overhead shaker. Subsequently, samples were measured in several runs

**Table 1**
Information for cores collected in Richards Bay Harbour. Refer to Fig. 2 for core locations.

| Core ID locality – year – core number | Recovery date | Latitude [°] | Longitude [°] | Water depth [m] | Core length [cm] |
|---|---|---|---|---|---|
| RBH18-10 | 25 Aug. 18 | −28.7976 | 32.0739 | 1.6 | 27.5 |
| RBH18-11 | 26 Aug. 18 | −28.7968 | 32.0392 | 20.5 | 80.5 |
| RBH18-12 | 26 Aug. 18 | −28.7980 | 32.0419 | 20.9 | 118.5 |
| RBH18-14 | 26 Aug. 18 | −28.8007 | 32.0439 | 21.0 | 135.0 |
| RBH18-21 | 27 Aug. 18 | −28.8284 | 32.0414 | 4.5 | 160.0 |
| RBH18-23 | 27 Aug. 18 | −28.8029 | 32.0220 | 3.2 | 72.5 |
| RBH18-25 | 27 Aug. 18 | −28.8034 | 32.0276 | 3.5 | 57.5 |

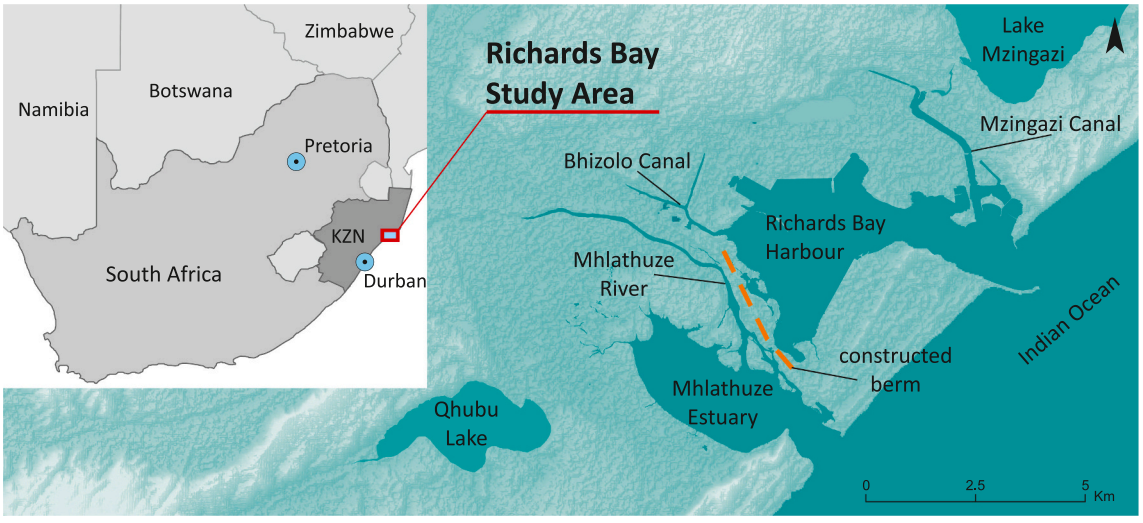


**Fig. 1.** Richards Bay in continental (left) and regional (right) context. The main river and adjacent lakes are indicated. Highlighted in orange is the berm constructed during the 1970s, which separates Richards Bay Harbour from the Richards Bay Sanctuary (Mhlatuze Estuary).

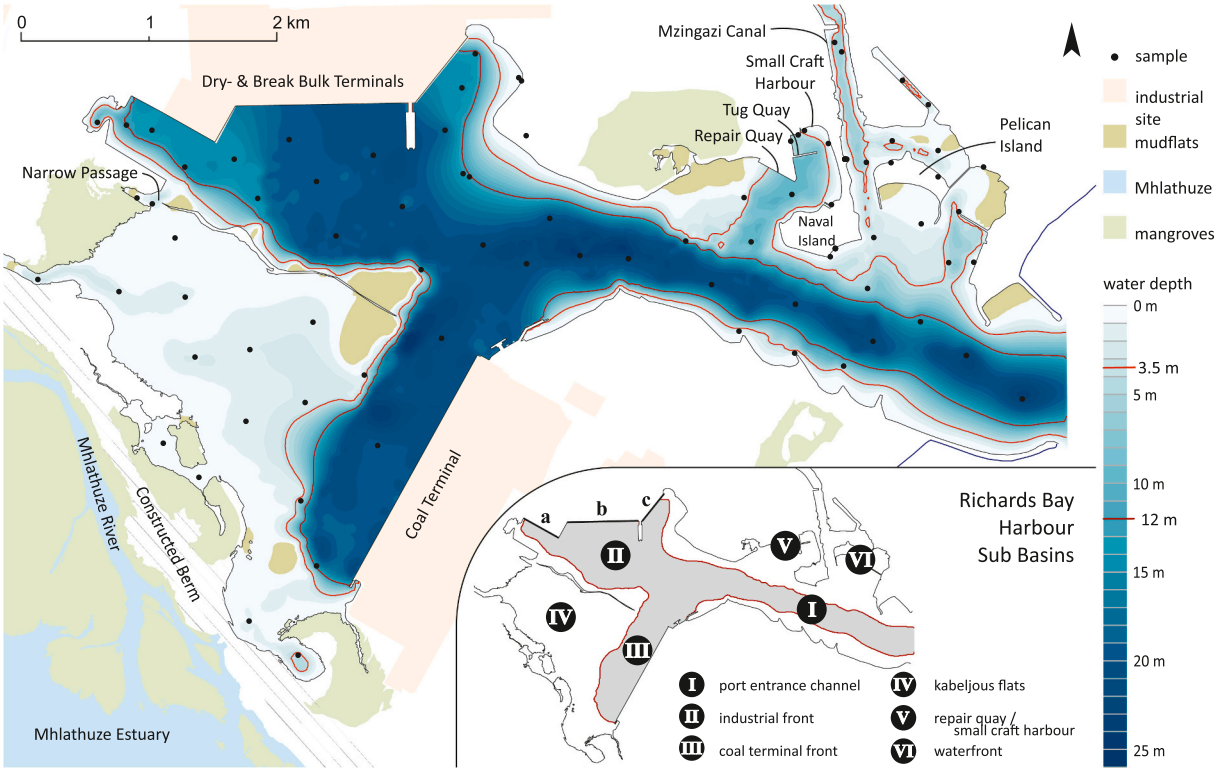


**Fig. 3.** Bathymetric map of Richards Bay Harbour (tide normalized). Indicated are surface sampling points (black symbols) and landmarks. Dredging results in a steep gradient within the basin marked by steep slope angles indicated by the proximity of the 3.5 and 12 m water depth contour lines. Also indicated are the six sub basins.

using a Laser Diffraction Particle Size Analyser (Fritsch Analysette 22; FRITSCH GmbH, Germany) until a reproducible signal was obtained. GRADISTAT 8.0 (Blott and Pye, 2001) was used to calculate grain-size statistics. End-member (EM) modelling was carried out using the R software package EMMAgeo v. 0.9.6. (Dietze and Dietze, 2019).

### 2.3. Sediment properties and geochemical analyses

Magnetic susceptibility was measured on freeze-dried samples, using a Bartington MS2B sensor and 10 ml plastic cups. For geochemical analyses, freeze-dried samples were ground to a particle size <60 μm and homogenized. Subsamples were digested using a modified aqua regia treatment (100 mg sample, 1.25 ml HCl 37% suprapur and 1.25 ml $HNO_3$ 65% suprapur) in PTFE crucible pressure bombs at 160 °C for 3 h. Quantitative element concentrations were measured using an Agilent 725 ES ICP-OES (Al, Ca Fe, K, Mg, Mn, Na, P, S, Sr, Ti) and a Thermo Fischer Scientific X-Series II ICP-MS (As, Cd, Co, Cr, Cu, Ni, Pb, Zn, Rb, Hg). Each digestion batch included laboratory blanks. Calibration was performed with multi element calibration standards. ICP measurements were evaluated using internal standards (20 μg $l^{-1}$ Ru and 10 μg $l^{-1}$ Re). During analysis, calibration verification standards were used regularly, and calibration curves evaluated. Each sample was measured three times, analysed for outliers (Grubbs's test), and reported as the mean and absolute standard deviation.

The Council for Scientific and Industrial Research (CSIR) analysed metal concentrations in 96 surface sediment samples collected in RBH using a van Veen grab in 2012. These data are included in this study for comparative purposes. About 1 g of freeze dried and ball milled sediment was weighed into a digestion vessel and digested in a mixture of $HNO_3$-HCl-$H_2O_2$ according to USEPA method 3050B. The concentrations of metals were measured using a Thermo ICap 6500 ICP-OES (Al, Fe, As, Cu, Cr, Co, Mn, Ni, Pb, Zn) and Agilent 7900 ICP-MS (Cd). Precision and extraction efficiency of the digestion and metal determination procedures was evaluated by repeatedly analysing marine sediment reference standard PACS-2 (National Research Council of Canada) and sample duplicates.

To properly interpret metal concentrations in sediment the factors that control their natural variation must be compensated for before background or baseline concentrations can be distinguished from enriched (higher than 'expected') concentrations. This is usually accomplished by the procedure of geochemical normalization, wherein metal concentrations are normalized to an element that provides a tracer of crustal decomposition (Hanson et al., 1993; Kerste and Smedes, 2002). In this manner, metal concentrations that are atypical of the bulk of the data can be identified.

Enrichment Factors (EF's) were used to compare metal enrichment of sediment sampled in RBH in 2012 and 2018. Baseline metal concentration models were defined for this purpose, using Al as the normalizer. The models were defined separately for each study since there were (usually small) differences in the nature of relationships between metal and Al concentrations. The differences likely reflect method related differences by the two laboratories that analysed the sediment. The baseline models were defined by fitting a linear regression and 99% prediction limits to scatter plots of metal versus Al concentrations. Metal concentrations falling outside the prediction limits were deemed outliers and sequentially trimmed, starting with the concentration presenting the largest residual and proceeding in this manner until all concentrations fell within the prediction limits. EF's were then computed as the ratio between measured metal concentrations and the concentration at the upper prediction limit at the corresponding Al concentration in the samples. EF's values >1 represent metal concentrations that are higher than expected (Newman and Watling, 2007).

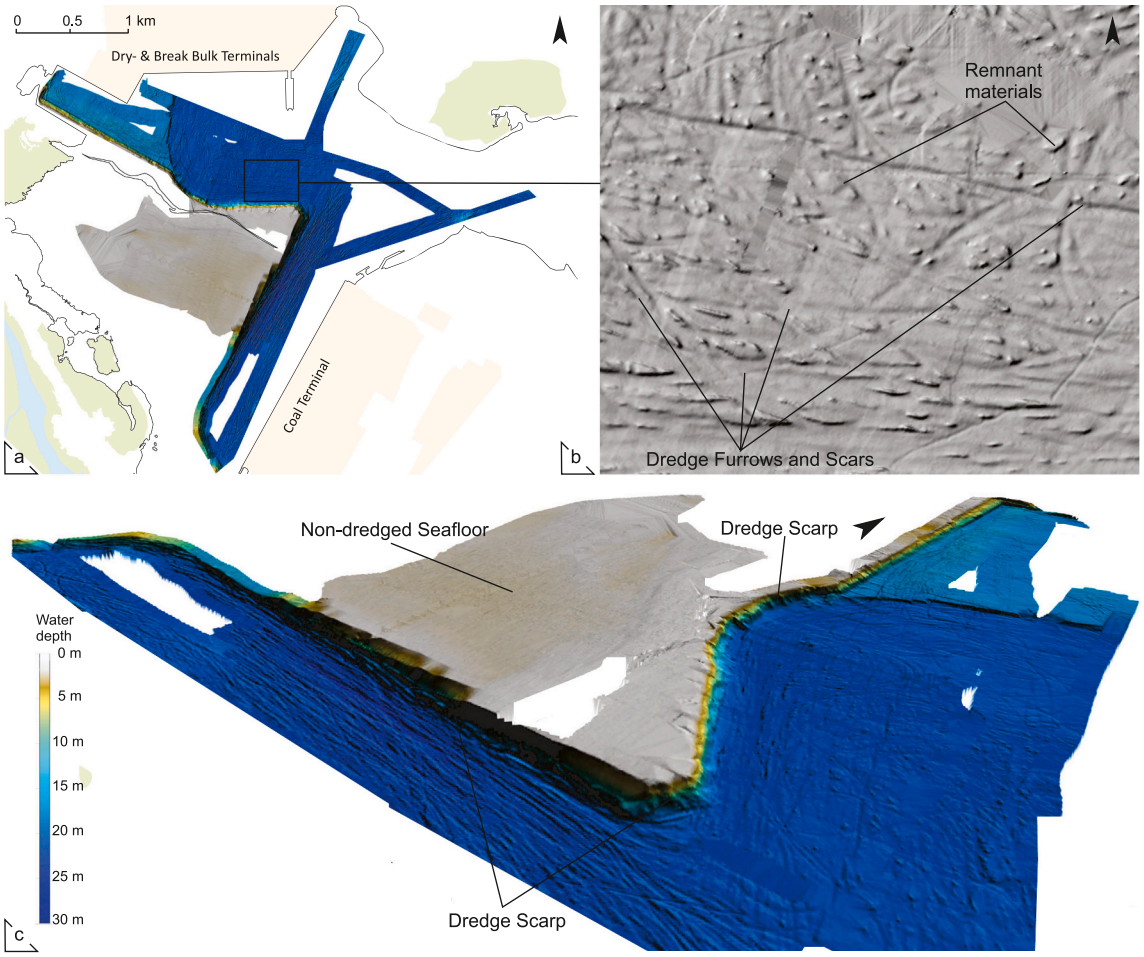


**Fig. 4.** a) Multibeam echosounder image of SB-I to IV. b) Furrows in sediment surface were created by dredging operations - note the remnants of the pre-dredged material outcrops. c) Steep scarps and sharp edges at the boundary between dredged and un-dredged areas.

### 2.4. Microplastic analysis

Prior to spectral analysis, freeze-dried samples were milled at 50 revolutions per second for 3 min and diluted with IR transparent Potassium bromide (KBr). The samples were analysed with a Bruker Vertex 70 spectrometer equipped with a MCT (Mercury–Cadmium–Telluride) detector and a KBr beam splitter. Spectra resulting from 128 sample scans in a range from 3750 $cm^{-1}$ to 400 $cm^{-1}$ were produced with a resolution of 4 $cm^{-1}$. For the semi-quantitative analysis of LDPE and PET contents on bulk sediments, we used the calibration models by Hahn et al. (2019), which are based on synthetic sediment mixtures with defined microplastic contents.

Microplastic analyses were complemented using microscopy-assisted handpicking of plastic remains >1 mm. Classification is based on three semi-quantitative categories: 0 particles found, 1–2 particles found, and 3–10 particles found.

### 2.5. Diatom analysis

Eight surface sediment samples representing different parts of RBH were prepared for diatom analysis (Fig. 2). Samples were chemically treated with 30% $H_2O_2$ and 10% HCl. The resultant supernatant was sieved and swirled to remove coarser materials and sediments. The supernatant was then repeatedly suspended, allowed to settle over 8 h periods, and the excess water decanted, thus systematically removing finer particulates such as clay and concentrating diatom frustules in the settled residue. Slides were mounted in Pleurax and diatoms were counted under a light microscope at up to 1000× magnification. Identification of diatom species was based on diatom manuals and catalogues (Bate et al., 2004; Taylor et al., 2007).

### 2.6. Ostracoda and Foraminifera analysis

Aliquots from sediment samples for diatom analysis were also analysed for Ostracoda and Foraminifera (Fig. 2). The volume of each sediment sample was measured as a reference for the calculation of abundance. Samples were wet sieved (using tap water) through a 63 μm sieve and dried. A floating technique using a sodium polytungstate solution (Parent et al., 2018) was used to separate microfossils from clastic sediment. The recovery rate is about 96% (Semensatto and Dias-Brito, 2007).

For quantitative foraminifer and ostracod analysis, samples were dry sieved through >200 μm and 125–200 μm mesh size sieves. The size fractions were split into sub-samples using a micro-splitter. Valves and tests from split samples were counted until 300 individuals of Foraminifera and Ostracoda for the >200 μm fraction, and >200 foraminifer tests for the >125 μm fraction were reached. All valves and tests were counted when the required number was not reached. Reworked individuals of both Foraminifera and Ostracoda were omitted from counts, e.g. those with abraded ornamentation or sediment inside the chambers. Ostracod carapaces were counted as two valves. Total abundance, diversity, and proportion of Ostracoda was calculated from the >200 μm

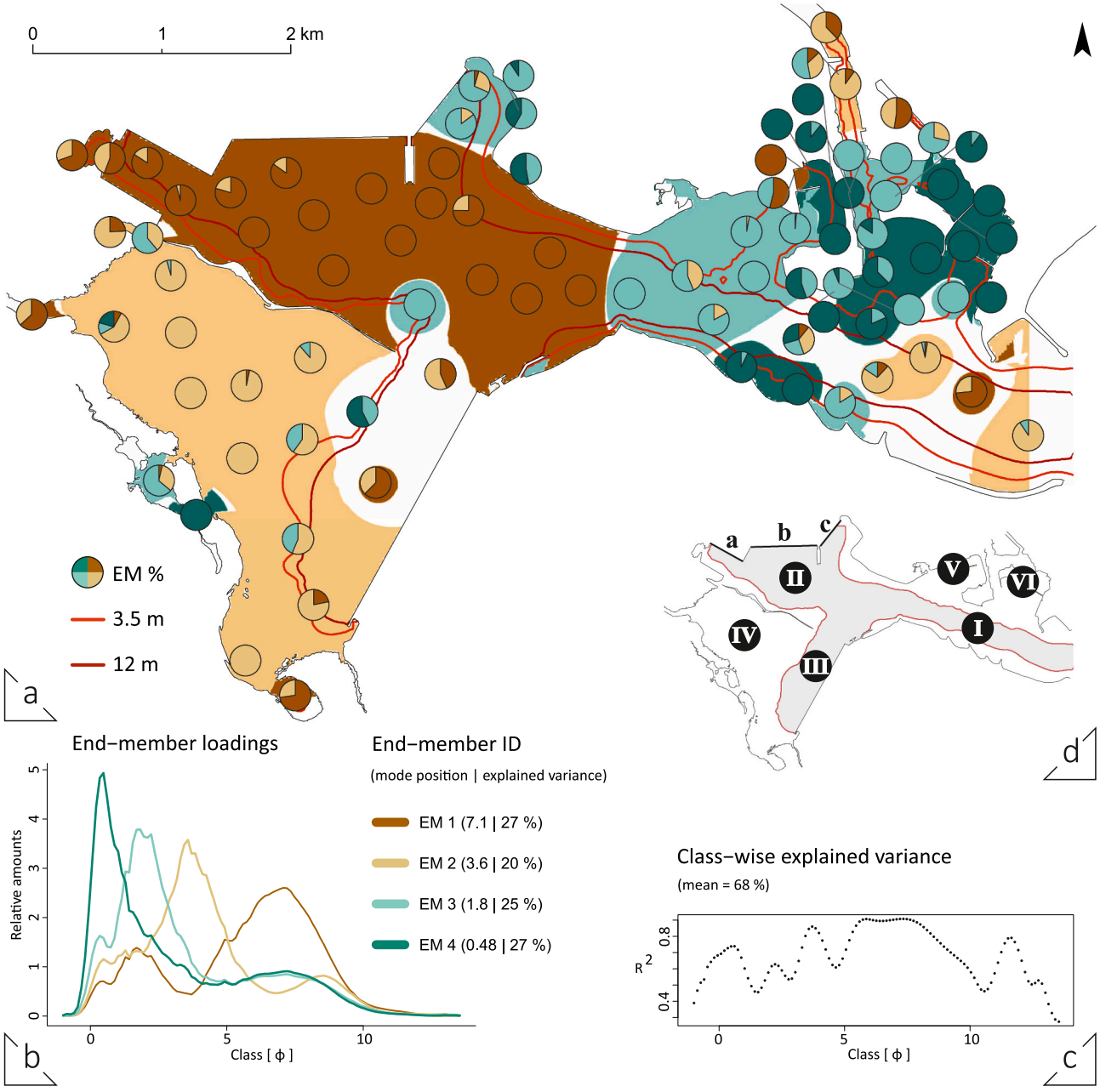


**Fig. 5.** a) Spatial distribution map of end-member scores (inverse distance weighting). Pie charts correspond to sample positions and detail the absolute end-member scores. Scores above 50% are coloured spatially. White areas indicate no dominant end-member score. Also indicated are the 3.5 and 12 m water depth contour lines. b) End-member loadings and explained variance. c) End-member class-wise explained variance. d) Sub-basin nomenclature. (For interpretation of the references to colour in this figure legend, the reader is referred to the web version of this article.)

size fraction count. Malformed foraminifera were counted separately in both size fractions to calculate a Foraminiferal Abnormality Index (FAI; Frontalini and Coccioni, 2008). Identification relied mainly on Benson and Maddocks (1964) and Dingle (1993, 1992) for Ostracoda, and Fürstenberg et al. (2017) and the World Register of Marine Species (http://www.marinespecies.org/) for Foraminifera. Species diversity was evaluated using Shannon's diversity (H′) index (Shannon, 1948).

### 2.7. Core processing

Sediment cores (Table 1) were split in half, photographed, and lithologically described at the Physical Geography department of the University of Greifswald. Magnetic susceptibility was measured on split cores using a Bartington MS2E point sensor (Bartington Instruments Ltd., Witney, UK) at 0.5 cm resolution. Core RBH18-12 and RBH18-23 were scanned with an ITRAX XRF-core scanner (COX analytical systems) at GEOPOLAR, University of Bremen. Sections were scanned with a Mo-tube with a step size of 2 mm, a count time of 20 s per step at a constant voltage of 30 kV, and a current of 50 mA. To account for matrix effects, data were normalized by total counts (element/kcps).

## 3. Results

### 3.1. Bathymetry and marine impact

RBH can be divided into six sub-basins (SB) (inset in Fig. 3), of which

**Table 2**
Mean, Standard Deviation, minimum and maximum concentrations (µg $g^{-1}$, dry weight) for bulk sediments sampled in 2018 (analytical methods are indexed below element symbol: MS = ICP-MS, OES = ICP-OES). Guideline levels are given according to the Department of Environmental Affairs (2012b).

| 2018 | Al | As | Ca | Cd | Co | Cr | Cu | Fe | K | Mg | Mn | Na | Ni | P | Pb | S | Sr | Ti | Zn | Rb |
|---|---|---|---|---|---|---|---|---|---|---|---|---|---|---|---|---|---|---|---|---|
| | OES | MS | OES | MS | MS | MS | MS | OES | OES | OES | OES | OES | MS | OES | MS | OES | OES | OES | MS | MS |
| Min | 4300 | 3 | 4841 | 0.1 | 2 | 11 | 2 | 4622 | 995 | 1776 | 100 | 1768 | 3 | 117 | 1 | 200 | 52 | 390 | 8 | 4 |
| Max | 72350 | 65 | 34241 | 1.5 | 25 | 969 | 353 | 67247 | 12625 | 13048 | 1495 | 31707 | 81 | 3125 | 49 | 9250 | 298 | 3582 | 274 | 90 |
| Mean | 30668 | 19 | 17388 | 0.2 | 12 | 169 | 38 | 31677 | 5612 | 6857 | 580 | 10953 | 28 | 941 | 14 | 2635 | 130 | 1643 | 79 | 36 |
| SD | 20538 | 16 | 5831 | 0.3 | 6 | 172 | 55 | 16205 | 3641 | 3318 | 320 | 7987 | 18 | 704 | 9 | 2263 | 38 | 763 | 55 | 26 |
| Warning Level | | 42 | | 1.2 | | 135/250 | 110 | | | | | | 62/88 | | 110 | | | | 270 | |
| Level I | | 57 | | 5.1 | | 260 | 230 | | | | | | 140 | | 218 | | | | 410 | |
| Level II | | 93 | | 9.6 | | 370 | 390 | | | | | | 370 | | 530 | | | | 960 | |

SB-I, -II, -III and V are dredged to maintain the operational water depth. As a result, the bathymetry clearly emphasizes marine traffic routes (Figs. 3, 4). Steep slopes (6-18°) – dredge scarps (Fig. 4c) – emerge towards the non-dredged sections, highlighted by the narrow separation of the 3.5 and 12 m water depth contour lines. Dredging operations scar the bottom and result in an uneven sediment surface (Fig. 4b). SB-II can further be subdivided based on proximity to three adjacent Dry- and Breakbulk terminals (a, b, c on inset in Fig. 3).

Salinities within RBH basins vary between about 34–35. The uniformly high salinity reflects tidal exchange with the Indian Ocean and limited inflow of freshwater. Lower salinities (30−31) occur north of Pelican Island (SB-VI, Fig. 3) and gradually decrease up Mzingazi Canal (reading 29), which connects RBH with the freshwater overflow of Lake Mzingazi (Fig. 1).

### 3.2. Grain-size distribution and end-member modelling

The steep bathymetric gradient formed by the dredge scarp is reflected in sediment granulometry. In general, the grain-size distribution in RBH reflects the bathymetry: mean grain-size (FWMphi; Folk and Ward, 1957) generally decreases with increasing water depth ($r = 0.71$, $p < 0.001$). Thus, deep basins SB-I, II and III – >12 m water depth – are dominated by silt, and shallower areas by sand.

Despite the positive correlation of surface sample mean grain-size and water depth, most grain-size distribution curves are bi- or tri-modal. Therefore, in the deposited sediment, mean grain-sizes reference a value that condenses two or three modes (local maxima), individual grain-size fractions, and eventually sediment sources. End-member modelling statistically decomposes grain-size distributions and allows for a genetic interpretation. Here, end-member (EM) modelling was used (Dietze et al., 2014) to facilitate the use of grain-size as an environmental parameter and to distinguish the main detrital processes that contribute to sedimentation (Fig. 5).

Four significant end-members were identified from RBH surface sediment samples, which explain 68% of the variance of grain-size classes (Fig. 5c). The finest end-member, EM1, occurs mainly in SB-II and partially in SB-I and III (Fig. 5). The main constituent is fine silt (mode 7.1φ, Fig. 5b), accompanied by a second fraction of medium to fine sand (mode 1.7φ). Samples containing >50 vol% EM1 occur at an average water depth of 15 m, which is largely in sub-basins SB-I, II and III. In various samples, EM2 occurs with EM1. The majority of EM2 is in SB-IV, with a predominant grain-size of very fine sand (mode 3.6φ) at an average water depth of 3 m. An array of less clustered samples is also classified as EM2 across much of RBH. EM3 occurs in various parts of the harbour, but predominates near the fairways at around 7 m water depth. Its main constituent is medium sand (mode 1.8φ, Fig. 5b). The coarsest end-member, EM4, occurs in close relation to EM3 in shallower water areas (~1.5 m), mainly at the harbour entrance and along shorelines (Fig. 5a). EM4 is dominated by coarse sand (mode 0.5φ, Fig. 5b).

### 3.3. Element concentrations in Richards Bay Harbour

The mean element concentrations in surface sediment sampled in 2018 follow the order Fe > Al > Ca > Na > Mg > K > S > Ti > P > Mn > Cr > Sr > Zn > Cu > Rb > Ni > As>Pb > Co > Cd (Table 2).

Apart from Ca, Cd, Sr and Ti, the elements (Table 2) correlate positively with one another. Aluminium (Fig. 14) is positively correlated with most elements ($r > 0.5$), bathymetry (Al/water depth; $r = 0.73$, $p < 0.001$) and mean grain-size (Al/FWMphi; $r = 0.95$, $p < 0.001$). Outliers – detected through geochemical normalization to Al – that in many cases reflect anthropogenic impact, alter the individual datasets, especially in the case of Cr and Cu. The removal of outliers results in an improved correlation to Al. Nevertheless, metal distribution patterns show significant spatial differences, despite their general correlation to Al.

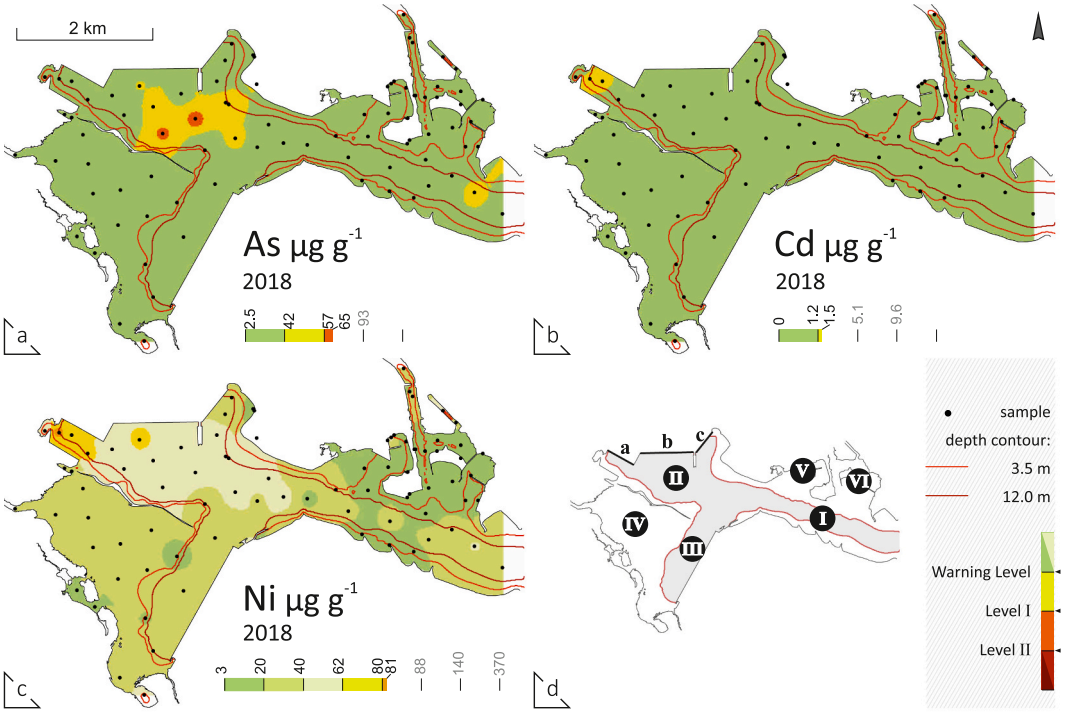


**Fig. 6.** Interpolated spatial distribution maps (inverse distance weighting) showing the concentration of As, Cd, and Ni. Each legend maxima refers to the guideline maxima (Department of Environmental Affairs, 2012b). Colour codes relate to guideline levels: ≤ Warning Level (green), > Warning Level and ≤ Level I (yellow), > Level I and ≤ Level II (orange), and > Level II (red). d) Sub-basin nomenclature. (For interpretation of the references to colour in this figure legend, the reader is referred to the web version of this article.)

### 3.4. Trace metals – As, Cd, Cr, Cu, Ni

The highest concentrations of most trace metals, including As, Cd, Cu, Cr and Ni, which are of concern from a toxicological perspective, were in SB-II (Fig. 6). The highest concentrations of As were in the middle part of SB-II, farthest from quays, and is unlikely to reflect contamination (Fig. 6a). High concentrations of Cd, Cr, Cu and Ni were found in SB-IIa (Figs. 6 and 7). Sediment in SB-IIb contained high concentrations of Cr, Cu and Ni, while Cu and Cr were also at a high concentration in SB-IIc (Fig. 7).

### 3.5. 2018 Cr and magnetic susceptibility distribution

The range of Cr concentrations in sediment sampled in RBH was wide, from 11 to 968 µg $g^{-1}$ (Table 2, Fig. 7c). The lowest Cr concentrations were near the port entrance. Moderate concentrations were found mainly in SB-III, IV and V. The highest concentrations were in SB II, with a distinct increase in front of the bulk goods terminals (a, b, c on inset in Fig. 7f).

Low-field mass-specific magnetic susceptibility ($\chi_{LF}$) values range from 0.15 to 4.48·$10^{-6}$ $m^3$ $kg^{-1}$, with consistently low values in SB-I, III, V and VI (Fig. 7e). Highest $\chi_{LF}$ values occur in front of the bulk goods terminals in SB-II and in the western part of SB-IV. Spatial magnetic susceptibility variations in surface sediment show similar patterns to Cr concentrations (Fig. 7c, e) and log-transformed datasets correlate positively (Cr $_{Translog}$/$\chi_{LF\ Translog}$: r = 0.71).

### 3.6. Baseline models and Enrichment Factors

The Al normalized baseline models for Cr in sediment sampled in RBH in 2012 and 2018 are provided in Fig. 8, with baseline and enriched concentrations superimposed. Additional spatial distributions of Cr EF's indicate only enriched sediment (EF ≥ 1). Hereby both maps show strong similarities in their distribution pattern. However, during 2012 samples were taken very close to the northern pier in SB-II and indicate Cr enrichment towards the pile wall. While 2012 data ranges up to an EF of 3.0, considered high enrichment, 2018 data ranges up to an EF of 5.5, considered as severe enrichment (Fig. 8a, c).

### 3.7. Sediment cores

Core RBH18-12 (1.2 m) – collected in SB-II (Fig. 2) – can be divided into three units (I-III) from base to surface (Fig. 9). Unit I comprised an olive-green mud with black mackles. This gradually changed into unit II, a homogeneous olive mud with two intercalated sand layers. The top section (unit III) reverts to an olive-green mud with increasing number of black mackles. This subdivision can also be observed in low field magnetic susceptibility ($\kappa_{LF}$), Cr and Cu counts (Fig. 9). $\kappa_{LF}$ and Cr show slightly lower values in unit II compared to unit I. However, both parameters show an increasing trend towards the top of unit III.

Sediment core RBH18-23 comprised an olive-green mud, with fine lamination and slight colour differentiation. The upper 23 cm were bioturbated and truncated by *Polychaeta* burrows. A subdivision into comparable units to RBH18-12 is not possible. Comparing the correlation factors between Cr/kcps and $\kappa_{LF}$ of core RBH18-23 (r = 0.8) to core RBH18-12 (r = 0.9), a similar dependence and rise in both parameters is noticed, which confirms the previously detected relationship between $\chi_{LF}$ and Cr in surface sediments.

In contrast to Cr, highest Cu counts were evident in unit I and III of core RBH18-12, with spikes at 100–90 cm and 45 cm (Fig. 9). Similar to $\kappa_{LF}$ and Cr, unit II had the lowest Cu counts. Cu counts were fairly constant through core RBH18-23.

A similar $\kappa_{LF}$ pattern as that evident in core RBH18-12 was evident in cores RBH18-11 and -14, which form a NW-SE-transect in SB-II from the

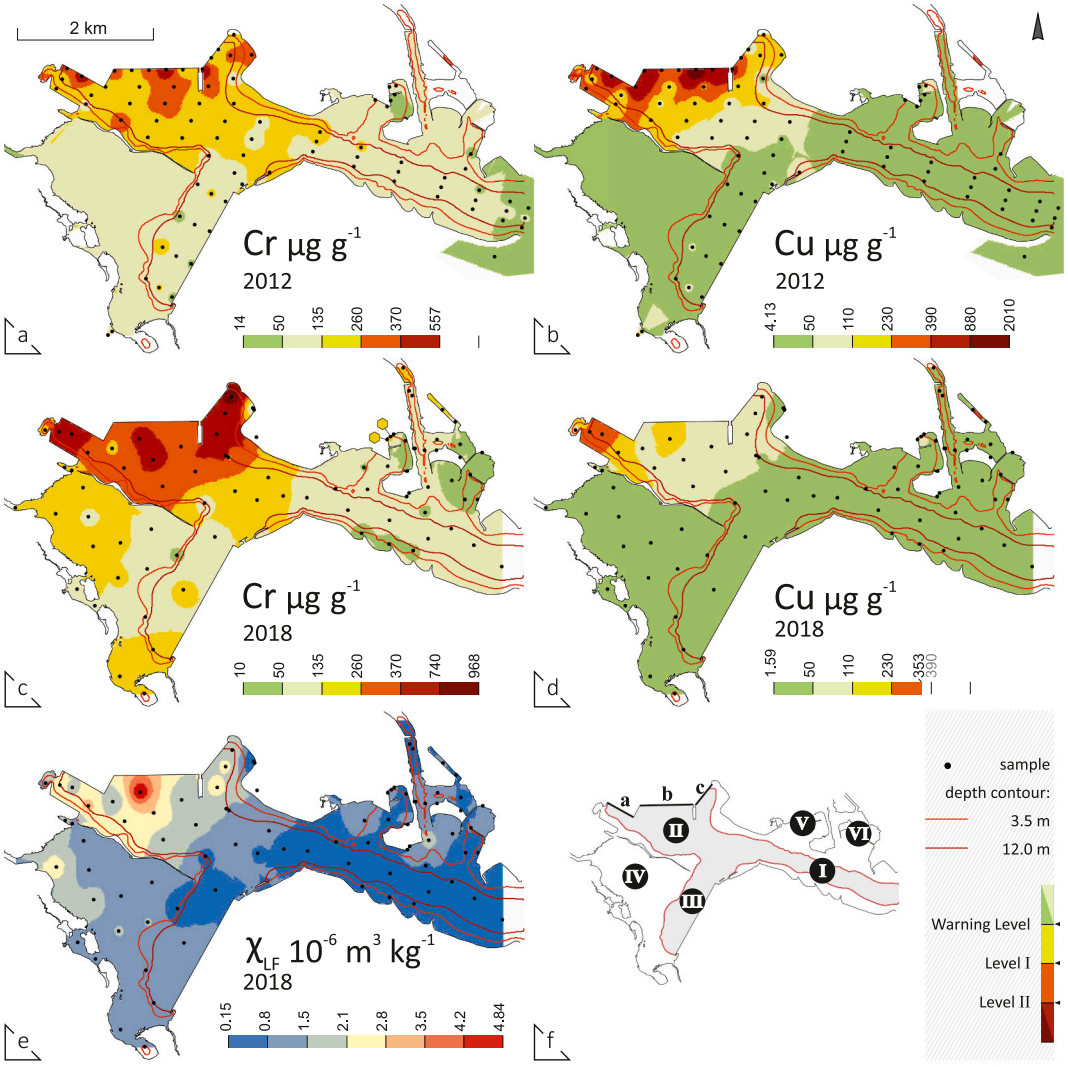


**Fig. 7.** Interpolated spatial distribution maps (inverse distance weighting) showing concentrations of Cr and Cu in 2012 (a, b) and 2018 (c, d). e) Pattern of magnetic susceptibility ($\chi_{LF}$) measured in 2018. Colour codes resemble element concentration limits as indexed by the Department of Environmental Affairs (2012b): ≤ Warning Level (green), > Warning Level and ≤ Level I (yellow), > Level I and ≤ Level II (orange), and > Level II (red). f) Sub-basin nomenclature. (For interpretation of the references to colour in this figure legend, the reader is referred to the web version of this article.)

bulk terminal towards the middle of the harbour. Moving away from apparent Cr concentration maxima in SB-II (a-c), $\chi_{LF}$ decreases in surface sediment towards the SE (Fig. 7). This observation is also evident in the SB-II core-transect: $\kappa_{LF}$ in the upper parts of the cores decreases from RBH18-11 to -14 (Fig. 10), the latter being furthest (about 1 km) from the bulk goods terminals (Fig. 2). Representative short cores from the western part of SB-IV, namely RBH18-23 and -25, also indicate increased $\kappa_{LF}$ in regions of increased $\chi_{LF}$ in surface sediments (Figs. 2, 7, 9 and 10). In contrast, almost no magnetic susceptibility variation was evident in cores RBH18-10 and -21, which were at a greater distance from the bulk goods terminals (Fig. 2).

### 3.8. Microplastics

FTIRS analyses revealed two types of plastic in RBH sediment: polyethylene terephthalate (PET) and low density polyethylene (LDPE). PET was found in most samples. The highest abundances were nearest the port entrance (SB-I, SB-V and SB-VI) and near the coal terminal (SB-III) (Fig. 11). LDPE was found mainly in the SW part of RBH, in sediment from SB-IV and small basins like SB-IIa and SB-V. The distribution of handpicked plastic pieces >1 mm visually resembles the PET-distribution, with higher abundances in SB-V. Correlation coefficients suggest a similar depositional behaviour of PET, EM4 ($r = 0.53$, $p < 0.001$) and medium sand ($r = 0.55$, $p < 0.001$).

PET and LDPE concentrations are negatively correlated ($r = -0.58$), and the individual distribution patterns visually oppose one another (Fig. 11). Therefore, the predominant occurrences can be assigned to different harbour sub-basins.

### 3.9. Bioindicators

The Foraminifera Abnormality Index (FAI) ranged between 0 and 9.1 for samples with at least 40 counted foraminifer tests (Table 4). Most samples contained high abundances of microfossils, mostly in good preservation, for all three groups. Exceptions were samples #62 and #64 directly in front of the bulk goods terminals in SB-II (SB-IIc and SB-IIa), where diatoms, foraminifers and ostracods showed low abundances and were often fragmented or poorly preserved. Foraminifera and

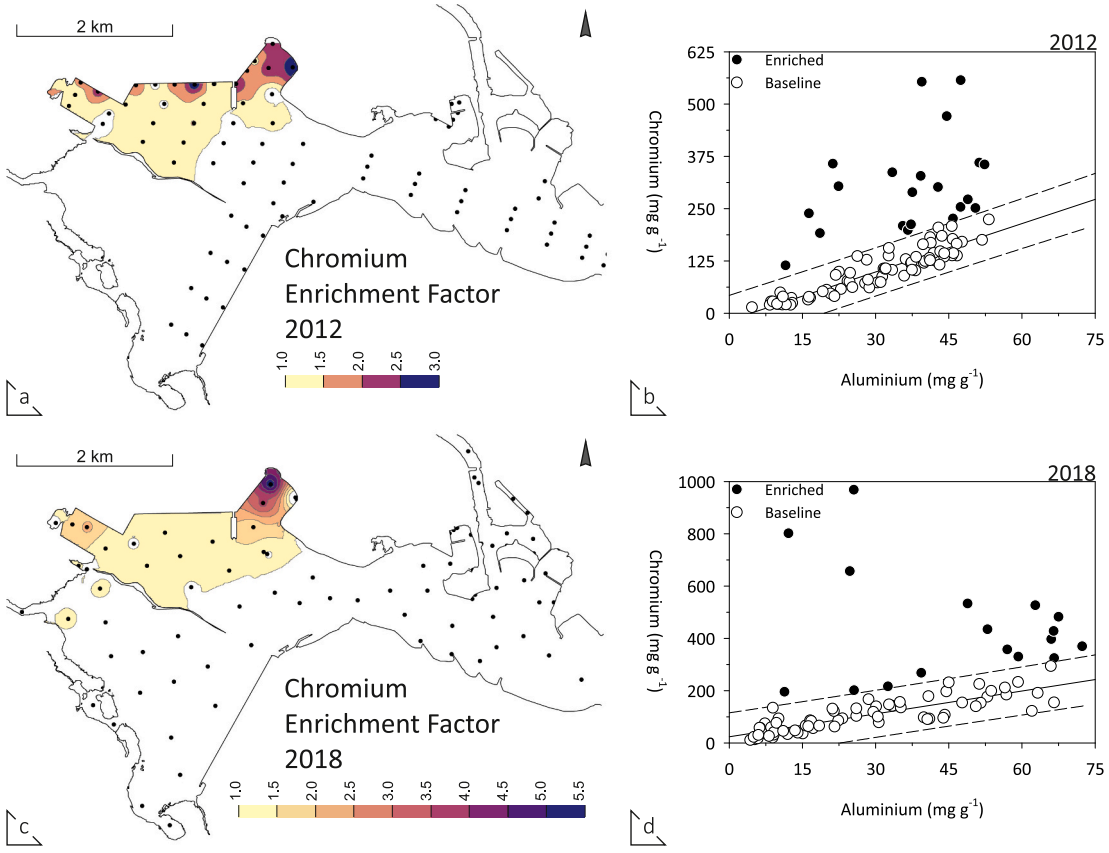


**Fig. 8.** Baseline models for Cr in surficial sediment sampled in Richards Bay Harbour in 2012 (b) and 2018 (d), enriched samples are black dotted. Associated spatial distribution maps (a, b) of Enrichment Factors (EF), interpolated via inverse distance weighting, are coloured if EF ≥ 1, whereby we categorize: low (EF ≥1–1.5), moderate (EF >1.5–2.5), high (EF >2.5–5), and severe (EF >5) enrichment.

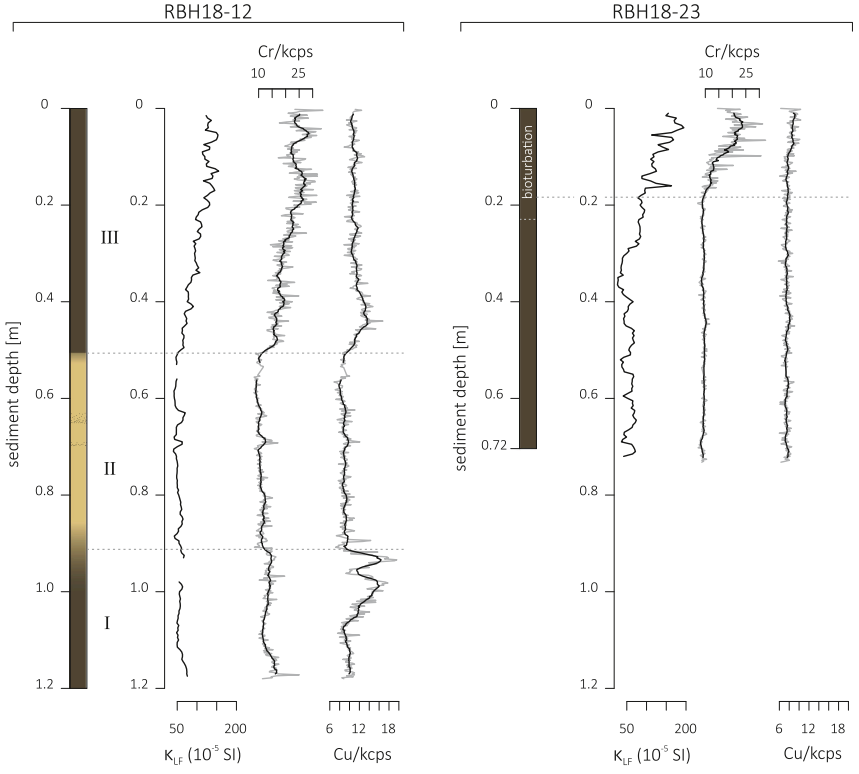


**Fig. 9.** Lithology, magnetic susceptibility and normalized XRF counts for Cr and Cu (grey line = original data at 2 mm resolution, black line = moving average (11 periods) from sediment cores RBH18-12 and -23.

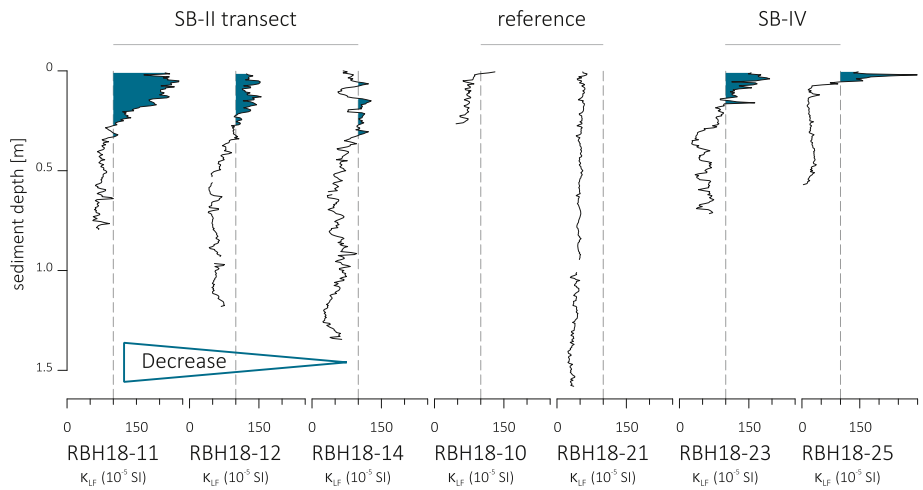


**Fig. 10.** Low field magnetic suceptibility ($\kappa_{LF}$) of selected sediment cores. All measurements are plotted on the same scale. Note the reference line at $100{\cdot}10^{-5}$ SI. Left: transect RBH18-11 to -14 indicates a decrease in susceptibility (with increasing distance from bulk terminals). RBH18-23 and -25 from SB-IV indicate comparable values to the transect. Reference cores RBH18-10 and -21 in which $\kappa_{LF}$ is below $100{\cdot}10^{-5}$ SI. For core locations see Fig. 2.

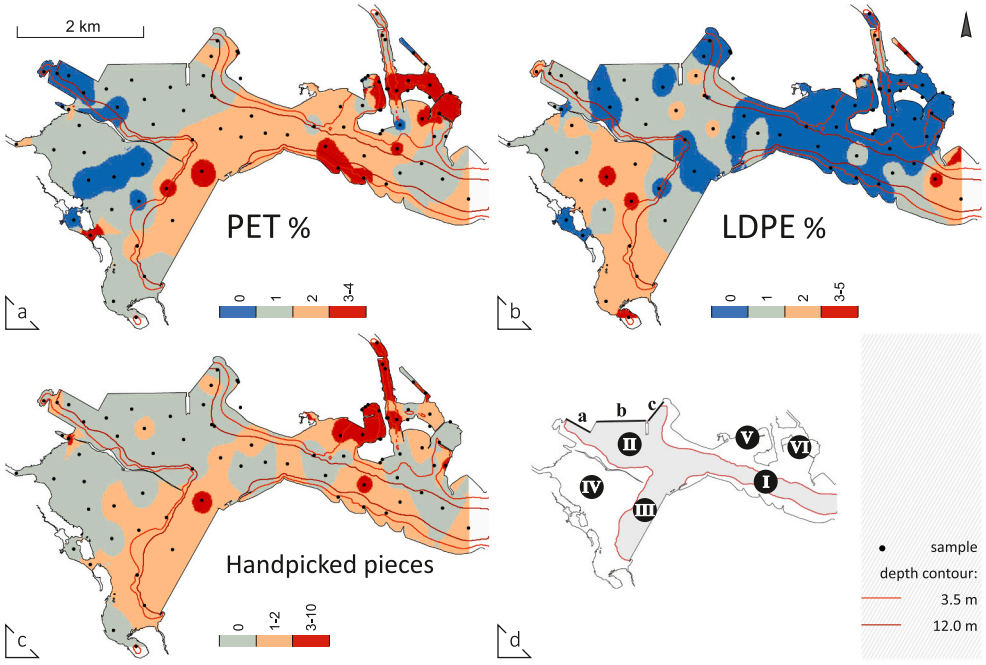


**Fig. 11.** Distribution maps of FTIRS spectroscopy inferred a) PET%, b) LDPE% and c) handpicked plastic pieces, interpolated by inverse distance weighting. Handpicked pieces refer to a categorical system (numbers identify pieces found; adopted from Schell, 2019). d) Sub-basin nomenclature.

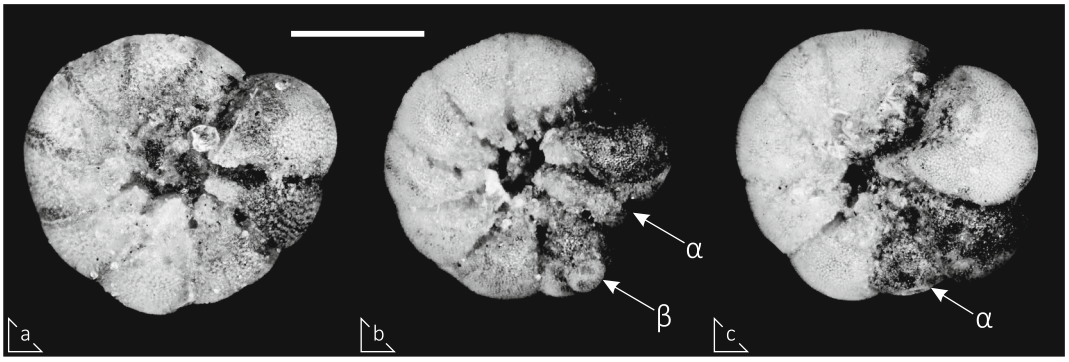


**Fig. 12.** Umbilical views of a) normal and b), c) malformed tests of Ammonia sp. from sample TR18-62, Richards Bay. The arrows point to malformation features such as dwarf chambers (α) or an accessory chamber (β). Scale bar = 200 μm.


**Fig. 13.** Left: Historical aerial image of Richards Bay Harbour during construction (© Klaus Jost – jostimages.com). Intensive sand (light brownish areas) relocation occurred during construction. The majority of sand features were temporary and do not exist today. Note that North is to the right. Right: Resuspension of surface sediment via berthing procedures at SB-II (source Google Earth). Sediment clouds – caused by propellers near to the seafloor – are often visible on aerial images.

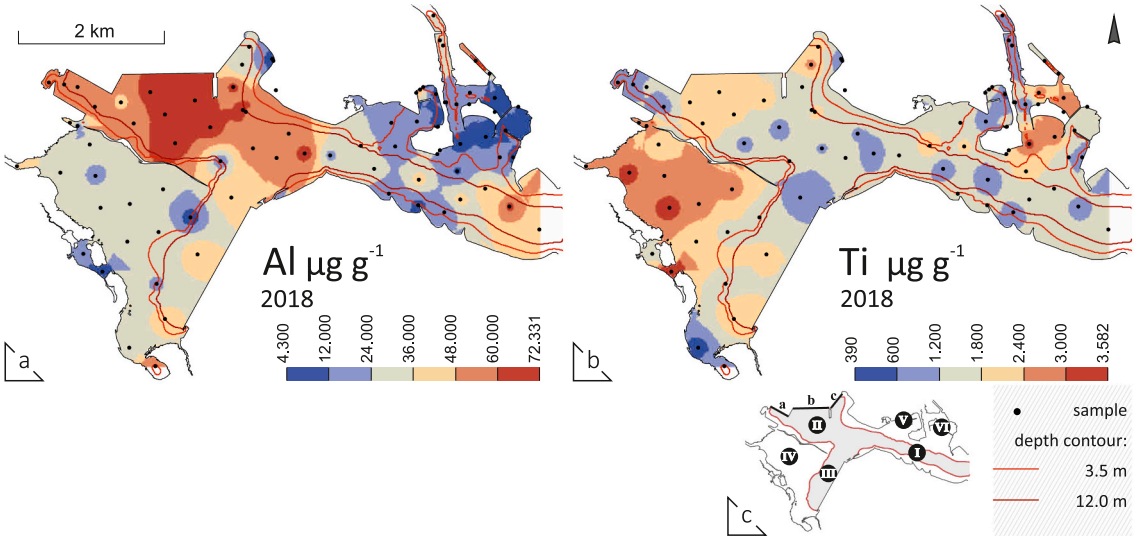


**Fig. 14.** Spatial distribution maps of a) Al and b) Ti, interpolated with inverse distance weighting. The elemental concentrations indicate a strong difference in accumulation patterns. c) Sub-basin nomenclature.

**Table 3**
Mean, Standard Deviation, minimum and maximum concentrations (µg $g^{-1}$, dry weight) for bulk sediments sampled in 2012 (analytical methods are indexed below element symbol: MS = ICP-MS, OES = ICP-OES). Guideline levels are given according to the Department of Environmental Affairs (2012b).

| 2012 | Al | As | Ca | Cd | Co | Cr | Cu | Fe | K | Mg | Mn | Na | Ni | P | Pb | S | Sr | Ti | Zn | Rb |
|---|---|---|---|---|---|---|---|---|---|---|---|---|---|---|---|---|---|---|---|---|
| | OES | MS | | MS | MS | MS | MS | OES | | | OES | OES | MS | | MS | | | | MS | |
| Min | 4665 | 1 | – | 0.0 | 2 | 14 | 4 | 3959 | – | – | 76 | – | 2 | – | 2 | – | – | – | 8 | – |
| Max | 53219 | 22 | – | 8.9 | 95 | 557 | 2016 | 55657 | – | – | 4746 | – | 1836 | – | 639 | – | – | – | 605 | – |
| Mean | 31494 | 9 | – | 0.4 | 14 | 143 | 117 | 30884 | – | – | 506 | – | 64 | – | 22 | – | – | – | 94 | – |
| SD | 13052 | 5 | – | 1.2 | 10 | 110 | 256 | 13772 | – | – | 489 | – | 186 | – | 64 | – | – | – | 87 | – |
| Warning Level | | 42 | | 1.2 | | 135/250 | 110 | | | | | | 62/88 | | 110 | | | | 270 | |
| Level I | | 57 | | 5.1 | | 260 | 230 | | | | | | 140 | | 218 | | | | 410 | |
| Level II | | 93 | | 9.6 | | 370 | 390 | | | | | | 370 | | 530 | | | | 960 | |

Ostracoda showed a general low diversity, and in particular *Ammonia* sp. showed malformations (Fig. 12) with an FAI of 4.2% and 5.1% for these two positions, respectively.

Sample #72 contained an abundant and well preserved diatom flora and a low to moderate number of calcareous microfauna, dominated by ostracods (Table 4). Similarly, sample #4 showed a low diversity of calcareous microfossils, a clear dominance of ostracods, and a very high FAI. Calcareous microfauna in sample #39 were virtually non-existent.

Within SB-IV, sample #47 showed a very high FAI (based on low counts) and a clear dominance of ostracods. Sample #50 showed the highest abundance of calcareous microfauna, with a slightly elevated FAI and ostracod dominance (Table 4). Sample #33 yield a well-preserved, rich diatom flora, while Ostracoda and Foraminifera showed a low abundance but a high diversity and the lowest FAI of the dataset (Table 4).

**Table 4**
Bioindicator data from RBH in 2018. Values in bold point to ecological stress; brackets are based on low counts. FAI = Foraminifer Abnormality Index; n.a. = not applicable. SB = sub-basin. Cr concentration is provided for comparison.

| Sample TR18- | Cr [μg g$^{-1}$] | Diatoms | | Foraminifera and Ostracoda | | | | SB |
|---|---|---|---|---|---|---|---|---|
| | | Number of species | Abundance and preservation | Abundance [spec./100 ml] | Diversity (Shannon H') | Ostracoda [%] | FAI [%] | |
| 4 | 185 | 68 | Good | 520 | **0.7** | **96** | **9.1** | V |
| 33 | 98 | 58 | Good | **118** | 1.9 | 5.3 | 0 | I |
| 39 | 233 | 78 | Good | **1** | **n.a.** | **n.a.** | n.a. | III |
| 47 | 197 | – | Good | 382 | 1 | **96.7** | **[33.3]** | IV |
| 50 | 140 | 65 | Good | 5729 | 1.4 | **60.4** | 2.1 | IV |
| 62 | 969 | **33** | **Poor** | **294** | **0.8** | 16.3 | **5.1** | II-c |
| 64 | 435 | **37** | **Poor** | 598 | 1.6 | **58** | **4.2** | II-a |
| 72 | 428 | – | Good | **255** | 1.1 | **75.8** | n.a. | II |

## 4. Interpretation

### 4.1. Sediment dynamics

Similar to mean grain-size, EM1 to EM4 indicate an increase in grain-size with a decrease in water depth. A distinct gap between mode positions of EM1 (7.1φ; fine silt) and EM2 (3.6φ, very fine sand) emphasizes a strict boundary between the two accommodation spaces (Fig. 5b). This is associated with the most prominent effect of dredging operations – the maintained steep depth gradient. Further, reoccurring dredging operations remove surficial sediments. However, the clustering of samples with a dominating end-member score (>50 vol%) in distinct areas and water depths of RBH indicates a non-random depositional pattern (Fig. 5). Therefore, we assume a stable accumulation space during the time of sampling. A second mode in the grain-size distribution curve of EM1 (Fig. 5b, also apparent in EM2 and EM3) represents an input of clastic material from a separate source. Marine operations, including traffic and propeller-induced sediment suspension (Fig. 13), probably affect the redistribution of sediment (end-members). EM2, outside of SB-IV, is process related and indicates downslope fining along fairways. EM4 represents tide-influenced shallow water conditions. This is in agreement with previous observations in which the sedimentary load deposited in coastal areas reflected a strong influence of longshore transport of beach sands, especially those deposited at the harbour entrance (Schoonees et al., 2006).

The predominance of EM4 in SB-VI, which is coupled to the occurrence of sand within the harbour sediments, might be related to intensive sand relocation during the construction phase of the harbour, which can be observed in historical aerial images (Fig. 13). At that time, construction material (according to our results probably mainly sand) was dumped to the north of the harbour entrance directly adjacent to SB-V and VI.

### 4.2. Al and Ti

Commonly used minerogenic input indicators are Al (Haberzettl et al., 2019; Strobel et al., 2019; Wündsch et al., 2016) and Ti (Haberzettl et al., 2009; Haberzettl et al., 2005; Kasper et al., 2012) (Fig. 14). The low correlation between Al and Ti is surprising at first, but can be explained by the surrounding geology. Ti is a major component of surrounding dune sands, which contain large amounts of heavy minerals and are mined nearby for ilmenite, rutile and zircon (Williams and Steenkamp, 2006). Density differences in minerals containing Ti and Al likely result in different transport and deposition processes. The highest Al concentrations were found in deeper water of SB-I, II and III. Ti was observed in higher-energy shallow water areas (Fig. 14b). As most other elements correlate positively to Al, we expect their distribution to depend on grain-size and the respective hydrodynamic regime in which they are deposited. This relationship between the spatial distribution of trace metals and grain-size has been often recognized (Förstner and Wittmann, 1981) and has been observed in comparable studies (Haberzettl et al., 2019; Haberzettl et al., 2010; Ohlendorf et al., 2014).

### 4.3. Cr and magnetic susceptibility distribution

Magnetic susceptibility is influenced by various factors, such as different mineralogical compositions, concentrations of magnetic minerals, and their magnetic grain-size and morphology (Ellwood et al., 2007; Haberzettl, 2015; Hatfield et al., 2013; Lisé-Pronovost et al., 2013). RBH has a low underlying magnetic susceptibility pattern that relates to a marine influence, which is larger at the harbour entrance. Marine sediments are usually enriched in diamagnetic minerals such as carbonates, and hence yield lower magnetic susceptibility values. The distinct increase in the magnitude of magnetic susceptibility and Cr concentration, which itself has a strong positive susceptibility (Dearing, 1994), in SB-II (front of the bulk goods terminals) indicates an additional input of Cr. This is likely associated with a point source rather than a hydrodynamic distribution.

### 4.4. Temporal pollution variations in sediment cores

The lowest Cu and Cr concentrations and magnetic susceptibility values in the lowermost part (lower part of unit I) of sediment cores RBH18-12 and RBH18-23 are assumed to reflect natural background conditions. The spike in the Cu concentration in the upper part of unit I in core RBH18-12, which is continued in the lower part of unit III (Fig. 9), indicates an additional, probably anthropogenic, Cu contribution.

We hypothesize that unit II of sediment core RBH18-12 consists of reworked material due to the distinctly different characteristics seen in all parameters (Fig. 9). Dredging activities might have caused a disturbance or reworked material. The susceptibility (and Cr and Cu concentration) is identical to lower unit III, and therefore comparable to the assumed background concentrations for the sediment characteristic of this core.

Progressively decreasing concentrations in the upper 40 cm reflect a decrease in Cu deposition towards the present time. At the same time, Cr and magnetic susceptibility increased in the recent past. Excluding the hypothesized reworked sediments of unit II, this spike in the Cu concentration and the increasing Cr concentration in sediment core RBH18-12 accords with the history of products exported through RBH. Copper ore was exported through the port until 2012. The abrupt increase in Cu concentrations (Fig. 9) in core RBH18-12 at around 100 cm sediment depth might indicate the onset of Cu ore export. Correspondingly, the return to lower levels at about 30 cm could represent the end of Cu export. However, Cu concentrations have not returned to background concentrations, probably reflecting residual contamination (Fig. 9). Comparing spatial distributions of Cu from 2012 to 2018 (Fig. 7), a decreasing trend is evident and the mean Cu concentration (Table 3) was about a third lower in 2018.

**Table 5**
Sediment quality guideline quotients (min, max and median) for individual metals, and the mean sediment quality guideline quotient for sediment sampled in the Port of Richards Bay in 2012 and 2018.

| | As | Cd | Cu | Cr | Ni | Pb | Zn | Mean quotient |
|---|---|---|---|---|---|---|---|---|
| 2012 | | | | | | | | |
| Minimum | 0.01 | 0 | 0.01 | 0.04 | 0.01 | 0 | 0.01 | 0.01 |
| Median | 0.09 | 0 | 0.09 | 0.33 | 0.1 | 0.03 | 0.08 | 0.11 |
| Maximum | 0.24 | 0.92 | 5.17 | 1.5 | 4.96 | 1.21 | 0.63 | 1.69 |
| 2018 | | | | | | | | |
| Minimum | 0.03 | 0 | 0 | 0.03 | 0.01 | 0 | 0.01 | 0.01 |
| Median | 0.15 | 0 | 0.05 | 0.32 | 0.07 | 0.02 | 0.07 | 0.12 |
| Maximum | 0.7 | 0.16 | 0.91 | 2.62 | 0.22 | 0.09 | 0.29 | 0.47 |

In contrast, Cr ore and ferrochrome are currently exported in high volumes through the harbour. The ore and ferrochrome are temporarily stored at open-air sites. Continuously increasing Cr concentrations in unit III (Fig. 9) possibly mirror increasing export volumes at the bulk goods terminal. Spillage during loading or strong winds could explain localized high Cr concentrations that decrease with distance from the source (bulk goods terminal). During the 2012 field campaign, ferrochrome nuggets were found in sediment samples collected in SB-IIb (Fig. 15).

The positive correlation between Cr concentration and $\chi_{LF}$ in RBH surface sediments and between Cr counts and $\kappa_{LF}$ in cores RBH18-12 and -23 allows the use of magnetic susceptibility ($\kappa_{LF}$) – measured on all cores – as a measure of Cr contamination in the cores (Fig. 10). The decreasing intensity in magnetic susceptibility in the sediment core transect RBH18-11 to -14 (Fig. 10) (especially at the upmost core-sediment) is similar to the modern surface distribution of Cr (Fig. 7), which indicates a decreasing trend with distance from the pollution source.

SB-IV is a restricted access area and in a more natural state (cf., bioindication). However, industrial runoff – linked to aluminium smelters and a fertilizer- and phosphoric acid plant in the surrounding – that enters upstream of Bhizolo Canal (cf., Fig. 1 for location) is responsible for contamination (Wepener and Vermeulen, 2005). While this might indeed be an explanation, we additionally recognize a similarity in the sediment cores – RBH18-12 and -23 – both showing an increased Cr content and susceptibility towards present sediment (Fig. 9). Therefore, we hypothesize a redistribution of fine particles by tidal currents, wind forcing or vessel propeller wash (Fig. 13) from SB-II via a small passage (Fig. 3) in the northeast of SB-IV and a distribution across SB-III during incoming tides.

### 4.5. Microplastics

The highest concentrations of PET or handpicked plastic pieces >1 mm were in sediment in public parts of RBH, especially at a beach in SB-VI. Recreational use of these beaches is high, particularly in summer, and the PET accumulation undoubtedly reflects plastic litter entering the harbour. Handpicked microplastic pieces were located predominantly in the Small Craft Harbour (restaurant and business area, and a popular bathing beach) of SB-V and along private jetties in Mzingazi Canal. Despite a slight difference in distribution patterns, PET and handpicked microplastic pieces show a clear link to areas of pronounced human use in the harbour.

Due to the high density of PET (1.33–1.41 g $cm^{-1}$; Fath, 2019) relative to seawater (~1.02 g $cm^{-1}$; Nayar et al., 2016; Sharqawy et al., 2010), PET particles likely sink to the bottom (Bellasi et al., 2020; Fath, 2019). Additionally, the density of PET enables preferential deposition within higher energy areas, explaining correlations to EM4 and medium sand. Lower energy transportation processes reduce the occurrence of PET and plastic pieces >1 mm towards inner basins of RBH (SB-IIa-c, SB-IV). However, PET particles still accumulate in lower energy, deep water areas that are affected by tidal currents and marine traffic induced currents and turbulence (Fig. 13).

Due to the density difference to seawater, Low Density Polyethylene (LDPE; 0.88–0.98 g $cm^{-1}$; Fath, 2019) has a tendency to float (Corcoran, 2015). Thus, current mediated transport occurs over a wider area, leading to LDPE accumulation in remote areas such as in SB-IIa, and at sites #4, #39 and #50 (Figs. 11, 2). To meet settling conditions certain factors are necessary (Bellasi et al., 2020; Corcoran, 2015; Fath, 2019), with biofouling being a compelling process. Based on the higher LDPE appearance in isolated basins (e.g. SB-IV, sites #39 and #50), isolated calm water conditions should also be preferential for deposition. The marine fairways were almost LDPE-free. LDPE appears mainly in the SW part of the harbour in SB-IV, and possibly relates to the main wind directions NE-SW (Begg, 1978). Surface waters would carry LDPE from their possible source (SB-V, VI) towards the SW. However, once settled, opposing wind turbulences towards NE will not redistribute the same amount. In addition, PET and handpicked remains preferentially occur in SW SB-III, which also underlines the influence of the prevailing wind from the NE.

Simultaneously, the individual distribution patterns of PET and LDPE indicate effects of hydrodynamic control in close relation to their density and resulting accumulation space. Reorganization of particles due to the prevailing wind direction, tidal currents and marine traffic-induced turbidity are considered plausible.

### 4.6. Bioindication

We used three taxonomic groups (diatoms, foraminifers and ostracods) as bioindicators to focus on effects of detected metal contamination in selected samples. This shortened approach is a reconnaissance study to test the abundance, species diversity, relative proportion of ostracods, and malformations in foraminifer tests. It is noteworthy that, according to our study, metal contamination, and especially Cr and Cu, enters RBH in the residual fraction, which is known to be less bioavailable (Sah et al., 2019). Based on investigations of all three groups we conclude that an increased level of metal contamination has adverse effects on the selected taxa, but affects them at a group level to different degrees and lowers the diversity in favour of opportunistic species. Hereby, diatoms and foraminifers seem to be more affected than ostracods. Generally, ostracods show higher abundances at severely metal contaminated sites, such as #47, #62 and #64. Ostracoda seem to have a greater physiological tolerance to elevated metal concentrations (Millward et al., 2004) and therefore dominate the calcareous microfauna under these conditions.

We interpret the moderate representation of opportunistic species at sites #47, #64 and #72 as a relatively recent pollution event. Additionally, the strong appearance of the diatom taxon *Fragilaria tenera* at site #72 is indicative of an incipient contamination event (Cattaneo et al., 2004). The highly fragmented nature and low concentrations of diatoms at site #62, correlating to the Cd warning level, may be evidence of negative effects of the metal on photosynthesis, resulting in reduced primary productivity and thus reproduction (Marshall and Mellinger, 1980).

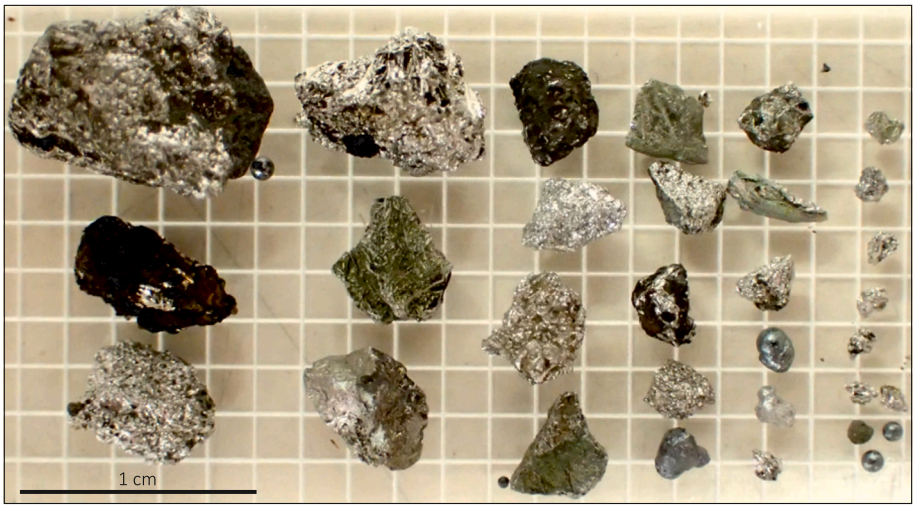


**Fig. 15.** Assorted ferrochrome particles of various sizes (gravel to fine sand) from 2012 survey samples collected in SB-IIb.

Ostracod proportions and FAI at the entrance to the Bhizolo Canal (site #47) appear very high, suggesting metal pollution. The rise in metal pollution at site #47 introduces diatom species, such as *Navicula salinicola*, that have been shown to propagate under increased metal and nutrient concentrations (Belando et al., 2017), while *Halamphora coffeaeformis*, which reaches its greatest representation at this site, is known to be tolerant of increased concentrations of metals such as zinc (Nguyen-Deroche et al., 2012).

The relatively low level of anthropogenic disturbance is seen at site #50 in SB-IV, which is separated by a sand barrier and thus more distal to pollution sources in SB-II (Figs. 2, 7). The highest diversity of calcareous microfossils at site #33 is likely due to the strong marine influence and also the least contaminated area relative to pollutants measured in our study. Frequent sediment reworking by tidal currents and vessel passage may also explain the low abundance of species. This hydrodynamic setting at site #33 can be inferred from the diatom community, which has a greater proportion of brackish-marine tycoplanktonics responding to high-energy coastal processes (Kirsten et al., 2018).

## 5. Discussion

### 5.1. Comparison of elemental distribution to guidelines

The South African Department of Environmental Affairs uses a National Action List to screen sediment identified for dredging in South African ports (Department of Environmental Affairs, 2012b). There are three guidelines for various metals: The Warning Level indicates an early stage of contamination, but is not used for decision-making. Action Level I and Level II are used for decision-making. Based on these guidelines, we highlight concentration thresholds of As, Cd, Cr, Cu, Ni and Zn (Figs. 6 and 7). The As concentrations exceed Action Level I in the middle harbour area, while the Cr and Cu concentration exceed Level I and Level II. The highest Cr and Cu concentrations in RBH exceed the Level I by a factor of >3.5 (968 μg $g^{-1}$ vs 260 μg $g^{-1}$) and >1.5 (353 μg $g^{-1}$ vs 230 μg $g^{-1}$), respectively (Fig. 7, Table 2). The mean Cr concentration in sediment near the terminal in SB-II is alarmingly high, at 351 μg $g^{-1}$, and in 42% of samples here exceed Level II. The Cr concentration in 45% of samples collected in 2018 (Fig. 7) was above the Warning Level (Cr > 135 μg $g^{-1}$), providing an aerial coverage of about 6.5 $km^2$. Additionally, the onset of increasing magnetic susceptibility (which correlates positively with Cr, Fig. 8) within the sediment core transects (Fig. 10) shows significant contamination in the top 30 cm of sediment. This results in an estimated volume of 1,950,000 $m^3$ of sediment with an elevated Cr concentration in RBH, which should be considered in future dredging operations and sediment disposal at the open water disposal site in the Indian Ocean.

### 5.2. Ecotoxicological implications

The ecological risk posed by As, Cd, Cr, Cu, Ni, Pb and Zn in sediment can be estimated using the sediment quality guideline quotient (SQGQ) approach (Long et al., 2006). The concentrations of these metals are divided by the Level II of the sediment quality guidelines defined by the Department of Environmental Affairs (2012b). For several of the metals these sediment quality guidelines are similar to the Effects Range Median (ERM) of the sediment quality guidelines derived by Long et al. (1995). As a further estimate of the risk for multiple metals in sediment, the mean sediment quality guideline quotient (mSQGQ) was calculated as the mean of the quotients for individual metals in each sediment sample.

The mSQGQ for surface sediment sampled in 2012 ranges from 0.01–1.69 (Table 5), indicating a risk of toxicity by metals in some samples. However, the median mSQGQ value of 0.11 shows a low risk of toxicity at most samples. Quotients >0.5 are exclusively for sediment in SB-II, near terminal operations. The highest individual SQGQs indicate severe contamination for Cu, Ni and Cr, at 5.17, 4.96 and 1.50 respectively. The mSQGQ for sediment sampled in 2018 ranges from 0.01–0.47 (Table 5), with a median of 0.12. The highest SQGQs, as for the 2012 survey, were calculated for sediment sampled in SB-II, at 0.91 and 2.62 for Cu and Cr respectively.

### 5.3. Comparison to earlier studies

In this section, we make use of and compare absolute maximum values from different surveys to metal concentrations in surface sediment in our study from RBH, noting that the strong dependence between elemental concentrations and grain-size distributions detracts somewhat from such comparisons.

A summary of concentration ranges for Al, Cu, Cr, Fe, Mn and Zn in studies dating back to 1976 is compiled in Wepener and Vermeulen (2005), indicating lowest Cu and Cr concentrations in sediment of 40 μg $g^{-1}$ (Cloete, 1979) and 74.8 μg $g^{-1}$ (Oliff and Turner, 1976), respectively in 1976 surveys. During their 1996–1997 survey's, Wepener and Vermeulen (2005) indicate an increase in concentrations: maximum concentrations for Cu (53.5 μg $g^{-1}$) and Cr (221.9 μg $g^{-1}$). These are already above present guidelines (Department of Environmental Affairs, 2012b) and are further exceeded in samples collected in 2012 (Cu 2016 μg $g^{-1}$;

Cr 557 μg $g^{-1}$) and 2018 (Cu 353 μg $g^{-1}$; Cr 969 μg $g^{-1}$).

Greenfield et al. (2011) and Wepener and Degger (2020) identified increased metal concentrations in the tissue of mussels (*Perna perna*) from buoys near Naval Island in 2008 and 2009. Compared to 2008, mussels of the 2009 survey show a decrease in Cu and an increase in Cr concentrations. This change, over the course of one year, is similar to anomalies in the sediment core XRF data, where a decreasing trend of Cu is accompanied by an increase in Cr (Fig. 7).

Wepener and Vermeulen (2005) relate temporal spikes in metal concentrations to activities like dredging, which cause a disturbance in oxic and anoxic conditions. However, the spatial distribution patterns in 2012 and 2018 indicate point sources on globally dredged surface sediment and cores RBH18-12 and -23 confirm the constant deposition of metals in sediment.

### 5.4. Regional comparison

In order to set the results in a regional context, we compare the results for RBH to ports in East London and Port Elizabeth in South Africa as presented in Fatoki and Mathabatha (2004). Maximum Pb concentrations in all three ports are below Warning Levels (Department of Environmental Affairs, 2012b), at 82.2 μg $g^{-1}$ in East London, 61.9 μg $g^{-1}$ in Port Elizabeth, and 48.8 μg $g^{-1}$ in RBH. Maximum Zn concentrations in East London (332 μg $g^{-1}$) and RBH (274.2 μg $g^{-1}$) were above, and in Port Elizabeth (126 μg $g^{-1}$) below the Warning Level. Maximum Cd concentrations surpass the Warning Level in all ports (Port Elizabeth 1.4 μg $g^{-1}$, RBH 1.5 μg $g^{-1}$, East London 1.63 μg $g^{-1}$).

In contrast, maximum Cu concentrations in RBH are twice as high compared to East London and four times higher than in Port Elizabeth (RBH: 353.4 μg $g^{-1}$, East London: 183 μg $g^{-1}$, Port Elizabeth: 92.5 μg $g^{-1}$; Fatoki and Mathabatha, 2004). Fatoki and Mathabatha (2004) present site-specific annual mean Cu concentrations in sediments at the Port Elizabeth Cruise Terminal and East London motor vehicle berth of 68.5 μg $g^{-1}$ and 106 μg $g^{-1}$ Cu, respectively. The mean Cu concentration of 88.6 μg $g^{-1}$ at RBH dry and breakbulk berths (SB-II) compares well to these findings. In this regard, local similarities, like surrounding industrial runoff and marine operations (ship maintenance), are likely the main contributors for elevated Cu concentrations at all three sites.

Birch et al. (2020) recently assessed sediment metal enrichment in ten ports and estuaries in the World Harbours Project. Concentrations found in RBH for Cr and Cu differ considerably to those reported by Birch et al. (2020). Cr concentrations in RBH exceed concentrations reported for sites by Birch et al. (2020) by a factor of 3.1 (overall harbour mean: 54 μg $g^{-1}$ and overall maximum 316 μg $g^{-1}$, Table 2). Mean Cu concentrations in RBH are below the average of 51 μg $g^{-1}$ (Birch et al., 2020), but maximum Cu concentrations in RBH (353 μg $g^{-1}$) are above the average maximum of 237 μg $g^{-1}$, thus indicating a wide span of concentrations in RBH that emphasize the point-source nature of Cu within RBH.

Similar to the current study, a high correlation between magnetic susceptibility and metals at harbour terminals was observed in Hong Kong Harbour (Chan et al., 2001; Yim et al., 2004), which was related to general shipping contamination. However, the strong Cr component, as found in RBH, was not determined in these studies.

### 5.5. Microplastics

The occurrence of microplastics is closely related to the magnitude of anthropogenic activity (population density and proximity; Bellasi et al., 2020). Bellasi et al. (2020) attribute common input sources for lakes and rivers to tributaries, on-water activities, tourism or improper dumping. In our study, the dependence on public areas is clearly reflected in the given PET concentration and distribution of handpicked plastic pieces (Fig. 11).

### 5.6. Bioindicators

Although no bioindication was mentioned in their study, Wepener and Degger (2020) showed an uptake of heavy metals in mussels from the open water column (buoys at RBH entrance channel) and thus demonstrated bioavailability of contaminants in RBH. It also indicates that Cr and Cu, although loaded as particulate matter that is believed to sink rapidly to the bottom, is in suspension long enough to be taken up by filter feeders. However, lower vulnerability was observed in ostracods in similar metal contaminated environments (Millward et al., 2004). It is reported that high metal concentrations in marine environments lead to increase in malformation rates in foraminifera, but these can also be triggered by strong salinity variation or oxygen deficiency (e.g. Frontalini and Coccioni, 2008; Geslin et al., 2000; Stouff et al., 1999). Based on our observations and in accordance with Yanko et al. (1998), increased metal concentrations reduced the abundance and diversity of calcareous microfauna and diatom flora in RBH.

The prevalence of metal contaminants in RBH is clearly observable and as a primary response, the autochthonous diatom community is composed of species that are adapted to tolerate critical to very heavy levels of pollution. In the current sample set, teratological forms do not occur to any significant level. This may be due timing between sampling and the most recent pollution event, with diatom community turnover already having been initiated. On a secondary level, diatom composition is responding to osmotic pressure variability brought about by environmental pressures (Taylor et al., 2007), such as salinity, and tidal currents. In summary, we strongly encourage a more detailed systematic study to elaborate the effective bioavailability to organisms including invertebrates and vertebrates. This does not only allow the development of a more detailed bioindication system, but also allows to evaluate a warning level of sea food collected in the harbour by local residents.

## 6. Conclusions

RBH is strongly impacted by anthropogenic activities. Sources of metals and plastic in sediment are clearly identified. Hydrodynamic processes, influenced by wind, tides, and vessel propeller wash, affect microplastic accumulation, sediment distribution, and associated elemental concentrations. Microplastic pollution is recognizable throughout publicly accessible parts of RBH (i.e. PET).

The zonation of RBH via endmember modelling defines distinct subbasins. Cu and Cr show very high concentrations in SB-II – the main operational basin with dry and breakbulk berths for import and export. Consequently, the bulk terminals (SB-II a-c; with increased Cr, Cu, Cd and Ni concentrations) and Small Craft Harbour (Cr, Cu) were identified as metal point sources. The metal pollution results in high malformation rates in foraminifera, and high proportions of ostracods within the calcareous microfauna at stations with highest metal concentrations. Diatoms are adversely affected by the high levels of contaminants in the harbour basin, to the extent of zones of low productivity and occurrences.

Cr and Cu concentrations in surface sediments from 2012 and 2018, as well as short sediment cores (recovered in 2018) mirror the pollution history, with increasing Cr concentrations towards the present time, preceded by a spike of Cu. Additionally, through correlating Cr concentrations and magnetic susceptibility, multiple cores reflect on spatial and historical metal pollution. This enables to quantify the load of metal (Cr) polluted sediment to an estimated volume of almost 2 million $m^3$.

The maximum Cr concentration measured in 2018 in RBH is about three times higher than the concentration recently reported for international ports. Consequently, metal contamination in RBH poses a potential environmental threat to the adjacent marine ecosystem by sediment resuspension and remobilization of accumulated metals, and by the dredging related transfer of contaminated dredged sediment to open water placement sites. However, it remains to be confirmed if metals such as Cr are present in the sediment in a bioavailable form

considering chromium ore and ferrochrome particles probably account for the high concentrations of this metal in sediment in RBH.

## CRediT authorship contribution statement

**Paul Mehlhorn:** Conceptualization, Investigation, Formal analysis, Writing – original draft, Writing – review & editing. **Finn Viehberg:** Conceptualization, Validation, Writing – original draft, Writing – review & editing, Funding acquisition. **Kelly Kirsten:** Investigation, Writing – original draft. **Brent Newman:** Investigation, Formal analysis, Writing – original draft, Writing – review & editing, Funding acquisition. **Peter Frenzel:** Investigation, Writing – original draft, Funding acquisition. **Olga Gildeeva:** Investigation, Writing – original draft. **Andrew Green:** Investigation, Visualization, Writing – original draft. **Annette Hahn:** Investigation, Writing – original draft. **Torsten Haberzettl:** Conceptualization, Writing – original draft, Supervision, Funding acquisition, Writing – review & editing, Project administration.

## Declaration of competing interest

The authors declare that they have no known competing financial interests or personal relationships that could have appeared to influence the work reported in this paper.

## Acknowledgements

This work was supported by the German Federal Ministry of Education and Research [grant numbers: 03F0798A, 03F0798B, 03F0798C] and is part of project TRACES (Tracing Human and Climate impact in South Africa) within the SPACES II Program (Science Partnerships for the Assessment of Complex Earth System Processes). The field work support by George Best is gratefully acknowledged. We acknowledge Anchor Energy (Pty) Ltd. for permission to use the multibeam data set. Doug Slogrove and Gaynor Deacon are acknowledged in this regard. We thank Transnet National Ports Authority for permission to use metal concentration data for the 2012 survey. The 2012 survey was funded by Transnet National Ports Authority and the CSIR through project Definition of baseline metal concentration models for assessing metal contamination of sediment from South African coastal waters (grant number: SIMS4401). We also thank Antonia Schell for semi-quantitative distribution data of plastic particles and Dirk Merten (both Friedrich-Schiller-University Jena) for ICP-MS and -OES analyses. Tammo Meyer (University of Greifswald) shared knowledge and equipment for aqua regia digestion. The cores were scanned with the ITRAX (CS-8) of GEOPOLAR at the University of Bremen. Klaus Jost kindly contributed the historical image of Richards Bay Harbour during the construction phase. Mike Steinich and Sebastian Lorenz (University of Greifswald) are acknowledged for their integral involvement in data collection.

## References

Bate, G.C., Smailes, P.A., Adams, J.B., 2004. Benthic Diatoms in the Rivers and Estuaries of South Africa Water Research Commission report, 1107.

Begg, G., 1978. The estuaries of Natal: a resource inventory report to the Natal Town and Regional Planning Commission conducted under the auspices of the Oceanographic Research Institute, Durban. In: Natal Town and Regional Planning Report, 41, pp. 1–657.

Belando, M.D., Marín, A., Aboal, M., García-Fernández, A.J., Marín-Guirao, L., 2017. Combined in situ effects of metals and nutrients on marine biofilms: shifts in the diatom assemblage structure and biological traits. Sci. Total Environ. 574, 381–389. https://doi.org/10.1016/j.scitotenv.2016.08.197.

Bellasi, A., Binda, G., Pozzi, A., Galafassi, S., Volta, P., Bettinetti, R., 2020. Microplastic contamination in freshwater environments: a review, focusing on interactions with sediments and benthic organisms. Environments 7 (4), 30. https://doi.org/10.3390/environments7040030.

Benson, R.H., Maddocks, R.F., 1964. In: Recent Ostracods of Knysna Estuary, Cape Province, Union of South Africa, 5. The University of Kansas Paleontological Contributions, pp. 1–39.

Birch, G.F., Lee, J.-H., Tanner, E., Fortune, J., Munksgaard, N., Whitehead, J., Coughanowr, C., Agius, J., Chrispijn, J., Taylor, U., Wells, F., Bellas, J., Besada, V., Viñas, L., Soares-Gomes, A., Cordeiro, R.C., Machado, W., Santelli, R.E., Vaughan, M., Cameron, M., Brooks, P., Crowe, T., Ponti, M., Airoldi, L., Guerra, R., Puente, A., Gómez, A.G., Zhou, G.J., Leung, K.M.Y., Steinberg, P., 2020. Sediment metal enrichment and ecological risk assessment of ten ports and estuaries in the world harbours project. Mar. Pollut. Bull. 155, 111129 https://doi.org/10.1016/j.marpolbul.2020.111129.

Blott, S.J., Pye, K., 2001. GRADISTAT: a grain size distribution and statistics package for the analysis of unconsolidated sediments. Earth Surf. Process. Landforms 26 (11), 1237–1248. https://doi.org/10.1002/esp.261.

Cattaneo, A., Couillard, Y., Wunsam, S., Courcelles, M., 2004. Diatom taxonomic and morphological changes as indicators of metal pollution and recovery in Lac Dufault (Québec, Canada). J. Paleolimnol. 32 (2), 163–175. https://doi.org/10.1023/B:JOPL.0000029430.78278.a5.

Chan, L., Ng, S., Davis, A., Yim, W., Yeung, C., 2001. Magnetic properties and heavy-metal contents of contaminated seabed sediments of Penny's Bay, Hong Kong. Mar. Pollut. Bull. 42 (7), 569–583. https://doi.org/10.1016/S0025-326X(00)00203-4.

Cloete, C.E., 1979. The transfer of pollutants in two southern hemispheric oceanic systems. In: Proceedings of a Workshop Held at Plettenberg Bay, South Africa, 23–26 April 1975. South African Scientific Programmes Report No 39.

Cloete, C.E., Oliff, W.D., 1976. South African Marine Pollution Survey Report 1974-1975. National Scientific Programmes Unit: CSIR.

Corcoran, P.L., 2015. Benthic plastic debris in marine and fresh water environments. Environ. Sci. Process. Impacts 17 (8), 1363–1369. https://doi.org/10.1039/C5EM00188A.

Dearing, J., 1994. Environmental Magnetic Susceptibility. Using the Bartington MS2 System. Chi Publ, Kenilworth.

Department of Environmental Affairs, 2012a. 2nd South Africa Environment Outlook. A Report on the State of the Environment. Executive Summary. Department of environmental Affairs, Pretoria, 60 pp.

Department of Environmental Affairs, 2012b. In: National Environmental Management: Integrated Coastal Management Act, 2008 (Act No. 24 of 2008). National Action List for the Screening of Dredged Material Proposed for Marine Disposal in Term of Section 73 of the National Environmental Management: Integrated Coastal Management Act, 2008 (Act No. 24 of 2008). Government Gazette (35602), pp. 6–9.

Dietze, E., Dietze, M., 2019. Grain-size distribution unmixing using the R package EMMAgeo. E&G Quat. Sci. J. 68 (1), 29–46. https://doi.org/10.5194/egqsj-68-29-2019.

Dietze, E., Maussion, F., Ahlborn, M., Diekmann, B., Hartmann, K., Henkel, K., Kasper, T., Lockot, G., Opitz, S., Haberzettl, T., 2014. Sediment transport processes across the tibetan plateau inferred from robust grain-size end members in lake sediments. Clim. Past 10 (1), 91–106. https://doi.org/10.5194/cp-10-91-2014.

Dingle, R.V., 1992. Quaternary ostracods from the continental margin off South-Western Africa. Part I. Dominant taxa. Ann. S. Afr. Mus. 102, 1–89.

Dingle, R.V., 1993. Quaternary ostracods from the continental margin off South-Western Africa. Part II. Minor taxa. Ann. S. Afr. Mus. 103, 1–165.

Ellwood, B.B., Brett, C.E., MacDonald, W.D., 2007. Magnetostratigraphy susceptibility of the upper ordovician kope formation, northern Kentucky. Palaeogeogr. Palaeoclimatol. Palaeoecol. 243 (1–2), 42–54. https://doi.org/10.1016/j.palaeo.2006.07.003.

Fath, A., 2019. Mikroplastik. Springer, Berlin Heidelberg.

Fatoki, O.S., Mathabatha, S., 2004. An assessment of heavy metal pollution in the East London and Port Elizabeth harbours. WSA 27 (2). https://doi.org/10.4314/wsa.v27i2.4997.

Folk, R.L., Ward, W.C., 1957. Brazos River bar [Texas]; a study in the significance of grain size parameters. J. Sediment. Res. 27 (1), 3–26. https://doi.org/10.1306/74D70646-2B21-11D7-8648000102C1865D.

Förstner, U., Wittmann, G.T.W., 1981. Metal Pollution in the Aquatic Environment. Springer, Berlin Heidelberg.

Frontalini, F., Coccioni, R., 2008. Benthic foraminifera for heavy metal pollution monitoring: a case study from the Central Adriatic Sea coast of Italy. Estuar. Coast. Shelf Sci. 76 (2), 404–417. https://doi.org/10.1016/j.ecss.2007.07.024.

Fürstenberg, S., Gründler, N., Meschner, S., Frenzel, P., 2017. Microfossils in surface sediments of brackish waters on the west coast of South Africa and their palaeoecological implications. Afr. J. Aquat. Sci. 42 (4), 329–339. https://doi.org/10.2989/16085914.2017.1406326.

Geslin, E., Stouff, V., Debenay, J.-P., Lesourd, M., 2000. Environmental variation and foraminiferal test abnormalities. In: Landman, N.H., Jones, D.S., Martin, R.E. (Eds.), Environmental Micropaleontology, 15. Springer US, Boston, MA, pp. 191–215.

Goodenough, C.K., 2003. The Local Global Nexus: A Case Study of Richards Bay.

Greenfield, R., Wepener, V., Degger, N., Brink, K., 2011. Richards Bay harbour: metal exposure monitoring over the last 34 years. Mar. Pollut. Bull. 62 (8), 1926–1931. https://doi.org/10.1016/j.marpolbul.2011.04.026.

Haberzettl, T., 2015. Advances in limnogeology and paleolimnology: with a special focus on corroborated chronologies using paleomagnetic secular variations. Jena, Univ., Habil.-Schr., 2015. Friedrich-Schiller-Universität Jena. http://nbn-resolving.de/urn:nbn:de:gbv:27-20160107-133023-6.

Haberzettl, T., Fey, M., Lücke, A., Maidana, N.I., Mayr, C., Ohlendorf, C., Schäbitz, F., Schleser, G.H., Wille, M., Zolitschka, B., 2005. Climatically induced lake level changes during the last two millennia as reflected in sediments of Laguna Potrok Aike, southern Patagonia (Santa Cruz, Argentina). J. Paleolimnol. 33 (3), 283–302. https://doi.org/10.1007/s10933-004-5331-z.

Haberzettl, T., Anselmetti, F.S., Bowen, S.W., Fey, M., Mayr, C., Zolitschka, B., Ariztegui, D., Mauz, B., Ohlendorf, C., Kastner, S., Lücke, A., Schäbitz, F., Wille, M., 2009. Late pleistocene dust deposition in the patagonian steppe - extending and refining the paleoenvironmental and tephrochronological record from Laguna

potrok aike back to 55ka. Quat. Sci. Rev. 28 (25–26), 2927–2939. https://doi.org/10.1016/j.quascirev.2009.07.021.
Haberzettl, T., St-Onge, G., Lajeunesse, P., 2010. Multi-proxy records of environmental changes in Hudson Bay and strait since the final outburst flood of Lake Agassiz-Ojibway. Mar. Geol. 271 (1–2), 93–105. https://doi.org/10.1016/j.margeo.2010.01.014.
Haberzettl, T., Kirsten, K.L., Kasper, T., Franz, S., Reinwarth, B., Baade, J., Daut, G., Meadows, M.E., Su, Y., Mäusbacher, R., 2019. Using 210Pb-data and paleomagnetic secular variations to date anthropogenic impact on a lake system in the Western Cape, South Africa. Quat. Geochronol. 51, 53–63. https://doi.org/10.1016/j.quageo.2018.12.004.
Hahn, A., Gerdts, G., Völker, C., Niebühr, V., 2019. Using FTIRS as pre-screening method for detection of microplastic in bulk sediment samples. Sci. Total Environ. 689, 341–346. https://doi.org/10.1016/j.scitotenv.2019.06.227.
Hanson, P.J., Evans, D.W., Colby, D.R., Zdanowicz, V.S., 1993. Assessment of elemental contamination in estuarine and coastal environments based on geochemical and statistical modeling of sediments. Mar. Environ. Res. 36, 237–266. https://doi.org/10.1016/0141-1136(93)90091-D.
Hatfield, R.G., Stoner, J.S., Carlson, A.E., Reyes, A.V., Housen, B.A., 2013. Source as a controlling factor on the quality and interpretation of sediment magnetic records from the northern North Atlantic. Earth Planet. Sci. Lett. 368, 69–77. https://doi.org/10.1016/j.epsl.2013.03.001.
Kasper, T., Haberzettl, T., Doberschütz, S., Daut, G., Wang, J., Zhu, L., Nowaczyk, N., Mäusbacher, R., 2012. Indian Ocean summer monsoon (IOSM)-dynamics within the past 4 ka recorded in the sediments of Lake Nam Co, central Tibetan Plateau (China). Quat. Sci. Rev. 39, 73–85. https://doi.org/10.1016/j.quascirev.2012.02.011.
Kerste, M., Smedes, F., 2002. Normalization procedures for sediment contaminants in spatial and temporal trend monitoring. J. Environ. Monit. 4, 109–115. https://doi.org/10.1039/b108102k.
Kirsten, K.L., Fell, J., Frenzel, P., Meschner, S., Kasper, T., Wündsch, M., Meadows, M.E., Haberzettl, T., 2018. The spatial heterogeneity of micro- and meio-organisms and their significance in understanding coastal system dynamics. Estuar. Coast. Shelf Sci. 213, 98–107. https://doi.org/10.1016/j.ecss.2018.08.011.
Lisé-Pronovost, A., St-Onge, G., Gogorza, C., Haberzettl, T., Preda, M., Kliem, P., Francus, P., Zolitschka, B., 2013. High-resolution paleomagnetic secular variations and relative paleointensity since the Late Pleistocene in southern South America. Quat. Sci. Rev. 71, 91–108. https://doi.org/10.1016/j.quascirev.2012.05.012.
Long, E.R., Macdonald, D.D., Smith, S.L., Calder, F.D., 1995. Incidence of adverse biological effects within ranges of chemical concentrations in marine and estuarine sediments. Environ. Manag. 19, 81–97. https://doi.org/10.1007/BF02472006.
Long, E.R., Ingersoll, C.G., Macdonald, D.D., 2006. Calculation and uses of mean sediment quality guideline quotients: a critical review. Environ. Sci. Technol. 40, 1726–1736. https://doi.org/10.1021/es058012d.
Marshall, J.S., Mellinger, D.L., 1980. An in situ experimental method for toxicological studies on natural plankton communities. In: Eaton, J.G., Parrish, P.R., Hendricks, A. C. (Eds.), Aquatic Toxicology. ASTM International, 100 Barr Harbor Drive, PO Box C700, West Conshohocken, PA 19428-2959, pp. 27–39.
Millward, R.N., Carman, K.R., Fleeger, J.W., Gambrell, R.P., Portier, R., 2004. Mixtures of metals and hydrocarbons elicit complex responses by a benthic invertebrate community. J. Exp. Mar. Biol. Ecol. 310 (1), 115–130. https://doi.org/10.1016/j.jembe.2004.04.004.
Nayar, K.G., Sharqawy, M.H., Banchik, L.D., Lienhard, V., J.H., 2016. Thermophysical properties of seawater: a review and new correlations that include pressure dependence. Desalination 390, 1–24. https://doi.org/10.1016/j.desal.2016.02.024.
Newman, B.K., Watling, R.J., 2007. Definition of baseline metal concentrations for assessing metal enrichment of sediment from the south-eastern cape Coastline of South Africa. Water SA 33. https://doi.org/10.4314/wsa.v33i5.184089.
Nguyen-Deroche, T.L.N., Caruso, A., Le, T.T., Bui, T.V., Schoefs, B., Tremblin, G., Morant-Manceau, A., 2012. Zinc affects differently growth, photosynthesis, antioxidant enzyme activities and phytochelatin synthase expression of four marine diatoms. Sci. World J. 2012, 982957 https://doi.org/10.1100/2012/982957.
Ohlendorf, C., Fey, M., Massaferro, J., Haberzettl, T., Laprida, C., Lücke, A., Maidana, N. I., Mayr, C., Oehlerich, M., Ramón Mercau, J., Wille, M., Corbella, H., St-Onge, G., Schäbitz, F., Zolitschka, B., 2014. Late Holocene hydrology inferred from lacustrine sediments of Laguna Cháltel (southeastern Argentina). Palaeogeogr. Palaeoclimatol. Palaeoecol. 411, 229–248. https://doi.org/10.1016/j.palaeo.2014.06.030.
Oliff, W.D., Turner, W.D., 1976. In: National Marine Pollution Surveys, East Coast Section: 2nd Annual Report. NIWR, Durban, p. 172.
Parent, B., Barras, C., Jorissen, F., 2018. An optimised method to concentrate living (Rose Bengal-stained) benthic foraminifera from sandy sediments by high density liquids. Mar. Micropaleontol. 144, 1–13. https://doi.org/10.1016/j.marmicro.2018.07.003.
Sah, D., Verma, P.K., Kandikonda, M.K., Lakhani, A., 2019. Chemical fractionation, bioavailability, and health risks of heavy metals in fine particulate matter at a site in the Indo-Gangetic Plain, India. Environ. Sci. Pollut. Res. Int. 26 (19), 19749–19762. https://doi.org/10.1007/s11356-019-05144-8.
Schell, A.C., 2019. Makrofauna, Schalenchemie und Sedimentkomponenten als Indikatoren Anthropogener Einflüsse im Hafengebiet von Richards Bay. Südafrika, Jena.
Schoonees, J.S., Theron, A.K., Bevis, D., 2006. Shoreline accretion and sand transport at groynes inside the port of Richards Bay. Coast. Eng. 53 (12), 1045–1058. https://doi.org/10.1016/j.coastaleng.2006.06.006.
Schwab, R., Becker, W. (Eds.), 2014. 1983/84, 1st ed. Springer Berlin, Berlin.
Semensatto, D.L., Dias-Brito, D., 2007. Alternative saline solutions to float foraminiferal tests. J. Foraminifer. Res. 37 (3), 265–269. https://doi.org/10.2113/gsjfr.37.3.265.
Shannon, C.E., 1948. A mathematical theory of communication. Bell Syst. Tech. J. 27 (3), 379–423. https://doi.org/10.1002/j.1538-7305.1948.tb01338.x.
Sharqawy, M.H., Lienhard, J.H., Zubair, S.M., 2010. Thermophysical properties of seawater: a review of existing correlations and data. Desalin. Water Treat. 16 (1–3), 354–380. https://doi.org/10.5004/dwt.2010.1079.
Stouff, V., Geslin, E., Debenay, J.-P., Lesourd, M., 1999. Origin of morphological abnormalities in ammonia (Foraminifera): studies in laboratory and natural environments. J. Foraminifer. Res. 29 (2), 152–170. https://doi.org/10.2113/gsjfr.29.2.152.
Strobel, P., Kasper, T., Frenzel, P., Schittek, K., Quick, L.J., Meadows, M.E., Mäusbacher, R., Haberzettl, T., 2019. Late quaternary palaeoenvironmental change in the year-round rainfall zone of South Africa derived from peat sediments from vankervelsvlei. Quat. Sci. Rev. 218, 200–214. https://doi.org/10.1016/j.quascirev.2019.06.014.
Taylor, J.C., Harding, W.R., Archibald, C.G.M., 2007. An Illustrated Guide to Some Common Diatom Species From South Africa. Water Research Commission, Gezina, South Africa, 11 pp.
Vermeulen, L.A., Wepener, V., 1999. Spatial and temporal variations of metals in Richards Bay Harbour (RBH), South Africa. Mar. Pollut. Bull. 39 (1–12), 304–307. https://doi.org/10.1016/S0025-326X(99)00083-1.
Wepener, V., Degger, N., 2020. Monitoring metals in South African harbours between 2008 and 2009, using resident mussels as indicator organisms. Afr. Zool. 1–11 https://doi.org/10.1080/15627020.2020.1799720.
Wepener, V., Vermeulen, L.A., 2005. A note on the concentrations and bioavailability of selected metals in sediments of Richards Bay Harbour, South Africa. Water SA 31 (4), 589–596. https://doi.org/10.4314/wsa.v31i4.5149.
Whitfield, A.K., 1992. A characterization of southern african estuarine systems. South. Afr. J. Aquat. Sci. 18 (1–2), 89–103. https://doi.org/10.1080/10183469.1992.9631327.
Williams, G.E., Steenkamp, J.D., 2006. Heavy mineral processing at Richards bay minerals. South. Afr. Pyrometall. 2006, 181–188.
Wündsch, M., Haberzettl, T., Kirsten, K.L., Kasper, T., Zabel, M., Dietze, E., Baade, J., Daut, G., Meschner, S., Meadows, M.E., Mäusbacher, R., 2016. Sea level and climate change at the southern Cape coast, South Africa, during the past 4.2 kyr. Palaeogeogr. Palaeoclimatol. Palaeoecol. 446, 295–307. https://doi.org/10.1016/j.palaeo.2016.01.027.
Yanko, V., Muna, A., Kaminski, M., 1998. Morphological deformities of benthic foraminiferal tests in response to pollution by heavy metals; implications for pollution monitoring. J. Foraminifer. Res. 28 (3), 177–200.
Yim, W.-S., Huang, G., Chan, L.S., 2004. Magnetic susceptibility study of late quaternary inner continental shelf sediments in the Hong Kong SAR,China. Quat. Int. 117 (1), 41–54. https://doi.org/10.1016/S1040-6182(03)00115-0.

# Chapter 3

# Comparison of different normalisers for identifying metal enrichment of sediment – a case study from Richards Bay Harbour, South Africa

Paul Mehlhorn[a], Brent Newman[b,c], Torsten Haberzettl[a]

[a] University of Greifswald, Institute for Geography and Geology, F.L.-Jahn Str. 16, 17489 Greifswald, Germany

[b] Coastal Systems Research Group, CSIR, P.O. Box 59081, Umbilo, 4075 Durban, South Africa

[c] Nelson Mandela University, P.O. Box 77000, Port Elizabeth 6031, South Africa

State of publication: Accepted (8 February 2022) and soon to be published (2022). In: von Maltitz, G., Midgley, G., Veitch, J., Brümmer, C., Viehberg, F., Rötter, R., Veste, M. (Eds). Sustainability of southern African ecosystems under global change: Science for management and policy interventions. Springer, Heidelberg (This citation may be subject to change).

## Abstract

South Africa's ecosystems are challenged in various ways by anthropogenic effects, such as land-use change, leading to soil erosion in concert with industrial or agricultural pollution, leading to an increase in pollutants in final depositional systems. Here we focus on metals in the marine environment of Richards Bay Harbour. The use for Al, Fe, Rb, Ti and the silt fraction of the sediment as normalisers of Cr, Cu, Co and Pb concentrations in sediment is compared to determine if they provide the same understanding on the enrichment. Baseline metal concentration models were defined and Enrichment Factors calculated to quantify the magnitude of enrichment.

Exceedingly high Cr and Cu concentrations in defined parts of the harbour lead to similar trends rather than a similar effectiveness of the normalisers. Probable biogeochemical processes hinder the effectiveness of Fe and geological background or hydrodynamic properties hinder the effectiveness of Ti as normaliser. Differences in the spatial extent of sediment identified as enriched and the area where metal concentrations exceed guidelines detracts from fully appreciating the extent of metal contamination of sediment using guidelines, with management implications. Furthermore, in the case of Cu the guidelines for this metal might be underproductive.

## Introduction

Metals are common, and often significant contaminants of sediment in ports (Birch et al. 2020; Mehlhorn et al. 2021) and are the subject of considerable attention in the scientific literature. The focus is founded on valid concerns, including that sediment is a major fate for, and through remobilisation a potential source of metals in aquatic ecosystems (Newman and Watling 2007), and metals are known to present ecological risks when present at elevated concentrations (Chapman and Wang 2001). A major challenge, however, is identifying metal concentrations that reflect the natural state and those that are enhanced through an anthropogenic contribution (i.e. contamination). This is complicated for several reasons. First, metals are a ubiquitous, naturally occurring component of sediment. The mere presence of metals in sediment does not thus infer contamination. Second, metal concentrations in uncontaminated sediment can vary by orders of magnitude over small spatial scales

depending on the sediment's mineralogy, granulometry and organic content amongst other factors (Amorosi et al. 2007; Balls et al. 1997; Du Laing et al. 2007; Grant and Middleton 1998; Kersten and Smedes 2002; Krumgalz et al. 1992; Loring 1991; Rubio et al. 2000; Schropp and Windom 1988; Thomas and Bendell-Young 1999; Windom et al. 1989; Woods et al. 2012). Third, despite input and transport dissimilarities, naturally occurring and anthropogenically introduced metals tend to accumulate in sediment in the same areas (Hanson et al. 1993; Loring 1991). Due to these complexities, similar metal concentrations in two sediment samples from the same system may reflect contamination in one sample but not the other, due to a difference in the sediments granulometry. Similarly, very different metal concentrations in two sediment samples from the same aquatic system might in both cases reflect the natural condition, for the same reasons. Therefore, "high" metal concentrations do not necessarily reflect increased levels of contamination and vice versa (Newman and Watling 2007). The direct comparison of metal concentrations amongst sediment samples is thus important in terms of ecological and human health, if certain thresholds are exceeded, but not in the context of identifying contamination itself.

To properly interpret metal concentrations in sediment it is necessary to compensate for the factors that control their natural variation before background or baseline concentrations can be distinguished from enriched (higher than 'expected') concentrations. There are two approaches to normalisation, namely: a) using a metal that acts conservatively – geochemical normalisation, or b) using a grainsize fraction – granulometric normalisation (Birch and Snowdon 2004; Newman and Watling 2007). In this way, metal concentrations that are atypical of the bulk of the data can be identified. The investigator must then decide if atypically high metal concentrations reflect contamination or can be explained by natural biogeochemical or hydrodynamic processes.

Geochemical normalisation makes use of a metal that acts as a proxy for the grain size variation of sediment, and more specifically for the silt and clay (mud) fraction (Birch and Snowdon 2004). A metal normaliser should (a) be highly refractory, (b) be structurally combined to one or more of the major metal-bearing phases of sediment, (c) co-vary in proportion to the naturally occurring concentrations of the metals of interest, (d) be insensitive to inputs from anthropogenic sources, and (e) be stable and not subject to environmental influences such as reduction/oxidation, adsorption/desorption and other diagenetic processes that may alter sediment concentrations (Luoma 1990). Commonly Al, Fe,

Li, Rb, or Ti are used as geochemical normalisers (Tůmová et al. 2019; Santos et al. 2005; Daskalakis und O'Connor 1995).

In granulometric normalisation, metal concentrations are either normalised to a specific grain size fraction of sediment, or metal concentrations are analysed in a defined grain size fraction of the sediment after sieving. Metals are predominantly incorporated in and preferentially bind to fine sediment rather than to coarse material, meaning that silt and clay are the most effective normalisers in this approach (Koigoora et al. 2013; Newman and Watling 2007; Szava-Kovats 2008). In addition, Ti is often associated with fine sand to silt or clay whereas K and Al are often associated with clay type minerals (Haberzettl et al. 2019; Watling 1977), while Zr has been reported as enriched in the silt fraction (Cuven et al. 2010; Kylander et al. 2011; Ohlendorf et al. 2014). Therefore, it is necessary to identify the best-fit grainsize-range for granulometric normalisation. However, caution is required when a grain size fraction is used as a normaliser since two separate samples are processed and analysed, one for grain size and one for metals. Errors in sample splitting can lead to errors in normalisation. Similarly, isolating a sediment fraction for metal analysis is usually done by wet sieving and this can lead to the loss of metals weakly adsorbed to the surface of sediment grains.

Site specific circumstances might alter the usefulness of normalisers. In this study we present data from Richards Bay Harbour on the northeast coast of South Africa, where different factors need to be considered in the choice of the normaliser. Industries near Richards Bay Harbour include two aluminium smelters and a ferrochrome smelter. These industries import alumina and export aluminium and ferroalloys through the port. The effect of open air bulk handling (e.g. of ferrochrome) can introduce metals to the harbour, and point sources of Cr or Cu at bulk handling terminals were recognised by Mehlhorn et al. (2021). Contamination arising from the spillage during import or export and from the smelters (e.g. through atmospheric deposition) could thus influence the utility of Al and Fe as normalisers. In a previous study (Mehlhorn et al. 2021), we used Al to normalize metal concentrations in sediment sampled in Richards Bay Harbour. However, considering the industrial impact outlined above, there are potential limitations to the use of Al and Fe as normalisers of metal concentrations in sediment in the harbour. Similarly, the catchment geology must be considered. For example, Ti-bearing heavy mineral dune sands of the Maputaland Group Sibayi Formation surrounding Richards Bay Harbour (Botha 2018; Kelbe 2010) question the usefulness of certain geochemical normalisers, such as Ti, as heavy minerals might be

differently influenced by prevailing hydrodynamic conditions compared to other normalisers. Furthermore, the basin topography of Richards Bay Harbour is optimized to serve marine port operations. To keep the port operational, the basin shape of the harbour is largely controlled by dredging (Greenfield et al. 2011, Dladla et al. 2021). Remobilization of metals from sediment by seabed disturbances can occur via bioturbation, increased current velocities (storms, tides) or dredging (Daskalakis and O'Connor 1995; Förstner 1989; Saulnier and Mucci 2000). Ship operations, especially propeller wash currents, impact the depositional environment (Mehlhorn et al. 2021) and disturb natural sedimentation processes.

To understand changes in an environment, it is necessary to identify a system's reference state using various proxies, in this case the release of (heavy) metals by surrounding industries and their potential health risks. This enables their comparability to past and future change (cf. Mehlhorn et al. 2021), but also shifts in the spatial extent of contamination, indicating sink and source relationships. However, each basin or catchment is subject to site-specific environmental influences that need special consideration when evaluating (normalising) parameters. In this study, we evaluate the efficacy of several potential normalisers for concentrations of Cr, Cu, Co and Pb in Richards Bay Harbour sediment, by defining baseline models using different normalisers and comparing trends in the enrichment of sediment identified by the models.

## Materials and methods

### Site description

Richards Bay Harbour (Fig. 3.1) is situated in the province of KwaZulu-Natal, on the subtropical northeast coast of South Africa. Prior to port construction, Richards Bay was a large, shallow estuary of about 30 km2 fed by five rivers (Begg 1978). Harbour development started in the early 1970's and involved the construction of an artificial berm that divided the estuary into two parts. The northern part was developed into Richards Bay Harbour. A new mouth was dredged for the southern part, which was designated a nature sanctuary (Mhlathuze Estuary), and part of the Mhlathuze River was canalised and diverted into this part. A major reason for the construction of Richards Bay Harbour was to facilitate the export of coal through the Richards Bay Coal Terminal, which is now one of the largest coal export terminals in the world (Nel et al. 2007). Other industry established in the area to take advantage of the import and

export opportunities provided by the harbour, including aluminium smelters, a phosphoric acid and fertilizer plant, a ferrochrome smelter, and heavy minerals mining and refining operations. A wide range of bulk materials are imported and exported through the harbour in addition to coal, including ferroalloys, sulphur, phosphoric acid, alumina, aluminium, heavy minerals, and woodchips.

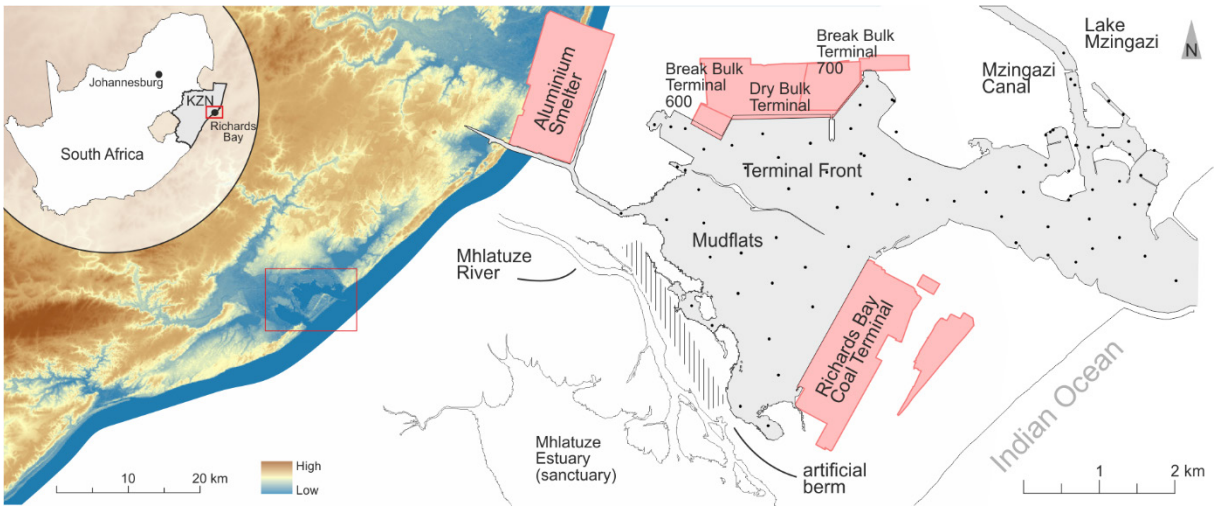


Fig. 3.1: The study area of Richards Bay Harbour. Indicated are the harbour area, which is separated from the Mhlatuze Estuary (sanctuary) by an artificial berm. Also shown are potential contamination sources (red) and sampling locations (black dots). A low altitude dune ridge extending from WNW to ESE divides the harbour and separates the shallow water Mudflats from the deep water Terminal Front.

## Sampling

Sampling was conducted in August and September of 2018. Eighty surface sediment samples were collected (Fig. 3.1) using an Ekman-Birge bottom sampler (HYDROBIOS, Kiel, Germany). Only the topmost 1 cm was sampled with a plastic spoon. Samples were stored in sterile polyethylene Nasco Whirl-Pak's and cooled until further processing.

## Granulometric and geochemical analysis

The sediment was prepared for granulometric analyses by soaking 0.5-2 g aliquots of wet sediment in 2 ml of hydrochloric acid (HCl, 10%) and 5 ml of hydrogen peroxide (H2O2, 10%). The residues were dispersed overnight in 5 ml tetrasodium pyrophosphate (Na4P2O7 10 H2O, 0.1 M) in an overhead shaker. The samples were then analysed using a Laser Diffraction Particle Size Analyser (Fritsch Analysette 22; FRITSCH GmbH, Germany).

Freeze-dried aliquots of sediment were ground to a particle size <60 µm. Subsamples of the sediment were digested at the University of Greifswald using a modified aqua regia treatment. The procedure involved the addition of 1.25 ml of HCl (37%, suprapur) and 1.25 ml of HNO3

(65%, suprapur) to 100 mg of sediment, which was then digested in PTFE crucible pressure bombs in an oven at 160°C for 3 hours. Each batch included a laboratory blank as well as a reference sediment sample of certified estuarine sediment (BCR-667) and indicated a good recovery range of 76.9-98.6% for the measured metals (Co = 86%; Cr = 96%; Cu = 96%; Fe = 99%; Pb = 77%). Elemental concentrations were measured at Friedrich Schiller University Jena using an Agilent 725 ES ICP-OES (Al, Ca Fe, K, Mg, Mn, Na, P, S, Sr, Ti) and a Thermo Fischer Scientific X-Series II ICP-MS (As, Co, Cr, Cu, Ni, Pb, Zn, Rb), as described in Mehlhorn et al. (2021).

### Data analysis

Scatterplots of the relationship between potential normalisers (Al, Rb, Ti, Fe, Silt) and co-occurring Cu, Cr, Co and Pb concentrations in sediment showed that, apart from Ti, there was a linear relationship between the bulk of the concentrations and the normalisers. Baseline models were thus defined by fitting a linear regression and 95% prediction limits to scatter plots of Cu, Cr, Co and Pb concentrations and the potential normalisers. Cu, Cr, Co and Pb concentrations falling outside the prediction limits were deemed outliers and sequentially trimmed, starting with the concentration with the largest residual, reiterating the regression, and proceeding in this manner until all concentrations fell on or within the prediction limits. The resultant regression and associated prediction limits define the baseline model. Apart from Ti, error terms for the regressions approximated normality but their variance was usually not homogenous. The Cu, Cr, Co and Pb concentrations were not transformed to approximate this assumption. In general, the lack of error term homogeneity does not result in biased estimates of regression parameters, but does result in an increase in variance about these estimates (Hanson et al. 1993). Schropp et al. (1990), Weisberg et al. (2000) and Woods et al. (2012) used a similar approach for defining baseline models, but continued to trim metal concentrations until the error terms were normally distributed and homogenous. This approach was not followed in this study since it required the trimming of a larger number of Cu, Cr, Co and Pb concentrations than the approach described above, including concentrations that were subjectively considered to be part of the baseline range.

Sediment with Cu, Cr, Co and Pb at a concentration above a baseline model upper prediction limit was interpreted as enriched (i.e. the metal concentration is in excess of the baseline). The upper prediction limit was thus used to discriminate baseline from enriched metal

concentrations. The magnitude of enrichment for each metal concentration was quantified by computing an Enrichment Factor (EF), which is calculated by dividing the observed metal/normaliser ratio by the reference (upper prediction limit) metal/normaliser ratio. EF´s >1 represent enriched concentrations, noting that this does not imply an enhancement through anthropogenic contribution, but rather that the concentration is atypical of the data that define the model (Horowitz 1991). Spatial trends for EF's were plotted using ArcMap v. 10.8.1., using inverse distance weighting with barrier function.

Reaching a conclusion on whether metal enrichment reflects contamination thus requires consideration of ancillary factors, including possible (bio)geochemical processes that can lead to natural enrichment (e.g. diagenetic enhancement), the absolute difference between a metal concentration and the baseline model upper prediction limit, the number of metals in a particular sediment sample at an enriched concentration, and the proximity of metal enriched sediment to known or strongly suspected anthropogenic sources of metals. The larger the difference between a metal concentration and the baseline model upper prediction limit, the closer the enriched sediment sampling site is to known or strongly suspected anthropogenic sources of metals, and the greater the number of metals enriched in sediment at a particular sampling site the more likely the excess concentrations reflect contamination.

## Results and discussion

### Evaluation of normaliser suitability

In a mineralogically homogenous area the absolute concentrations of metals in sediment are largely controlled by the sediments grain size (Förstner 1989; Horowitz 1991; Horowitz and Elrick 1987; Larrose et al. 2010; Liang et al. 2019; Loring 1991; Matys Grygar and Popelka 2016; Taylor and McLennan 1981). Aluminosilicates, the dominant natural metal-bearing phase of sediment, predominate in silt and clay (mud). Sand, in contrast, is comprised largely of metal deficient quartz. Metals naturally adsorb onto Fe/Mn oxides and organic matter in sediment in quantities that are usually proportional to grain size (Kersten and Smedes 2002). As a result, there is usually a strong positive correlation between the concentration of metals and the mud fraction, and between the concentration of different metals in uncontaminated sediment (Coynel et al. 2016; Rubio et al. 2000; Sabadini-Santos et al. 2009; but see Jung et al. 2014; Jung et al. 2016; Matys Grygar et al. 2013; Matys Grygar et al. 2014 for evidence of non-linear

relationships). These relationships provide the basis for geochemical normalisation, by modelling the linear relationship between metal and co-occurring element (Hanson et al. 1993; Kersten and Smedes 2002; Weisberg et al. 2000). Geochemical normalisation through linear regression is premised on a two-component linear mixing model, one end member representing metal deficient quartz (sand) and the other metal rich aluminosilicates (mud; Hanson et al. 1993). A fundamental requirement for the use of a metal as a geochemical normaliser, therefore, is that the metal must be strongly correlated to the fine-grained fraction of the sediment for which it acts as a proxy.

Richards Bay Harbour includes multiple heterogeneous sedimentary environments (Mehlhorn et al. 2021). To identify the most effective granulometric normaliser we plotted correlation coefficients of individual elements to different grain size classes (Fig. 3.2). Several elements show a high positive correlation with parts of the clay and silt fraction. The curve shape of Al is highlighted as an example in Fig. 3.2. Therefore, this grain size fraction appears to be a good normalizer. As the grain size increases the correlation coefficient decreases and changes to strongly negative at the onset of 250 µm (medium sand). Elements showing a visually similar pattern to Al, but at a lower correlation coefficient of r = 0.5, include Cu, Cr and Mn. Other elements, like Sr, Ti and Ca, show no distinct correlation to any grain size class. The correlation between the Silt and Mud (Clay + Silt, which appear to be good normalisers) fractions of sediment in Richards Bay Harbour is strong (r = 0.993, p < 0.01). Consequently, only Silt is hereafter considered as a normaliser of metal concentrations in sediment in the harbour.

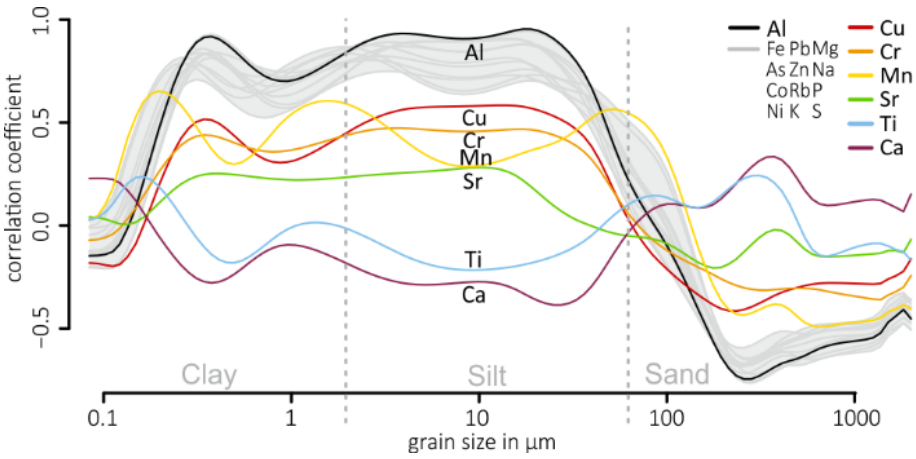


Fig. 3.2: Correlation coefficient vs grain size. The unique distribution curves indicate the varying correlation coefficients of individual elements against grain size classes. Elements displayed by grey lines show a similar behaviour to Al. Coloured curves indicate a differing and individual behaviour when plotted against grain size.

Al and Rb concentrations in sediment in Richards Bay Harbour are highly correlated to the silt fraction ($r > 0.954$, $p < 0.001$), but less so to the clay fraction ($r = 0.782 - 0.792$, $p < 0.001$). The implication is that Al and Rb are closely associated with or incorporated in the silt fraction of the sediment and are thus effective proxies for this fraction. Despite the import of alumina, export of aluminium, and presence of two large aluminium smelters near Richards Bay Harbour, sediment in the harbour does not indicate contamination by Al. This conclusion is based on the strong correlation of Al with most of the elements, and by the absence of pronounced outliers in the relationship between Al and the silt fraction of the sediment and elements that are unlikely to be influenced by anthropogenic activities, such as Rb.

Fe concentrations are also highly correlated to the silt fraction of the sediment ($r = 0.834$, $p < 0.001$), but less so to the clay fraction ($r = 0.798$, $p < 0.001$). The weaker correlation of Fe concentrations to the silt fraction compared to Al and Rb is a result of anomalously high Fe concentrations in sediment at five stations in a shallow area opposite the Richards Bay Coal Terminal, colloquially known as the Mudflats (Fig. 3.1). If the data for sediment sampled on the Mudflats is excluded, the correlation between Fe concentrations and the silt fraction increases ($r = 0.928$, $p < 0.001$), but the correlation to the clay fraction remains moderate ($r = 0.777$, $p < 0.001$). The implication is that Fe is closely associated with or incorporated into the silt fraction of the sediment and is thus an effective proxy for this fraction across most of the harbour, but not on the Mudflats.

Ti concentrations in sediment of Richards Bay Harbour are not correlated to the silt ($r = 0.094$, $p = 0.405$) or clay ($r = 0.061$, $p = 0.589$) fractions. Ti is thus not an effective proxy for these fractions of sediment in the harbour, and by implication also not for the concentrations of other metals.

The concentrations/values of normalisers should be strongly positively correlated to the concentrations of metals in uncontaminated sediment. However, in some parts of Richards Bay Harbour the sediment is metal contaminated (Mehlhorn et al. 2021). The baseline models for Cu, Cr, Co and Pb do not thus represent background concentrations since it is possible, and for Cu and Cr likely that certain concentrations included in the baseline models reflect low magnitude contamination of the sediment but are not identified as outliers through the approach used to define the models. Nevertheless, the stronger the relationship between the normalisers and metals the more effective the baseline model should theoretically be in identifying metal enrichment of sediment.

There is not much difference in the coefficients of determination for baseline models apart from Ti, for which coefficients are consistently very low (Table 3.1). The Fe normalised baseline models provide the highest coefficients for Cu, Cr and Co, and the Rb model for Pb. The baseline model coefficients of determination suggest, therefore, that Fe is the best normaliser for Cu, Cr and Co, and Rb for Pb. However, the Fe normalised baseline models are strongly influenced by the exclusion of Cu and Cr and inclusion of Co and Pb concentrations in sediment on parts of the Mudflats due to the anomalous concentrations of Fe, Co and Pb in this part of the harbour. The anomalous concentrations of Fe might be caused by a local change in redox processes (Wündsch et al. 2014; Zolitschka et al. 2019). The critical Eh for the reduction of $Fe^{3+}$ to more soluble $Fe^{2+}$ is 100 mV (Sigg and Stumm 1996). If the redox potential is lowered, Fe ions start to migrate in pore water. When an Eh above 100 mV is encountered, the ions will oxidize and precipitate, leading to the enrichment of sediment that is not necessarily linked to an anthropogenic impact (Brunschön et al. 2010; Haberzettl et al. 2007).

Table 3.1: Coefficients of determination (r2) for copper, chromium, cobalt, and lead baseline models defined using different normalisers.

| | | Metal | | | |
|---|---|---|---|---|---|
| | | Cu | Cr | Co | Pb |
| Normaliser | Al | 0.935 | 0.813 | 0.962 | 0.966 |
| | Fe | 0.95 | 0.931 | 0.988 | 0.897 |
| | Rb | 0.929 | 0.768 | 0.959 | 0.967 |
| | Ti | 0.002 | 0.031 | 0.007 | 0.003 |
| | Silt | 0.932 | 0.898 | 0.923 | 0.877 |

## Baseline model comparison

If normalisers are to be considered similarly effective, then (a) they should identify a similar number of sediment samples as enriched by any metal, (b) the spatial extent of the enrichment should be similar, (c) the magnitude of the enrichment should be similar, and (d) the enrichment should be logical in the context of known or potential anthropogenic sources of the metal. The baseline models defined for Cu, Cr, Co, and Pb using different normalisers are provided in Fig. 3.3 - Fig. 3.6, with outlier concentrations superimposed. Parameters for the baseline models are provided in Table 3.2.

Table 3.2: Baseline model regression parameters, number of samples included in the baseline model (n), number of outliers, coefficient of determination ($r^2$), and assessment of normality and constant variance for metal concentrations included in the models.

| Metal | Normaliser | Model regression formula | n | Outliers | $r^2$ | Normality | Constant Variance |
|---|---|---|---|---|---|---|---|
| Chromium | Al | Cr = 15.273 + (3.102 × Al) | 59 | 21 | 0.813 | Passed | Failed |
| | Fe | Cr = -28.061 + (4.935 × Fe) | 53 | 27 | 0.931 | Passed | Failed |
| | Rb | Cr = 21.723 + (2.363 × Rb) | 60 | 20 | 0.768 | Passed | Failed |
| | Ti | Cr = 77.428 + (13.009 × Ti) | 63 | 17 | 0.031 | Failed | Passed |
| | Silt | Cr = 38.500 + (1.949 × SILT) | 55 | 25 | 0.898 | Passed | Failed |
| | | | | | | | |
| Copper | Al | Cu = -0.625 + (0.660 × Al) | 57 | 23 | 0.935 | Passed | Failed |
| | Fe | Cu = -3.439 + (0.764 × Fe) | 42 | 38 | 0.950 | Passed | Passed |
| | Rb | Cu = 0.0983 + (0.546 × Rb) | 56 | 24 | 0.929 | Passed | Failed |
| | Ti | Cu = 11.071 + (0.345 × Ti) | 49 | 31 | 0.002 | Failed | Passed |
| | Silt | Cu = 6.004 + (0.332 × SILT) | 57 | 23 | 0.932 | Passed | Failed |
| | | | | | | | |
| Lead | Al | Pb = 0.715 + (0.388 × Al) | 68 | 12 | 0.966 | Passed | Failed |
| | Fe | Pb = -0.869 + (0.417 × Fe) | 66 | 14 | 0.897 | Passed | Failed |
| | Rb | Pb = 0.984 + (0.315 × Rb) | 67 | 13 | 0.967 | Passed | Failed |
| | Ti | Pb = 14.769 - (0.647 × Ti) | 79 | 1 | 0.003 | Failed | Passed |
| | Silt | Pb = 4.334 + (0.215 × SILT) | 70 | 10 | 0.877 | Passed | Failed |
| | | | | | | | |
| Cobalt | Al | Co = 2.918 + (0.245 × Al) | 65 | 15 | 0.962 | Passed | Passed |
| | Fe | Co = 0.198 + (0.366 × Fe) | 73 | 7 | 0.988 | Passed | Failed |
| | Rb | Co = 3.066 + (0.200 × Rb) | 63 | 17 | 0.959 | Passed | Failed |
| | Ti | Co = 10.741 + (0.644 × Ti) | 78 | 2 | 0.007 | Failed | Passed |
| | Silt | Co = 5.053 + (0.151 × SILT) | 69 | 11 | 0.923 | Passed | Passed |

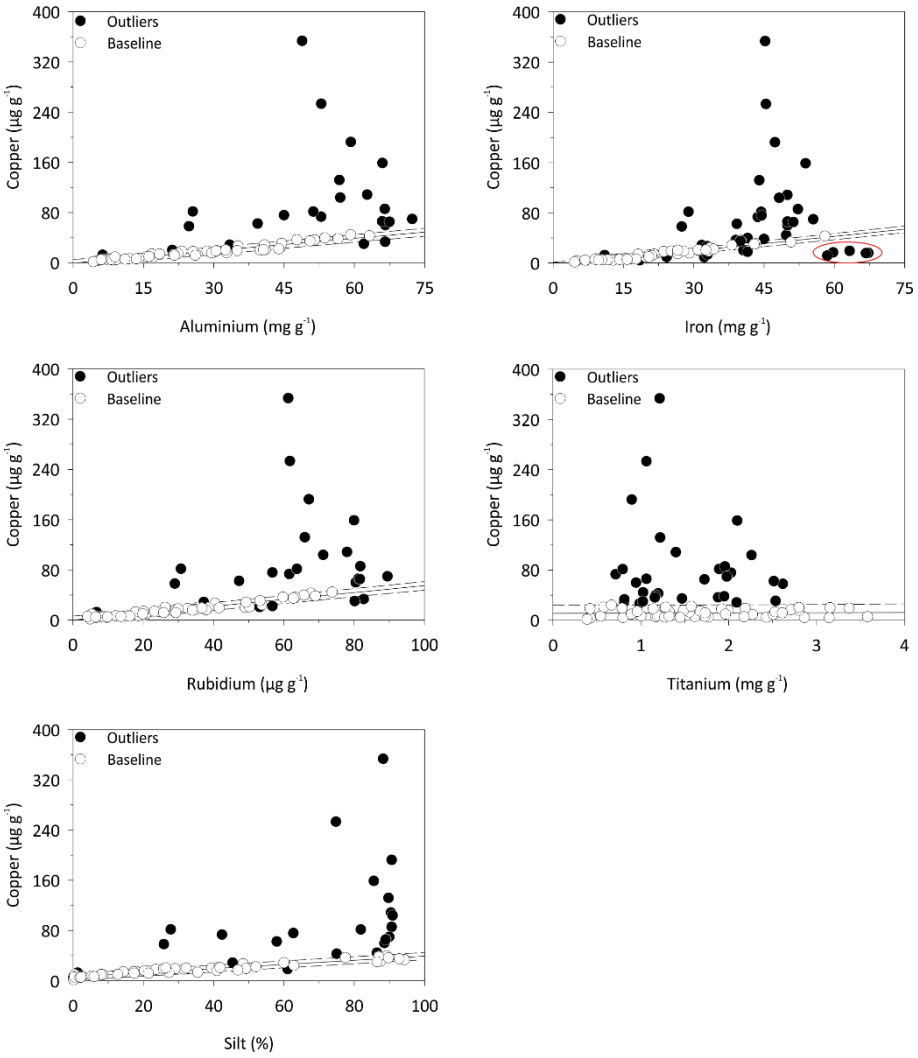


Fig. 3.3: Baseline models for copper defined using different normalisers, with outlier concentrations superimposed (black filled dots). Samples of the mudflat region are highlighted (red circle) in the iron-normalised model.

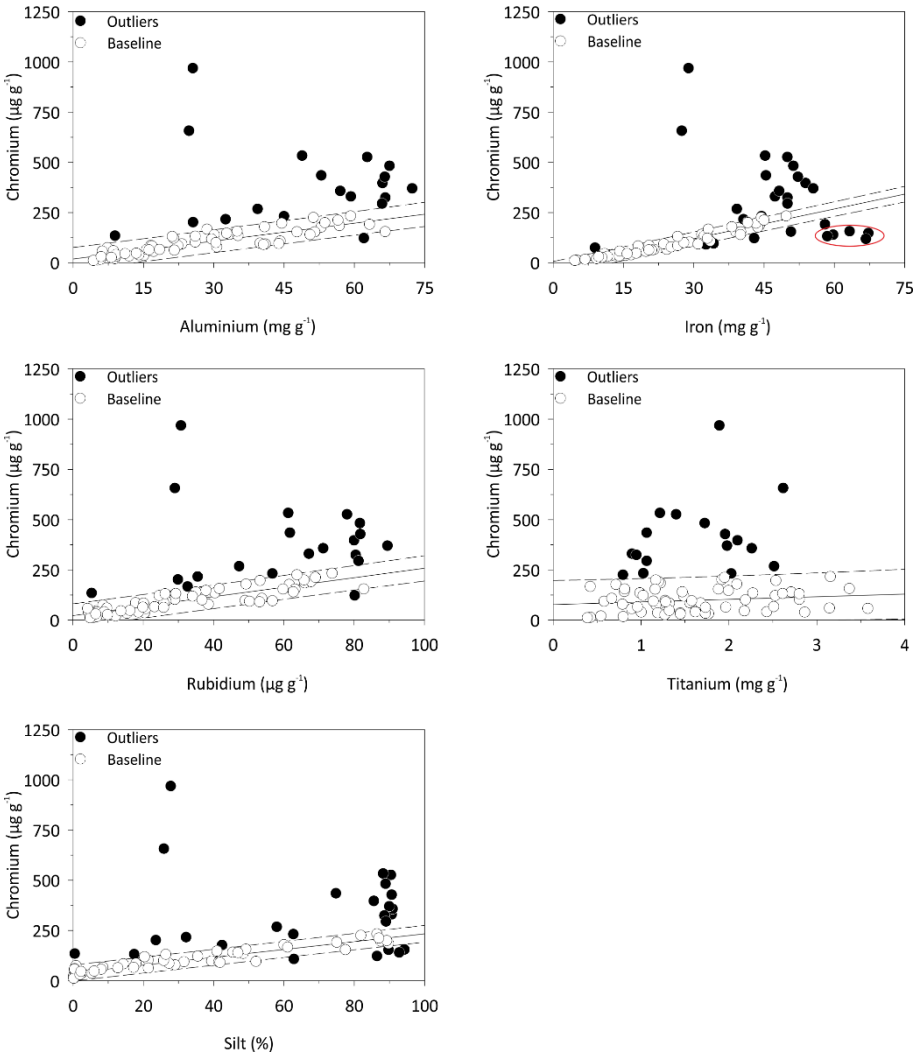


Fig. 3.4: Baseline models for chromium defined using different normalisers, with outlier concentrations superimposed (black filled dots). Samples of the mudflat region are highlighted (red circle) in the iron-normalised model.

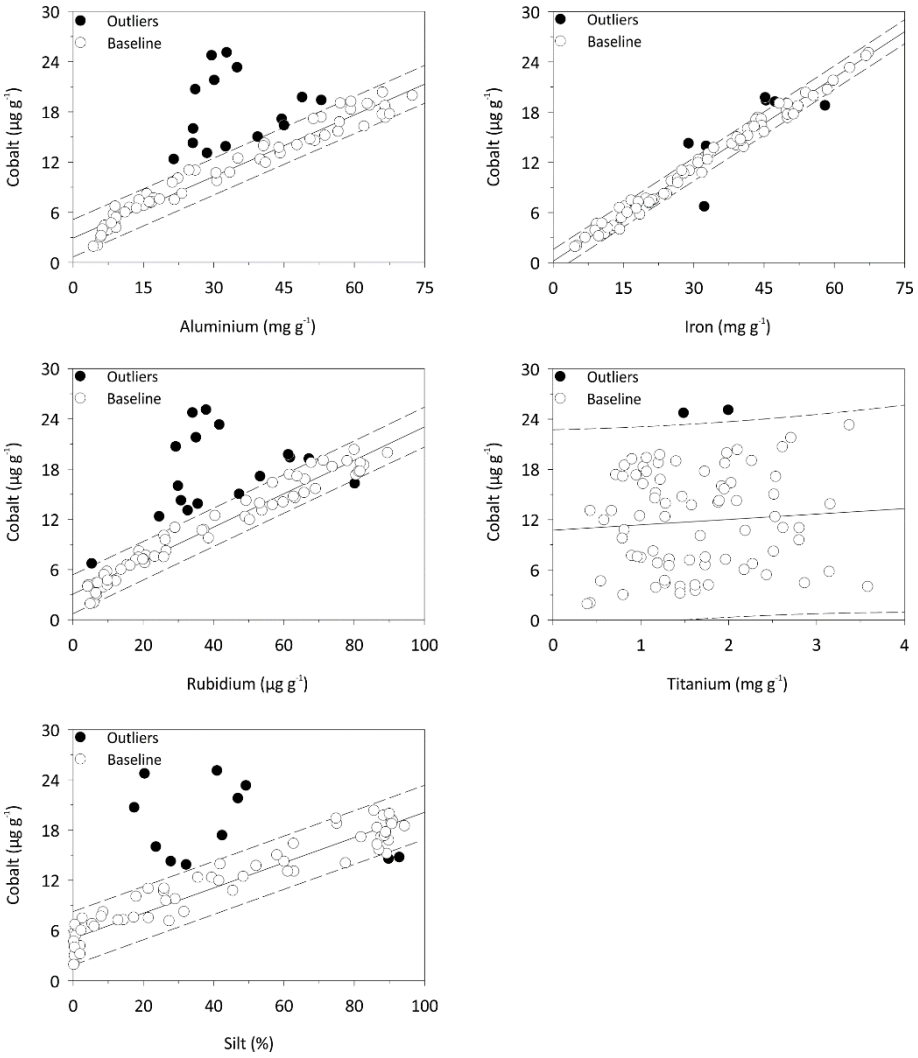


Fig. 3.5: Baseline models for cobalt defined using different normalisers, with outlier concentrations superimposed (black filled dots).

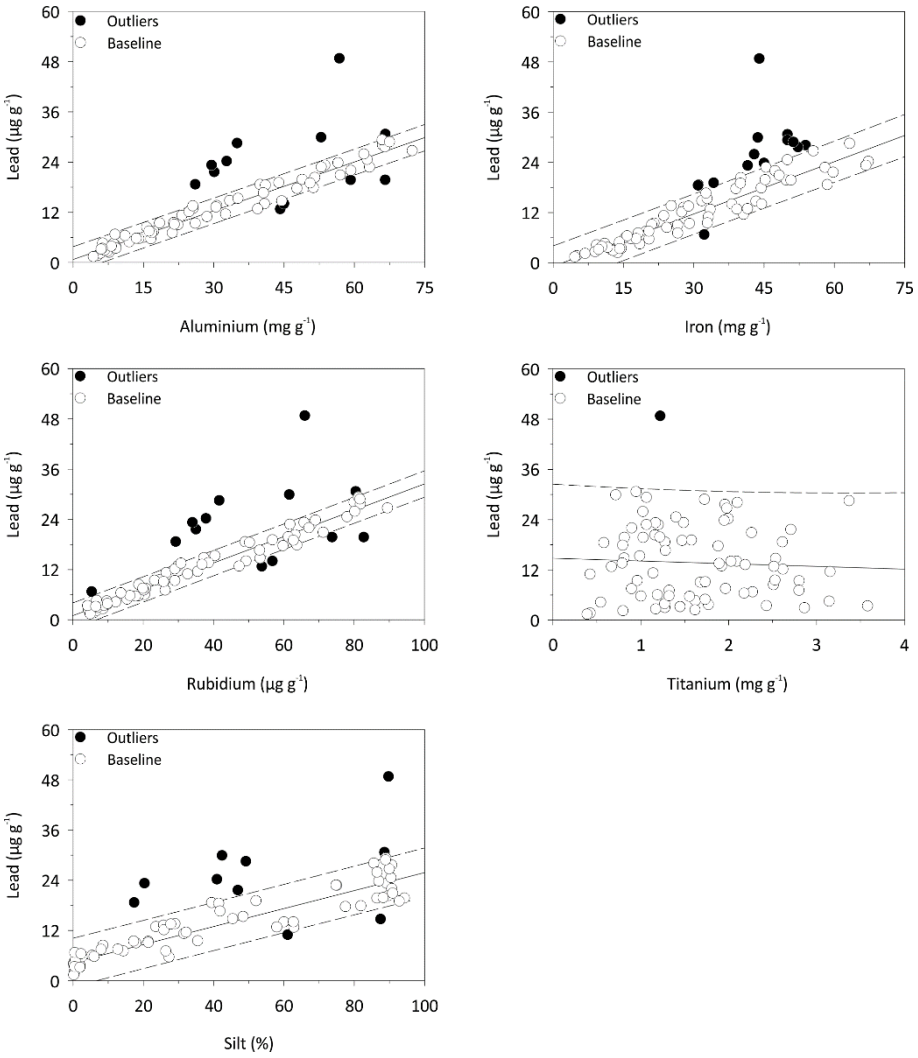


Fig. 3.6: Baseline models for lead defined using different normalisers, with outlier concentrations superimposed (black filled dots).

As stated previously, sediment with metals at a concentration above the upper prediction limit was deemed to be enriched by the metal. The number of sediment samples identified as enriched by individual baseline models is provided in Fig. 3.7.

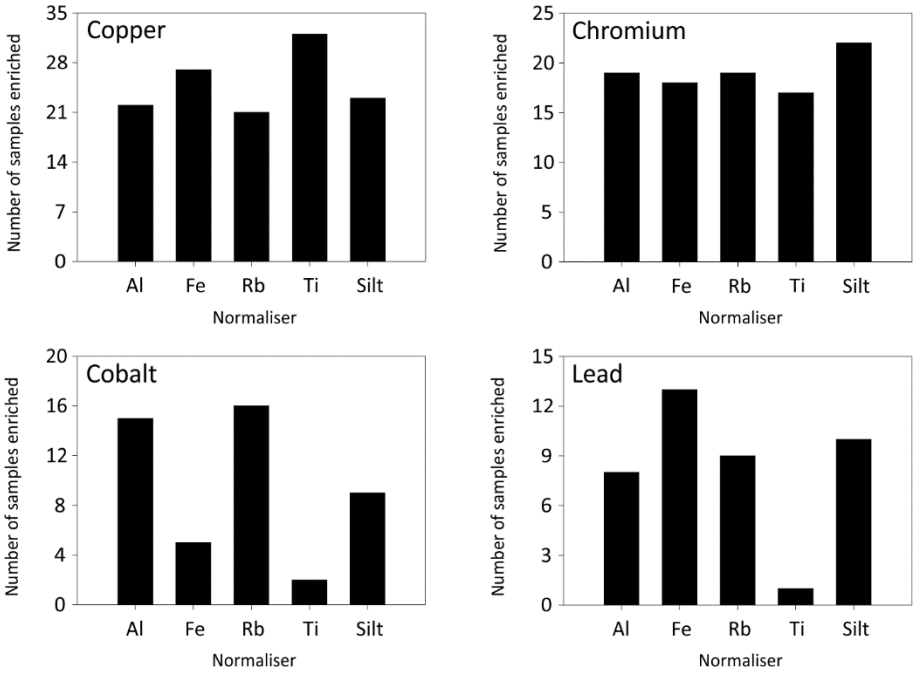


Fig. 3.7: Number of sediment samples with copper, chromium, cobalt, and lead concentrations identified as enriched by baseline models defined using different normalisers.

The number of sediment samples identified as enriched by Cu is similar for the Al, Rb, and Silt normalised baseline models, but the Fe and Ti models identify a higher number. The Al, Fe, Rb, and Ti normalised baseline models identify a similar number of sediment samples as enriched with Cr, but the Silt model identifies a higher number. The number of samples identified as Co and Pb enriched varies widely amongst the normalisers and is most similar for Al, Rb, and Silt and the lowest for Ti. The number of metals identified as enriched by baseline models defined using different normalisers is not particularly convincing as to which of the normalisers is more effective than others. However, we consider those normalisers that identify a comparable number of sediment samples as enriched by a metal are likely more effective than others.

## Spatial enrichment trends

The spatial trend for Cu and Cr EF´s that are >1 is comparable when computed using Al, Rb, or Silt normalised baseline models (Fig. 3.8 – Fig. 3.11). However, the trend for EF's computed using Fe and Ti normalised models are different, especially for Co and Pb (Fig. 3.10, Fig. 3.11). A larger area of sediment is identified as Cu enriched by the Fe and Ti normalised baseline models, the additional area extending from the 700 series berth basin into the northern part of the Richards Bay Coal Terminal basin and also including one or more isolated areas in the latter basin (Fig. 3.8). Fe and Ti identify a similar area of the 600 and 700 series berth basins (part of the Dry Bulk Terminal, Fig. 3.1) as Cr enriched compared to other normalisers but identify little (Fe) or no (Ti) Cr enrichment of sediment on the Mudflats.

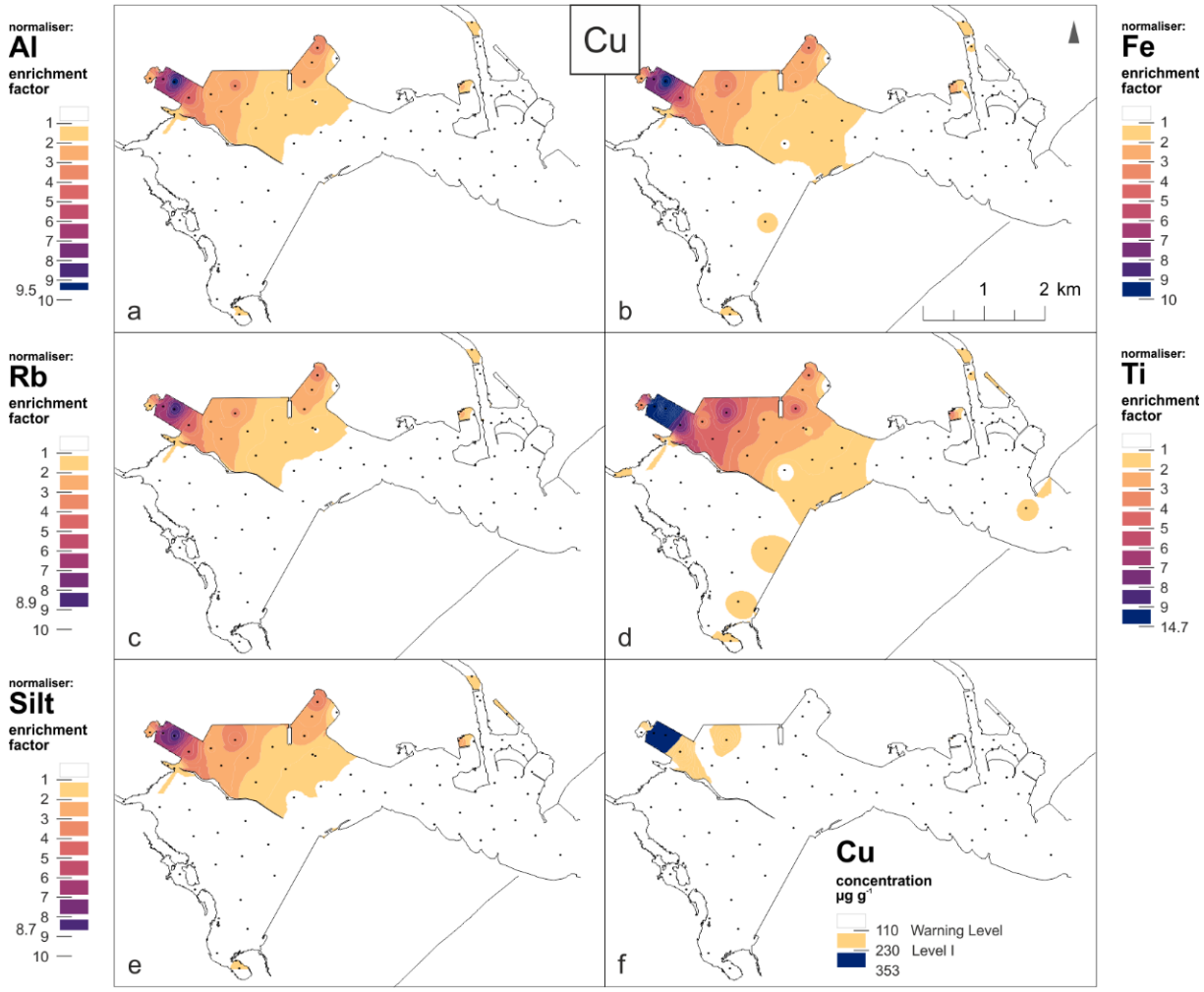


Fig. 3.8: Spatial distributions of the Copper (Cu) Baseline models normalised to a) Al, b) Fe, c) Rb, d) Ti and e) Silt. The Enrichment Factors are plotted to the same scale to achieve visual comparability, note the extended Legend of Ti ($EF_{max}$=14.7), maximum values are shown next to the classification. For additional comparison, the distribution map of Cu (f) in surface sediments of Richards Bay Harbour is plotted, making use of guideline concentrations as presented by the Department of Environmental Affairs (2012).

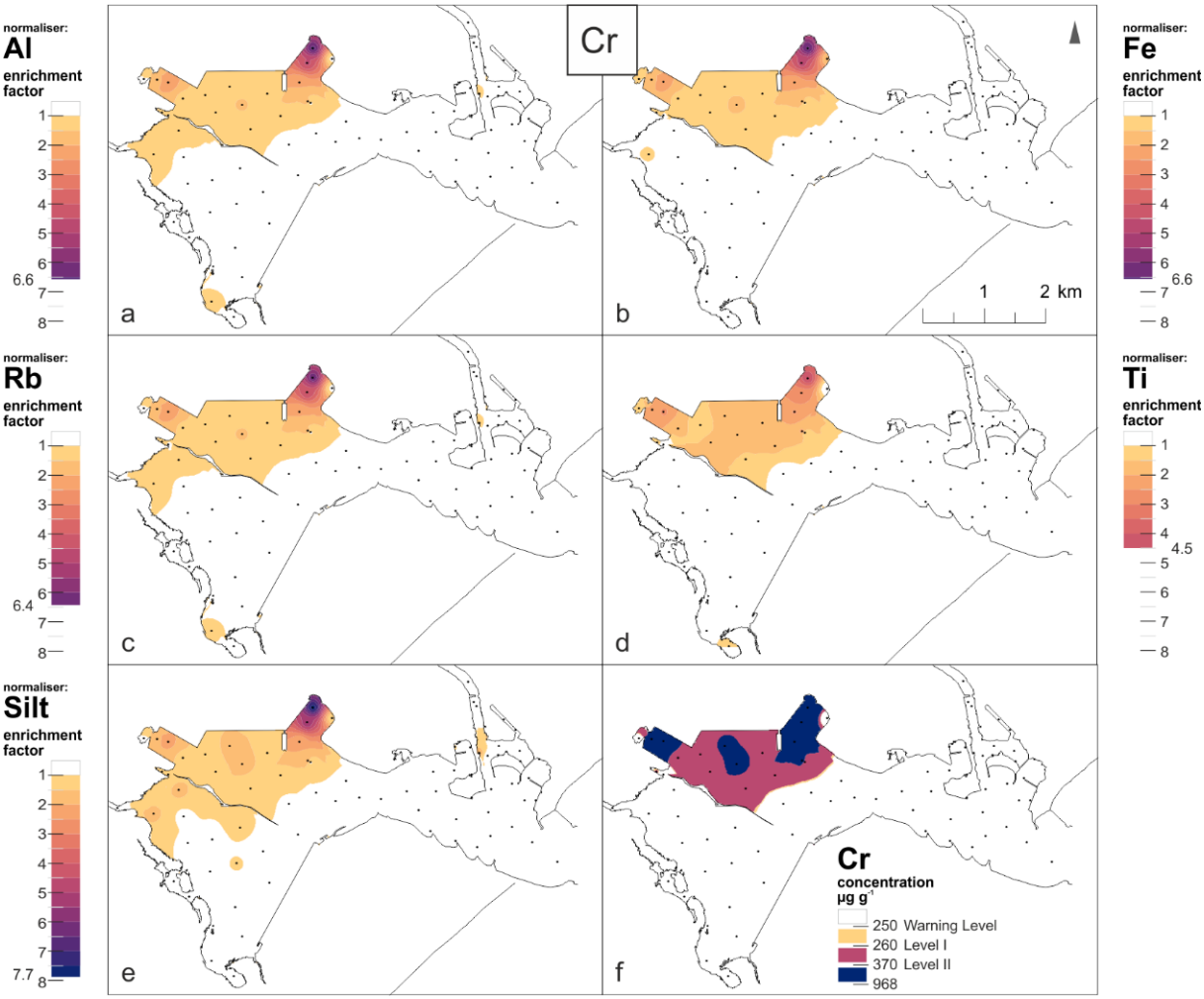


Fig. 3.9: Spatial distributions of the Chromium (Cr) Baseline models normalised to a) Al, b) Fe, c) Rb, d) Ti and e) Silt. The Enrichment Factors are plotted to the same scale; maximum values are shown next to the classification. For additional comparison, the distribution map of Cr (f) in surface sediments of Richards Bay Harbour is plotted, making use of guideline concentrations as presented by the Department of Environmental Affairs (2012).

There is clear evidence for significant anthropogenic inputs of Cu and Cr in Richards Bay Harbour. Chromium ore and ferrochrome are exported through the harbour. During export, chromium ore and ferrochrome particles are spilled into the harbour and account for the Cr contamination (Mehlhorn et al. 2021). The source of the excess Cu in sediment is less certain. Cu concentrate was historically exported through the harbour and the contamination might reflect the spillage of Cu concentrate particles during export, noting that exports ceased in 2012. The Cu and Cr enrichment of sediment sampled across much of the 600 and 700 series berth basins (dry bulk terminals) is of such a high magnitude that comparable areas of sediment are identified as enriched by baseline models defined using different normalisers, regardless of the effectiveness of the normalisers. The sediment in part of the Small Craft

Harbour is identified as Cu enriched by all normalisers (Fig. 3.8), possibly reflecting inputs from antifouling coatings on vessel hulls amongst other possible sources. Some of the baseline models also identify Cu enrichment of sediment in canals joining the north-eastern part of the port, but the source of the Cu is uncertain.

All baseline models identify Cu and Cr enrichment near the 600 and 700 series berths. An extension of the Cu enrichment from the 700 series berth basin to the northern part of the Richards Bay Coal Terminal basin is identified using the Fe and Ti normalised baseline models (Fig. 3.8). This is contradictory as it seems unlikely that Cu but not Cr (Fig. 3.9) would be dispersed to and accumulated in this area considering the strong similarity in parts of the 600 and 700 series berth basins where the sediment is identified as Cu and Cr enriched by Al, Rb, and Silt normalised baseline models. The wider area of Cu enrichment identified by the Fe normalised baseline model is probably related to the wider scatter of Cu versus Fe concentrations compared to other normalisers, which led to the trimming of a larger number of concentrations compared to other normalisers (Table 3.2). The Cr enrichment of sediment identified on the Mudflats using the Al, Rb, and Silt normalised baseline models, but absence of Cu enrichment also seems illogical for the same reason discussed above for Cu enrichment extending to the Richards Bay Coal Terminal basin. As stated above, the magnitude of Cu and Cr enrichment of sediment at many stations in the 600 and 700 series berth basins is large and it is almost inevitable the sediment will be identified as enriched regardless of the effectiveness of the baseline models defined using different normalisers.

Trends in Co and Pb enrichment of sediment are more revealing on the effectiveness of different normalisers. Sediment on the Mudflats of Richards Bay Harbour is identified as enriched by Co and Pb using Al, Rb, and Silt normalised baseline models, but not by Fe and/or Ti normalised baseline models (Fig. 3.10 and Fig. 3.11). These elements might share a similar accumulation mechanism or be affected similarly by sediment biogeochemical processes.

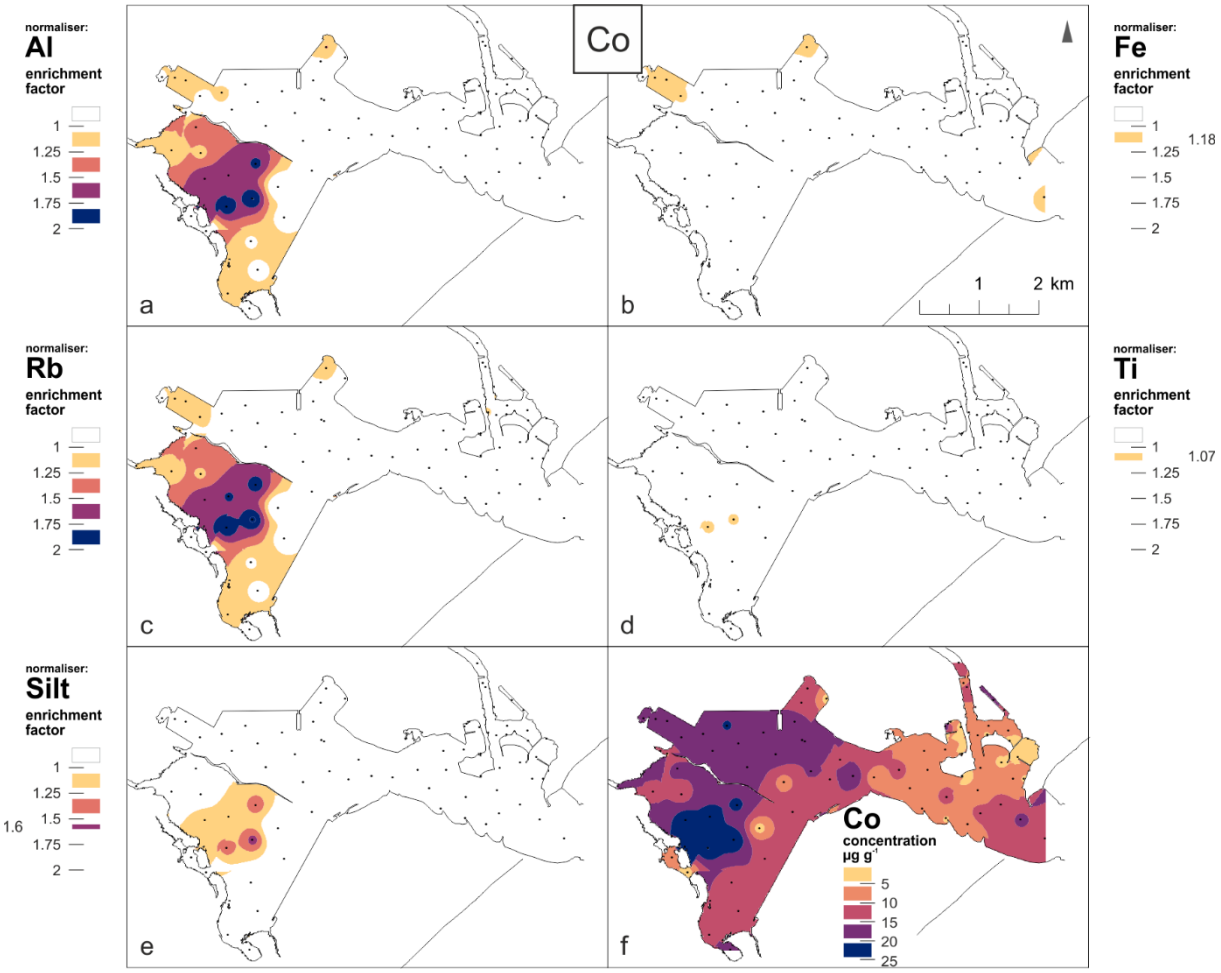


Fig. 3.10: Spatial distributions of the Cobalt (Co) Baseline models normalised to a) Al, b) Fe, c) Rb, d) Ti and e) Silt. The Enrichment Factors are plotted to the same scale; maximum values are shown next to the classification. For additional comparison, the concentration of Co (f) in surface sediments of Richards Bay Harbour is plotted.

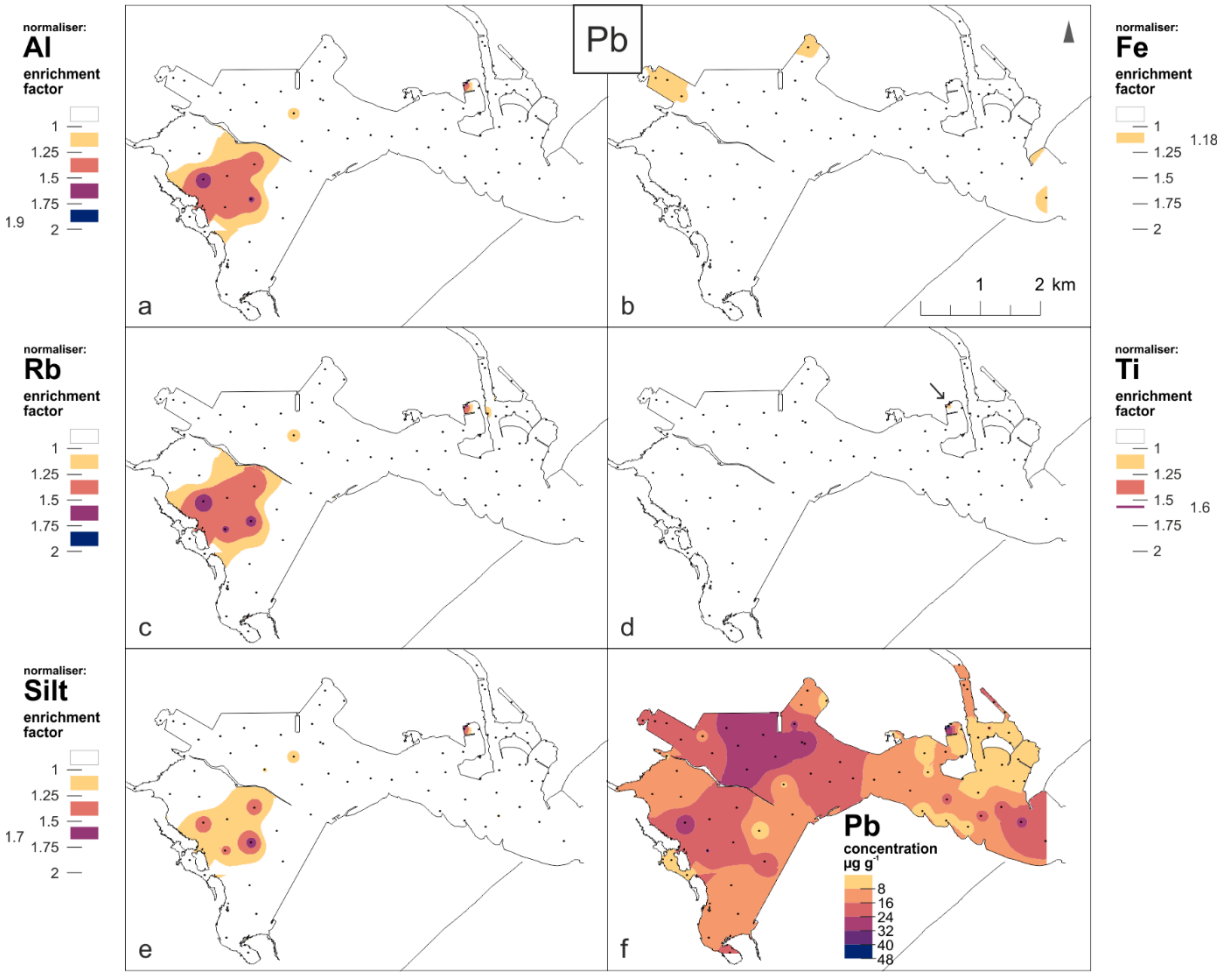


Fig. 3.11: Spatial distributions of the Lead (Pb) Baseline models normalised to a) Al, b) Fe, c) Rb, d) Ti and e) Silt. The Enrichment Factors are plotted to the same scale; maximum values are shown next to the classification. For additional comparison, the concentration of Pb (f) in surface sediments of Richards Bay Harbour is plotted.

Examples of Fe enrichment identified using Al and Silt as the normaliser are provided in Fig. 3.12. The consequence is that Fe normalised Co and Pb concentrations are shifted to the right in scatterplots, to the extent they fall within the prediction limits of baseline models defined using the data (Fig. 3.13). In contrast, the Cu and Cr concentrations in sediment at these stations were trimmed during baseline model definition and fall below the lower prediction limit (Fig. 3.3 and Fig. 3.4). The anomalous concentrations do not thus have the same influence on the baseline models as the Co and Pb concentrations.

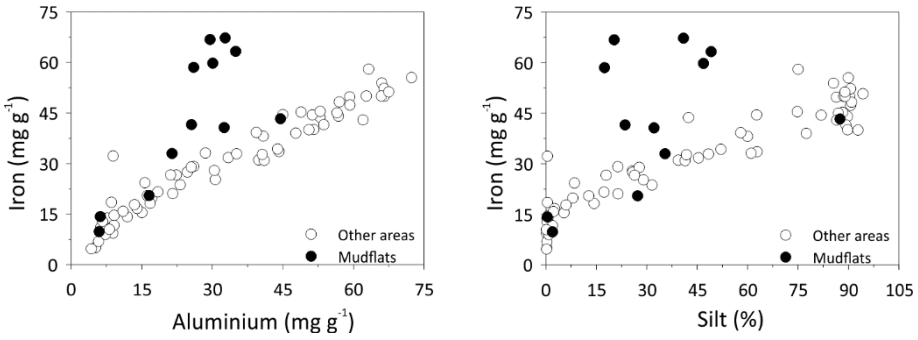


Fig. 3.12: Relationship between the aluminium concentration and silt fraction and co-occurring iron concentrations in sediment in Richards Bay Harbour. Iron concentrations in sediment sampled on the Mudflats are highlighted (black filled dots).

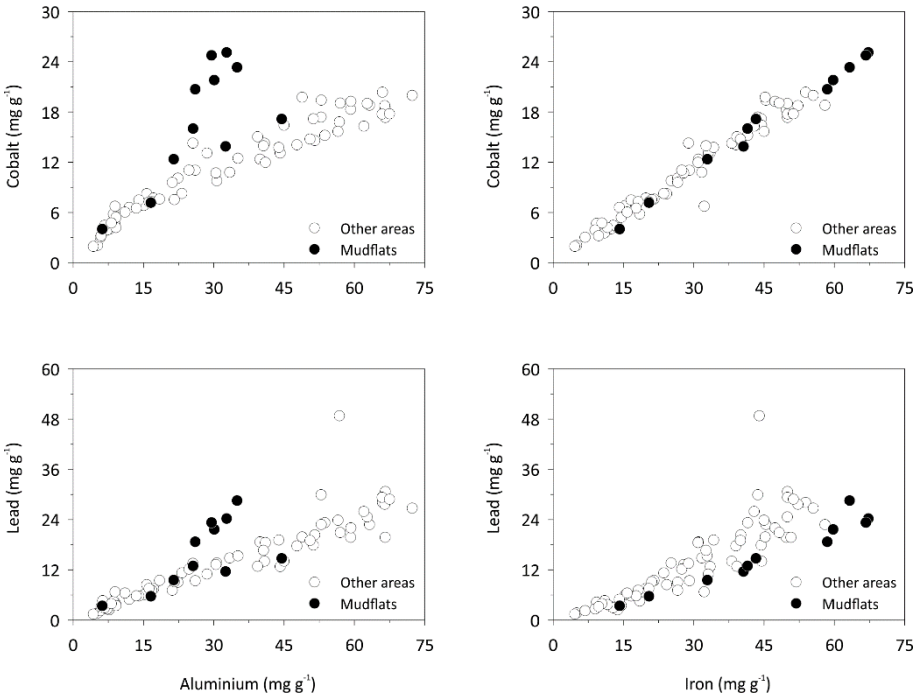


Fig. 3.13: Relationship between aluminium and iron concentrations and co-occurring cobalt and lead concentrations in sediment in Richards Bay Harbour. Cobalt and lead concentrations in sediment sampled on the Mudflats are highlighted (black filled dots). Note how the anomalously high cobalt and lead concentrations in the aluminium normalised plots are shifted to the right in the iron normalised plots.

The differences between Al, Rb, and Silt normalised baseline models, and the Fe baseline model for Co and Pb suggests there is either an anthropogenic source of Fe, Co and Pb to the Mudflats, or there is a biogeochemical or hydrodynamic process leading to the enrichment of these metals in sediment in this part of the harbour. The Bhizolo Canal connects to the Mudflats and is a potential source of effluents from adjacent aluminium smelters, but it seems unlikely this will be limited largely to Fe, Co and Pb, but rather to the introduction of Al. A more likely explanation is that redox processes resulted in an inhomogeneous Fe distribution

(Brunschön et al. 2010; Demory et al. 2005). Support for this hypothesis is provided by Mn, which is also a redox sensitive metal (Haberzettl et al. 2007) and which is also identified as enriched in sediment on the Mudflats (data not reported here) using Al, Rb, and Silt normalised baseline models.

The EF plots presented in Fig. 3.8 – Fig. 3.11 make it easy to visually compare the spatial extent of enrichment of sediment by various metals in Richards Bay Harbour and to identify areas where the highest enrichment is evident, but it is not easy to visually compare areas of low magnitude enrichment. To facilitate such comparison the relationship between EF's is provided for Cu and Co in Fig. 3.14 and Fig. 3.15. The oblique lines in the graphs represent a 1:1 relationship. The more similar the EF's are to one another the nearer they fall to the 1:1 line. The graphs also reveal if the baseline model defined using a normaliser provides consistently higher or lower EF's compared to baseline models defined using other normalisers depending on whether the EF's fall above or below the 1:1 line. In Fig. 3.14 (and Fig. 3.8), for example, the Ti normalised baseline model provides higher EF's for Cu in a large proportion of sediment samples compared to other baseline models. The most similar EF's for Cu and Cr are for combinations of Al, Fe, Rb, and Silt normalised baseline models. For Co (Fig. 3.15) and Pb (not shown), combinations of Al, Rb, and Silt normalised baseline models provide similar EFs, but these differ to EFs computed using Fe and Ti normalised models. The differences for Co and Pb reflect the influence of the high Fe, Co and Pb concentrations in sediment on the Mudflats on baseline models defined using Al, Rb and Silt (Fig. 3.12 and Fig. 3.13). Thus, while these sediment samples are included in the baseline models for Co and Pb, the Cu and Cr concentrations fall below the lower prediction limit of the Fe normalized models. They do not thus exert a similarly pronounced influence on the baseline model parameters.

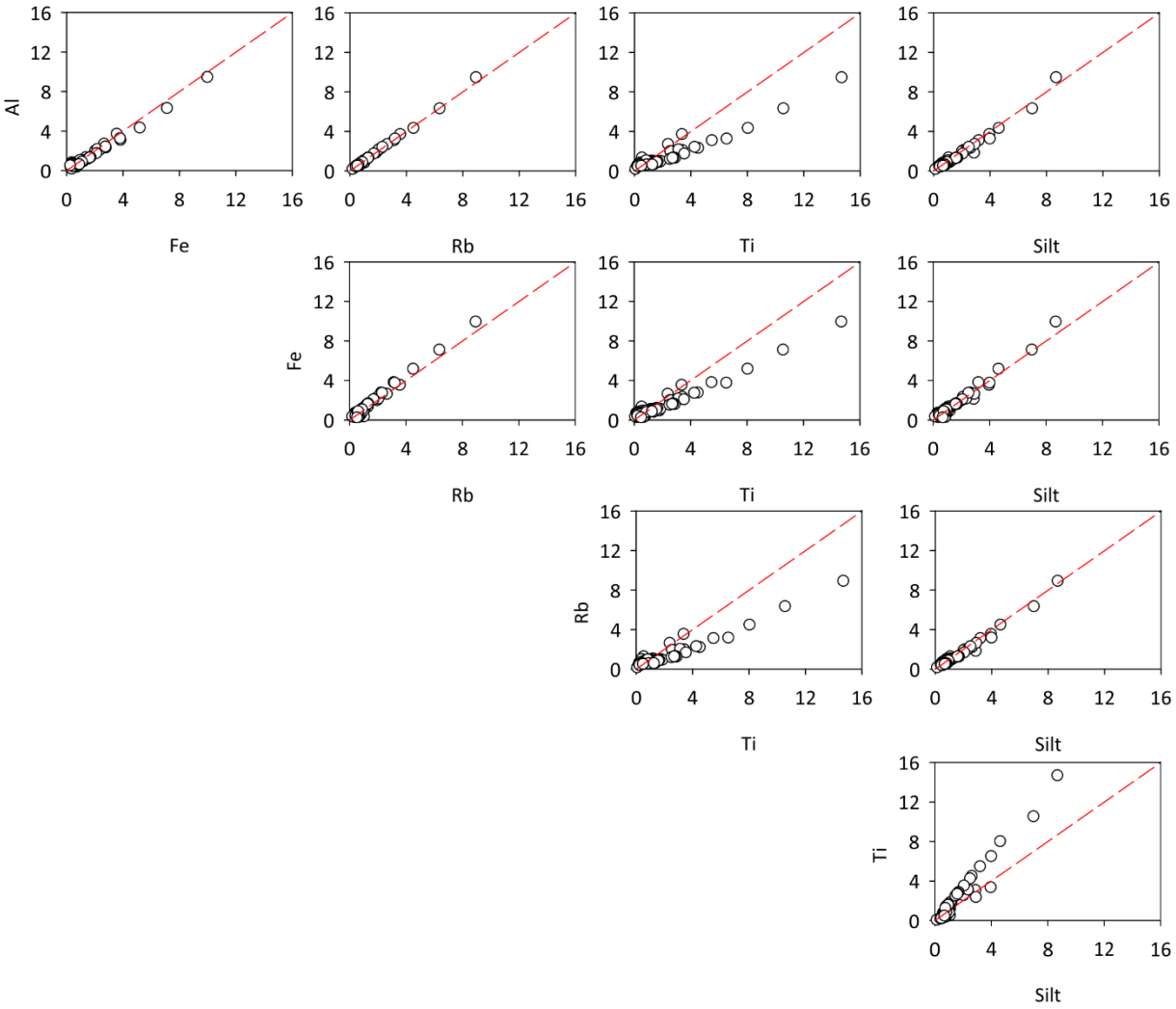


Fig. 3.14: Relationship between copper Enrichment Factors computed using baseline models defined using different normalisers. The diagonal dashed line represents a 1:1 line.

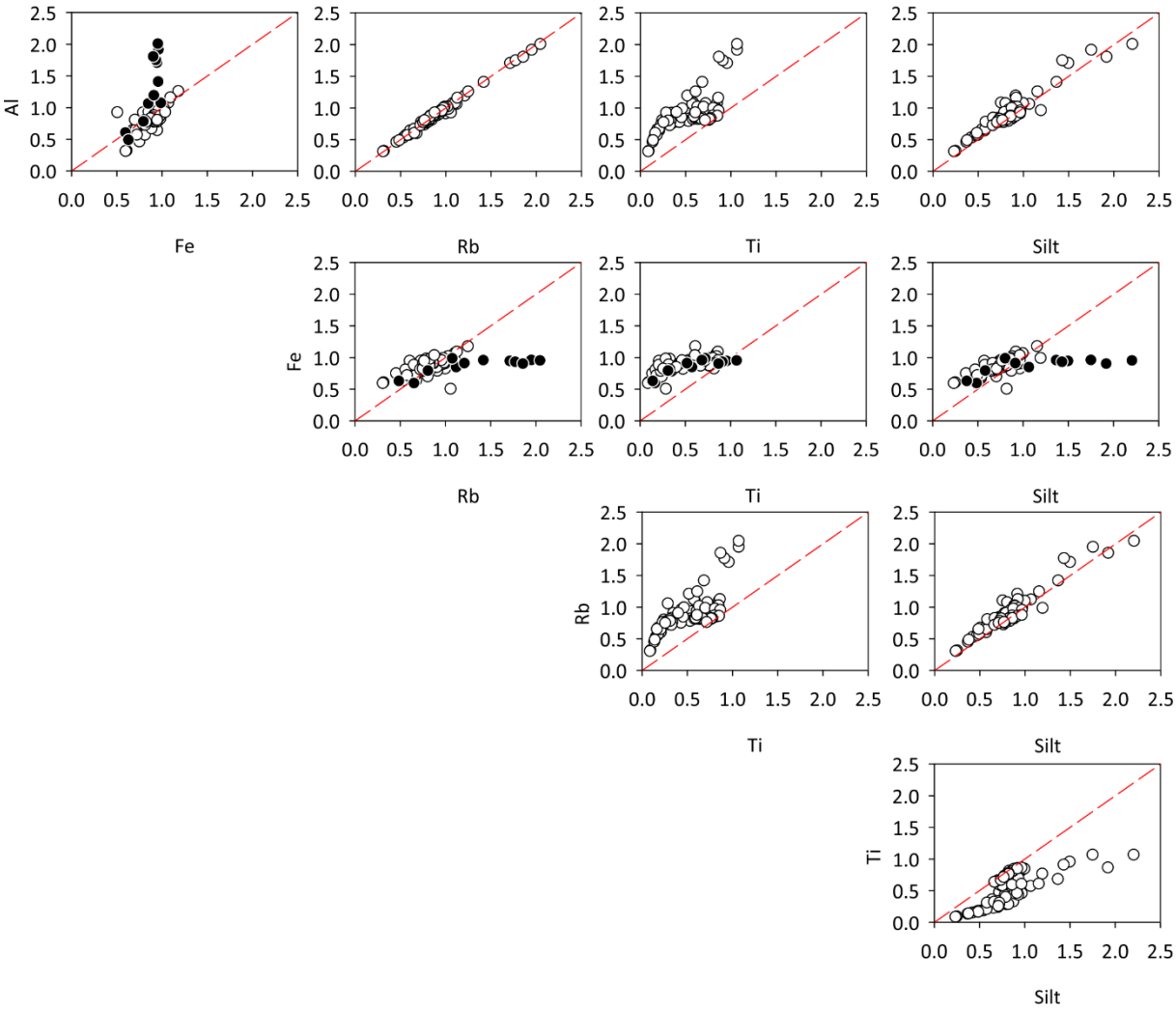


Fig. 3.15: Relationship between cobalt Enrichment Factors computed using baseline models defined using different normalisers. The diagonal dashed line represents a 1:1 line. Black symbols represent Enrichment Factors for sediment sampled on the Mudflats.

A random choice of any of the normalisers considered in this study will thus provide a different understanding on the spatial extent and magnitude of enrichment. The differences will vary depending on the chosen normaliser, but are small when Al, Rb and Silt are used as normalisers. If only Fe was considered for normalisation, then this would have provided a different understanding on metal enrichment of sediment in some parts of the harbour compared to that provided by Al, Rb and Silt normalised baseline models. Ti provides a very different understanding of enrichment for most metals compared to other normalisers, reflecting its unsuitability as a normaliser in the case of Richards Bay Harbour.

## Comparison to guidelines

A common approach to estimating the toxicological significance of metal concentrations in sediment is to compare them to sediment quality guidelines. A misconception is that sediment quality guidelines indicate the onset of metal contamination of sediment. Although this is usually true for metal concentrations that exceed a guideline, depending on how conservative the guideline is, the sediment might be contaminated by a metal at concentrations well below the guideline. As examples, spatial trends for Cu and Cr concentrations in sediment in Richards Bay Harbour that exceed sediment quality guidelines used by the Department of Environmental Affairs (2012) to manage dredged material in South Africa are included in Fig. 3.8 and Fig. 3.9. There are three guidelines, known as the Warning Level, Level I and Level II. The Warning Level provides a warning of incipient metal contamination but is not used for decision-making. Sediment with metals at a concentration below the Level I is considered to pose a low risk and is suitable for open water disposal. Sediment with metals at a concentration between the Level I and Level II is considered cause for concern, with the degree of concern increasing as the concentrations approach the Level II. Sediment with metals at a concentration exceeding the Level II is considered to pose a high risk and is unsuitable for open water disposal unless other evidence (e.g. toxicity testing) shows the metals are not toxic to sediment-dwelling organisms.

There are large differences in the spatial extent of sediment identified as Cu enriched by baseline models defined using different normalisers and the area of sediment with Cu at a concentration exceeding the guidelines (Fig. 3.8). The area of maximum intensity (either concentration or EF) is confined to the 600 series berth basin. However, the area defined by EF´s > 1 extends into the 700 berth basin (Terminal Front) and to other areas, such as the Small Craft Harbour.

The difference in the spatial extent of sediment identified as metal enriched using the baseline models and the spatial extent of sediment with metals at a concentration exceeding Action List guidelines is often pronounced. This alludes to the guidelines perhaps being under or over-protective, noting that the guidelines were not derived using empirical data from South African coastal waters but rather were adopted from guidelines used in North America. The guidelines might not, therefore, be appropriate to (all) parts of the South African coastline. Taking Cu as an example, large areas of sediment in the harbour are identified as enriched by this metal, yet the area where Cu concentrations exceed sediment quality guidelines is quite

small. The use of the guidelines thus fails to identify sediment that is quite significantly enriched by Cu as potentially problematic, and alludes to management challenges larger than those alluded to by using the guidelines alone. This may mean the Cu guidelines are under-protective, that is, the guideline concentrations are too high for sediment in Richards Bay Harbour.

## Conclusion

This study compares the effectiveness of different normalisers on assorted metal in sediment in Richards Bay Harbour. The aim was to define metal concentration baselines and to identify areas of the harbour that are currently metal enriched, to aid in the tracking of changes in metal enrichment of sediment over time. The baseline models defined using some normalisers provide a powerful tool for this purpose, compensating for grain size influences on natural metal concentrations and reducing subjectivity in deciding if sediment is metal enriched. The models are equally effective in identifying changes in metal concentrations that may result from anthropogenic metal inputs and those that might arise from future climate changes, such as the introduction of increased metal and sediment loads to coastal waters associated with changes in precipitation patterns.

The use of different normalisers provides a different understanding on metal enrichment of sediment in Richards Bay Harbour. Despite the import of alumina and the presence of two large aluminium smelters near Richards Bay harbour, this does not appear to result in a significant Al contamination of sediment in the harbour affecting its use as a normaliser. The EF trends for metals in Richards Bay Harbour, including those not discussed here, are most similar when Al, Rb or Silt are used as normalisers. The EF trends using Fe as the normaliser are similar to the trends for most other metals normalised by Al, Rb, and Silt. However, the (potential hydrodynamic or redox induced) enhancement of Co, Pb and Mn concentrations in sediment across part of the Mudflats influences the Fe normalised baseline model parameters and results in differences in EF trends for these metals in this part of the harbour. Ti is not considered an effective normaliser of metal concentrations in sediment of Richards Bay Harbour, as it is not correlated with the fine-grained fraction of sediment or other metal concentrations. However, if contamination is of a very high magnitude contaminated areas will be identified using different normalisers, regardless of the effectiveness of the

normalisers. The comparison of baseline models to Action List guidelines shows that baseline models reveal a wider area of contamination (e.g. Cu), thus leading to a better understanding of the system`s state.

The findings of this study highlight the need to investigate the utility of different normalisers before a decision is made on the most effective one. Different normalisers should not be expected to provide precisely the same understanding on metal enrichment of sediment, even if this might be an aspirational outcome. Small differences in sample processing and analysis, and biogeochemical processes in sediment, will lead to small differences in the identification of enrichment, especially if it is of a low magnitude. Further, baseline models should not be used as precise boundaries, to clearly delineate enriched from unenriched sediment. Certain normalisers might prove more effective for certain metals than others. This does not imply different normalisers should be used for different metals, but by investigating the utility of different normalisers anomalies in relationships for metals that allude to important features in the environment that need to be considered may be identified. The implication is that more than one, and preferably several potential normalisers should be analysed in studies focussing on metals in sediment if the aim is to identify enrichment that reflects contamination. Although the inclusion of several potential normalisers has financial implications from an analytical perspective, the ecological or management implications based on conclusions reached using a single (faulty) normaliser that might over- or underestimate enrichment may be significant and warrants such investment.

## Acknowledgements

This work was supported by the German Federal Ministry of Education and Research [grant number: 03F0798C] and is part of project TRACES (Tracing Human and Climate impact in South Africa) within the SPACES II Program (Science Partnerships for the Assessment of Complex Earth System Processes). The field work support by Andrew Green (University of KwaZulu-Natal), Peter Frenzel, Olga Gildeeva (both Friedrich-Schiller-University Jena) and George Best is gratefully acknowledged. We also thank Tammo Meyer (University of Greifswald) for providing help for sample digestion and Dirk Merten (Friedrich-Schiller-University Jena) for ICP-MS and -OES analyses.

## References

Amorosi A, Sammartino I, Tateo F (2007) Evolution patterns of glaucony maturity: A mineralogical and geochemical approach. Deep Sea Research Part II: Topical Studies in Oceanography 54:1364–1374. https://doi.org/10.1016/j.dsr2.2007.04.006

Balls PW, Hull S, Miller BS, Pirie JM, Proctor W (1997) Trace metal in Scottish estuarine and coastal sediments. Marine Pollution Bulletin 34:42–50. https://doi.org/10.1016/S0025-326X(96)00056-2

Begg G (1978) The estuaries of Natal: a resource inventory report to the Natal Town and Regional Planning Commission conducted under the auspices of the Oceanographic Research Institute, Durban. Natal Town and Regional Planning Report: 1–657

Birch GF, Snowdon RT (2004) The Use of Size-Normalisation Techniques in Interpretation of Soil Contaminant Distributions. Water, Air, & Soil Pollution 157:1–12. https://doi.org/10.1023/B:WATE.0000038854.02927.1f

Birch GF, Lee J-H, Tanner E, Fortune J, Munksgaard N, Whitehead J, Coughanowr C, Agius J, Chrispijn J, Taylor U, Wells F, Bellas J, Besada V, Viñas L, Soares-Gomes A, Cordeiro RC, Machado W, Santelli RE, Vaughan M, Cameron M, Brooks P, Crowe T, Ponti M, Airoldi L, Guerra R, Puente A, Gómez AG, Zhou GJ, Leung KMY, Steinberg P (2020) Sediment metal enrichment and ecological risk assessment of ten ports and estuaries in the World Harbours Project. Marine Pollution Bulletin 155:111129. https://doi.org/10.1016/j.marpolbul.2020.111129

Botha GA (2018) Lithostratigraphy of the late Cenozoic Maputaland Group. South African Journal of Geology 121:95–108. https://doi.org/10.25131/sajg.121.0007

Brunschön C, Haberzettl T, Behling H (2010) High-resolution studies on vegetation succession, hydrological variations, anthropogenic impact and genesis of a subrecent lake in southern Ecuador. Vegetation History and Archaeobotany 19:191–206. https://doi.org/10.1007/s00334-010-0236-4

Chapman PM, Wang F (2001) Assessing sediment contamination in estuaries. Environmental Toxicology and Chemistry 20:3–22. https://doi.org/10.1002/etc.5620200102

Coynel A, Gorse L, Curti C, Schafer J, Grosbois C, Morelli G, Ducassou E, Blanc G, Maillet GM, Mojtahid M (2016) Spatial distribution of trace elements in the surface sediments of a major European estuary (Loire Estuary, France): Source identification and evaluation of anthropogenic contribution. Journal of Sea Research 118:77–91. https://doi.org/10.1016/j.seares.2016.08.005

Cuven S, Francus P, Lamoureux SF (2010) Estimation of grain size variability with micro X-ray fluorescence in laminated lacustrine sediments, Cape Bounty, Canadian High Arctic. Journal of Paleolimnology 44:803–817. https://doi.org/10.1007/s10933-010-9453-1

Daskalakis KD, O'Connor TP (1995) Normalization and elemental sediment contamination in the coastal United States. Environmental Science and Technology 29:470–477

Demory F, Oberhänsli H, Nowaczyk NR, Gottschalk M, Wirth R, Naumann R (2005) Detrital input and early diagenesis in sediments from Lake Baikal revealed by rock magnetism. Global and Planetary Change 46 (1-4):145–166. DOI: 10.1016/j.gloplacha.2004.11.010.

Department of Environmental Affairs (2012) National Environmental Management: Integrated Coastal management Act, 2008 (Act No. 24 of 2008). National Action List for the screening of dredged material proposed for marine disposal in term of section 73 of the National Environmental Management: Integrated Coastal management Act, 2008 (Act No. 24 of 2008). Government Gazette:6–9

Dladla NN, Green AN, Cooper J, Mehlhorn P, Haberzettl T (2021) Bayhead delta evolution in the context of late Quaternary and Holocene sea-level change, Richards Bay, South Africa. Marine Geology 441:106608. doi: 10.1016/j.margeo.2021.106608

Du Laing G, Vandecasteele B, Grauwe P de, Moors W, Lesage E, Meers E, Tack FMG, Verloo MG (2007) Factors affecting metal concentrations in the upper sediment layer of intertidal reedbeds along the river Scheldt. Journal of Environmental Monitoring 9:449–455. https://doi.org/10.1039/B618772B

Förstner U (1989) Contaminated Sediments. Springer Berlin; Germany

Grant A, Middleton R (1998) Contaminants in Sediments: Using Robust Regression for Grain-Size Normalization. Estuaries 21:197. https://doi.org/10.2307/1352468

Greenfield R, Wepener V, Degger N, Brink K (2011) Richards Bay Harbour: metal exposure monitoring over the last 34 years. Marine Pollution Bulletin 62:1926–1931. https://doi.org/10.1016/j.marpolbul.2011.04.026

Haberzettl T, Corbella H, Fey M, Janssen S, Lücke A, Mayr C, Ohlendorf C, Schäbitz F, Schleser GH, Wille M, Wulf S, Zolitschka B (2007) Lateglacial and Holocene wet—dry cycles in southern Patagonia: chronology, sedimentology and geochemistry of a lacustrine record from Laguna Potrok Aike, Argentina. The Holocene 17:297–310. https://doi.org/10.1177/0959683607076437

Haberzettl T, Kirsten KL, Kasper T, Franz S, Reinwarth B, Baade J, Daut G, Meadows ME, Su Y, Mäusbacher R (2019) Using 210Pb-data and paleomagnetic secular variations to date anthropogenic impact on a lake system in the Western Cape, South Africa. Quaternary Geochronology 51:53–63. https://doi.org/10.1016/j.quageo.2018.12.004

Hanson PJ, Evans DW, Colby DR, Zdanowicz VS (1993) Assessment of elemental contamination in estuarine and coastal environments based on geochemical and statistical modeling of sediments. Marine Environmental Research 36:237–266. https://doi.org/10.1016/0141-1136(93)90091-D

Horowitz AJ (1991) A primer on sediment-trace element chemistry. Lewis Publishers Chelsea

Horowitz AJ, Elrick KA (1987) The relation of stream sediment surface area, grain size and composition to trace element chemistry. Applied Geochemistry 2:437–451. https://doi.org/10.1016/0883-2927(87)90027-8

Jung H-S, Lim D, Xu Z, Kang J-H (2014) Quantitative compensation of grain-size effects in elemental concentration: A Korean coastal sediments case study. Estuarine, Coastal and Shelf Science 151:69–77. https://doi.org/10.1016/j.ecss.2014.09.024

Jung H, Lim D, Xu Z, Jeong K (2016) Secondary grain-size effects on Li and Cs concentrations and appropriate normalization procedures for coastal sediments. Estuarine, Coastal and Shelf Science 175:57–61. https://doi.org/10.1016/j.ecss.2016.03.028

Kelbe B (2010) Hydrology and water resources of the Richards Bay EMF area

Kersten M, Smedes F (2002) Normalization procedures for sediment contaminants in spatial and temporal trend monitoring. Journal of Environmental Monitoring 4:109–115. https://doi.org/10.1039/b108102k

Koigoora S, Ahmad I, Pallela R, Janapala VR (2013) Spatial variation of potentially toxic elements in different grain size fractions of marine sediments from Gulf of Mannar, India. Environmental Monitoring and Assessment 185:7581–7589. https://doi.org/10.1007/s10661-013-3120-8

Krumgalz BS, Fainshtein G, Cohen A (1992) Grain size effect on anthropogenic trace metal and organic matter distribution in marine sediments. Science of The Total Environment 116:15–30. https://doi.org/10.1016/0048-9697(92)90362-V

Kylander ME, Ampel L, Wohlfarth B, Veres D (2011) High-resolution X-ray fluorescence core scanning analysis of Les Echets (France) sedimentary sequence: new insights from chemical proxies. Journal of Quaternary Science. 26:109–117. https://doi.org/10.1002/jqs.1438

Larrose A, Coynel A, Schäfer J, Blanc G, Massé L, Maneux E (2010) Assessing the current state of the Gironde Estuary by mapping priority contaminant distribution and risk potential in surface sediment. Applied Geochemistry 25:1912–1923. https://doi.org/10.1016/j.apgeochem.2010.10.007

Liang J, Liu J, Xu G, Chen B (2019) Distribution and transport of heavy metals in surface sediments of the Zhejiang nearshore area, East China Sea: Sedimentary environmental effects. Marine Pollution Bulletin 146:542–551. https://doi.org/10.1016/j.marpolbul.2019.07.001

Loring DH (1991) Normalization of heavy-metal data from estuarine and coastal sediments. ICES Journal of Marine Science 48:101–115. https://doi.org/10.1093/icesjms/48.1.101

Luoma SN (1990) Processes affecting metal concentrations in estuarine and coastal marine sediments. In: Furness, R.W., Rainbow, P.S. (Eds), Heavy Metals in the Marine Environment. CRC Press, Boca Raton.

Matys Grygar T, Popelka J (2016) Revisiting geochemical methods of distinguishing natural concentrations and pollution by risk elements in fluvial sediments. Journal of Geochemical Exploration 170:39–57. https://doi.org/10.1016/j.gexplo.2016.08.003

Matys Grygar T, Nováková T, Bábek O, Elznicová J, Vadinová N (2013) Robust assessment of moderate heavy metal contamination levels in floodplain sediments: a case study on the Jizera River, Czech Republic. Science of The Total Environment 452-453:233–245. https://doi.org/10.1016/j.scitotenv.2013.02.085

Matys Grygar T, Elznicová J, Bábek O, Hošek M, Engel Z, Kiss T (2014) Obtaining isochrones from pollution signals in a fluvial sediment record: A case study in a uranium-polluted floodplain of the Ploučnice River, Czech Republic. Applied Geochemistry 48:1–15. https://doi.org/10.1016/j.apgeochem.2014.06.021

Mehlhorn P, Viehberg F, Kirsten K, Newman B, Frenzel P, Gildeeva O, Green A, Hahn A, Haberzettl T (2021) Spatial distribution and consequences of contaminants in harbour sediments - A case study from Richards Bay Harbour, South Africa. Marine Pollution Bulletin 172:112764. https://doi.org/10.1016/j.marpolbul.2021.112764

Nel EL, Hill TR, Goodenough C (2007) Multi-Stakeholder Driven Local Economic Development: Reflections on the Experience of Richards Bay and the uMhlathuze Municipality. Urban Forum 18:31–47. https://doi.org/10.1007/s12132-007-9004-7

Newman BK, Watling RJ (2007) Definition of baseline metal concentrations for assessing metal enrichment of sediment from the south-eastern Cape coastline of South Africa. Water SA 33. https://doi.org/10.4314/wsa.v33i5.184089

Ohlendorf C, Fey M, Massaferro J, Haberzettl T, Laprida C, Lücke A, Maidana NI, Mayr C, Oehlerich M, Ramón Mercau J, Wille M, Corbella H, St-Onge G, Schäbitz F, Zolitschka B (2014) Late Holocene hydrology inferred from lacustrine sediments of Laguna Cháltel (southeastern Argentina). Palaeogeography, Palaeoclimatology, Palaeoecology 411:229–248. https://doi.org/10.1016/j.palaeo.2014.06.030

Rubio B, Nombela M, Vilas F (2000) Geochemistry of Major and Trace Elements in Sediments of the Ria de Vigo (NW Spain): an Assessment of Metal Pollution. Marine Pollution Bulletin 40:968–980. https://doi.org/10.1016/S0025-326X(00)00039-4

Sabadini-Santos E, Knoppers BA, Oliveira EP, Leipe T, Santelli RE (2009) Regional geochemical baselines for sedimentary metals of the tropical São Francisco estuary, NE-Brazil. Marine Pollution Bulletin 58:601–606

Santos IR, Silva-Filho EV, Schaefer CEGR, Albuquerque-Filho MR, Campos LS 2005: Heavy metal contamination in coastal sediments and soils near the Brazilian Antarctic Station, King George Island. Marine Pollution Bulletin 50 (2), S. 185–194. DOI: 10.1016/j.marpolbul.2004.10.009.

Saulnier I, Mucci A (2000) Trace metal remobilization following the resuspension of estuarine sediments: Saguenay Fjord, Canada. Applied Geochemistry 15:191–210. https://doi.org/10.1016/S0883-2927(99)00034-7

Schropp SJ, Windom HL (1988) A guide to the interpretation of metal concentrations in estuarine sediments coastal zone management section. Florida: Florida Department of Environmental Regulation

Schropp SJ, Lewis FG, Windom HL, Ryan JD, Calder FD, Burney LC (1990) Interpretation of Metal Concentrations in Estuarine Sediments of Florida Using Aluminum as a Reference Element. Estuaries 13:227. https://doi.org/10.2307/1351913

Sigg L, Stumm W (1996) Aquatische Chemie: eine Einführung in die Chemie wässriger Lösungen und natürlicher Gewässer. vdf, Hochschulverl.-AG an d. ETH Zürich

Szava-Kovats RC (2008) Grain-size normalization as a tool to assess contamination in marine sediments: is the <63 micron fraction fine enough? Marine Pollution Bulletin 56:629–632. https://doi.org/10.1016/j.marpolbul.2008.01.017

Taylor SR, McLennan SM (1981) The composition and evolution of the continental crust: rare earth element evidence from sedimentary rocks. Philosophical Transactions of the Royal Society A 301:381–399. https://doi.org/10.1098/rsta.1981.0119

Thomas C, Bendell-Young L (1999) The Significance of Diagenesis versus Riverine Input in Contributing to the Sediment Geochemical Matrix of Iron and Manganese in an Intertidal Region. Estuarine, Coastal and Shelf Science 48:635–647. https://doi.org/10.1006/ecss.1998.0473

Tůmová Š, Hrubešová D, Vorm P, Hošek M, Grygar TM (2019) Common flaws in the analysis of river sediments polluted by risk elements and how to avoid them: case study in the Ploučnice River system, Czech Republic. Journal of Soils and Sediments 19 (4), 2020–2033. DOI: 10.1007/s11368-018-2215-9.

Watling RJ (1977) Trace metal distribution in the Wilderness-lakes. CSIR Special Report FIS 147

Weisberg SB, Wilson HT, Heimbuch DG, Windom HL, Summers JK (2000) Comparison of sediment metal:aluminum relationships between the eastern and gulf coasts of the United States. Environmental Monitoring and Assessment 61:373–385. https://doi.org/10.1023/A:1006113631027

Wepener V, Vermeulen LA (2005) A note on the concentrations and bioavailability of selected metals in sediments of Richards Bay Harbour, South Africa. Water SA 31 (4):589–596. DOI: 10.4314/wsa.v31i4.5149.

Windom HL, Schropp SJ, Calder FD, Ryan JD, Smith Jr RG, Burney LC, Lewis FG, Rawlinson CH (1989) Natural trace metal concentrations in estuarine and coastal marine sediments of the southeastern United States. Environmental Science and Technology 23:314–320

Woods AM, Lloyd JM, Zong Y, Brodie CR (2012) Spatial mapping of Pearl River Estuary surface sediment geochemistry: Influence of data analysis on environmental interpretation. Estuarine, Coastal and Shelf Science 115:218–233. https://doi.org/10.1016/j.ecss.2012.09.005

Wündsch M, Biagioni S, Behling H, Reinwarth B, Franz S, Bierbaß P, Daut G, Mäusbacher R, Haberzettl T (2014) ENSO and monsoon variability during the past 1.5 kyr as reflected in sediments from Lake Kalimpaa, Central Sulawesi (Indonesia). The Holocene 24:1743–1756. https://doi.org/10.1177/0959683614551217

Zolitschka B, Fey M, Janssen S, Maidana NI, Mayr C, Wulf S, Haberzettl T, Corbella H, Lücke A, Ohlendorf C, Schäbitz F (2019) Southern Hemispheric Westerlies control sedimentary processes of Laguna Azul (south-eastern Patagonia, Argentina). The Holocene 29:403–420. https://doi.org/10.1177/0959683618816446

# Chapter 4

# Bayhead delta evolution in the context of late Quaternary and Holocene sea-level change, Richards Bay, South Africa

N.N. Dladla[a], A.N. Green[a,b], J.A.G. Cooper[a,b], P. Mehlhorn[c], T. Haberzettl[c]

[a] Geological Sciences, School of Agricultural, Earth and Environmental Sciences, University of KwaZulu-Natal, South Africa

[b] School of Geography and Environmental Sciences, Ulster University, United Kingdom

[c] Physical Geography, Institute for Geography and Geology, University of Greifswald, Germany

Published in: Marine Geology 441 (2021) 106608

Marine Geology 441 (2021) 106608

Contents lists available at ScienceDirect

Marine Geology

journal homepage: www.elsevier.com/locate/margo

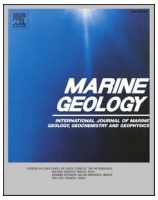

# Bayhead delta evolution in the context of late Quaternary and Holocene sea-level change, Richards Bay, South Africa.

N.N. Dladla [a,*], A.N. Green [a,b], J.A.G. Cooper [a,b], P. Mehlhorn [c], T. Haberzettl [c]

[a] Geological Sciences, School of Agricultural, Earth and Environmental Sciences, University of KwaZulu-Natal, South Africa
[b] School of Geography and Environmental Sciences, Ulster University, United Kingdom
[c] Physical Geography, Institute for Geography and Geology, University of Greifswald, Germany

ARTICLE INFO

Editor: Edward Anthony

*Keywords:*
Bayhead delta
Incised valleys
Backstepping
Meltwater pulses
Antecedent gradient

ABSTRACT

Richards Bay is part of a back-barrier lagoon fronted by high coastal dunes on the NE, Indian Ocean coast of South Africa. In the early 1970s, a berm was constructed, dividing the original Mhlathuze Estuary into two separate systems; the Richards Bay Harbour and the new Mhlathuze Estuary. This study investigates the stratigraphic evolution of the incised valley system and bayhead delta in the Richards Bay Harbour segment. Seven seismic units (Units 1–7) were imaged. A single regionally developed sequence boundary (SB) along with two tidal ravinement surfaces (tRS1 and tRS2) were identified. Surface SB is associated with the LGM lowstand which developed when sea levels were ~ 130 m below present, until ~18,000 year BP. Cretaceous age siltstones (Unit 1) form the basement. Transgressive material overlying SB (Unit 2) reflects the filling of an incised valley located in the middle segment of a wave-dominated back-barrier system. It is overlain by a bayhead delta (Unit 3), the geometry and seismic signature of which indicate alternating periods of aggradation/progradation and backstepping. The behaviour is attributed to episodic jumps in sea-level, and is tentatively (on the basis of elevations in relation to the regional sea-level curve) linked to periods of rapidly rising sea-level (8.2 ka event and Meltwater Pulse (MWP)-1d). These intervals of rapidly rising sea-level, combined with relatively low gradient settings facilitated backstepping of the delta. Fills (Unit 4) occur within minor incisions along the delta top. These are interpreted as distributary channels that fed sediment to the seaward edge of the bayhead delta system. Elongated mounds on the seafloor (Unit 5) are interpreted as spoil from contemporary port dredging. Slump deposits (Unit 6) along the delta front are attributed to a combination of oversteepening of the delta by dredging, as well as deposition of modern sediments brought into the system by tidal currents. The system is capped by fine-grained, tidally redistributed and deposited sediments (Unit 7) which were possibly sourced from older organic material of an indeterminate source. This site is especially sensitive to episodic rates of sea-level change due to the relatively small Glacial Isostatic Adjustments (GIA) during the postglacial transgression and the flat antecedent gradients of both the subaerial unconformity and the overlying tidal ravinement.

## 1. Introduction

Bayhead deltas are defined as fluvially-dominated deltas that prograde into a semi-enclosed body of marine water (Nichol et al., 1997). On a transgressive coastline bayhead deltas form where the rate of sediment input from a fluvial source surpasses the rate of sea-level rise (Aschoff et al., 2018). As such, bayhead deltas are an integral component of most classic wave-dominated lagoon/embayment systems (Dalrymple et al., 1992). They provide a link between the fluvial and central basin depositional environments of many incised valley systems (Simms and Rodriguez, 2015). However, they are not restricted to incised valley systems (Bhattacharya and Giosan, 2003) and also form in fjords, structural basins, interdistributary bays, and other backbarrier environments (see Simms et al., 2018).

In most cases, fluvial systems associated with bayhead deltas provide the majority of the sediment and freshwater input to the upper portions of these systems (Smith et al., 2013). They are also an important part of the rock record, providing vital information for sequence stratigraphic models, and play host to important hydrocarbon reservoirs worldwide (Simms et al., 2018). Many ports and coastal cities are also partly constructed on bayhead deltas, underlining the importance of these shallow and flat-lying areas for land reclamation.

* Corresponding author.
*E-mail address:* dladlan2@ukzn.ac.za (N.N. Dladla).

https://doi.org/10.1016/j.margeo.2021.106608
Received 3 June 2021; Received in revised form 12 August 2021; Accepted 17 August 2021
Available online 20 August 2021

Here we document the stratigraphic evolution of a bayhead delta and incised valley system on which one of the busiest ports in Africa, Richards Bay Harbour, is situated. The purpose of this study is to: (1) provide a detailed and complete stratigraphic framework of the underlying incised valley network of the palaeo-Mhlatuze Estuary, now the site of Richards Bay Harbour; (2) describe the stratigraphic evolution of the backbarrier system and its bayhead delta and (3) determine the process and controls on bayhead delta backstepping in the local context of sea-level change.

## 2. Regional setting

### 2.1. Physiography

The Richards Bay Harbour is situated on the subtropical northeast coast of South Africa (approximately 28°47′55.15" S, 32°03'26.71" E) and lies adjacent to the Mhlathuze Estuary (Fig. 1). Before the harbour was developed, the two systems comprised a single large lagoonal system (Weerts and Cyrus, 2002) connected to the Indian Ocean via a narrow inlet roughly in the location of the modern harbour entrance (Jerling, 2003) (Fig. 1).

The original estuary system had five rivers flowing into it, the Mhlathuze, Bhizolo, Mzingazi, Mtantatweni and Manzinyama rivers (Jerling, 2003), of which the west-east-trending Mhlathuze River was dominant. The construction of a berm that divided the estuary into two systems, commenced in 1972 and allowed the two embayments to now function independently, with two separate inlets (Fig. 1) situated 4 km from each other (Weerts and Cyrus, 2002). The Mhlathuze River was redirected to flow into the new Mhlathuze Estuary and not into the harbour (Jerling, 2003), though a small channel still occurs where the palaeo-Mhlatuze River had previously entered. Large portions of the former back-barrier have now been reclaimed and converted into various docks and industrial spaces (Fig. 1).

To the north of the harbour lies Lake Mzingazi, which enters the system via the Mzingazi Canal (Weerts et al., 2014). Apart from the tidal inlets, the system is separated from the Indian Ocean by a peninsula comprising a coastal dune-ridge with an elevation of approximately 20–30 m to its west and 5 m in the east (Maud and Orr, 1975).

### 2.2. Hydrodynamic regime

Semi-diurnal tides dominate the northern KwaZulu-Natal coastal plain. The neap tidal range in the Richards Bay area is 0.52 m, whereas the mean spring range is approximately 1.80 m (Schoonees et al., 2006). The KwaZulu-Natal coast is thus described as microtidal (Davies, 1964) or lower mesotidal (Hayes, 1979; cf. Flemming, 2005).

The open coast is dominated by high energy waves (Salzmann and Green, 2012). The average significant wave height offshore Richards Bay is 1.5 m (Moes and Rossouw, 2008) and there are only small seasonal changes in wave height and direction (Rossouw, 1984). For approximately 40% of the time, southeast prevailing high-amplitude swells are dominant in the area (Begg, 1978; Rossouw, 1984). However, when northeasterly winds prevail, low-amplitude and short period waves develop for a further 40% of the time (Van Heerden and Swart, 1986). Offshore the harbour, the middle to outer shelf is dominated by the Agulhas Current, a swiftly-flowing western boundary current that can reach speeds of up to 2 m s-1

(Lutjeharms, 2006) and which removes most of the sediment that accumulates along the shelf edge since the early Holocene (Flemming, 1981).

Schoonees et al. (2006) outline both the swell and wind-wave climate of the harbour interior. Significant wave heights in the centre of the main channel (Fig. 1) were modelled and values of 0.7 m and 1.1 m obtained for return periods of 1 and 100 years respectively. Wave penetration decreases substantially to landward in the backbarrier (Schoonees et al., 2006).

### 2.3. Fluvial sediment load

Before the development of the Richards Bay Harbour, the Mhlathuze River delivered a sediment load of approximately 20,500 $m^3$ pear year to the unaltered estuary (Anon, 1972, cited in Weerts, 2002). Subsequent to the harbour development, this increased to approximately 237,000 $m^3$ per annum in the now separated Mhlatuze estuary to the south (Huizinga and Van Niekerk, 2000, cited in Weerts, 2002). Sediment delivery to the current harbour is limited to almost entirely marine materials (Begg, 1978), with very little fluvial sediment entering the system (Cloete and Oliff, 1976).

## 3. Methods

### 3.1. Seismic reflection data

This study focuses on a series of incised valleys and sedimentation related to the palaeo-Mhlatuze River entrance to the Richards Bay backbarrier system. High resolution, single-channel seismic data were collected using a Design Projects Boomer and a 20-element hydrophone array at a power level of 175 J. Data were collected along coastal strike with a line spacing of 25–50 m. Several tie lines were collected down-dip with a line spacing of ≤200 m totalling approximately 180 line kilometres (Fig .1). These data were recorded using the Hypack™ hydrographic software package and positioning was achieved using a Real Time Kinematic DGPS of ~ decimetre accuracy. The raw seismic data were processed using the Hypack SBP utility. Bandpass filtering and time-varied gains were applied to all data. Constant sound velocities in water (1500 ms − 1) and sediment (1650 ms − 1) were used to extrapolate the time-depth conversions. Post-processing, the vertical resolution of the Boomer system is between 0.5 and 0.7 m. All data were interpreted according to standard seismic stratigraphic principles (Mitchum and Vail, 1977).

### 3.2. Bathymetry

Multibeam bathymetry data were collected using a Norbit iWBMS narrow beam multibeam echosounder with an integrated Applanix Wavemaster II inertial navigation unit. Sound velocity in water was measured using an AML Base X system, and tides were corrected in real time using the RTK GPS position. All data were processed in Hypack and the final product exported as 0.5 × 0.5 m grid.

### 3.3. Coring and sediment sampling

Several gravity cores were collected to sample some of the key seismic surfaces and facies observed in the seismic records. The cores were collected using a Uwitec large-gauge gravity corer with an 86 mm diameter barrel. The cores were split, described, photographed, and sampled for AMS $C^{14}$ dating. Samples of organic sediment were sent for radiocarbon analysis from two cores, RBH-18-23 and RBH-18-18. All samples were calibrated using the marine20.14c model (Heaton et al., 2020), with a reservoir effect of 716 ±26 years (Maboya et al., 2018).

## 4. Results

### 4.1. Bathymetry

The study area encompasses a shallow, low-gradient intertidal-subtidal bayhead delta of sediment adjacent to the entry point of the palaeo-Mhlatuze River into the Richards Bay Harbour. The platform is fringed landward by mangroves and is modified along its southeastern and northeastern margins by regular seafloor dredging (Fig. 2). A clear, planar morphology is evident, with the platform widening seaward (Fig. 2). Platform elevations range from +1 m MSL along the mangrove fringes in the northwest of the study area, to −24 m where the bayhead

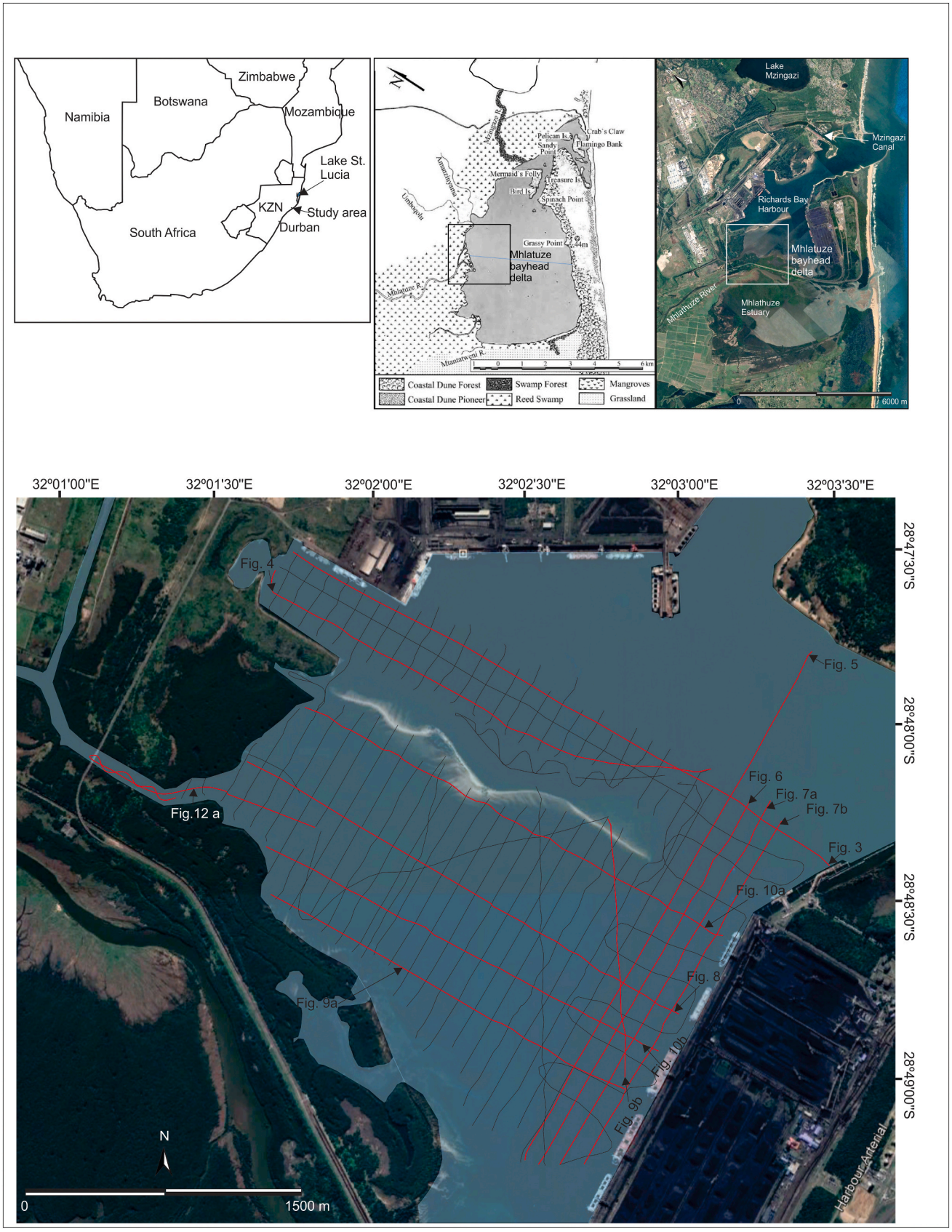


**Fig. 1.** Locality map of the study area, outlining the Richards Bay Harbour situated on the northeast coast of South Africa. Note the pre- and post-harbour development geomorphology of the system (top right).

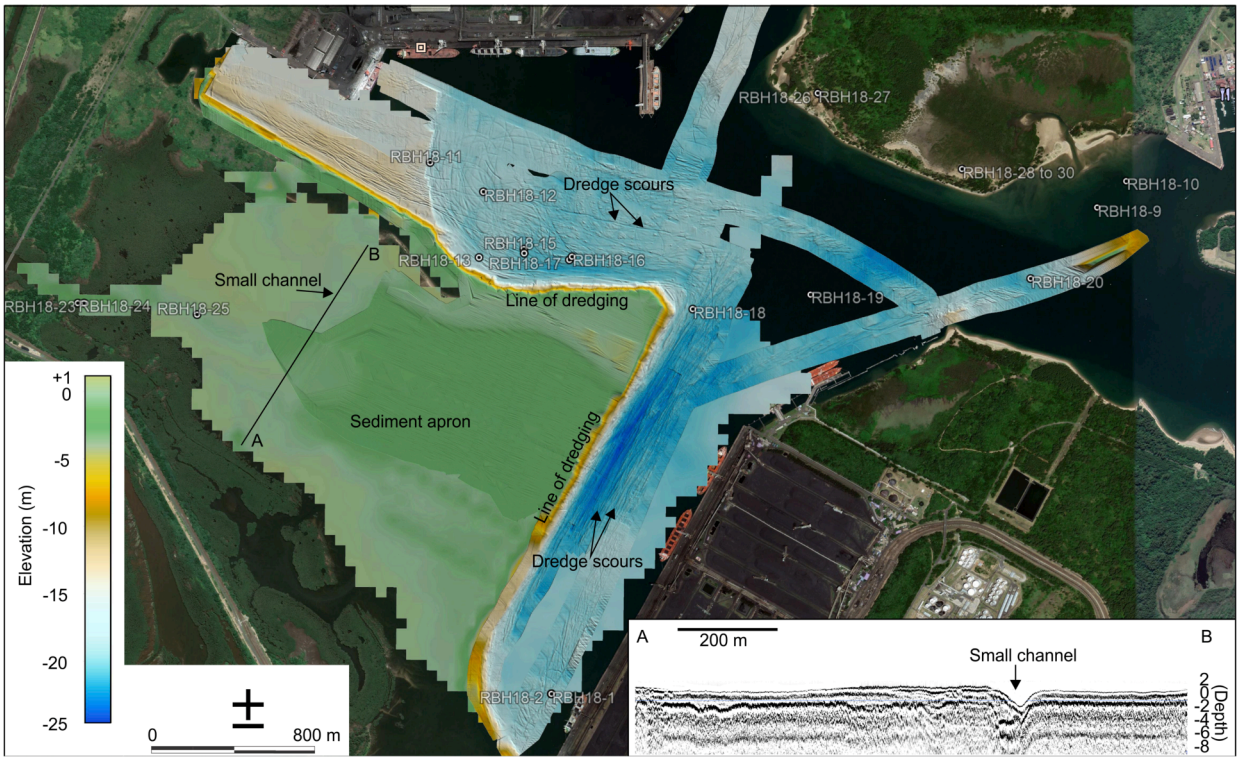


**Fig. 2.** Multibeam bathymetry of the study area with core locations. Note the clear apron-like morphology that is between +1 to −10 m in elevation. The platform is modified along its southeastern and northeastern margins by seafloor dredging (clear irregular lines in the bathymetry). Note the presence of small channels ≤2 m deep in the northeastern portions of the study area (lower right inset A to B). These are near imperceptible at the scale presented in the bathymetry and at the gridding resolution of the shallow water areas.

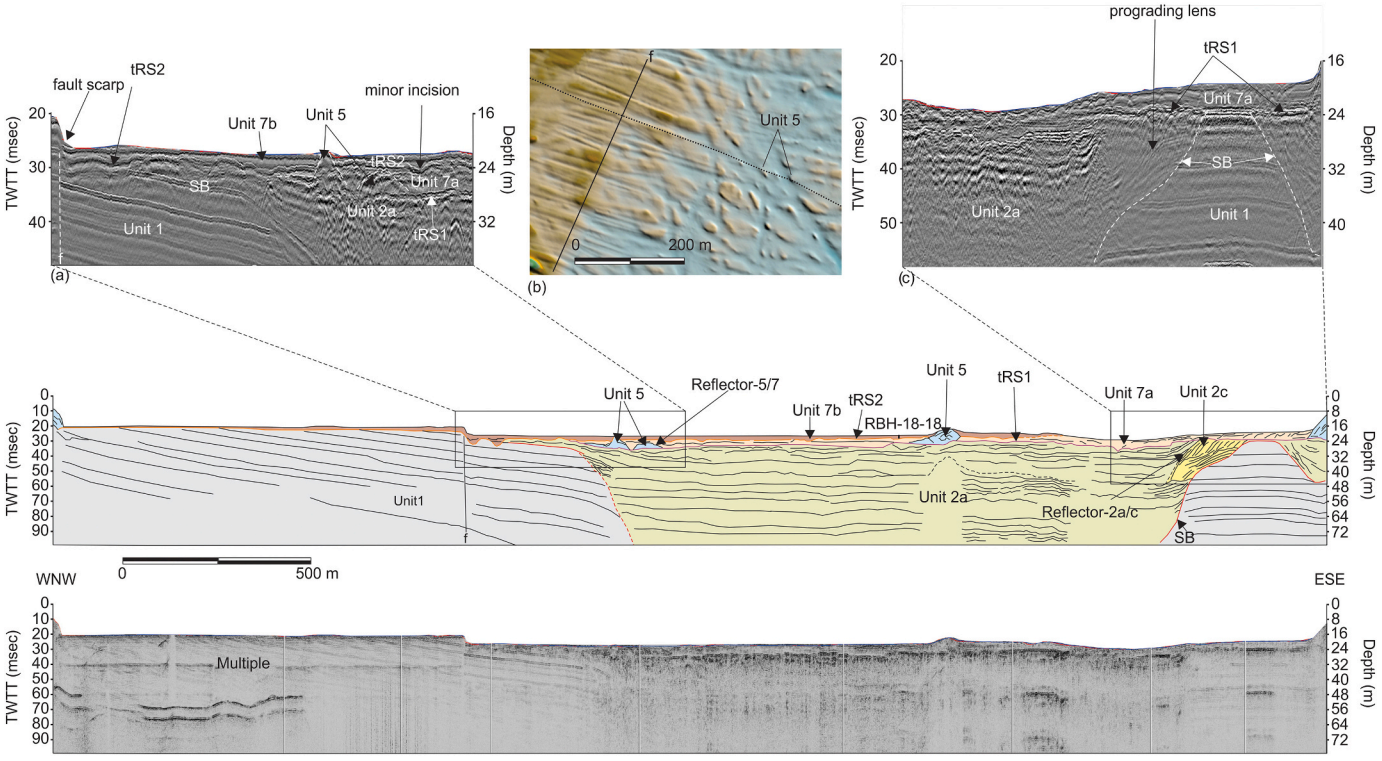


**Fig. 3.** WNW-ESE seismic profile displaying interpreted (top) and raw (bottom) seismic data. Unit 2a dominates the incised valley fill. Units 2b, 3, 4 and 6 are absent from this seismic line. Enlarged seismic data (insets a and c) show the three major surfaces (SB, tRS1 and tRS2). A prograding bedform (Unit 2c) is truncated by tRS1 (Fig. 3c). The seafloor is displaced by faulting. Note the minor incisions formed by tRS2. Inset b shows the modern-day seabed corresponding to inset a (dashed line), with pinnacles of intact or more cohesive material surrounded by dredge scars. These correspond to Unit 5. The fault scarp at the seabed is labelled f. Note the position of core RBH-18-18.

delta drops off steeply and where dredging is common in the main shipping channels. A series of shallow channels incise the surface of the platform. They are up to 100 m-wide and ≤ 2 m deep. These extend from the current channel that enters the port, to the southeastern terminus of the platform (Fig. 2), decreasing in relief until they are barely perceptible in the gridded bathymetry.

### 4.2. Seismic stratigraphy

Seven seismic units (Unit 1–7) were imaged beneath Richards Bay Harbour (Figs. 3-10). Of these, Units 2 and 7 are subdivided into a number of sub-units (e.g. Unit 2a, b and c) (Figs. 3 and 4). Acoustic reflectors separate these units from each other (e.g. Reflector-1/3 separates Unit 1 and Unit 3). Unit 1 is separated from the overlying units by Surface SB. Unit 2 occurs between Surface SB and tRS1. Units 3, 4 and 6 occur above Reflector-1/3 and crop out on the seabed. Unit 5 occurs between tRS1 and tRS2 or between tRS1 and the seabed, and Unit 7a occurs between tRS1 and tRS2 or between tRS1 and the seabed. Unit 7b exclusively occurs between tRS2 and the seabed. The elevations of the main seismic surfaces are presented in Fig. 11.

Unit 1

Unit 1 is the oldest unit resolved in the study area. This unit is characterised by continuous, parallel, seaward dipping and prograding reflectors of moderate amplitude. These reflectors are truncated by high amplitude erosional surfaces SB and tRS1 or tRS2 (Figs. 3-10) or may crop out on the seabed (Figs. 4 and 7b). In places, this unit also directly underlies Unit 3, where the lateral extent of Surface SB is unknown (Figs. 8-10). The maximum thickness of this unit cannot be determined but is at least 58 m.

Unit 2

Unit 2 occurs as fills within incisions of Surface SB. This unit is subdivided into three sub-units (2a, b and c) which are present to varying degrees throughout the study area.

Unit 2a

Unit 2a occurs throughout the study area, forming the majority of the valley fills (Figs. 3-10). It mainly manifests itself as aggrading/draping reflectors of low to moderate amplitude (e.g. Fig. 3-7 and 9a). These either onlap Surface SB (Figs. 3-7 and 9a) or Reflector-2a/c (Figs. 3, 5-7a). In some incisions, these reflectors are randomly oriented, showing no particular configuration (e.g. Figs. 7b and 10), while in others they are sigmoidal to oblique-parallel. They downlap Surface SB and onlap Reflector- 2a/b (Figs. 8 and 9b). In all instances, reflectors of Unit 2a are truncated by the overlying tRS1. The average thickness of this unit cannot be determined as its basal surface is mainly beyond the penetration depth of the Boomer but appears to reach maximum thicknesses of more than 30 m.

Unit 2b

Unit 2b occurs sporadically in the study area, comprising low amplitude, concave down to oblique-parallel, valley-flank attached reflectors which form mounds (Figs. 7a, 8 and 9). These reflectors onlap and downlap Surface SB. Where present, this unit is mainly attached to only one valley-flank and is separated from Unit 2a by Reflector-2a/b. This unit attains a maximum thickness of 2.5 m.

Unit 2c

Unit 2c occurs as lenses of prograding, sigmoid to oblique-parallel reflectors of low to moderate amplitude (Figs. 3, 5-7a and 10). These onlap Surface SB and downlap Reflector-2a/c. In all cases, this unit is truncated by tRS1 and is mainly attached to incised valley-flanks. This unit is 4 to 8 m thick and lies approximately 24 m below sea-level.

Unit 3

With a maximum thickness of 22 m, Unit 3 consists of continuous, high to moderate amplitude, aggrading and prograding reflectors (Figs. 8-10). The unit is overall planar, with very flat topsets confined to the distal margins. Clinoforms of this unit aggrade and also backstep, with successive rollovers initiated further landwards and at shallower elevations. They all prograde into and over the underlying incised valley fill of Unit 2 (Figs. 8-10). Along the delta bottomsets, the reflectors are sub-parallel, exhibiting dip angles of 6 to 11° and either abut against Unit 6 (Figs. 8, 9b and 10b) or intercalate with Unit 7 (Figs. 9a and 10a). The rollover of Unit 3's clinoforms are associated with three distinct

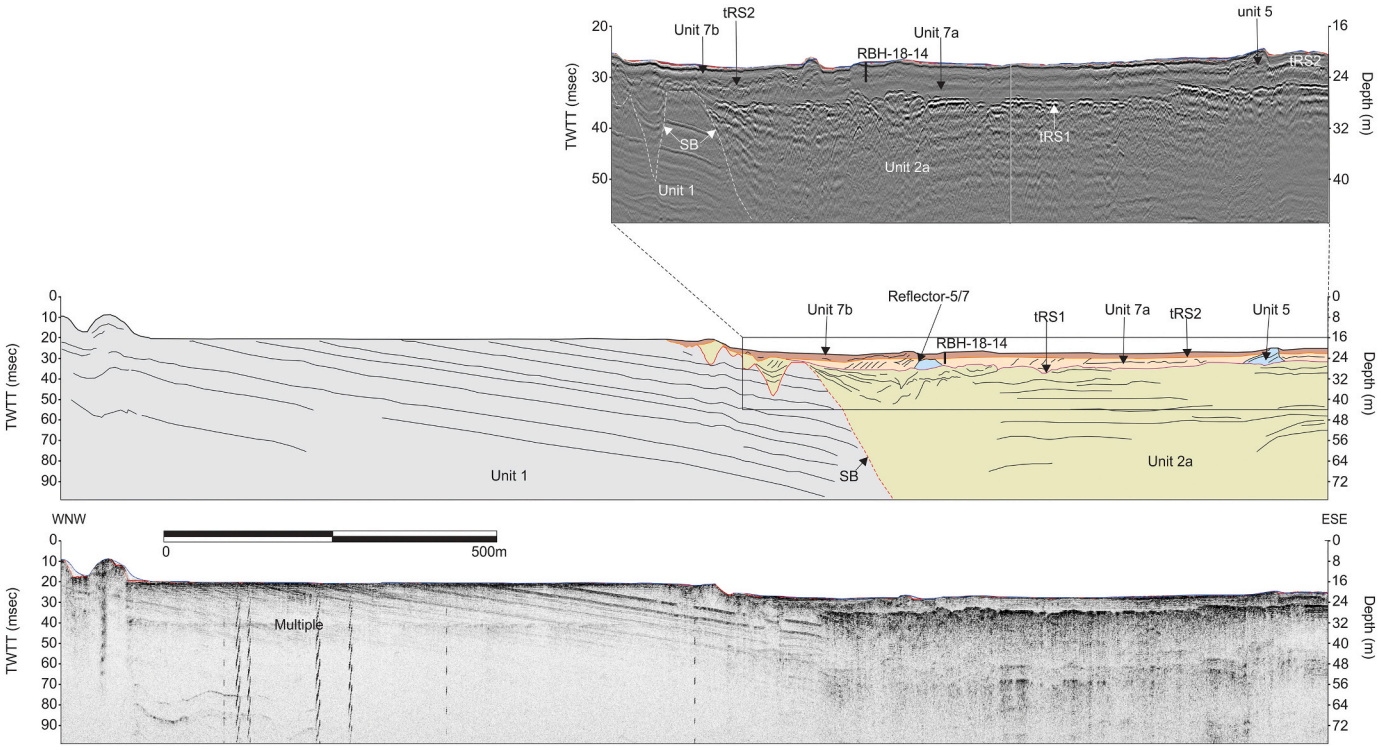


**Fig. 4.** WNW-ESE seismic profile displaying interpreted (top) and raw (bottom) seismic data. Units 2b, 2c, 3, 4 and 6 are absent from this seismic line. Unit 2a dominates the fills. Enlarged seismic data clearly show the LGM-age incisions (SB), tRS1 and tRS2. Note the position of core RBH-18-14.

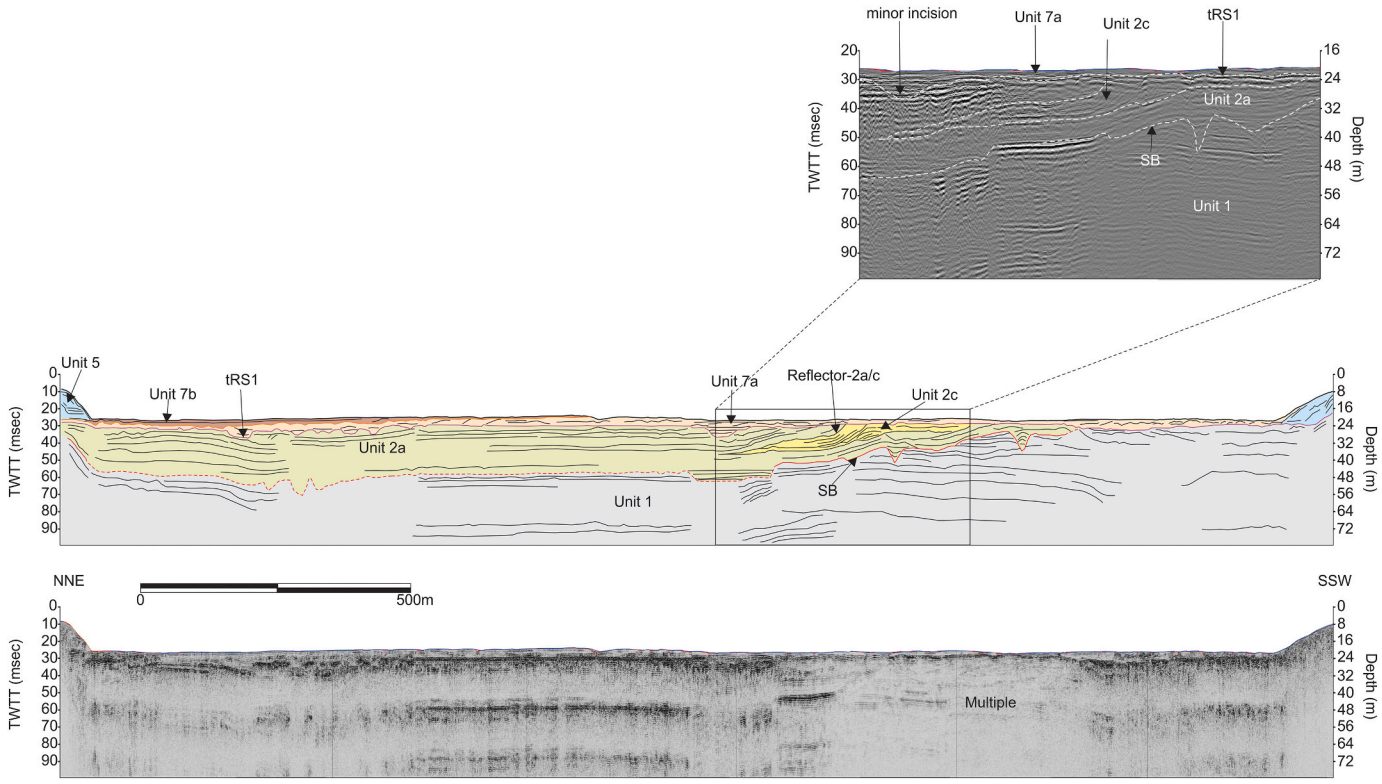


**Fig. 5.** NNE-SSW seismic profile displaying interpreted (top) and raw (bottom) seismic data. Only Units 1, 2a, 2c, 5, and 7 are present on this seismic line. All major surfaces are also noted. The enlarged seismic data show the prograding tidal bedform attached to tRS1. Note the numerous minor incisions formed by tRS1.

elevations at ~ −12.5 m, ~ −11 m and ~ −7.5 m (Fig. 11f).

Unit 4

Unit 4 forms fills within small, isolated incisions (Fig, 8, 9b and 10b). These incisions are exclusively found within the upper portions of Unit 3 and reach depths of 7–15 m (Fig. 11). This unit comprises low to moderate amplitude, aggrading to concave up reflectors.

Unit 5

Unit 5 forms as isolated mounds with chaotic, high amplitude reflectors showing no particular configuration (Figs. 3-6). These mounds are found within or crop out of Unit 7 and lie directly on tRS1. These form small peaks on the seafloor, surrounded by contemporary furrows formed by active dredging (Fig. 3b).

Unit 6

Unit 6 forms adjacent to Unit 3 and comprises moderate to high amplitude, randomly oriented to sigmoid parallel reflectors (Figs. 8, 9b and 10b). These may either onlap Reflector-2/6 (e.g. Fig. 8) or Reflector-3/6 (e.g. Figs. 9b and 10b). This unit reaches maximum thicknesses of approximately 10 m.

Unit 7

Capping most incised valleys is Unit 7, which can be divided into two sub-units (7a and b). This unit may either be laterally extensive or may pinch out landward or seaward.

Unit 7a

Unit 7a occurs throughout the study area and consists of aggrading and prograding, moderate to low amplitude reflectors (Figs. 3-10). The reflectors are mostly parallel and, drape the depressions formed by the underlying tRS1 surface (e.g. Fig. 5). They may also be sigmoidal, discontinuous, randomly oriented or show no particular internal configuration (Fig. 3-10). Where sigmoidal, they downlap tRS1 and in places, onlap Reflector-6/7 (Fig. 9b and 10b). This unit underlies tRS2 (Figs. 3-5 and 9a) and may be up to 5.5 m thick.

Unit 7b

Where present, Unit 7b lies directly above Unit 7a (Figs. 3-5 and 9a). This unit comprises very low to low amplitude reflectors with no apparent configuration. The unit pinches out landward and/or seaward and attains a maximum thickness of approximately 2 m.

Stratigraphic surfaces

Three major stratigraphic surfaces characterise the study area (SB, tRS1 and tRS2). Their orientation, depth and attributes are shown in Fig. 11. Throughout the study area, reflectors of Unit 1 are erosionally truncated by the high amplitude, continuous, rugged, undulating Surface SB. Numerous incisions of various widths and depths characterise this surface. The incisions in Surface SB either trend N-S or W-E and reach depths greater than 40 m (Fig. 11a).

Surface tRS1 occurs throughout the study area. This erosional surface is characterised by the presence of numerous minor incisions and may either be limited to the major incised valley network (Figs. 8-10) or may extend laterally beyond the incised valleys where it merges with SB on the incision interfluves (Figs. 3-7). Where Units 3 and 6 are present, tRS1 abuts gently against either of them (Figs. 8-10). Surface tRS1 reaches depths of ~29 m (Fig. 11b). The combined tRS1 and SB surfaces (over which unit 3 progrades) are generally flat (Fig. 11c), with an average gradient of ~0.1°. Local gradients of this combined surface increase where there has been excavation by subsequent erosion during formation of tRS2 to remove tRS1. This usually occurs where pronounced valleys are present in SB.

As mentioned, surface tRS2 is erosional, consisting of numerous minor incisions and small scarps. This surface is not continuous across the system (Figs. 3-5 and 9a). Surface tRS2 extends to a depth of ~24 m (Fig. 11d). The small channels that house Unit 4 reach depths of 15 m relative to mean sea-level (Fig. 11e).

Faults

A number of prominent normal faults are recognised in the study area. They are visible in the NNE-SSW (e.g. Figs. 6 and 7a) and WNW-ESE (Fig. 3) trending seismic lines as well as the N-S trending seismic line (Fig. 9b). Most of these faults occur within Unit 1 (Figs. 3, 6, 7a and

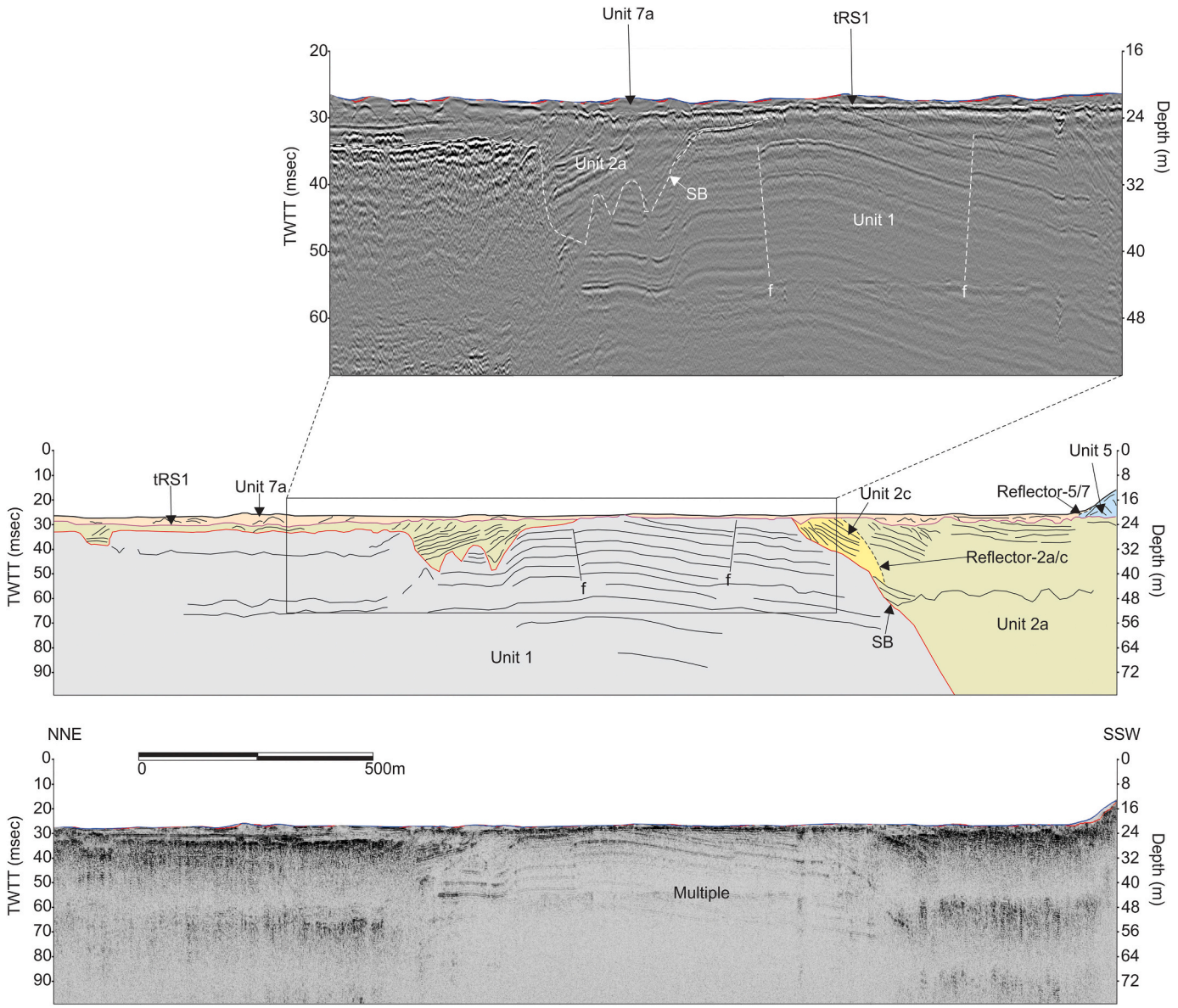


**Fig. 6.** NNE-SSW seismic profile displaying interpreted (top) and raw (bottom) seismic data. Only Units 1, 2a, 2c, 5 and 7a are present on this seismic line. Note the absence of tRS2. Enlarged seismic data clearly show the prominent faulting that characterises the area.

9b), with a single fault observed within the incised valley fill itself (Unit 2a) in Fig. 7a. In some instances, the faults influence the seabed morphology, displacing the seafloor by approximately 2 m (e.g. Fig. 3a and b).

### 4.3. Core lithology

The cores grouped in the landward-most part of the study site (RBH-18-23 and 24) are dominated by rhythmically interbedded silts and clays, with occasional sandy laminae and regular organic-rich horizons (Fig. 12). Occasional, high-angle plan cross-bedded sandy laminae occur. Towards the core tops, burrows are apparent. Core RBH-18-25 collected from the more distal parts of the platform-top channel is more organic-rich, with few laminations present and a lack of rhythmic interbedding (Fig. 12). Occasional shell debris occurs, marking very crude, flat-lying beds. Mottling and burrowing are common in the upper portions of the core where the sand content increases to medium sands with larger, grit-sized (2–4 mm) shell fragments. These cores intersect only Unit 7b. The landward expression of Unit 7b appears (Fig. 12a) sedimentologically different to the more seaward variant, as described below.

In the main dredge depression, cores RBH-18-18, RBH-18-11, RBH-18-12 and RBH-18-14 show similar alternating dark black and light brown silty laminations (Fig. 12b). RBH-18-14 has a brown, clay-rich basal section with very faint black laminae. Flat-lying sand lenses up to 1 cm-thick occur sporadically. Above the stratigraphically highest lens (~ 1.3 m downcore) the core comprises uniform brown clay which is sharply overlain by rhythmic interbeds of black and brown clays. These grade into dark black clays with stratigraphic height. The core intersects both Unit 7a and b (Fig. 4), with tRS2 reconciled to the uppermost sand lens at 92 cm downcore (Fig. 12b).

The deepest parts of RBH-18-12 intersect a basal set of dark black clay laminae which are sharply overlain by a faintly laminated brown clay with gently inclined sandy layers (Fig. 12b). This grades vertically into a dark brown and light brown interbedded clay unit. The core intersects tRS2 which is marked by a cm-thick sandy layer. Unit 7b can be reconciled with the lower, faintly laminated brown clay, and Unit 7a the overlying darker materials. RBH-18-11 consists almost entirely of the

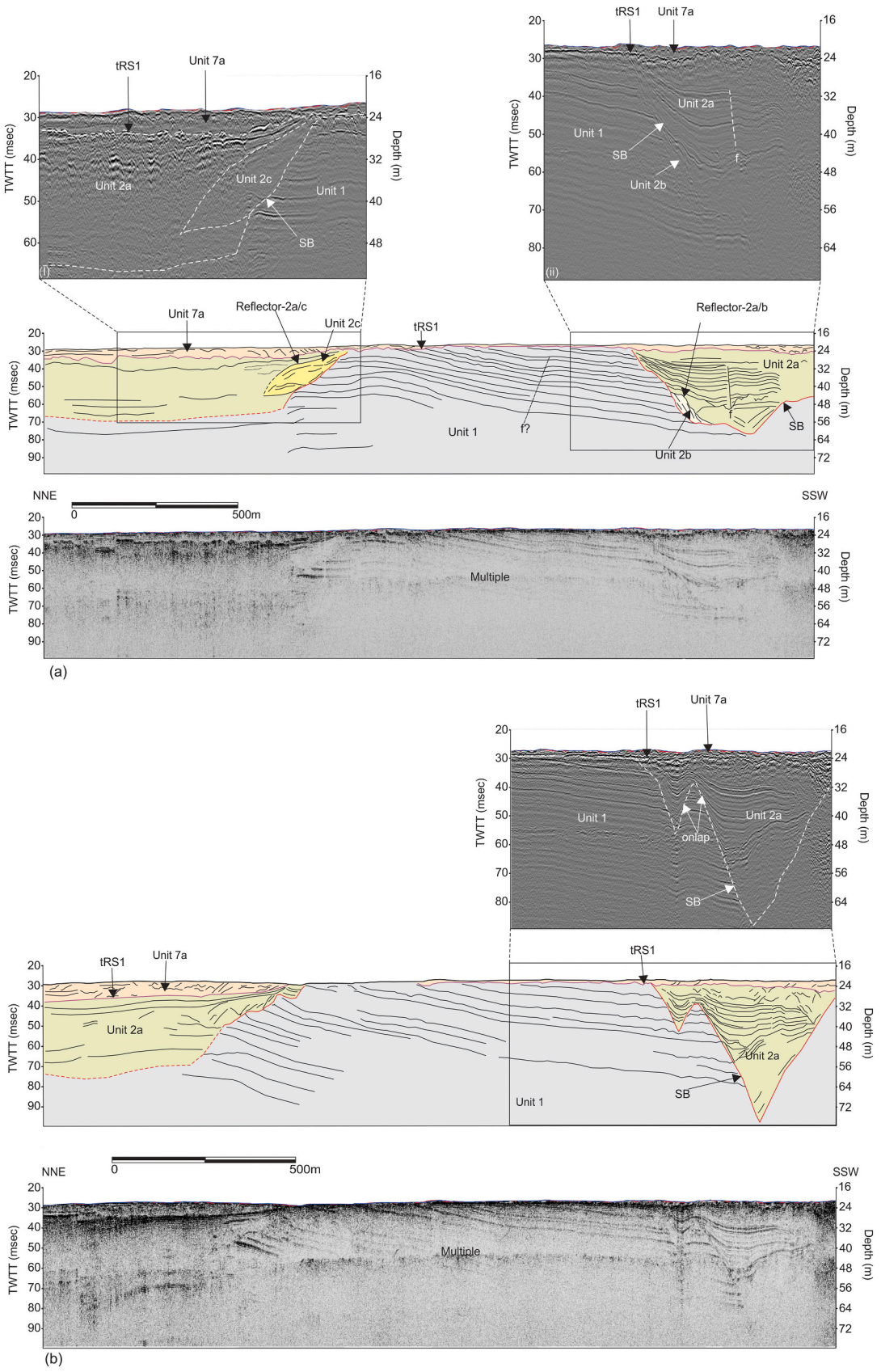


**Fig. 7.** (a) Shows a NNE-SSW seismic profile displaying interpreted (top) and raw (bottom) seismic data. Units 3, 4, 5, 6, 7b, as well as surface tRS2 are absent from this seismic line. Possible faulting of Unit 1 is observed. a(i) Shows the prograding bedform attached to tRS1. a(ii) Shows faulting within the incision itself. Draping fills dominate the incised valley. (b) Shows a WNW-ESE seismic profile displaying interpreted (top) and raw (bottom) seismic data. Only Unit 1, 2a and 7a are present on this seismic line. The incised valley fill may have randomly oriented or aggrading draping reflectors. Note the randomly oriented reflectors of Unit 7a. Surface tRS2 is absent from this line.

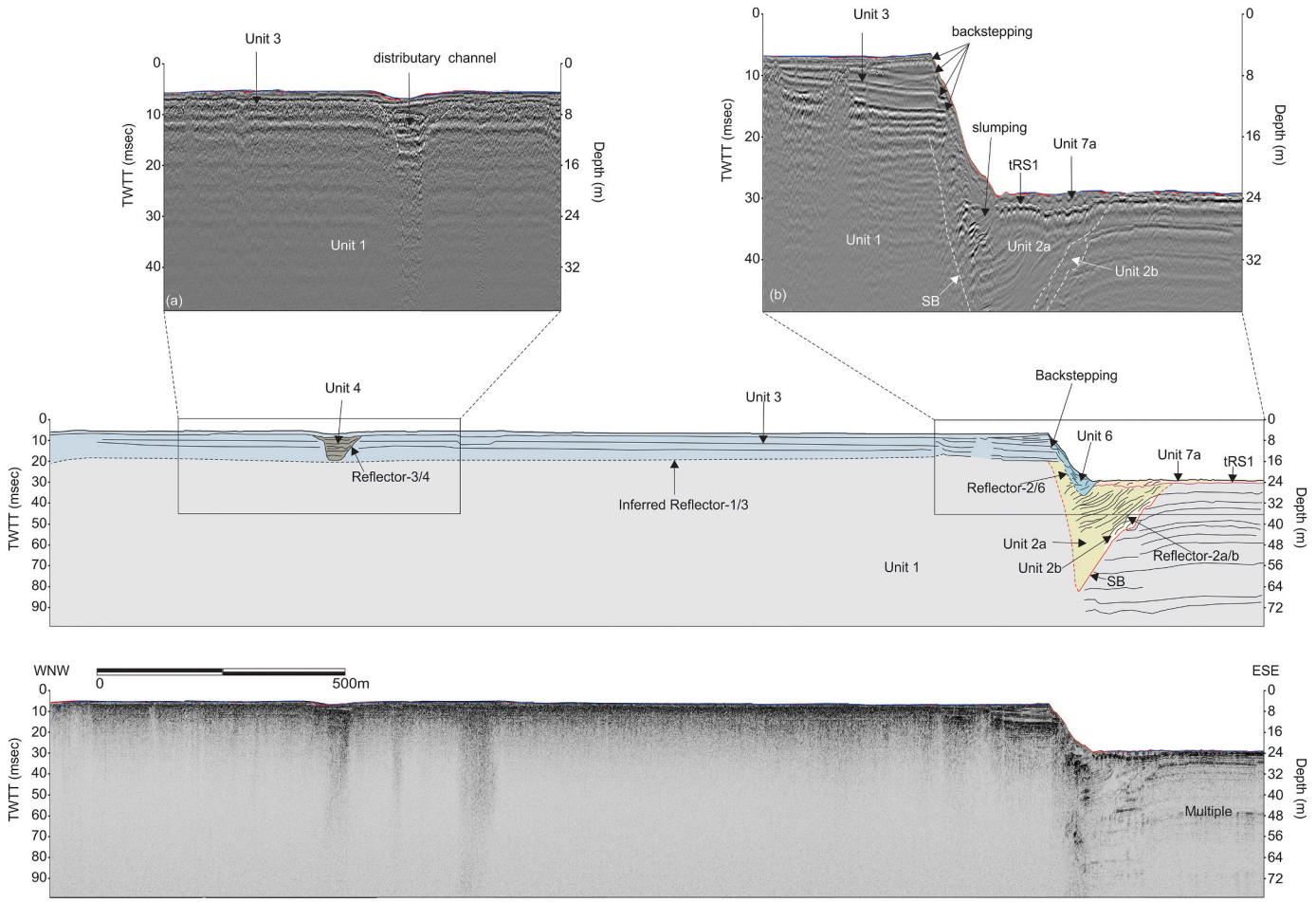


**Fig. 8.** WNW-ESE seismic profile displaying interpreted (top) and raw (bottom) seismic data. A single incised valley, dominated by sigmoid to oblique-parallel reflectors of Unit 2a, is present. Units 2c, 5 and 7b are absent from this seismic line. Enlarged seismic data (Fig. 8a) displays a feeder channel within Unit 3. Note the backstepping bayhead delta (Unit 3) as well as the slumping (Unit 6) occurring in front of it (Fig. 8b).

dark black laminae that marks the upper horizons of the other cores and appears to have terminated at tRS2 (Fig. 12b). RBH-18-18 comprises a similar dark black upper laminated package that terminates sharply on a lower stiff grey clay. The entire core represents Unit 7b.

The dates on RBH-18-23 are stratigraphically inconsistent. Organic sediment from a core depth of 70–71 cm dated to 1845 ± 30 BP. This is overlain at 33–34 cm by organic sediment dated at 3745 ± 30 BP (Fig. 12B). A single organic sediment date from RBH-18-18 at a core depth of 42–43 cm returned an age of 6060 ± 165 cal BP.

## 5. Discussion

### 5.1. Seismic stratigraphic interpretation

#### 5.1.1. Acoustic basement and LGM lowstand (Unit 1 and Surface SB)

Unit 1 forms the acoustic basement to the study area. This unit is intersected by numerous boreholes in the region (Maud and Orr, 1975) and represents the Cretaceous age siltstones that have been widely recognised along the shelf and underlying the coastal water bodies of the east coast of South Africa (Green and Garlick, 2011; Green et al., 2013; Benallack et al., 2016; Dladla et al., 2019). A series of incised valleys, represented by Surface SB, are cut into the Cretaceous siltstones. This unconformity surface can be traced onto the shelf and for several hundred kilometres along the east coast. Cores from incised valleys of similar stratigraphic positions on the Durban shelf (Pretorius et al., 2016) and in Lake St Lucia (Dladla et al., 2019) reveal the infilling materials to be Holocene in age. We thus associate this surface with the LGM lowstand, when sea levels occupied a position of the shelf break at ~130 m below present, ~18,000 year BP (Ramsay and Cooper, 2002; Cooper et al., 2018).

#### 5.1.2. Post-LGM incised valley fills (Unit 2)

The incised valley network is dominated by the thick and homogenous fills of Unit 2a. Though these may occasionally show no particular reflector configuration, they are mainly aggrading in nature, forming onlapping drapes with the valley walls. This architecture closely resembles the central basin fills recognised in incised valleys to the south (e.g. Green et al., 2013) and to the north (e.g. Benallack et al., 2016; Dladla et al., 2019) of the study area, suggesting that Unit 2 is mainly characterised by central basin deposits (Unit 2a), intercalated with other deposits (e.g. Unit 2b). The thick nature of the central basin fill is in keeping with the location of the incised valley in the middle segment of a wave-dominated back-barrier system (e.g. Zaitlin et al., 1994).

The valley flank deposits of Unit 2b show strong similarity to the prograding point bars that other authors have recognised from incised valley fills (e.g. Weber et al., 2004; Chaumillon et al., 2008; Dladla et al., 2019). The high-angle, inclined reflectors and their location usually on the gentler bank of the valley support this interpretation.

Unit 2c forms as flank attached or isolated prograding packages with sigmoid to oblique-parallel reflectors. Simms et al. (2010) reported a similar, prograding, valley-flank attached package in the Baffin Bay incised valley. Here, they suggest that a package with this type of appearance can either be interpreted as buried prograding subtidal spits or lobes of a bayhead delta. They propose that the attached nature of the

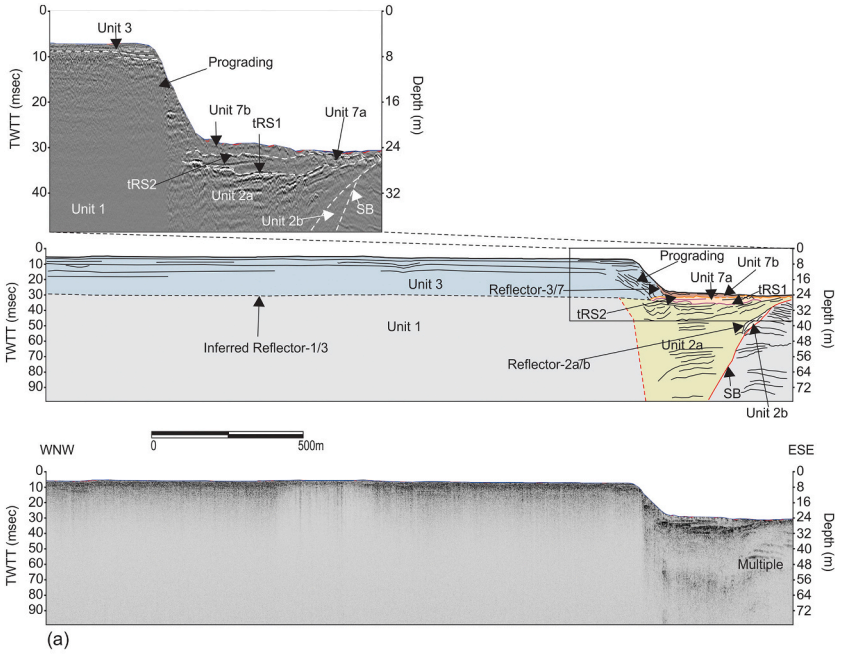


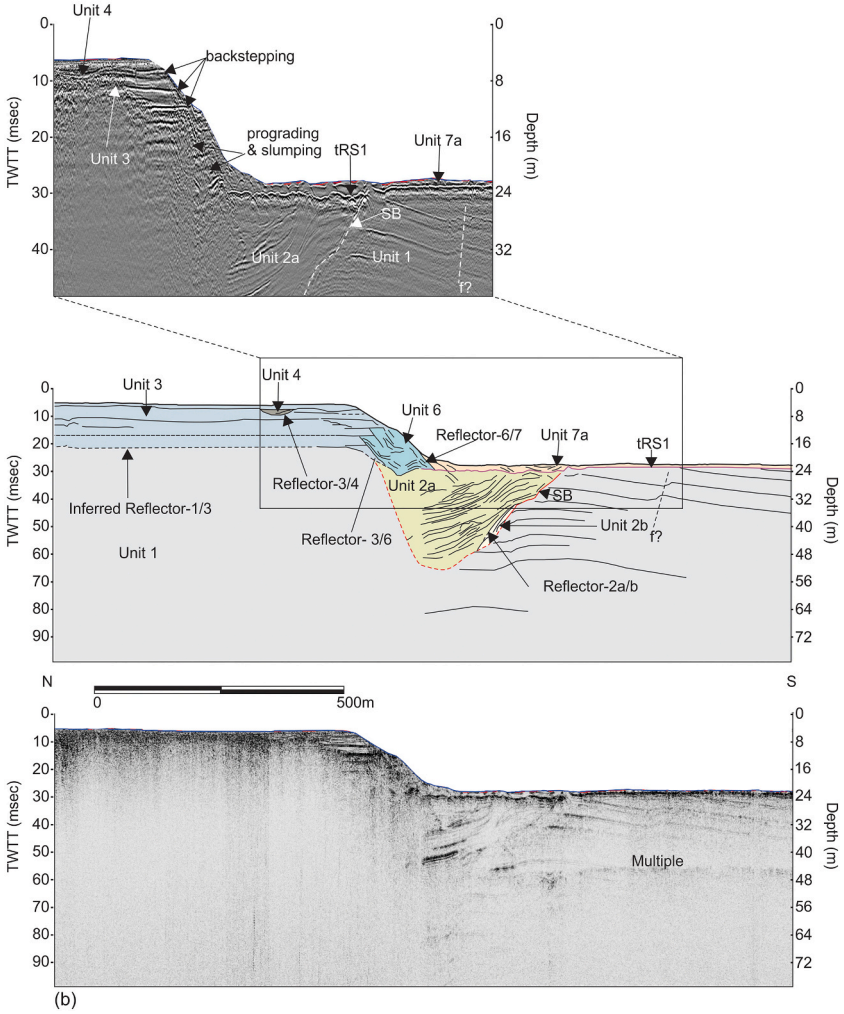


**Fig. 9.** (a) Shows a WNW-ESE seismic profile displaying interpreted (top) and raw (bottom) seismic data. A single incision formed by the LGM-age Surface SB is displayed. Unit 2a dominates the fills, with aggrading reflectors. Only Units 1, 2a, 2b, 3 and 7 are present on this seismic line. Note the presence of the prograding and backstepping bayhead delta. Both tRS1 and tRS2 are present. (b) Shows N-S seismic profile displaying interpreted (top) and raw (bottom) seismic data. An LGM-age incision is shown, dominated by Unit 2a. Units 2c, 5 and 7b, as well as surface tRS2, are absent from this seismic line. The enlargement clearly shows the prograding and backstepping bayhead delta, with slumping occurring in front of it. Also, note the presence of the feeder channel within the bayhead delta as well as the possible faulting of Unit 1.

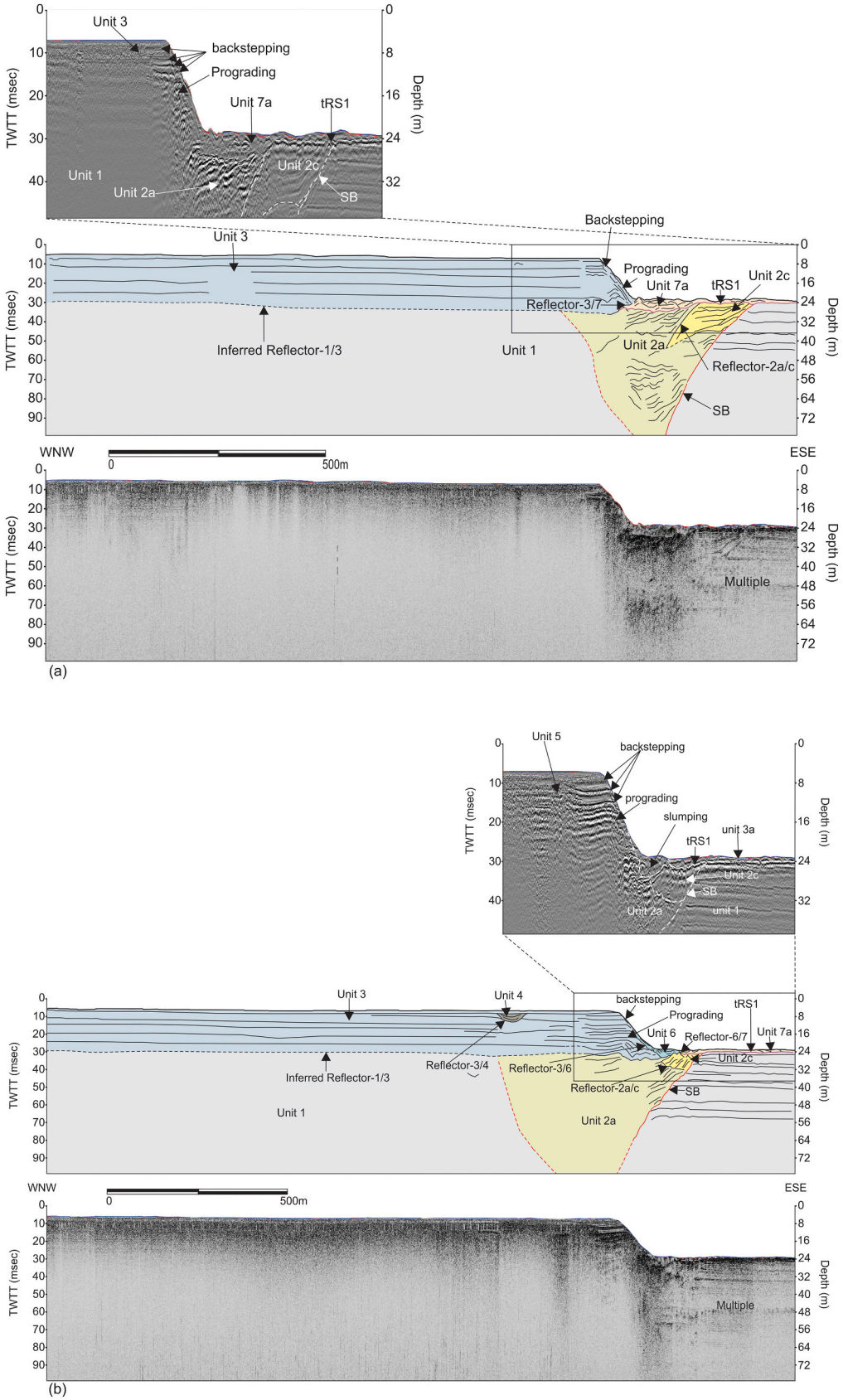


**Fig. 10.** (a) Shows a WNW-ESE seismic profile displaying interpreted (top) and raw (bottom) seismic data. The incision is dominated by thick Unit 2a fills, which are aggrading in nature. Units 2b, 4,5 and 6 are absent from this line. The three major surfaces are present. The bayhead delta progrades into the underlying LGM-age incision. (b) Shows a WNW-ESE seismic profile displaying interpreted (top) and raw (bottom) seismic data. Only Units 1, 2a, 2c, 3, 4, 6 and 7a are present on this seismic. On the enlargement, note the prograding and backstepping bayhead delta (Unit 3) as well as the slumping (Unit 6) that occurs in front of it.

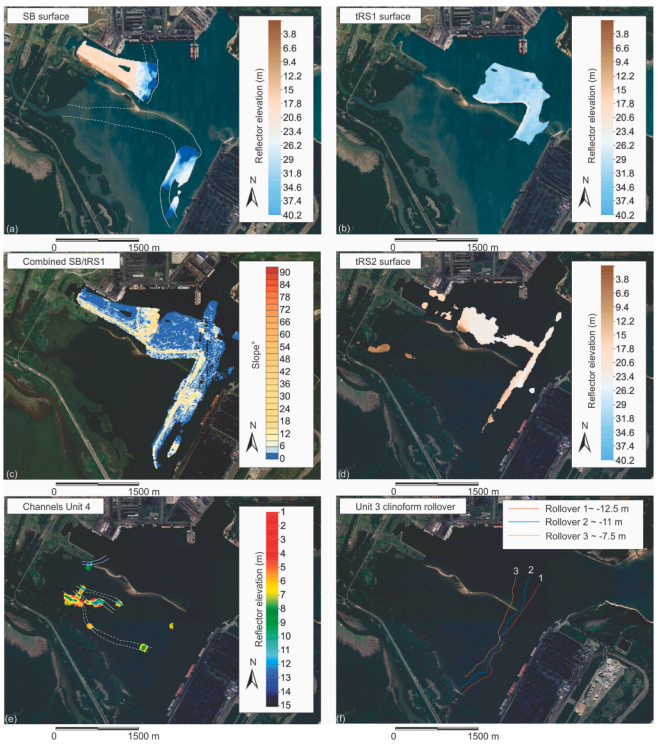


**Fig. 11.** Sun-shaded relief surface of (a) the SB unconformity, (b) tRS1, (c) gradient of the combined SB and tRS1 surfaces reflecting the antecedent gradient beneath Unit 3 (d) tRS2 and (e) feeder channels of Unit 4. (f) Shows the three positions of the clinoform rollover of Unit 3.

unit to valley flanks favours a buried spit interpretation over bayhead delta lobes. We similarly interpret Unit 2c as representing buried subtidal spits. In Lake St. Lucia, Dladla et al. (2019) recognise units of similar seismic architecture and describe these as wind-driven prograding sand spits. Such deposits are suggested to have formed due to the transport and reworking of sediment by wind-induced bottom currents (e.g. Nutz et al., 2015). These are commonly recognised in other large coastal water bodies of the area (Wright et al., 2000). The spits (Unit 2c) were later truncated by modern tidal processes (tRS1).

Surface tRS1 is characterised by numerous minor incisions, the morphology and scale of which are similar to those of contemporary tidal creeks and channels of the modern back-barrier system. tRS1 has a similar seismic expression to tidal ravinement surfaces documented elswhere (Menier et al., 2006; Nordfjord et al., 2006; Benallack et al., 2016; Dladla et al., 2019; Engelbrecht et al., 2020). Such surfaces form due to migrating tidal inlets or channels during sea-level rise (Catuneanu et al., 2009; Green et al., 2015).

### 5.1.3. Bayhead delta (Units 3 and 4)

The aggrading-prograding and backstepping seismic reflection architecture of Unit 3 closely resembles that of bayhead deltas subject to episodic jumps in sea-level. Such features have previously been recognised worldwide (e.g. Allen and Posamentier, 1993; Nichol et al., 1997; Rodriguez et al., 2010; Smith et al., 2013; Benallack et al., 2016; Aschoff et al., 2018). Episodic landward shifts of many of these features have been directly linked to rapid sea-level rise during the early Holocene period (Rodriguez et al., 2010; Kendall et al., 2008; Törnqvist et al., 2004).

Unit 4 occurs as fills within minor incisions along the delta top (Fig. 11e). We interpret these as tidal channels on the bayhead delta surface (distributaries) that fed sediment to the seaward edge of the system. A similar series of small, shallow channels incise the surface of the modern platform and are visible in the bathymetry (Fig. 2). The overall seismic architecture of Unit 3 and 4 is in combination similar to the bayhead deltas described from Florianopolis Bay of southern Brazil (Meireles et al., 2016). The fact that clinoforms are restricted to the seaward margin, points to vertical aggradation of the delta surface since its inception when sea-level reached ca. -20 m.

The distinct elevations in delta clinoform rollover at ~ −12.5 m, ~ −11 m and ~ −7.5 m (Fig. 11f) are discussed below in Section 5.3.2. Each of these can be considered approximate upper intertidal palaeo-shoreline positions and thus markers of palaeo-sea level. Their degree of accuracy can be related to palaeo-tidal influences, with larger tides extending the error of interpretation. In most instances, and in the absence of data, the palaeo-tidal ranges are related to the modern heights of these datums (Hijma et al., 2015). In the case of our study and the palaeo-shorelines above, the underlying incised valley stratigraphy, in combination with the wave-dominated shape of the delta, illustrates a former wave-dominated setting for an open bayhead delta (Simms et al., 2018). When related to the upper micro-tidal framework currently experienced in the area, these provide good sea-level indicators with an approximate error of half the tidal amplitude (cf. Hijma et al., 2015). Given the contemporary spring tide amplitude of 1.8 m, this error equates to <0.9 m.

Despite the evidence for neotectonism presented later in Section 5.2, the modelled glacial isostatic adjustment (GIA) for the last deglaciation in the study area reveals local sea levels to be within 1 m of the global predicted values (Milne and Mitrovica, 2008). This points to a relatively good fit between palaeo-sea level inferences based on the stratigraphy and global episodes of sea-level variation.

### 5.1.4. Anthropogenic features (Unit 5)

Figs. 2 and 3 show several elongate mounded features of seafloor that crop out as semi-cohesive sediment piles of Unit 5, surrounded by fainter reflectors of Unit 7. These are clearly remnants of the dredging process, where small ridges remain between furrows that have been scoured. The erosional furrows represent the excavation of the seabed and formation of the tRS2 surface (discussed in Section 5.1.6).

### 5.1.5. Slump deposits (Unit 6)

With randomly oriented reflectors, Unit 6 occurs in front of the bayhead delta and intercalates with valley fill material. Based on its position and chaotic seismic architecture, we interpret this unit as slump deposits, formed on the steepest part of the delta (distal delta front; cf. Aschoff et al., 2018). This could be the result of the oversteepening of the delta by dredging along its margins. However, we also recognise a strong association between the slumping (Unit 6) and the feeder channels (Unit 4), as all the seismic lines with feeder channels are characterised by the presence of slumping in front of the delta. We therefore suggest that the slumping may be due to the steepness of the delta front (Aschoff et al., 2018).

### 5.1.6. Fine-grained tidally deposited sediment (Unit 7)

Unit 7 caps the incised valley stratigraphy and is subdivided into two sub-units (Unit 7a and b). This unit is mostly characterised by low to moderate amplitude reflectors, which drape underlying units or may lack any internal reflector configuration, suggesting low energy depositional environments prevailed at the time of formation. Core data reveal that the uppermost portions of the stratigraphy are characterised by laminated silts and clays. tRS2 is revealed to be a sandy layer that separates a lower brown from upper dark black laminated clay. The building of the harbour and construction of a second mouth increased the tidal range in the area, leading to larger areas being exposed to tidal influences (Huizinga and van Niekerk (2000). Surface tRS2 likely represents remobilisation and winnowing of the seabed, possibly due to a combination of modern tidal reworking and dredging of the area.

The stratigraphical inconsistency of the dates of Unit 7b can be ascribed to reworking and redeposition of older-aged carbon that has been transported into the system as organic sediment. Their mixed age

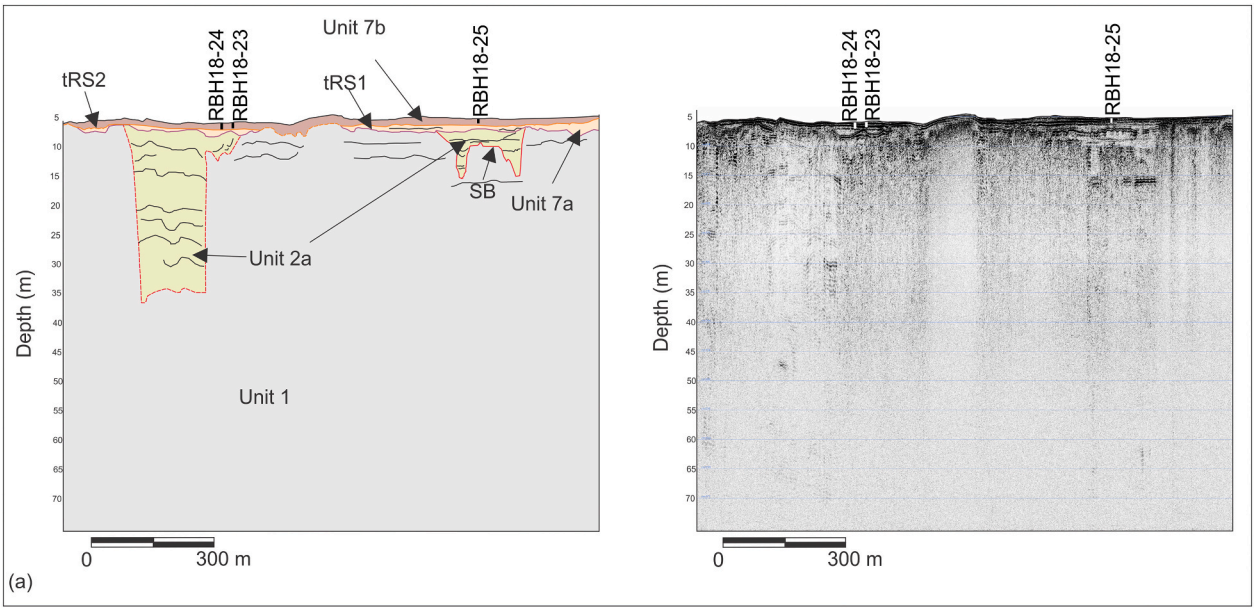


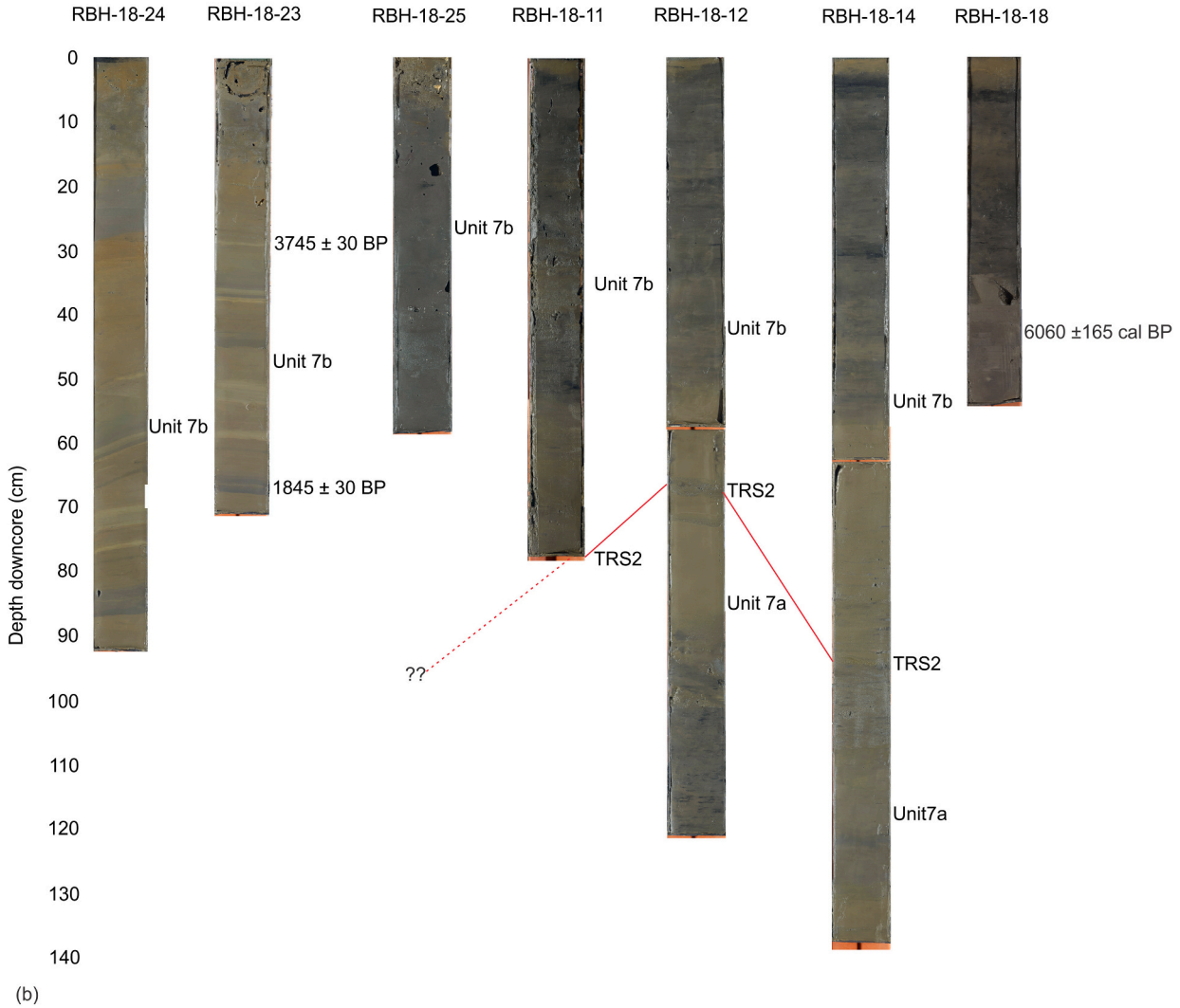


**Fig. 12.** (a) WNW-ESE seismic profile displaying interpreted (left) and raw (right) seismic data. Note the position cores RBH18–23; 24 and 25. (b) Shows seven cores from the study area. RBH18–18; 23; 24 and 25 only intersect Unit 7a. RBH18–11; 12 and 14 intersect both Unit 7a and 7b. Note the position of tRS2 on the uppermost sand lens at 92 cm downcore on core RBH18–11 and 14.

suggests that this unit is likely of recent origin, and that the seabed materials have been reworked from a sediment source of older organic material.

### 5.2. Neotectonics

Numerous faults were recorded in the seismic records. Neotectonism is identified as being pervasive across South Africa (Andreoli et al., 1996) and faults are found along the coastal regions and on the ocean floor. Late Pleistocene to Holocene faults are exposed from Port Durnford (Jackson and Hobday, 1980) northwards along the northern KwaZulu-Natal coastal plain (Kruger and Meyer, 1988) all the way to south Mozambique (cf. Andreoli et al., 1996). The faults reported in this study area are consistent with these other indicators of neotectonics.

### 5.3. Coastal evolution

We summarise the early geological evolution of the palaeo-Mhlatuze River and estuarine complex as follows (Fig. 13):

The stratigraphy is underlain by Cretaceous age siltstones (Unit 1; forming the acoustic basement), into which a single episode of incision occurred (SB), formed by the Mhlathuze River. This was associated with the Last Glacial Maximum when sea-level fell ~130 m below present (Fig. 13a). This produced a very flat antecedent slope along the valley interfluves.

The subsequent initial transgressive material overlying SB (Unit 2) reflects the filling of an incised valley located in the middle segment of a wave-dominated system (Fig. 13b). During a period of sea-level stability, a bayhead delta (Unit 3) prograded into the underlying incised valley system, over a flat tidal ravinement surface (tRS1). This completely filled the remaining accommodation space of the valley (Fig. 13b and c).

#### 5.3.1. Backstepping of the bayhead delta

Factors such as sediment supply, climatic changes, sea-level variations, gradient, etc., govern the development and architecture of a sedimentary system (Feng et al., 2019). As such, the progradation and eventual backstepping of bayhead deltas can be attributed to a number of these processes. The position of multiple delta offset breaks can be used to describe changing palaeo-shoreline trajectories and overall coastal changes over time (Helland-Hansen and Gjelberg, 1994; Aschoff et al., 2018; Engelbrecht et al., 2020).

Factor 1. Sediment supply and local accommodation?

Apart from sea-level rise, Muto and Steel (1992) and Feng et al. (2019) suggest that the main driving factors of the autogenic evolution of deltas are the availability of accommodation as well as sediment supply. A system's response to rapidly rising sea levels is dependent on the sediment supply/accommodation creation ratio (Rodriguez et al., 2008). In general, a system with a low sediment supply/accommodation creation ratio should respond instantaneously to increases in sea-level, whereas one that has a high sediment supply/accommodation ratio should have very little to no response to rising sea levels (Cooper, 1993; Rodriguez et al., 2010).

Several lines of evidence suggest that the Mhlatuze lagoon had low sediment supply during the mid- to late Holocene since sea-level reached the present. In contrast to most large estuaries in the region where sedimentation infilled the estuarine valleys with fluvial sediment (Cooper, 1993, 2002), the pre-engineered Mhlatuze lagoon was not completely infilled but had a tripartite division with tidal inlet and deltas, central basin and bayhead delta. This was associated with a large tidal prism that maintained the tidal inlet and is characteristic of gradually infilling estuarine basins.

In our study area, other authors have noted a decrease in sediment supply since the separation of the Mhlatuze River from the modern harbour (Cloete and Oliff, 1976), however this post-dates the bayhead delta development reported above by several thousand years. No data currently exist concerning sediment supply to the system, though seismic profiling directly offshore the Richards Bay area, revealed an up to 4 m-thick depocenter containing ~11.78 × 106 $m^3$ of Holocene-age sediment (Martin and Flemming, 1985). Assuming no significant erosion, this equates to an average rate of sedimentation of 1000 $m^3$ of sediment per year since the Holocene began 11,650 cal BP. This is significantly less than the 20,500 $m^3$ per year measured prior to the harbour construction, and given the shelf exposure to the strong Agulhas Current in the area, likely reflects significant alongshore and off-shelf dispersal. Nonetheless, on geomorphological evidence, we consider the Mhlatuze system to exhibit a low sediment supply/accommodation ratio based on the shallow bedrock and thinly-developed sediment fill, so backstepping may have indeed been exacerbated by a low local sediment supply.

Factor 2. Meltwater pulses: the "other" driving force behind backstepping bayhead deltas?

Rapid increases in the rate of sea-level rise as a result of sudden pro- or subglacial meltwater, are referred to as meltwater pulses (Blanchon, 2011). Meltwater pulses, associated with the collapse of ice sheets, are prominent in the deglaciation phase of the last glacial period (e.g. Fairbanks, 1989). The study of these pulses is important as it provides a link between climatic, glacial and oceanic systems (Tian et al., 2020). During the deglaciation period from 16.5 and 8.2 ka BP, global warming triggered the extensive melting of ice sheets, resulting in a eustatic sea-level rise of ~130 m (Lambeck et al., 2014). Given the local GIA, which is relatively minor in the context of the far field location of Richards Bay, the behaviour of the bayhead delta is thus most probably a strong reflection of adjustments to sea-level related to melt water pulses.

The first rollover that approximates palaeo-sea level occurs at −12.5 m, an elevation that places a constraint on the timing for delta development to an age of >8.3 ka, based on the local sea-level curve of Cooper et al. (2018). The aggrading landward planar reflectors of the delta indicate a slow rise in sea-level, corroborated by the data of De Lecea et al. (2017) who observed a period of slowly rising sea level between 8.8 ka BP and 8.5 ka BP. We consider this period the point where the delta first formed, followed by a sharp rise in sea-level to cause the first stage of backstepping in the clinoform rollovers from −12.5 to −11 m. Given the lack of sea-level data for this time in South Africa, we tentatively ascribe this to the 8.2 ka event described by Liu et al. (2004). This hypothesis however remains to be tested by further coring and radiocarbon dating.

A further jump in sea-level has been ascribed to MWP-1d (Liu et al., 2004). Though not widely recognised, this meltwater pulse is considered to have occurred between ~8.0 and 7.0 ka BP (Liu et al., 2004). Here, sea levels are thought to have risen by 6 m (Blanchon and Shaw, 1995). The final retreat of the delta may possibly have been related to this event. The rollover depth at −7.5 m implies that the delta stabilised at ~8 ka (Cooper et al., 2018), which matches well with these slightly younger ages reported for the most recent episodic jump in sea-level (Blanchon and Shaw, 1995). Kirkpatrick et al. (2019) similarly link backstepping delta geometries from the inner shelf of southern Namibia to these two episodes (8.2 ka event and MWP-1d). We again emphasize that these are hypotheses, however the seismic and stratigraphic data from the study area provide an alluring argument for the influence of meltwater pulses as drivers of stratigraphic change in this bayhead delta.

Factor 3. Antecedent topography

Low topographic gradients, when coupled with abruptly rising sea levels, may be crucial in the overall preservation of coastal systems (Sanders and Kumar, 1975) and the eventual backstepping of the shoreline as a whole (Törnqvist et al., 2004). Rodriguez et al. (2010) suggest that estuaries fringed by low lying gradients are more sensitive to low amplitude and sudden sea-level rises, as is evident for the northern Gulf of Mexico estuaries. Locally, a flat topographic surface and stepped rise in sea-level has most likely aided in the preservation and backstepping of the deltaic body offshore on the wave dominated Thukela Shelf (Engelbrecht et al., 2020). Studies show that the inundation of flat-lying areas most likely exacerbates the backstepping of

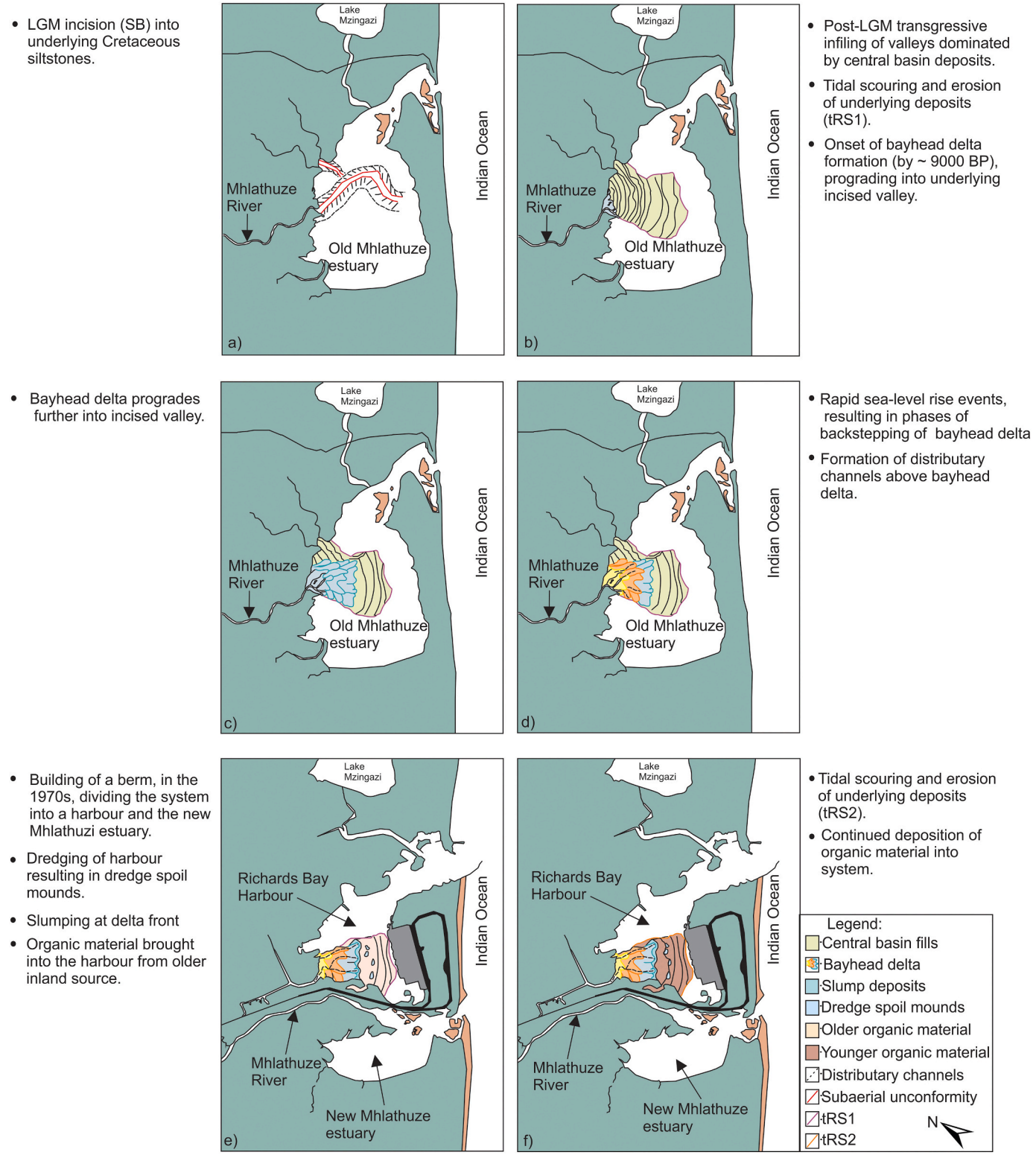


**Fig. 13.** The schematic evolution model of the Richards Bay Harbour estuarine stratigraphy. (a) LGM-age incision into Cretaceous siltstones. (b) Post-LGM transgressive infilling of incised valleys, tidal scouring (forming tRS1) and Prograding bayhead delta formation. (c) Continued prograding of delta into underlying incised valleys. (d) Rapid sea-level rise events resulting in backstepping of the bayhead delta. Increased sediment brought into the system by feeder channels. (e) Dividing of the system into the harbour and the Mhlathuze Estuary. Dredging of harbour, formation of dredge mounds and slumping on the delta front. Deposition of organic sediment from an inland source (Unit 7a). (f) Tidal scouring (tRS2) and continued deposition of organic material (Unit 7b).

bayhead delta systems (Rodriguez et al., 2005), as the system is especially sensitive to any sea-level variations in this case. The combined subaerial unconformity and tRS1 surfaces over which the deltas have prograded and been preserved on are exceptionally flat (between 0.1 and 0.02° on average-Fig. 11c). In tandem with stepped sea-level rise, this flat antecedent gradient has exaggerated the translation of the shoreline. We therefore suggest that the backstepping nature of the bayhead delta here is also partly a result of an autogenic response to rapid sea-level changing its shoreline trajectory over the gentle antecedent topography. This likely dampened the bayline erosion along the edge of the bayhead delta and as such we consider this area a particularly good site for further sea-level reconstructions using palaeo-bayhead delta stratigraphy.

Considering the above arguments, we link the backstepping of the bayhead delta to rapid sea-level rise during the early Holocene, initiated by the 8.2 ka event (Fig. 13.d). Minor incisions, in the form of distributary channels, occurred above the bayhead delta and introduced further sediment into the system (Fig. 13d). A second phase of backstepping occurred after another relatively stable period of sea-level at ~8 ka BP. This backstepping is possibly related to MWP-1d.

#### 5.3.2. *Anthropogenic influences*

In the early 1970s, a berm was constructed, dividing the original Mhlathuze Estuary into two separate systems; the Richards Bay Harbour and the new Mhlathuze Estuary (Fig. 13e). Here, the Mhlathuze River was redirected to flow into the new Mhlathuze Estuary. The low rates of sediment supply since have allowed the delta morphology to remain mostly unchanged apart from the modifications of the steeply dipping margins by dredging and gravity collapse. Dredging of the harbour has periodically occurred, pooling organic rich materials (Unit 7) around isolated mounds of undredged sediment (Unit 5) and produced a steepened delta front that has resulted in slumping (Unit 6) (Fig. 13e).

The tRS2 surface represents modern anthropogenic influence. The remobilisation and winnowing of the seabottom is currently due to a combination of modern tidal reworking and dredging of the area (Fig. 13f).

The changes in system configuration from the pre-harbour to post development states can be linked to a reduction in water volumes and tidal prism respectively.

## 6. Conclusion

The backstepping of bayhead deltas into underlying incised valleys is a global phenomenon. The prograding and eventual backstepping of these bayhead deltas may be attributed to a number of different factors. These include: (1) the amount of sediment brought into the system by rivers, (2) the rate at which this sediment comes into the system, (3) the rate of accommodation creation, (4) rapidly rising sea levels, (5) the gradient of the palaeo-landscape surface, etc. For the Richards Bay Harbour bayhead delta, pulses of rapidly rising sea levels in combination with a relatively low gradient setting were key factors that played a role in the backstepping of the delta. The landward shift of the bayhead delta is proposed to have been linked to both the 8.2 ka event and to MWP-1d. Given the (1) relatively small GIA during the postglacial transgression and (2) the flat antecedent gradients of both the subaerial unconformity and the overlying tidal ravinement, this site is especially sensitive to episodic rates of sea-level change. As such, it poses a key target for investigating these phenomena in the far field.

## Data availability

The data used for the research described in this article are proprietary and were released to us. They can be made available on request to Anchor Energy (Pty)Ltd.

## Declaration of Competing Interest

The authors declare that they have no known competing financial interests or personal relationships that could have appeared to influence the work reported in this paper.

## Acknowledgments

This work was supported by the German Federal Ministry of Education and Research [grant numbers: 03F0798A, 03F0798B, 03F0798C] and is part of project TRACES (Tracing Human and Climate impact in South Africa) within the SPACES II Program (Science Partnerships for the Assessment of Complex Earth System Processes). The field work support by George Best is gratefully acknowledged. We acknowledge Dr. Peter Ramsay and Anchor Energy (Pty) Ltd. for permission to use the geophysical data sets. Doug Slogrove and Gaynor Deacon are acknowledged in this regard.

## References

Allen, G.P., Posamentier, H.W., 1993. Sequence stratigraphy and facies model of an incised valley fill: Gironde estuary, France. J. Sediment. Petrol. 63, 378–391.
Andreoli, M.A.G., Doucouré, M., Van Bever Donker, J., 1996. Neotectonics of southern Africa - a review. Afr. Geosci. Rev. 3, 1–16.
Anon, 1972. Richards Bay Harbour project. In: The South African Shipping News and Fishing Industry Review, 27, pp. 25–27.
Aschoff, J.L., Olariu, C., Steel, R.J., 2018. Recognition and significance of bayhead delta deposits in the rock record: a comparison of modern and ancient systems. Sedimentology 65, 62–95.
Begg, G.W., 1978. The estuaries of Natal. In: Natal Town and Regional Planning Report, 41, 657pp.
Benallack, K., Green, A.N., Humphries, M.S., Cooper, J.A.G., Dladla, N.N., Finch, J.M., 2016. The stratigraphic evolution of a large back-barrier lagoon system with a non-migrating barrier. Mar. Geol. 379, 64–77.
Bhattacharya, J.P., Giosan, L., 2003. Wave-influenced deltas: geomorphological implications for facies reconstruction. Sedimentology 50, 187–210.
Blanchon, P., 2011. Meltwater pulses. In: Hopley, D. (Ed.), Encyclopedia of Mordern Coral Reefs: Structure, Form and Process. Springer-Verlag Earth Science Series, pp. 683–690.
Blanchon, P., Shaw, J., 1995. Reef drowning during the last deglaciation: evidence for catastrophic sea level rise and ice-sheet collapse. Geology 23, 4–8.
Catuneanu, O., Abreu, V., Bhattacharya, J.P., Blum, M.D., Dalrymple, R.W., Eriksson, P. G., Fielding, C.R., Fisher, W.L., Galloway, W.E., Gibling, M.R., Giles, K.A., Holbrook, J.M., Jordan, R., Kendall, C.G.St.C, Macurda, B., Martinsen, O.J., Miall, A. D., Neal, J.E., Nummedal, D., Pomar, L., Posamentier, H.W., Pratt, B.R., Sarg, J.F., Shanley, K.W., Steel, R.J., Strasser, A., Tucker, M.E., Winker, C., 2009. Towards the standardization of sequence stratigraphy. Earth Sci. Rev. 92, 1–33.
Chaumillon, E., Proust, J.-N., Menier, D., Weber, N., 2008. Incised-valley morphologies and, sedimentary-fills within the inner shelf of the Bay of Biscay (France): a synthesis. J. Mar. Syst. 72, 383–396.
Cloete, C.E., Oliff, W.D., 1976. South African marine pollution survey report 1974-1975. In: National Scientific Programmes Unit. CSIR.
Cooper, J.A.G., 1993. Sedimentation in a river dominated estuary. Sedimentology 40, 979–1017.
Cooper, J.A.G., 2002. The role of extreme floods in estuary-coastal behaviour: contrasts between river-and tide-dominted microtidal estuaries. Sediment. Geol. 150, 123–137.
Cooper, J.A.G., Green, A.N., Compton, J.S., 2018. Sea-level change in southern Africa since the Last Glacial Maximum. Quat. Sci. Rev. 201, 303–318.
Dalrymple, R.W., Zaitlin, B.A., Boyd, R., 1992. Estuarine facies models: conceptual basis and stratigraphic implications. J. Sediment. Petrol. 62, 1130–1146.
Davies, J.L., 1964. A morphogenic approach to world shorelines. Z. Geomorphol. 8, 27–42.
De Lecea, A.M., Green, A.N., Strachan, K.L., Cooper, J.A.G., Wiles, E.A., 2017. Stepped Holocene sea-level rise and its influence on sedimentation in a large marine embayment: Maputo Bay, Mozambique. Estuar. Coast. Shelf Sci. 193, 25–36.
Dladla, N.N., Green, A.N., Cooper, J.A.G., Humphries, M.S., 2019. Geological inheritance and its role in the geomorphological and sedimentological evolution of bedrock-hosted incised valleys, lake St Lucia, South Africa. Estuar. Coast. Shelf Sci. 222, 154–167.
Engelbrecht, L., Green, A.N., Cooper, J.A.G., Hahn, A., Zabel, M., Mackay, D., 2020. Construction and evolution of submerged deltaic bodies on the high energy SE African coastline: the interplay between relative sea level and antecedent controls. Mar. Geol. 424, 106170.
Fairbanks, R.G., 1989. A 17,000-year glacio-eustatic sea level record: influence of glacial melting rates on the younger dryas event and deep-ocean circulation. Nature 342, 637–642.
Feng, W.-J., Zhang, C.-M., Yin, T.-J., Yin, S.-Y., Liu, J.-L., Zhu, R., Xu, Q.-H., Chen, Z., 2019. Sedimentary characteristics and internal architecture of a river-dominated

delta controlled by autogenic process: implications from a flume tank experiment. Pet. Sci. 16, 1237–1254.
Flemming, B.W., 1981. Factors controlling shelf sediment dispersal along the southeast African continental margin. Mar. Geol. 42, 259–277.
Flemming, B.W., 2005. Tidal environments. In: Schwartz, M.L. (Ed.), Encyclopedia of Coastal Science. Springer, Dordrecht, pp. 954–958.
Green, A.N., Garlick, G.L., 2011. A sequence stratigraphic for a narrow, current-swept continental shelf: the Durban Bight, Central KwaZulu-Natal, South Africa. J. Afr. Earth Sci. 60, 303–314.
Green, A.N., Dladla, N., Garlick, G.L., 2013. Spatial and temporal variations in incised valley systems from the Durban continental shelf, KwaZulu-Natal, South Africa. Mar. Geol. 335, 148–161.
Green, A.N., Cooper, J.A.G., Wiles, E.A., De Lecea, A.M., 2015. Seismic architecture, stratigraphy and evolution of a subtropical marine embayment: Maphuto Bay, Mozambique. Mar. Geol. 369, 300–309.
Hayes, M.O., 1979. Barrier island morphology as a function of tidal and wave regime. In: Leatherman, S.P. (Ed.), Barrier Islands from the Gulf of Mexico. Academic Press, New York, pp. 1–29.
Heaton, T.J., Köhler, P., Butzin, M., Bard, E., Reimer, R.W., Austin, W.E., Ramsey, C.B., Grootes, P.M., Hughen, K.A., Kromer, B., Reimer, P.J., 2020. Marine20—the marine radiocarbon age calibration curve (0–55,000 cal BP). Radiocarbon 62, 779–820.
Helland-Hansen, W., Gjelberg, J.G., 1994. Conceptual basis and variability in sequence stratigraphy: a different perspective. Sediment. Geol. 92, 31–52.
Hijma, M.P., Engelhart, S.E., Törnqvist, T.E., Horton, B.P., Hu, P., Hill, D.F., 2015. A protocol for a geological sea-level database. In: Shennan, I., Long, A.J., Horton, B. P. (Eds.), Handbook of Sea-Level Research. Wiley Blackwell, pp. 536–553.
Huizinga, P., Van Niekerk, L., 2000. Mhlathuze estuary — physical aspects. In: Mahlathuze System Ecological Reserve (quantity) Study. Department of Water Affairs and Forestry, Pretoria. Unpublished report. Report No. W120-00-1499.
Jackson, M.P.A., Hobday, D.K., 1980. Gravity gliding and clay diapirism in Pleistocene shoreline sequence in Zululand South Africa. Am. J. Sci. 280, 333–362.
Jerling, H.L., 2003. The Zoopankton community of the Mhlathuze (Richards Bay) Estuary: two decades after construction of the Harbour. Afr. J. Mar. Sci. 25, 289–299.
Kendall, R.A., Mitrovica, J.X., Milne, G.A., Törnqvist, T.E., Li, Y., 2008. The sea-level fingerprint of the 8.2 ka climate event. Geology 36, 423–426.
Kirkpatrick, L.H., Green, A.N., Pether, A.N., 2019. The seismic stratigraphy of the inner shelf of southern Namibia: the development of an unusual nearshore shelf stratigraphy. Mar. Geol. 408, 18–35.
Kruger, G.P., Meyer, R., 1988. A sedimentological model for the norther Zululand coastal plain. In: Abstract of the 22nd Earth Science Congress of the Geological Society of South Africa. University of Natal, Durban, pp. 423–425.
Lambeck, K., Rouby, H., Purcell, A., Sun, Y., Sambridge, M., 2014. Sea level and global ice volumes from the last glacial maximum to the Holocene. Proc. Nat. Acad. Sci. United States of America 111, 15296–15303.
Liu, J.P., Milliman, J.D., Gao, S., Cheng, P., 2004. Holocene development of the Yellow River's subaqueous delta North Yellow Sea. Mar. Geol. 209, 45–67.
Lutjeharms, J.R.E., 2006. The Agulhas Current. Springer-Verlag, Berlin, Heidelberg, p. 329.
Maboya, M.L., Meadows, M.E., Reimer, P.J., Backeberg, B.C., Haberzettl, T., 2018. Late Holocene marine radiocarbon reservoir correction for the southern and eastern coasts of South Africa. Radiocarbon 60, 571–582.
Martin, A.K., Flemming, B.W., 1985. The distribution and thickness of Holocene sediments on the Zululand continental shelf between 28° and 29°S. In: CSIR Report C/SEA, 8524, pp. 1–13.
Maud, R.R., Orr, W.N., 1975. Aspects of post-Karroo geology in the Richards Bay area. Trans. Geol. Soc. South Afr. 78, 101–109.
Meireles, R.P., Cooper, J.A.G., Klein, A.H.F., de Abreu, J.G.N., Green, A.N., de Souza, L. H.P., Told Jr., E.E., 2016. Holocene Submarine Bayhead Delta Deposits: An Example from Southern Brazil (VII Simpósio Brasiliero de Geofísica).
Menier, D., Raynaud, J.-Y., Proust, J.-N., Guillocheau, F., Gunennoc, P., Bonnet, S., Tessier, B., Gouert, E., 2006. Basement control on shaping and infilling of valleys incised at the southern coast of Brittany, France. In: Dalrymple, R.W., Leckie, D.A., Tillman, R.W. (Eds.), Incised Valleys in Time and Space, Society of Palaeontologists and Mineralogists Special Publication, vol. 85, pp. 37–55.
Milne, G.A., Mitrovica, J.X., 2008. Searching for eustacy in deglacial sea-level histories. Quat. Sci. Rev. 27, 2292–2302.
Mitchum, R.M., Vail, P.R., 1977. Seismic stratigraphy and global changes of sea level, part 7: Seismic stratigraphy interpretation procedure. In: Payton, C.E. (Ed.), Seismic Stratigraphy-Applications to Hydrocarbon Exploration, American Association of Petroleum Geologists Memoir, vol. 26, pp. 135–143.
Moes, H., Rossouw, M., 2008. Considerations for the Utilization of Wave Power around South Africa: Workshop on Ocean Energy, 46. University of Stellenbosch, Centre for Renewable and Sustainable Energy Studies, Abstracts, Stellenbosch, South Africa.
Muto, T., Steel, R.J., 1992. Retreat of the front in a prograding delta. Geology 20, 967–970.
Nichol, S.l., Zaitlin, B.A., Thom, B.G., 1997. The upper Hawkesbury River, New South Wales, Australia: a Holocene example of an estuarine bayhead delta. Sedimentology 44, 263–286.
Nordfjord, S., Goff, J.A., Austin, J.A., Gulick, S.P.S., 2006. Seismic facies of incised valley fills, New Jersey Continental Shelf: implications for erosion and preservation processes acting during latest Pleistocene-Holocene transgression. J. Sediment. Res. 76, 1284–1303.
Nutz, A., Schuster, M., Ghienne, J.-F., Roquin, C., Hay, M.B., Retif, F., Certain, R., Robin, N., Raynal, O., Cousineau, P.A., Team, S., Bouchette, F., 2015. Wind-driven bottom currents and related sedimentary bodies in Lake Saint-Jean (Québec, Canada). Geol. Soc. Am. Bull. 127, 1194–1208.
Pretorius, L., Green, A., Cooper, A., 2016. Submerged shoreline preservation and ravinement during rapid postglacial sea-level rise and subsequent "slowstand". Geol. Soc. Am. Bull. 128, 1059–1069.
Ramsay, P.J., Cooper, J.A.G., 2002. Late Quaternary Sea-level change in South Africa. Quat. Res. 57, 82–90.
Rodriguez, A.B., Anderson, J.B., Simms, A.R., 2005. Terrace inundation as an autocyclic mechanism for parasequence formation: Galveston estuary, Texas, USA. J. Sediment. Res. 75, 608–620.
Rodriguez, A.B., Greene, D.L., Anderson, J.B., Simms, A.R., 2008. Response of Mobile Bay and eastern Mississippi Sound, Alabama, to changes in sediment accommodation and accumulation. In: Anderson, J.B., Rodriguez, A.B. (Eds.), Response to Upper Gulf Coast Estuaries to Holocene Climate Change and Sea-Level Rise. Geological Society of America Special paper, 443, pp. 12–29.
Rodriguez, A.B., Simms, A.R., Anderson, J.B., 2010. Bay-head deltas across the northern Gulf of Mexico back step in response to the 8.2 ka cooling event. Quat. Sci. Rev. 29, 3983–3993.
Rossouw, J., 1984. Review of Existing Wave Data, Wave Climate and Design Waves for South Africa and West African (Namibian) Coastal Waters. Coastal Engineering and Hydraulics, National Research Institute for Oceanology, CSIR Report T/SEA 8401, Stellenbosch, 61 pp.
Salzmann, L., Green, A., 2012. Boulder emplacement on a tectonically stable, wave-dominated coastline, Mission Rocks, northern KwaZulu-Natal, South Africa. Mar. Geol. 323-325, 96–106.
Sanders, J.E., Kumar, N., 1975. Evidence of shoreface retreat and in-place "drowning" during Holocene submergence of barriers, Shelf of Fire Island, New York. Geol. Soc. Am. Bull. 86, 65–76.
Schoonees, J.S., Theron, A.K., Bevis, D., 2006. Shoreline accretion and sand transport at groynes inside the Port of Richards Bay. Coast. Eng. 53, 1045–1058.
Simms, A.R., Rodriguez, A.B., 2015. The influence of valley morphology on the rate of bayhead delta progradation. J. Sediment. Res. 85, 38–44.
Simms, A.R., Aryal, N., Miller, L., Yokoyama, Y., 2010. The incised valley of Baffin Bay, Texas: a tale of two climates. Sedimentology 57, 642–669.
Simms, A.R., Rodriguez, A.B., Anderson, J.B., 2018. Bayhead deltas and shorelines: insights from modern and ancient examples. Sediment. Geol. 374, 17–35.
Smith, C.G., Osterman, L.E., Poore, R.Z., 2013. An examination of historical inorganic sedimentation and organic matter accumulation in several marsh types within the Mobile Bay and Mobile-Tensaw River Delta region. J. Coast. Res. 63, 68–83.
Tian, S.Y., Yasuhara, M., Hong, Y., Huang, H.-H.M., Iwatani, H., Chiu, W.-T.R., Briony, M., Okahashi, H., Rasmussen, T.L., 2020. Deglacial–Holocene Svalbard Paleoceanography and Evidence of Meltwater Pulse 1B.
Törnqvist, T.E., Bick, S.J., González, J.L., 2004. Tracking the sea-level signature of the 8.2 ka cooling event: new constraints from the Mississippi Delta. Geophys. Res. Lett. 31. L23309.
Van Heerden, I.L., Swart, D.H., 1986. An assessment of past and present geomorphological and sedimentary process operative in the St. Lucia estuary and environs. In: Marine Geoscience and Sediment Dynamics Division, National Research Institute for Oceanology, CSIR Research Report No. 569.
Weber, N., Chaumillon, E., Tesson, M., Garlan, T., 2004. Architecture and morphology of the outer segment of a mixed tide and wave-dominated-incised valley, revealed by HR seismic reflection profiling: the palaeo-Charente River, France. Mar. Geol. 207, 17–38.
Weerts, S.P., 2002. Habitat Utilisation by Juvenile Fishes in Mhlathuze Estuary and Richards Bay Harbour. Unpublished M.Sc. thesis. University of Zululand, South Africa, 199pp.
Weerts, S.P., Cyrus, D.P., 2002. Occurrence of young and small-sized fishes in different habitats within a subtropical South African estuary and adjacent harbor. Mar. Freshw. Res. 53, 447–456.
Weerts, S.P., MacKay, C.F., Cyrus, D.P., 2014. The potential for a fish ladder to mitigate against the loss of marine-estuarine-freshwater connectivity in the subtropical coastal lake. Water SA 40, 27–38.
Wright, C.I., Miller, W.R., Cooper, J.A.G., 2000. The Cenozoic evolution of coastal water bodies in northern KwaZulu-Natal, South Africa. Mar. Geol. 167, 207–229.
Zaitlin, B.A., Dalrymple, R.W., Boyd, R., 1994. The stratigraphic organization of incised-valley systems associated with relative sea level change. In: Dalrymple, R.W., Boyd, R., Zaitlin, B.A. (Eds.), Incised Valley Systems: Origin and Sedimentary Sequences, Society of Economic Palaeontologists and Mineralogists Special Publication, vol. 51, pp. 45–60.

# Chapter 5

# Organochlorine pesticide contamination in sediments from Richards Bay, South Africa: spatial trends and ecotoxicological risks

Paul Mehlhorn[a], Marc Humphries[b], Julia Gensel[c], Archibold Buah-Kwofie[b,d], Raymond Lubem Tyohemba[b], Torsten Haberzettl[a]

[a] University of Greifswald, Institute for Geography and Geology, F.L.-Jahn Str. 16, 17489 Greifswald, Germany

[b] University of the Witwatersrand, School of Chemistry, Johannesburg, South Africa

[c] MARUM - Center for Marine Environmental Sciences, University of Bremen, Bremen, Germany

[d] Nuclear Power Institute, Ghana Atomic Energy Commission, P. O Box LG 80, Legon, Accra, Ghana

State of publication: Submitted (25.12.2021) to Environmental Science and Pollution Research.

## Abstract

The occurrence and distribution of organochlorine pesticides (OCPs) in aquatic systems is a matter of global concern and poses significant toxicological threats to both organisms and human health. Despite the extensive use of OCPs for pest and disease control in southern Africa, relatively few studies have examined the occurrence and toxicological risks of OCP residues in the region. This study investigates on the nature, distribution and potential sources of OCP contamination in sediments from Richards Bay, a rapidly developing industrial port on the northeast coast of South Africa.

Surface sediments collected from Richards Bay harbour and surrounding areas indicate that OCP contamination in the region is widespread. Total concentrations (∑OCP) in surface samples ranged from 135 to 1020 ng $g^{-1}$, with hexachlorocyclohexanes (∑HCH, 35 – 230 ng $g^{-1}$) and dichlorodiphenyltrichloroethanes (∑DDT, 12 – 350 ng $g^{-1}$) the dominant contaminant groups detected. Metabolite isomeric compositions indicate that the presence of aldrin and endosulfan likely result from historical agricultural usage, while recent input of γ-HCH, heptachlor and endrin may be linked to the illegal use of old pesticide stockpiles. Total DDT concentrations were dominated by p,p'-DDT (80 ± 64 ng $g^{-1}$), which was attributed to its ongoing use in malaria vector control in the region. A $^{210}$Pb-dated sediment core revealed that OCP input to the local environment increased dramatically from relatively low concentrations in the mid-1940s (∑OCP, 355 ng $g^{-1}$) to peak levels (∑OCP, 781 ng $g^{-1}$) in the 1980s/1990s. An overall decrease in ∑OCP concentration from the mid-2000s is likely related to restrictions on use following the Stockholm Convention in 2004. Despite current restrictions on use, OCP concentrations exceeded sediment quality guidelines in the vast majority of cases, raising concerns for protected estuarine and mangrove habitats in the area, as well as for local fishing and farming communities.


## Introduction

Organochlorine pesticides (OCPs) are of great environmental concern due to their environmental persistence and potential for bioaccumulation (Potapowicz et al. 2020). Once introduced into the environment, various transport processes result in their widespread dispersal and accumulation in different media, with aquatic coastal ecosystems, such as

estuaries and coastal lakes, acting as important sinks for agricultural and industrial pollution (Saulnier and Mucci 2000, Mestres et al. 2006). Bioaccumulation (bio-concentration and bio-magnification) of OCPs through the food chain can pose ecological and human health risks in local and regional communities (Bornman et al. 2010, Humphries 2013, Gerber et al. 2016, Buah-Kwofie and Humphries 2021).Their bioaccumulation potential, toxicity and ability for endocrine disruption make these pesticides a matter of global concern (Bouwman 2004, Buah-Kwofie et al. 2018, 2019, Tyohemba et al. 2020).

South Africa is the largest consumer of pesticide products in Africa and is ranked as the 20$^{th}$ highest user in the world (FAO 2020). The use of OCPs in agriculture and disease vector programs in South Africa dates back to the 1940s (Fischer et al. 2011, Quinn et al. 2011, Buah-Kwofie et al. 2018). Although environmental and human health concerns led to their ban in the early 1970 in most developed countries, OCPs remained widely in use in South Africa until the signing of the Stockholm Convention on Persistent Organic Pollutants (POPs) in 2004 (Bouwman 2004). While use of most OCP compounds is today banned in South Africa, DDT is still used to control the spread of malaria in the north-eastern parts of the country. The application of DDT by indoor residual spraying (IRS) remains the primary method of control by local health departments, particularly in the province of KwaZulu-Natal (Maharaj et al. 2019)(Fig. 51). As a result, DDT and other legacy OCP compounds continue to be detected in environmentally significant concentrations in the region, with several studies reporting on the widespread prevalence of OCPs in both sediment (Humphries 2013, Buah-Kwofie and Humphries 2017) and wildlife species (Buah-Kwofie et al. 2017, Bouwman et al. 2019, Humphries et al. 2021) from iSimangaliso Wetland Park (Fig. 5.1).

Apart from the work conducted in iSimangaliso Wetland Park, little is known about the prevalence of OCPs elsewhere along the coastline of KwaZulu-Natal. Early studies carried out by the South African marine pollution survey on sediments and fish at Richards Bay Harbour, located about 60 km south of iSimangaliso (Fig. 5.1), indicated only low quantities of DDT and dieldrin in samples of fish (Cloete and Oliff 1976). A few years later, the detection of DDT in fish from Richards Bay Harbour suggested recent inputs of technical DDT from local mosquito control activities (Gardner et al. 1983). More recently, high concentrations of hexachlorocyclohexanes (HCHs) in sediments from Richards Bay were reported by Roos (2010), however, the sampling conducted as part of this survey was limited in scope and did

not consider sediments found within Richards Bay Harbour itself. Richards Bay Harbour functions as South Africa's leading coal export facility, around which various other industries and bulk cargo export facilities have developed. Although Richards Bay is one of the fastest developing industrial nodes in the country and host to some of the largest sub-tropical mangrove forests (Fig. 5.1) in South Africa (Naidoo 2016), a detailed evaluation of OCP contamination in the region is yet to be conducted.

This study aimed to examine the concentration and distribution of OCPs in the Richards Bay area. Using a combination of surface sediment and core sampling, we examine spatial and temporal trends in OCP concentrations to identify potential sinks and sources of contaminants. We integrate our findings with results from previous studies and assess the ecotoxicological implications of OCPs in Richards Bay.

## Materials and Methods

### Study site

Established in 1976, Richards Bay Harbour has become one of the largest exporting ports in Africa. Prior to port construction, Richards Bay was the direct estuary of the Mhlatuze River. This connection was cut off during port construction to minimize the effect of siltation, separating Richards Bay Harbour from the Mhlatuze River, which today flows into the Richards Bay Sanctuary (Fig. 5.1). Industries associated with the port of Richards Bay include the Richards Bay Coal Terminal, an aluminium smelter and exporting freight terminals (Terminal Front) (Fig. 5.1). Freshwater input to Richards Bay Harbour is supplied via the Mzingazi Canal, which connects the port to Lake Mzingazi (Fig. 5.1c). Black Bass Pool is a small, freshwater lake located within rural residences of Richards Bay and is not hydrologically connected to Lake Mzingazi or Richards Bay Harbour.

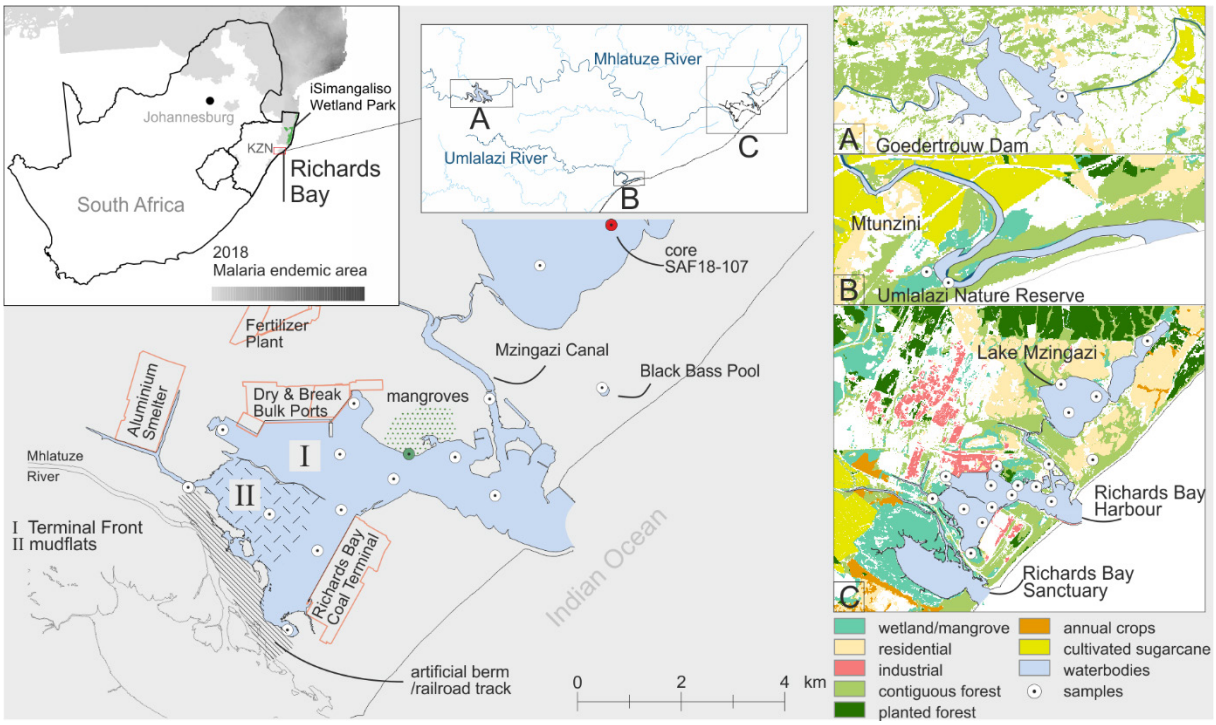


Fig. 5.1: Top-Left: Malaria endemic regions of South Africa (modified from Weiss et al. 2019) (KZN = KwaZulu-Natal), Top Centre: catchment area of Mhlatuze and Umlalazi Rivers. Right: sampling locations and regional overview of Goedertrouw Dam (A), Umlalazi Nature Reserve (B) and Richards Bay (C) showing dominant land use (modified from Thompson 2019). Note the characteristic change in land-use from north-east (residential and industrial) to south-west (wetland/mangrove habitat) of Richards Bay. Centre: Richards Bay Harbour and adjacent industries, as well as the mangrove forest sampling location (green).

## Sample collection

Surface sediment samples were collected during two surveys carried out in 2018 and 2019. Samples from Richards Bay Harbour (n = 12), Lake Mzingazi (n = 3), Black Bass Pool (n = 1), Mangroves at RBH (n = 1), Goedertrouw Dam (n = 1) and Umlalazi Nature Reserve (n = 2) were retrieved using an Ekman-Birge bottom sampler (HYDROBIOS, Kiel, Germany). The topmost 1 cm of the grab was removed with a metal spoon, transferred into a 10 ml glass vial and kept frozen until further processing (Mehlhorn et al. 2021).

To examine temporal variations in OCP accumulation, a 113 cm sediment core (SAF18-107; Fig. 5.1) was retrieved from Lake Mzingazi using a modified ETH-gravity corer (Kelts et al. 1986) with 63 mm tube diameter. The core was split longitudinally, photographed, and lithologically described at the Physical Geography Department of the University of Greifswald. Surface sediments and core subsamples (4 cm intervals, n = 4) were subsequently freeze-dried and ground into fine powder using a ball mill for analysis.

The area of Richards Bay is regarded the final sink for sediments originating from within the Mhlatuze catchment area (Fig. 5.1b). In order to assess the input of contaminants originating

from farther inland, the Goedertrouw Dam was sampled. The Umlalazi Nature Reserve (UMR), near the township of Mtunzini, extends the sample range to the next southern catchment. Two sampling sites were selected, at the border of the mangrove forest and within the Umlalazi River, close to a slipway (Fig. 5.1b).

### Dating

The top 15 cm of sediment core SAF18-107 was radiometric dated using $^{210}$Pb. Measurements of $^{210}$Pb were made by gamma ray spectrometry using a high-purity Germanium detector system at the Laboratoire de Radiochronologie, Université Laval, Quebec, Canada. To establish a chronology, age-depth modelling was performed following the procedure by Aquino-López et al. (2018), using the R package *rplum* version 0.2.2 (Blaauw et al. 2021).

### TOC measurement

Total organic carbon (TOC) was determined by combustion of dried and homogenized samples with a CNS elemental analyser (EuroEA) at the University of Greifswald. Inorganic carbon was removed from sediments prior to measurement using 20% HCl. Control samples were measured in triplicate and did not exceed an error of 3%.

### OCP extraction and analysis

The extraction of OCPs was carried out at the University of the Witwatersrand following previously validated methods (Buah-Kwofie and Humphries 2017). Briefly, 3 – 5 g of dried material were rehydrated in water and extracted with 10 ml acetonitrile (containing 1% glacial acetic acid). A mixture of anhydrous magnesium sulphate ($MgSO_4$), sodium acetate (NaOAc) and sodium acetate trihydrate ($NaOAc{\cdot}3H_2O$) was added to aid in the separation of aqueous and organic phases. The sample was centrifuged and an aliquot of the organic phase was cleaned using a combination of $MgSO_4$, C18 and primary secondary amine (PSA). This mixture was vortexed and then centrifuged to isolate the clean extract. An aliquot of the extract was concentrated to dryness under vacuum at a temperature of < 40°C, reconstituted in hexane and spiked with internal standard (Pentachloronitrobenzene) for final analysis. The recovery efficiency of this method has been shown to range between 68 – 115% (Buah-Kwofie and Humphries 2017).

A total of 17 OCPs were analysed, which included: dichlorodiphenyltrichloroethanes (DDTs; p,p'-DDT, p,p'-DDE and p,p'-DDD; sum expressed as ∑DDT), hexachlorocyclohexanes

(HCHs; α-, β-, γ-, δ-HCH, sum expressed as ∑HCH), drin-residues (aldrin, dieldrin, endrin and endrin ketone; sum expressed as ∑drins), endosulfans (α-, β-endosulfan and endosulfan-sulfate; sum expressed as ∑endosulfans) and chlor-residues (heptachlor, heptachlor epoxide and methoxychlor; sum expressed as ∑chlors). Analysis was performed by two-dimensional gas chromatography – time-of-flight mass spectrometry (GC X GC-TOFMS) using an Agilent 7890 GC coupled to a Leco Pegasus 4D TOF mass spectrometer, as previously described by Buah-Kwofie and Humphries (2017). Quantification was performed using high-purity (> 98%) PESTANAL® reference standards purchased from Sigma Aldrich. Correlation coefficients derived from linear regressions obtained from matrix-matched calibration curves were > 0.99 in all cases.

Sample extracts were analysed in duplicate with relative standard deviations typically < 15%. Quality control standards were run after every third sample to monitor and correct for variations in instrument response. Detection limits ranged between 0.42 and 3.1 ng $g^{-1}$ dry weight (dw).

### Data treatment

Descriptive data analysis was performed using R version 4.1.0 (R Core Team 2021). To test for normal distribution of the data, the Shapiro-Wilk test was performed, revealing summed data to be mainly non-parametric (with the exception of ∑HCH and ∑DDT/TOC). Hence, Spearman rank correlation coefficients were calculated using the function "cor.test(...,method="spearman")", and probability values less than $p < 0.05$ were considered statistically significant. Concentrations below detection limit were assigned a value of zero. Spatial distribution maps were created using the Inverse distance weighted technique of the Spatial Analyst function in ArcMap 10.6.1.

## Results and Discussion

### OCP concentrations and spatial distributions

OCPs were detected at all sampling sites with total concentrations (∑OCP) ranging between 135 and 1020 ng $g^{-1}$ (Table 5.1). All target residues were detected in the vast majority of samples analysed. ∑HCH varied from 35 to 230 ng $g^{-1}$, ∑DDT from 12 to 350 ng $g^{-1}$, ∑drins from 43 to 270 ng $g^{-1}$, ∑endosulfans from 21 to 260 ng $g^{-1}$ and ∑chlor from 18 to 280 ng $g^{-1}$.

| Analytes | Concentration (ng $g^{-1}$) dw | | | | | |
|---|---|---|---|---|---|---|
| | Richards Bay Harbour n = 12 | Lake Mzingazi n = 3 | Black Bass Pool n = 1 | Mangroves at RBH n = 1 | Goedertrouw dam n = 1 | Umlalazi Nature Reserve n = 2 |
| α-HCH | 28 ± 14 (11 – 53) | 25 ± 5.7 (18 – 32) | 27 | 26 | 22 | 9.5 (8.0 – 11) |
| β-HCH | 34 ± 14 (12 – 58) | 46 ± 24 (18 – 76) | 76 | 31 | 24 | 14 (9.0 – 18) |
| δ-HCH | 14 ± 6.1 (7.0 – 28) | 37 ± 20 (12 – 60) | 58 | 20 | 13 | 11 (7.0 – 14) |
| γ-HCH | 51 ± 34 (10 – 110) | 37 ± 6.8 (32 – 47) | 35 | 17 | 47 | 8.5 (7.0 – 10) |
| **∑HCHs** | **130 ± 64 (42 – 230)** | **150 ± 55 (81 – 220)** | **200** | **94** | **110** | **43 (35 – 50)** |
| Aldrin | 9.6 ± 3.1 (6.0 – 15) | 3.0 ± 4.2 (n.d. – 9.0) | 9 | 18 | 12 | 6.5 (4.0 – 9.0) |
| Dieldrin | 15 ± 3.5 (8.0 – 21) | 32 ± 14 (13 – 48) | 59 | 22 | 15 | 11 (4.0 – 18) |
| Endrin | 18 ± 5.0 (11 – 27) | 51 ± 26 (16 – 80) | 26 | 18 | 18 | 18 (10 – 25) |
| Endrin Aldehyde | 15 ± 8.0 (1.0 – 27) | 17 ± 7.0 (8.0 – 25) | 30 | 14 | 15 | 9.0 (8.0 – 10) |
| Endrin ketone | 86 ± 66 (3.0 – 192) | 10 ± 15 (n.d. – 31) | n.d. | 9 | 36 | 0.5 (n.d. – 1.0) |
| **∑Drins** | **140 ± 77 (49 – 270)** | **110 ± 31 (77 – 150)** | **120** | **81** | **96** | **44 (43 – 45)** |
| Heptachlor | 17 ± 6.6 (4.0 – 31) | 35 ± 17 (15 – 56) | n.d. | 10 | 21 | 8.0 (3.0 – 13) |
| Heptachlor epoxide | 9.7 ± 3.3 (5.0 – 17) | 22 ± 10 (8.0 – 33) | 25 | 15 | 9 | 6.0 (5.0 – 7.0) |
| Methoxychlor | 18 ± 8.2 (5.0 – 34) | 42 ± 50 (n.d. – 110) | 250 | 10 | 21 | 6.5 (n.d. – 13) |
| **∑Chlors** | **43 ± 17 (18 – 82)** | **99 ± 56 (37 – 170)** | **208** | **35** | **50** | **20 (18 – 23)** |
| p,p'-DDE | 7.5 ± 2.8 (4.0 – 13) | 15 ± 6.2 (6.0 – 20) | 83 | 11 | 7 | 5.5 (3.0 – 8.0) |
| p,p'-DDD | 13 ± 5.0 (3.0 – 19) | 13 ± 4.5 (8.0 – 19) | 53 | 10 | 7 | 5.0 (4.0 – 6.0) |
| p,p'-DDT | 50 ± 53 (4.0 – 200) | 53 ± 59 (n.d. – 140) | 220 | 17 | 77 | 23 (n.d. – 45) |
| **∑DDTs** | **70 ± 53 (15 – 210)** | **81 ± 65 (31 – 170)** | **350** | **38** | **92** | **33 (12 – 54)** |
| α-Endosulfan | 12 ± 3.2 (7.7 – 19) | 24 ± 11 (9.6 – 35) | 45 | 15 | 12 | 6.8 (5.2 – 8.4) |
| β-Endosulfan | 18 ± 7.7 (8.6 – 33) | 13 ± 7.2 (6.3 – 23) | 17 | 14 | 15 | 6.2 (6.1 – 6.4) |
| Endosulfan sulfate | 71 ± 73 (7.3 – 220) | 22 ± 5.4 (17 – 30) | 11 | 13 | 31 | 7.7 (6.4 – 9.1) |
| **∑Endosulfans** | **100 ± 78 (29 – 261)** | **60 ± 21 (37 – 87)** | **72** | **42** | **58** | **21 (21 – 21)** |
| **∑OCP** | **480 ± 220 (150 – 830)** | **500 ± 180 (270 – 720)** | **1020** | **290** | **400** | **160 (140 – 190)** |

Table 5.1: Mean concentrations ± SD and (min – max) of OCP metabolites in surface sediment samples from Richards Bay (ng $g^{-1}$ dw). n.d. - not detected.

The average ∑OCP concentration in Richards Bay Harbour was 480 ± 220 ng $g^{-1}$ and was similar to total concentrations measured in Lake Mzingazi (500 ± 180 ng $g^{-1}$) and at Goedertrouw Dam (400 ng $g^{-1}$) (Fig. 5.2). Samples from the Umlalazi Nature Reserve (160 ± 25 ng $g^{-1}$) were characterised by overall lower concentrations. Sediment from the mangroves at Richards Bay Harbour indicated intermediate amounts of OCPs (290 ng $g^{-1}$), while Black Bass Pool exhibited the highest ∑OCP concentration (1020 ng $g^{-1}$).

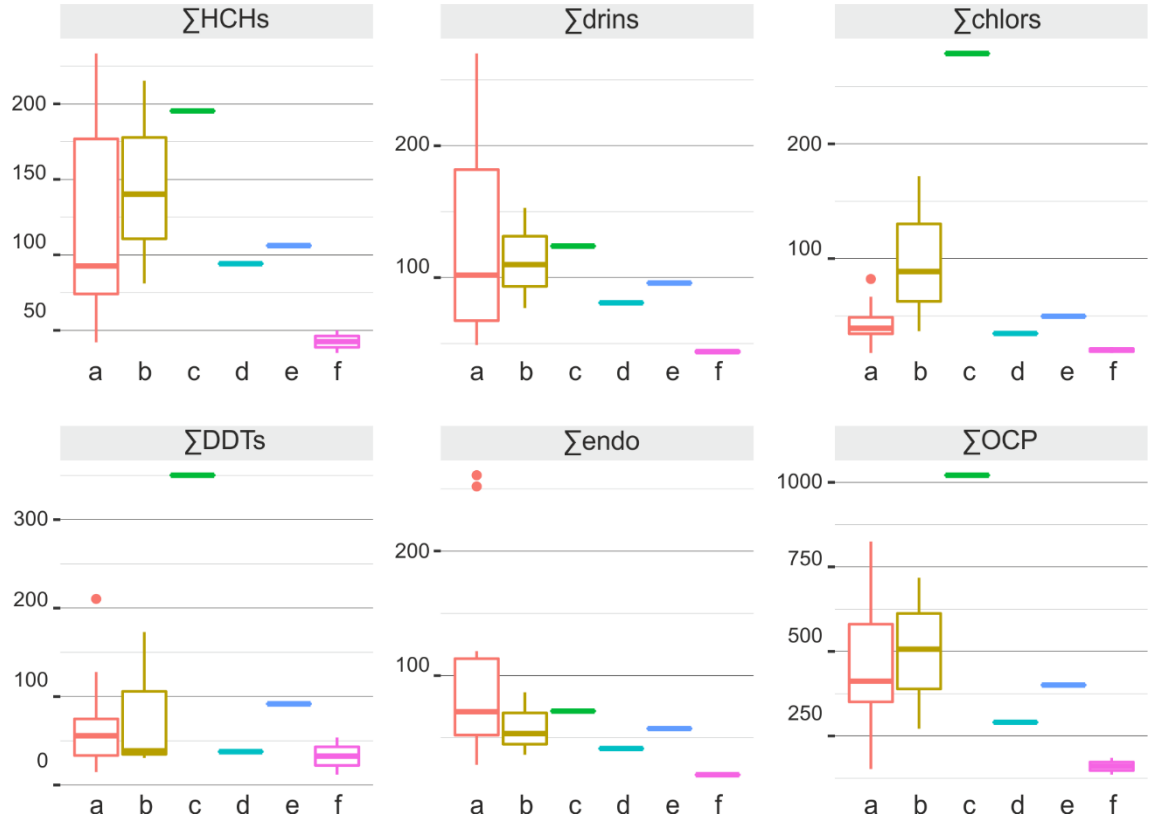


Fig. 5.2: Summed analyte classes and total OCP concentration (∑OCP) ordered by sampling location: a) Richards Bay Harbour, b) Lake Mzingazi, c) Black Bass Pool, d) Mangroves at Richards Bay Harbour, e) Goedertrouw Dam and f) Umlalazi Nature Reserve. The Whiskers of the box plot indicate the 1.5 IQR, dots indicate outliers. See Fig. 5.1 for locations of sampling sites.

DDT

∑DDT concentration in surface sediments from Richards Bay Harbour varied from 15 to 210 ng $g^{-1}$ (Fig. 5.2). Highest concentrations occurred at the Terminal Front (Fig. 5.3), with a general decline towards the Indian Ocean. Sediments from Lake Mzingazi were characterised by similar ∑DDT concentrations, ranging between 32 and 170 ng $g^{-1}$. Black Bass Pool revealed the highest ∑DDT values at 350 ng $g^{-1}$, while substantially lower concentrations were detected in river bed (54 ng $g^{-1}$) and mangrove (12 ng $g^{-1}$) sediments from Umlalazi Nature Reserve, and in sediment from Goedertrouw Dam (92 ng $g^{-1}$).

### HCH

∑HCH concentrations in surface sediments from Richards Bay Harbour ranged from 42 to 230 ng $g^{-1}$, with highest concentrations detected near the Coal Terminal (Fig. 5.3). ∑HCH in surface sediments from Lake Mzingazi varied from 80 to 215 ng $g^{-1}$ and showed a similar distribution to ∑DDT. Total HCH concentrations at Black Bass Pool (195 ng $g^{-1}$) were similar to maximum concentrations in Richards Bay Harbour and Lake Mzingazi, while samples from Umlalazi indicated lower concentrations (35 -50 ng $g^{-1}$). The inland location at Goedertrouw Dam indicated an intermediate concentration of 110 ng $g^{-1}$ (Fig. 5.2).

### Other OCP residues

The distribution of chlor residues in Richards Bay Harbour was confined to three local maxima: mid-port, at the north-western bulk-terminal and inside the Mzingazi Canal. In Lake Mzingazi, high concentrations were found in the centre of the main lake (90 ng $g^{-1}$) and the north-eastern lake (170 ng $g^{-1}$). Highest chlor concentrations were found at Black Bass Pool (280 ng $g^{-1}$), while relatively low levels were detected at Umlalazi Nature Reserve (avg. 20 ng $g^{-1}$) and Goedertrouw Dam (50 ng $g^{-1}$).

Concentrations of ∑drins and ∑endosulfans in Richards Bay varied from 50 to 270 ng $g^{-1}$ and 30 to 260 ng $g^{-1}$, respectively. In general, ∑drins, ∑endosulfans and ∑OCP showed similar distribution patterns to ∑HCHs, as indicated by correlation factors of 0.9 ($p < 0.001$), 0.81 ($p < 0.001$) and 0.95 ($p < 0.001$), respectively.

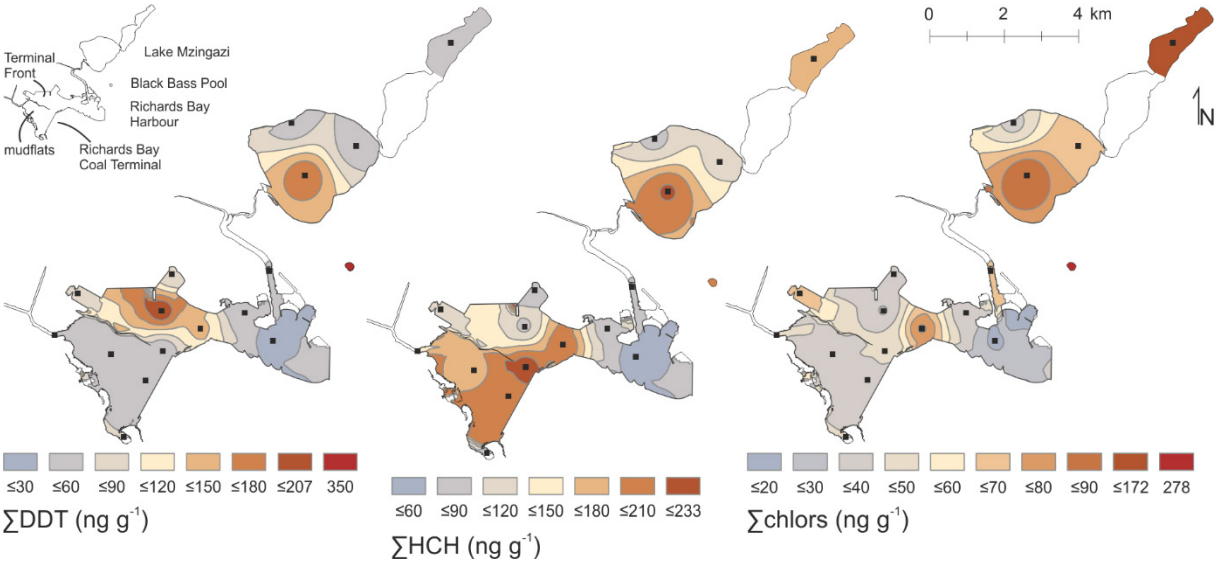


Fig. 5.3: Spatial distribution maps of the metabolite sums ∑DDT, ∑HCH and ∑chlors (left to right).

## Temporal variations in OCP accumulation

The $^{210}$Pb-derived age-model for the top 15 cm of core SAF18-107 provided a chronology for the past ~85 ± 30 years (Fig. 5.4). The concentration of ∑OCPs steadily increases from 355 ng g$^{-1}$ in 1947 (± 15 years) to 781 ng g$^{-1}$ in 1992 (± 10 years), and then decreases to 400 ng g$^{-1}$ in the most recent sample (2011 ± 8 years) (Fig. 5.5). Total concentrations measured of individual metabolite sums indicate very similar trends (Fig. 5.5) and correspond well with the rise in pesticide usage in South Africa during the mid-1940s to mid-1990s. The peak in pesticide concentrations from 1982 to 2003 covers a time period where OCPs were used extensively in agriculture and for disease vector control. Observed decreases in OCP concentration over the last two decades correspond with government actions limiting the use of OCPs in the 1990s and eventual ban under the Stockholm Convention in 2004. Although use of DDT was reintroduced in 2000 and continues to be employed today, application is implemented in a more targeted manner through IRS.

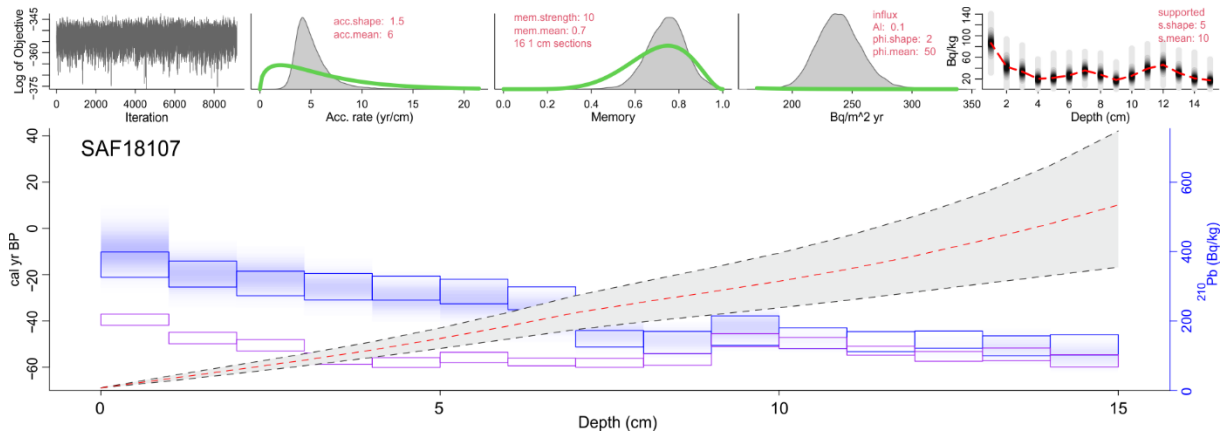


Fig. 5.4: $^{210}$Pb-derived age-depth model of sediment core SAF18-107 using the Bayesian chronological approach of Aquino-López et al. (2018).

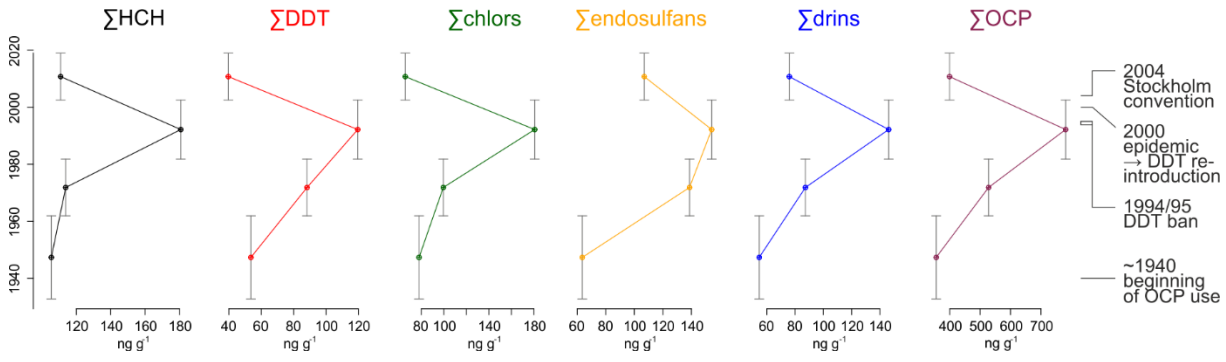


Fig. 5.5: Concentrations of OCP metabolites over time from sediment core SAF18-107 recovered from Richards Bay Harbour. Historical events are modified from Coetzee et al. (2013).

## OCP compositions and potential sources

On average, ∑DDT concentrations in Richards Bay surface sediment samples were composed of 68% p,p'-DDT, 14% p,p'-DDD and 18% p,p'-DDE (Fig. 5.6). Technical DDT consists of ~77% p,p'-DDT, 15% o,p'-DDT, and negligible percentages of its metabolites p,p'-DDD (0.3%) and p,p'-DDE (4%) (World Health Organization (WHO) 1989). The relatively high proportion of p,p'-DDT measured in samples thus suggests recent input of technical DDT into the environment at Richards Bay.

The ratio between the parent compound and the sum of its metabolites ($\frac{p,p'-DDT}{p,p'-DDD + p,p'-DDE}$) can be used to distinguish between current and historical usage of DDT (Qian et al. 2006). Over time, the proportion of metabolites is expected to increase, with relatively low DDT/(DDD+DDE) ratios being indicative of historical inputs. Hiller et al. (2011) used a ratio of 0.4 to distinguish between recent and historical DDT inputs. Sediments from Richards Bay Harbour and surrounding environments are characterised by DDT/(DDD+DDE)-ratios that greatly exceed 1 (mean: 2.7), suggesting the recent use of DDT as part of ongoing malaria vector control through IRS. In contrast, very low DDT-ratios (<0.4) were reported for iSimangaliso Wetland Park (Humphries 2013, Buah-Kwofie and Humphries 2017), indicating relatively long term degradation. The comparably high DDT-ratios measured in sediments from Richards Bay likely reflect a close proximity to IRS-treated areas.

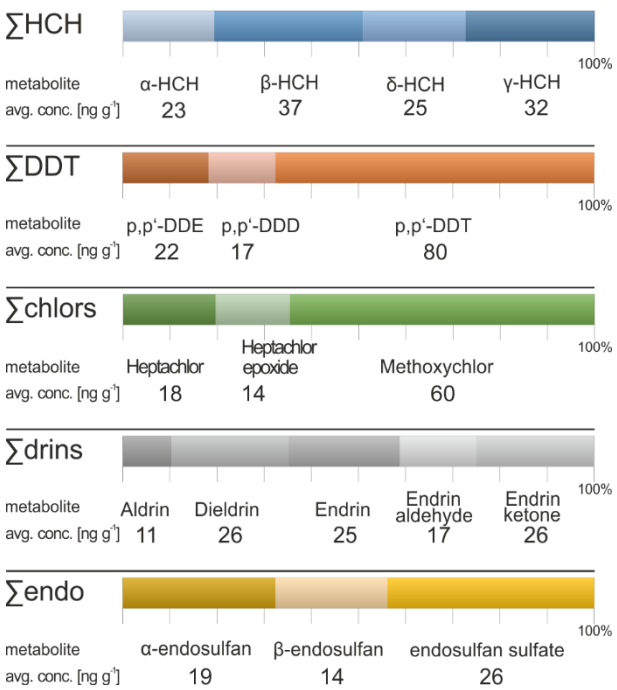


Fig. 5.6: Average composition and concentration of individual metabolite in surface sediments from the Richards Bay region.

Lindane (pure γ-HCH) has a half-life of about two weeks, and is degraded by microorganisms (Benezet and Matsumura 1973) and photo-chemically isomerized to α-HCH (Malaiyandi and Shah 1984). The α- and γ-isomers degrade to the more stable β-form (Walker et al. 1999, Willett et al. 1998), which is highly persistent in the environment (Malik et al. 2007). In contrast, technical HCH usually contains only 10-12% γ-HCH (Saadati et al. 2012). At Richards Bay, γ-HCH comprises an average of 27% of ∑HCH (Fig. 5.6), suggesting the recent input of lindane at all sites. This is in contrast to sites situated in northern KwaZulu-Natal where γ-HCH was rarely detected in sediments from Lake Sibaya and Kosi Bay (Buah-Kwofie and Humphries, 2017).

Aldrin was present in lower abundance compared to dieldrin (aldrin/dieldrin ratio = 0.6; Fig. 5.6), which is attributed to the long-term degradation of aldrin to the more stable and persistent dieldrin metabolite. This is similar to what Buah-Kwofie and Humphries (2017) reported in sediments from iSimangaliso Wetland Park.

Although endrin has a half-life of 12-20 years and was banned in South Africa during the 1980s (Fischer et al. 2011), the detection of relatively high proportions of endrin relative to its metabolites (endrin ketone and endrin aldehyde) in surface sediment samples suggest possible recent contamination/use. In sediment, the rapid metabolization of heptachlor (half-life of 1 – 3.5 days; Reed and Koshlukova 2014) to the more stable heptachlor epoxide is expected (World Health Organization (WHO) 2006). However, at most sampling sites the heptachlor/heptachlor-epoxide ratio exceeded 1, indicating potential recent inputs in Richards Bay. This contrasts with northern sites in iSimangaliso Wetland Park (Buah-Kwofie and Humphries 2017) and surrounding river catchments (Buah-Kwofie and Humphries 2021) which indicate historical use of heptachlor.

β-endosulfan degrades slower than α-endosulfan towards the more stable endosulfan-sulfate (Ghadiri and Rose 2001). Sediments from Richards Bay were characterised by average α-endosulfan/β-endosulfan metabolite ratios of < 1 and suggest historic input, correspond to sites in iSimangaliso Wetland Park (Buah-Kwofie and Humphries 2017).

### Sources and sinks of contamination

OCPs bind strongly to organic matter, which can affect their representation in heterogeneously composed surface samples. In order to reduce matrix effects and identify potential sources of contamination, OCP concentrations were normalised to TOC.

The distribution map of p,p'-DDT/TOC shows elevated ratios inside the industrial port section of Richards Bay Harbour and along the western margin of Lake Mzingazi (Fig. 5.7). Extensive development (residential and industrial, Fig. 5.7) associated with the town of Richards Bay is a likely source for DDT entry (i.e. by IRS).

In contrast, high γ-HCH/TOC ratios are found in front of the Richards Bay Coal Terminal and extend into the mudflats, a non-dredged, shallow water area of the port that experiences little marine traffic (Fig. 5.1, Fig. 5.7). Farmland directly west of Richards Bay Harbour, including commercial sugar cane cultivation and subsistence farming is a likely source of γ-HCH contamination, which enters the port via nearby canals on the western side of the mudflats. In Lake Mzingazi, highest normalised p,p'-DDT and γ-HCH values are found along the north western margin of the lake. The adjacent land use is characterised by densely populated residential areas and commercial forestry to the north of Lake Mzingazi (Fig. 5.7), which is the likely origin of these pollutants.

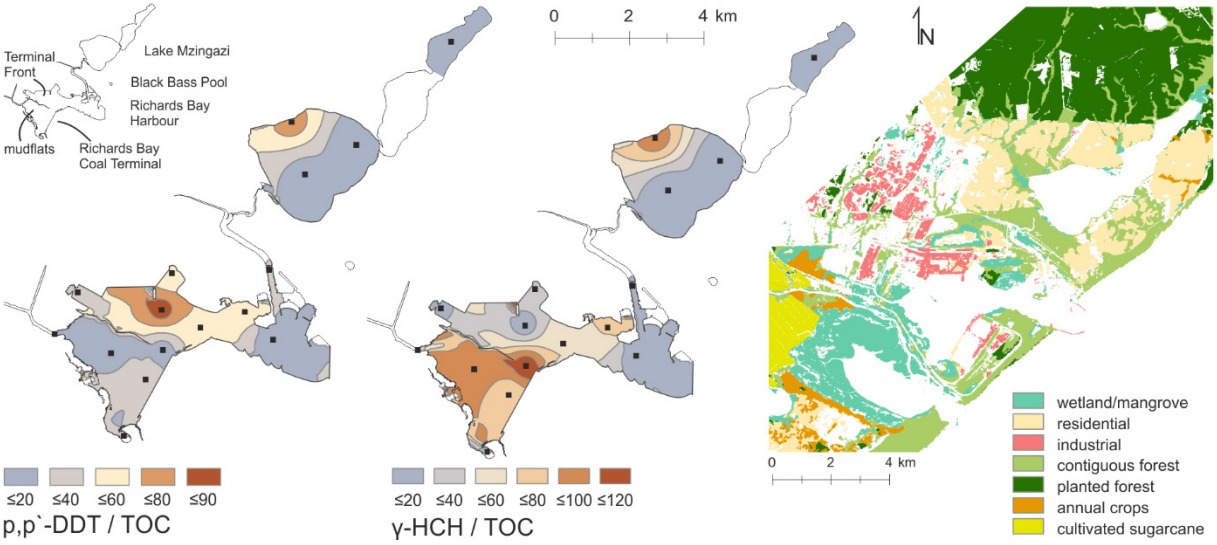


Fig. 5.7: Spatial distribution patterns of p,p'-DDT/TOC (left), γ-HCH/TOC (middle) and land use data (right; modified from Thompson 2019). To account for matrix effects, isomeric metabolite concentrations are normalised to TOC. At Lake Mzingazi elevated ratios occur in the northwest of the lake. In Richards Bay Harbour, increased p,p'-DDT ratios locate at the Terminal Front, in conjunction with the main industrial site of the port. γ-HCH ratios locate at the mudflats and the Coal Terminal where effluents of nearby farmland might drain into the port via the canal systems.

The TOC-normalised distribution patterns of heptachlor (r = 0.81), endrin (r = 0.79), aldrin (r = 0.78) and α-endosulfan (r = 0.82) correlated well with γ-HCH, which indicates a similar source to HCH (i.e. agriculture and forestry).

## Ecotoxicological evaluation

OCPs in sediment have the potential for biological uptake. To evaluate the potential toxicological effects, sediment quality guidelines (SQG) proposed by National Oceanic and Atmospheric Administration (NOAA) (MacDonald et al. 1996, MacDonald et al. 2000, Long et al. 1995) were employed. Using this approach, each chemical is classified by two guideline values, the effect range low (ERL) which represents the concentration below which adverse effects are rarely observed, and the effect range medium (ERM), above which adverse toxicological effects would frequently occur. Moderate toxicological incidence is expected at concentrations between the ERL and ERM values (Birch and Hutson 2009).

In this study, the ERL threshold is exceeded at all sampling points (Fig. 5.8). Additionally, all samples (100%) exceeded the γ-HCH and ∑Chlors ERM values, while most (> 90%) also exceeded the p,p'-DDT and dieldrin ERM values (Fig. 5.8). Therefore, the majority of the samples also indicate a high probability of adverse toxicological effects.

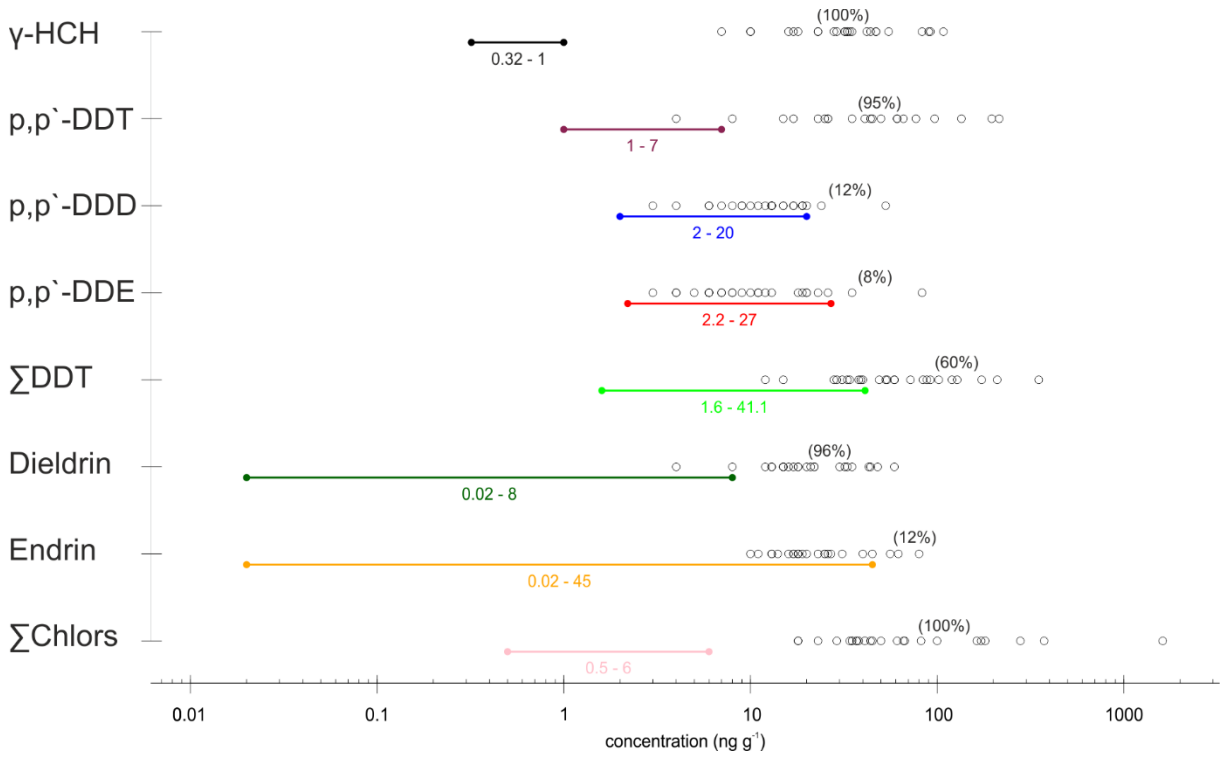


Fig. 5.8: Comparison of individual OCP concentrations (circles) measured in surface sediments from Richards Bay, with sediment quality guidelines proposed by NOAA (Long et al. 1995). Effect Range Low (ERL) and Effect Range Median (ERM) are depicted by coloured dots connected by a line. Percentages are given for samples exceeding the ERM.

The OCP concentrations measured in sediments from Richards Bay raise ecological and human health concerns. As shown in studies from iSimangaliso Wetland Park, OCPs readily enter the food chain and bioaccumulate in aquatic species (Bouwman et al. 2019, Buah-Kwofie and

Humphries 2021, Humphries et al. 2021). Potential human health risks also exist to local communities who catch fish from the harbour and lakes in Richards Bay, or who cultivate crops within the area (e.g. Buah-Kwofie et al. 2019). Additional studies examining bioaccumulation and human health exposure to OCPs at Richards Bay are therefore recommended.

### Regional comparison

The sediment OCP concentrations measured at Richards Bay fall within the range previously reported for other coastal systems in northern KZN (Buah-Kwofie and Humphries, 2017; Fig. 5.9). While comparisons between different systems are potentially complicated by variances in the time of sampling, nature of the sediment analysed and the sampling strategy employed, regional trends in concentration are evident. In general, catchment size and proximity to potential sources of contamination are important factors influencing total OCP concentrations. Systems associated with large catchment areas impacted by agriculture (e.g. the Mkhuze wetlands) typically show higher levels of OCP accumulation than sites that receive limited amounts of catchment runoff (e.g. Kosi Bay and Lake Sibaya). Total OCP concentrations at Richards Bay are similar to those reported for Kosi Bay and Lake Sibaya, likely indicative of the relatively confined catchment area that characterises the modern-day system.

Buah-Kwofie and Humphries (2017) noted a clear north to south decreasing gradient in ∑DDT concentrations, which was attributed to IRS and the extent to which DDT is used within the respective catchment areas. St Lucia and Mkhuze are considered relatively low-risk malaria areas, while outbreaks of malaria have historically been more common in areas farther north. However, DDT concentrations at Richards Bay do not follow this trend, which we attribute to the close proximity of contamination sources (IRS) at this site. ∑DDT concentrations in iSimangaliso Wetland Park are composed predominantly of the metabolites p,p'-DDD and p,p'-DDE. In contrast, p,p'-DDT is the major (80%) DDT metabolite at Richards Bay, indicating that total DDT concentrations at this site are strongly influenced by current IRS practices.

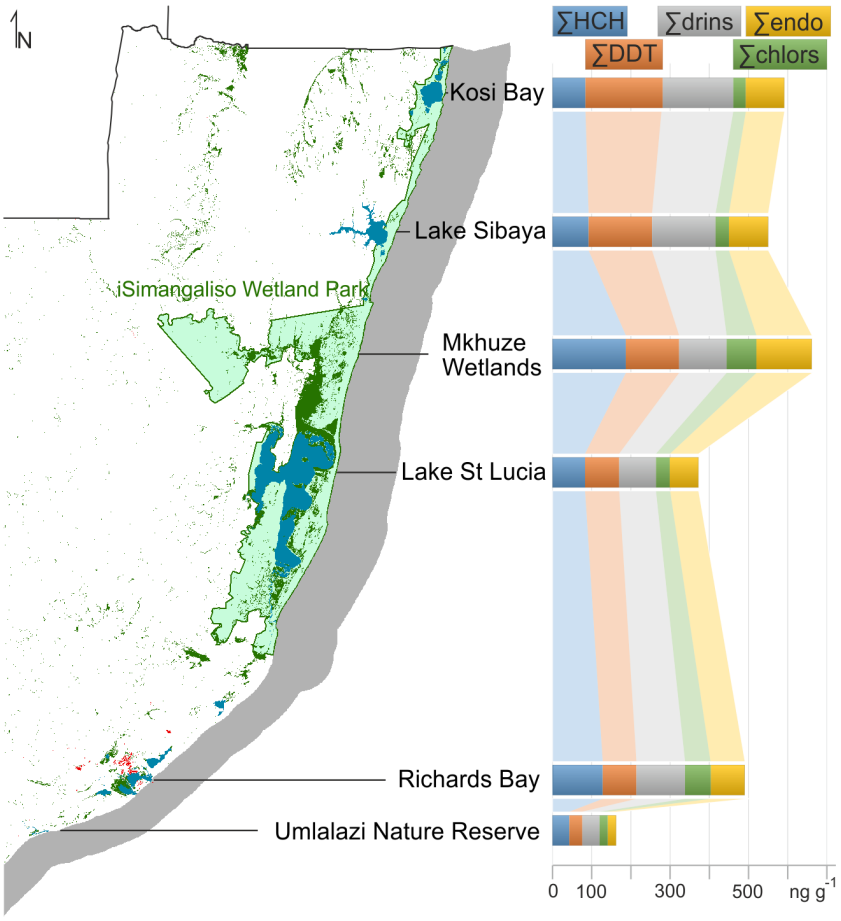


Fig. 5.9: Regional overview of South Africa's east coast, modified from SANLC 2018 (Thompson 2019) and additionally indicating locations of previous OCP investigations by Buah-Kwofie and Humphries (2017). In side-to-side comparison, locations match the concentrations of OCPs measured in that area. The graph indicates the effect of increased use of pesticides in Richards Bay and the Mkhuze Wetlands. Note general decreasing DDT concentrations from north to south, whereby Lake St Lucia and Richards Bay indicate similar amounts, despite the regional difference.

## Conclusions

This study shows that harbour sediments can be an important sink for organic contaminants. OCPs were widely found in sediments from Richards Bay, the distribution of which could be linked to land use and anthropogenic activities in the region. Agriculture was identified as an important source of legacy OCP contamination, although the recent use of lindane, heptachlor and endrin, possibly from old stockpiles, is suspected. The prevalence of DDT in sediments was linked to ongoing malaria control measures, with highest concentrations found at sites adjacent to densely populated residential areas. Decreases in OCP concentration over the past two decades indicate the effectiveness of restrictions in reducing contaminant input to the environment. However, despite current restrictions, many of the OCP concentrations measured exceeded sediment quality guidelines and are therefore likely to have adverse impacts on both human and ecosystem health. The accumulation of substantial quantities of

OCP residues within Richards Bay Harbour indicates the need for further monitoring and this study provides important baseline data for future assessments. Furthermore, a detailed investigation into the bioaccumulation of OCPs and associated toxicological risks to biological ecosystems and human health is urgently required.

## Acknowledgements

This work was supported by the German Federal Ministry of Education and Research [grant number: 03F0798C] and is part of project TRACES (Tracing Human and Climate impact in South Africa) within the SPACES II Program (Science Partnerships for the Assessment of Complex Earth System Processes). PM and JG would like to thank the DAAD for the scholarship and the opportunity to visit the University of the Witwatersrand. Further, we would like to acknowledge the support by the University of the Witwatersrand. We acknowledge Andrew Green from the University of KwaZulu-Natal and George Best, as well as Olga Gildeeva and Peter Frenzel from the Friedrich-Schiller-University Jena, who assisted in the field.

## References

Aquino-López MA, Blaauw M, Christen JA, Sanderson NK (2018) Bayesian Analysis of $^{210}$Pb Dating. JABES 23(3):317–333. doi: 10.1007/s13253-018-0328-7

Benezet HJ, Matsumura F (1973) Isomerization of γ-BHC to α-BHC in the Environment. Nature 243(5408):480–481. doi: 10.1038/243480a0

Birch GF, Hutson P (2009) Use of sediment risk and ecological/conservation value for strategic management of estuarine environments: Sydney estuary, Australia. Environmental Management 44(4):836–850. doi: 10.1007/s00267-009-9362-0

Blaauw MJ, Christen A, Aquino-Lopez MA (2021) rplum: Bayesian Age-Depth Modelling of Cores Dated by Pb-210. R package version 0.2.1.

Bornman MS, Barnhoorn IE, Genthe B, van Vuuren JH, Pieterse GM, Aneck-Hahn NH (2010) DDT for malaria control: effects in indicators and health risk. Water Research Commission Report 1674(1):9

Bouwman H (2004) South Africa and the Stockholm Convention on Persistent Organic Pollutants. South African Journal of Science 100(7):323–328

Bouwman H, Yohannes YB, Nakayama SMM, Motohira K, Ishizuka M, Humphries MS, van der Schyff V, Du Preez M, Dinkelmann A, Ikenaka Y (2019) Evidence of impacts from DDT in pelican, cormorant, stork, and egret eggs from KwaZulu-Natal, South Africa. Chemosphere 225:647–658. doi: 10.1016/j.chemosphere.2019.03.043

Buah-Kwofie A, Humphries MS (2017) The distribution of organochlorine pesticides in sediments from iSimangaliso Wetland Park: Ecological risks and implications for conservation in a biodiversity hotspot. Environmental Pollution (Barking, Essex : 1987) 229:715–723. doi: 10.1016/j.envpol.2017.07.031

Buah-Kwofie A, Humphries MS (2021) Organochlorine pesticide accumulation in fish and catchment sediments of Lake St Lucia: Risks for Africa's largest estuary. Chemosphere 274:129712. doi: 10.1016/j.chemosphere.2021.129712

Buah-Kwofie A, Humphries MS, Pillay L (2018) Bioaccumulation and risk assessment of organochlorine pesticides in fish from a global biodiversity hotspot: iSimangaliso Wetland Park, South Africa. The Science of the Total Environment 621:273–281. doi: 10.1016/j.scitotenv.2017.11.212

Buah-Kwofie A, Humphries MS, Pillay L (2019) Dietary exposure and risk assessment of organochlorine pesticide residues in rural communities living within catchment areas of iSimangaliso World Heritage Site, South Africa. Environmental Science and Pollution Research International 26(17):17774–17786. doi: 10.1007/s11356-019-05046-9

Cloete CE, Oliff WD (1976) South African Marine Pollution Survey Report 1974-1975. National Scientific Programmes Unit: CSIR

Coetzee M, Kruger P, Hunt RH, Durrheim DN, Urbach J, Hansford CF (2013) Malaria in South Africa: 110 years of learning to control the disease. South African Medical Journal 103(10 Pt 2):770–778. doi: 10.7196/SAMJ.7446

FAO (2020) FAOSTAT Pesticide Use Dataset. http://www.fao.org/faostat/en/#data/RP

Fischer D, Costley S, Moloi M, Jila X, Khauoe G (2011) South Africa National Implementation Plan for the Stockholm Convention on Persistent Organic Pollutants

Gardner BD, Connel AD, Eagle GA, Molden AG, Oliff WD, Orren MJ, Watling RJ (1983) South African Marine Pollution Survey Report 1976-1979

Gerber R, Smit NJ, van Vuren JHJ, Nakayama SMM, Yohannes YB, Ikenaka Y, Ishizuka M, Wepener V (2016) Bioaccumulation and human health risk assessment of DDT and other organochlorine pesticides in an apex aquatic predator from a premier conservation area. The Science of the Total Environment 550:522–533. doi: 10.1016/j.scitotenv.2016.01.129

Ghadiri H, Rose CW (2001) Degradation of endosulfan in a clay soil from cotton farms of western Queensland. Journal of Environmental Management 62(2):155–169. doi: 10.1006/jema.2001.0428

Hiller E, Sirotiak M, Tatarková V, Jurkovič Ľ (2011) Occurrence of selected organochlorine pesticide residues in surface sediments from the Velke Kozmalovce, Ruzin, and Zemplinska Sirava water reservoirs, Slovakia. Journal of Hydrology and Hydromechanics 59(1). doi: 10.2478/v10098-011-0004-x

Humphries MS (2013) DDT residue contamination in sediments from Lake Sibaya in northern KwaZulu-Natal, South Africa: implications for conservation in a World Heritage Site. Chemosphere 93(8):1494–1499. doi: 10.1016/j.chemosphere.2013.07.047

Humphries MS, Myburgh JG, Campbell R, Buah-Kwofie A, Combrink X (2021) Organochlorine pesticide bioaccumulation in wild Nile crocodile (Crocodylus niloticus) fat tissues: Environmental influences on changing residue levels and contaminant profiles. The Science of the Total Environment 753:142068. doi: 10.1016/j.scitotenv.2020.142068

Kelts K, Briegel U, Ghilardi K, Hsu K (1986) The limnogeology-ETH coring system. Schweiz. Z. Hydrol 48(1):104–115. doi: 10.1007/bf02544119

Long ER, Macdonald DD, Smith SL, Calder FD (1995) Incidence of adverse biological effects within ranges of chemical concentrations in marine and estuarine sediments. Environmental Management 19(1):81–97. doi: 10.1007/BF02472006

MacDonald DD, Carr RS, Calder FD, Long ER, Ingersoll CG (1996) Development and evaluation of sediment quality guidelines for Florida coastal waters. Ecotoxicology (London, England) 5(4):253–278. doi: 10.1007/BF00118995

MacDonald DD, Ingersoll CG, Berger TA (2000) Development and evaluation of consensus-based sediment quality guidelines for freshwater ecosystems. Archives of Environmental Contamination and Toxicology 39(1):20–31. doi: 10.1007/s002440010075

Maharaj R, Seocharan I, Qwabe B, Mkhabela M, Kissoon S, Lakan V (2019) Decadal epidemiology of malaria in KwaZulu-Natal, a province in South Africa targeting elimination. Malaria Journal 18(1):368. doi: 10.1186/s12936-019-3001-x

Malaiyandi M, Shah SM (1984) Evidence of photoisomerization of hexachlorocyclohexane isomers in the ecosphere. Journal of Environmental Science and Health . Part A: Environmental Science and Engineering 19(8):887–910. doi: 10.1080/10934528409375200

Malik A, Singh KP, Ojha P (2007) Residues of organochlorine pesticides in fish from the Gomti river, India. Bulletin of Environmental Contamination and Toxicology 78(5):335–340. doi: 10.1007/s00128-007-9188-5

Mestres M, Sanchéz-Arcilla A, Sierra JP, Mösso C, Tagliani PRA, Möller Junior OO, Niencheski LFH (2006) Coastal bays as a sink for pollutants and sediment. 0749-0208

Potapowicz J, Lambropoulou D, Nannou C, Kozioł K, Polkowska Ż (2020) Occurrences, sources, and transport of organochlorine pesticides in the aquatic environment of Antarctica. The Science of the Total Environment 735:139475. doi: 10.1016/j.scitotenv.2020.139475

Qian Y, Zheng M, Zhang B, Gao L, Liu W (2006) Determination and assessment of HCHs and DDTs residues in sediments from Lake Dongting, China. Environmental Monitoring and Assessment 116(1-3):157–167. doi: 10.1007/s10661-006-7233-1

Quinn LP, de Vos BJ, Fernandes-Whaley M, Roos C, Bouwman H, Kylin H, Pieters R, van den Berg J (2011) Pesticide Use in South Africa: One of the Largest Importers of Pesticides in Africa. In: Stoytcheva M (ed) Pesticides in the Modern World - Pesticides Use and Management. InTech, Croatia, pp 49–96

R Core Team (2021) A language and environment for statistical computing. R Foundation for Statistical Computing, Vienna, Austria

Reed NR, Koshlukova S (2014) Heptachlor. In: Encyclopedia of Toxicology. Elsevier, pp 840–844

Roos C (2010) Characterising the scale and significance of persistent organic pollutants in South African sediments. Doctoral dissertation, North-West University

Saadati N, Abdullah MP, Zakaria Z, Rezayi M, Hosseinizare N (2012) Distribution and fate of HCH isomers and DDT metabolites in a tropical environment-case study Cameron Highlands-Malaysia. Chemistry Central Journal 6(1):130. doi: 10.1186/1752-153X-6-130

Saulnier I, Mucci A (2000) Trace metal remobilization following the resuspension of estuarine sediments: Saguenay Fjord, Canada. Applied Geochemistry 15(2):191–210. doi: 10.1016/S0883-2927(99)00034-7

Thompson M (2019) DEA E1434 Land-Cover South African National Land-Cover 2018 Report & Accuracy Assessment

Tyohemba RL, Pillay L, Humphries MS (2020) Herbicide residues in sediments from Lake St Lucia (iSimangaliso World Heritage Site, South Africa) and its catchment areas: Occurrence and ecological risk assessment. Environmental Pollution (Barking, Essex : 1987) 267:115566. doi: 10.1016/j.envpol.2020.115566

Walker K, Vallero DA, Lewis RG (1999) Factors Influencing the Distribution of Lindane and Other Hexachlorocyclohexanes in the Environment. Environmental Science & Technology 33(24):4373–4378. doi: 10.1021/es990647n

Weiss DJ, Lucas TCD, Nguyen M, Nandi AK, Bisanzio D, Battle KE, Cameron E, Twohig KA, Pfeffer DA, Rozier JA, Gibson HS, Rao PC, Casey D, Bertozzi-Villa A, Collins EL, Dalrymple U, Gray N, Harris JR, Howes RE, Kang SY, Keddie SH, May D, Rumisha S, Thorn MP, Barber R, Fullman N, Huynh CK, Kulikoff X, Kutz MJ, Lopez AD, Mokdad AH, Naghavi M, Nguyen G, Shackelford KA, Vos T, Wang H, Smith DL, Lim SS, Murray CJL, Bhatt S, Hay SI, Gething PW (2019) Mapping the global prevalence, incidence, and mortality of Plasmodium falciparum, 2000–17: a spatial and temporal modelling study. The Lancet 394(10195):322–331. doi: 10.1016/S0140-6736(19)31097-9

Willett KL, Ulrich EM, Hites RA (1998) Differential Toxicity and Environmental Fates of Hexachlorocyclohexane Isomers. Environmental Science & Technology 32(15):2197–2207. doi: 10.1021/es9708530

World Health Organization (WHO) (1989) DDT and its Derivates, Environmental Aspects. World health organization, Geneva, Switzerland

World Health Organization (WHO) (2006) Heptachlor. Concise International Chemical Assessment Document, vol 70. World health organization, Geneva

## Statements and Declarations

### Funding

This work was supported by the German Federal Ministry of Education and Research [grant number: 03F0798C] and is part of project TRACES (Tracing Human and Climate impact in South Africa) within the SPACES II Program (Science Partnerships for the Assessment of Complex Earth System Processes).

### Competing interests

The authors declare no competing interests.

### Author contribution

Conceptualisation: PM, MH, JG, ABK, RLT, TH; Data Curation: PM; Formal analysis: PM, MH, JG, ABK, RLT; Funding acquisition: MH, TH; Investigation: PM, JG, ABK, RLT; Project administration: MH, TH; Resources: MH; Visualisation: PM; Writing – original draft: PM; Writing – review and editing: MH, JG, AKB, RLT, TH.

### Data availability

The datasets used or analysed during the current study are available from the corresponding author on reasonable request.

### Ethics approval and consent to participate

Not applicable

### Consent for publication

Not applicable

# Chapter 6
# Synthesis

## Synthesis
### Chronological challenges in sediments from Richards Bay Harbour

The very invasive 1970's port construction and ongoing maintenance dredging has been posing an ever-present concern for dating in sediment cores. Ages obtained in sediment cores have been stratigraphically inconsistent and much older than expected, given the age of the port itself (Fig. 6.1).

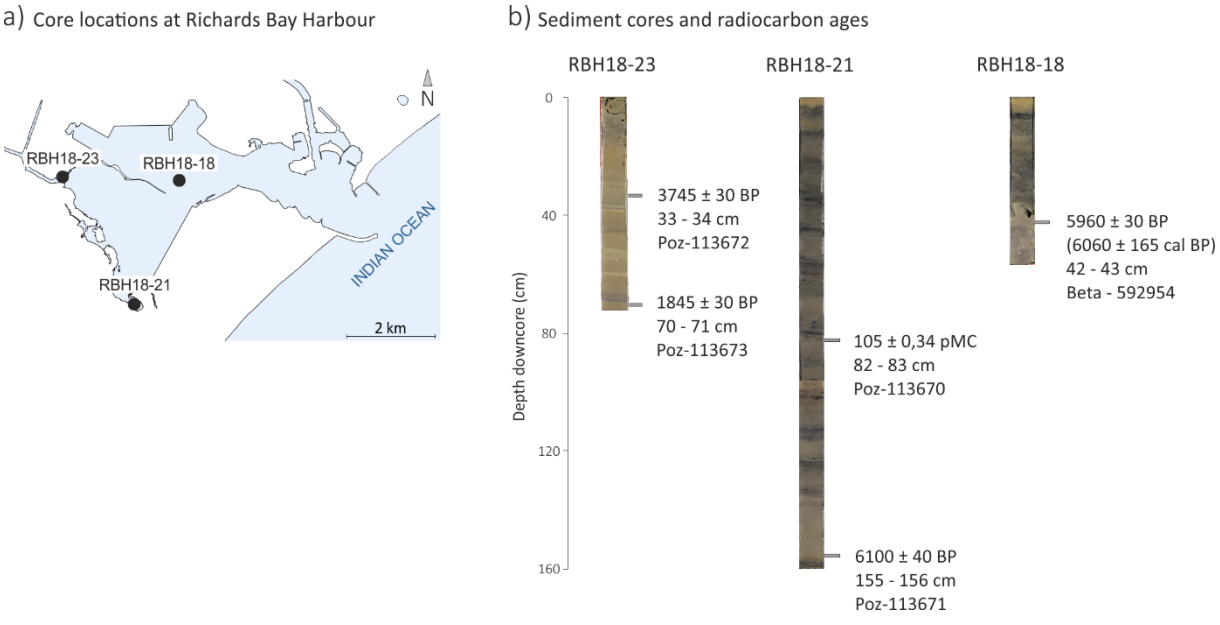


Fig. 6.1: Results of radiocarbon dating on cores from Richards Bay Harbour. a) Locations of sediment cores obtained from Richards Bay Harbour. b) Sediment core images to scale with radiocarbon age, sampling depth and Laboratory Number from the Poznań Radiocarbon Laboratory (Poz) and Beta Analytic (Beta).

The longest core, RBH18-21, indicated a basal age of 6100 ± 40 BP at a depth of 160 cm, while at 80 cm modern carbon was confirmed. Core RBH18-23 indicted an age inversion.

The inconsistency of measured ages may be partially ascribed to the change in tidal range, which increased due to the estuary port conversion and led to the reworking of older organic material in the sediment (Chapter 4). The base of sediment core RBH18-18 gave access to a stiff grey clay with a sharp transition to modern sedimentation, which was otherwise noticed in fragments and far deeper within the sedimentary record. Given the maximum age of 6060 ± 165 cal BP for this grey clay, a hiatus to older strata caused by dredging is very likely. An otherwise continuous modern sedimentation was assumed above this hiatus by comparing multiple sediment cores all over the port area. The cores show a homogeneous trend in magnetic susceptibility, often with increasing intensity to the surface of the sediment (Chapter 2). Seismic data giving insights to the internal structure of the sediments in Richards Bay Harbour also indicate coherent sediment units (Unit 7a and 7b; Chapter 4), while direct signs of dredging are found in the bathymetrical data at the sediment surface (Chapter 2, 4). A rough age estimate for some sediment cores may be based on the change (decrease) of Cu concentrations from 2012 to 2018, which is also recorded as decreasing Cu counts in sediment cores (Chapter 2).

### On the origin of pollutants

The analyses of potential pollutants within Richards Bay Harbour indicate multiple stressors from different sources. Ongoing economic development, particularly industrialisation, has been affecting the harbour's environment and ultimately its sediment. Transhipment at export and import terminals lead to the input of various (heavy) metals. Anthropogenically induced variations in spatial extent and intensity of metal concentration are noticeable in surface sediment, especially regarding Cr and Cu distributions (Chapter 2, 3; Fig. 6.2). The analysis of organochlorine pesticides (Chapter 5) reveals DDT concentrations to be similarly distributed within the harbour (Fig. 6.2). These contaminants indicate increased amounts in the sub-basin close to the Terminal Front. Despite their sink relationship, different factors are assumed to cause pollution. DDT-based vector control is legal in malaria endemic regions and used in residential areas (by indoor residual spraying). Unlike the primarily industrial induced metal contamination, the source of DDT contamination should originate from urbanised districts, presumably north of the industrialised sector.

Besides economical aspects, the embayment is also used for recreational purposes. Microplastics contamination is especially high in samples related to publically accessible,

recreational beaches, which are crowded during weekends. Bound to the hydrodynamic regime and physicochemical properties, PET and LDPE particles are deposited nearshore public beaches and in sub-basins of low current velocity further away, respectively (Fig. 6.2).

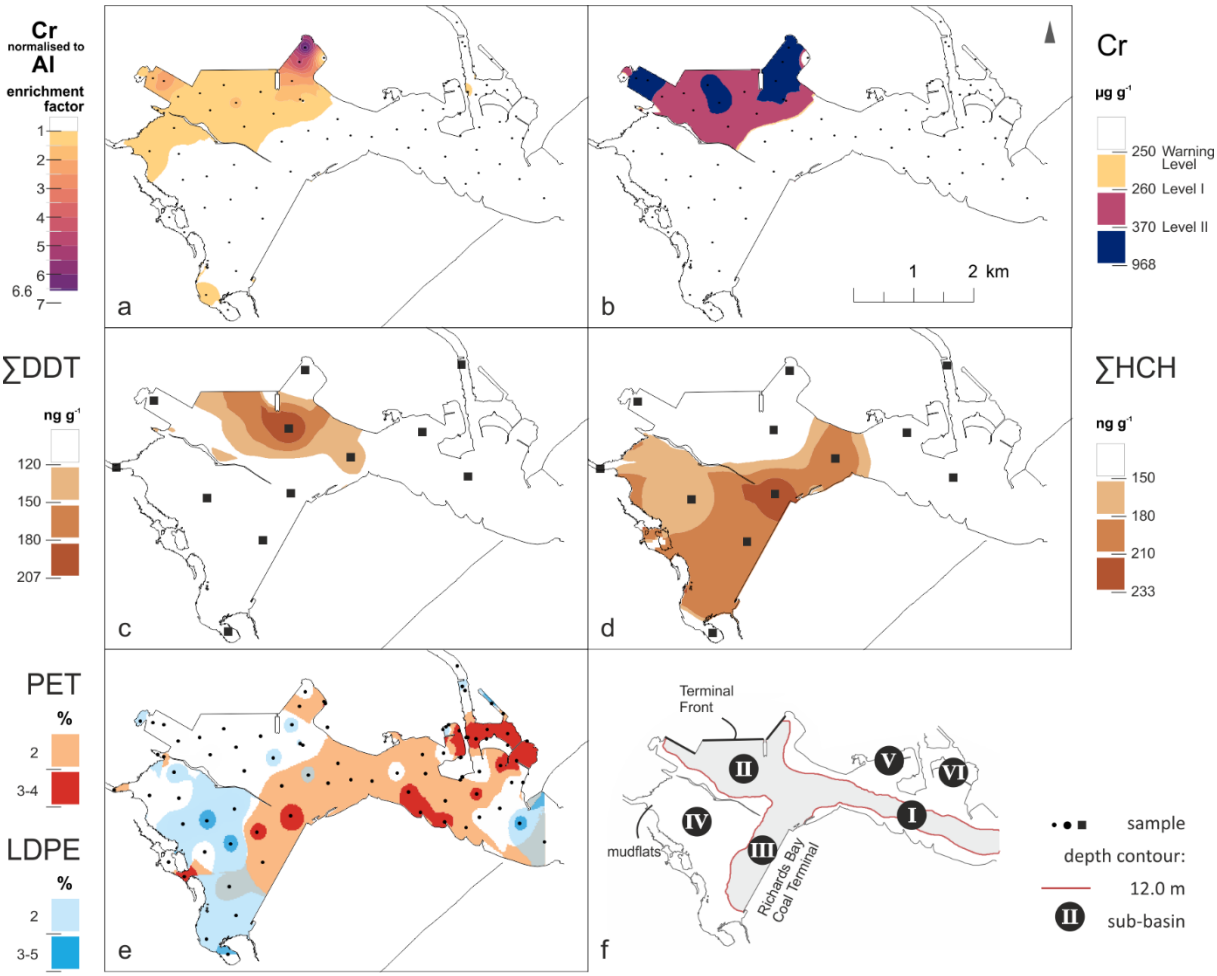


Fig. 6.2: Compilation of spatial distribution maps of exemplary pollutants analysed in this thesis. a) spatial distribution of the Chromium (Cr) Baseline model normalised to Aluminium (Al). The Enrichment Factors maximum values are shown next to the classification. Modified from Chapter 3 (Mehlhorn et al. [accepted]); b) the distribution map of Cr in surface sediments of Richards Bay Harbour is plotted, making use of guideline concentrations as presented by the Department of Environmental Affairs (2012). Modified from Chapter 3 (Mehlhorn et al. [accepted]); The spatial distribution of ∑DDT (c) elevated in northern sub-basins and ∑HCH (d) increased in southern sub-basins. Modified from Chapter 5 (Mehlhorn et al. [subm.]); e) distribution of PET and LDPE percentages in bulk sediments. Note the transition from PET deposited northeast to LDPE southwest. Modified from Mehlhorn et al. 2021; f) overview of the six sub-basins and generalised bathymetry of Richards Bay Harbour. Modified from Mehlhorn et al. 2021.

While recognising industrial sites and urban districts as possible sources of pollution in the northern region of Richards Bay Harbour, a primary N–S gradient (populated – unpopulated, industrialised – protected) is assumed. However, compounds of formerly used agricultural insecticides are found particularly in the south-western sub-basins (Fig. 6.2). The adjacent Mhlatuze Estuary and its alluvial fan is used extensively as farmland for sugarcane or annual crops. The area poses a reasonable source of pesticide contamination by legacy pesticides or

old stockpiles (e.g. of lindane, heptachlor or endrin), as metabolite ratios indicate recent use (Chapter 5). Since this thesis provides evidence that malformations of bioindicators occur in samples of increased metal contamination (Chapter 2), further risk assessments regarding the effect of organochlorine pesticides will be useful.

While further temporal information on the spatial distribution of pesticide and microplastics contamination at Richards Bay Harbour is to be raised, data on metal distribution allows noticing system reaction to the burden and relief of contaminants. Short sediment cores and spatial data from 2012 and 2018 used in this thesis mirror changing metal accumulation in sediments, especially regarding the shift from Cu to Cr related bulk export. Organochlorine pesticide concentrations in a core from Lake Mzingazi show a similar effect of increasing and decreasing contamination, linked to the effectiveness of environmental protective measures (Chapter 5). Hereby, the used sedimentary records and geochemical analyses indicate the potential to identify an ecological burden as well as its relief. Further, the potential of harbour and lake sediment, to record contamination history, is to be highlighted in this regard.

## Conclusions

This thesis contributes to a better understanding of the environmental status of the Richards Bay region at the east coast of South Africa. With a focus on metal concentrations in sediment of the port of Richards Bay, it adds valuable data to the years 2012 and 2018. The amount and density of samples used in this thesis is unprecedented in the record of publically available surveys at Richards Bay Harbour and proved beneficial for the assessment of source and sink relationships – a research goal also emphasized in the project TRACES. The stratigraphically supported development model on the evolution of the incised valley system and bayhead delta at Richards Bay Harbour insights the historic and recent basin changes. The port is structured in sub-basins with different grainsize characteristics and hydrodynamic implications. This proved fundamental for understanding the depositional behaviour of contaminants. Microplastics distribution in the harbour was found to be hydrodynamically controlled. PET particles tend to accumulate in wave and tide impacted sands of the north-eastern harbour, LDPE particles are deposited at the south-western sub-basins under low current velocity. Despite hydrodynamic processes affecting the sediment distribution and

associated elemental concentrations, different metal point sources were identified. Increased amounts and partly severe concentrations of As, Cd, Cr, Cu, or Ni were noticed. Evidence was found that anthropogenically introduced heavy metals, especially Cr and Cu, are in strong coherence with port operations and transhipment, confirming preceding assumptions. Investigations on the usefulness of different normalisers at Richards Bay Harbour have shown that the substantial increase of Cu and Cr concentration in confined areas was reflected by any of the normalisers tested. Further, the use of Ti and Fe as normaliser is compromised by the geological background or in some places by redox processes. However, the usefulness of Al or Rb as normaliser in Richards Bay was confirmed for future studies. Assumptions on the impact of metal enrichment on local microfaunal assemblies were confirmed. The identified bioindicators in samples of high metal exposure have shown deformities and changes in species composition. Exposure to organochlorine pesticides has been detected in all areas of Richards Bay and could be linked to anthropogenic activities and land use. Metabolite isomeric compositions reveal past and present use of pesticides in agriculture, as well as the prevalence of DDT, which indicates ongoing malaria control measures in residential areas.

Due to their different geochemical and sedimentological properties, the pollutants examined in this thesis link to different sediment properties or depositional mechanisms. Each sample revealed to be affected by a varying number of pollutants, depending on its location and relation to the pollution source. Herby, each pollutant forms individual problems that can be spatially differentiated and addressed separately.

This thesis shows that harbour sediment is an important sink for inorganic and organic contaminants, including environmental pollutants like metals, microplastics and organochlorine pesticides. Geochemical and sedimentological investigation on various environmental pollutants reveal that multiple stressors affect the harbour and raise concern for the environmental health of the system. Consequently, the analyses imply the need for further toxicological risk assessments in different ecosystems.

## Outlook

The work presented here focuses on the status of Richards Bay Harbour, based on sedimentological and geochemical analyses. During investigations, it became evident that the unique geological setting, including mineral rich sand dunes, or uncertainties in port development and maintenance would challenge a national comparison. In foresight, further investigations as part of the Project TRACES, included the search for comparable environmental reference systems in the vicinity of Richards Bay. The formally proposed reference-location of choice, the adjacent Mhlatuze Estuary, unfortunately was inaccessible (Fig. 6.3).

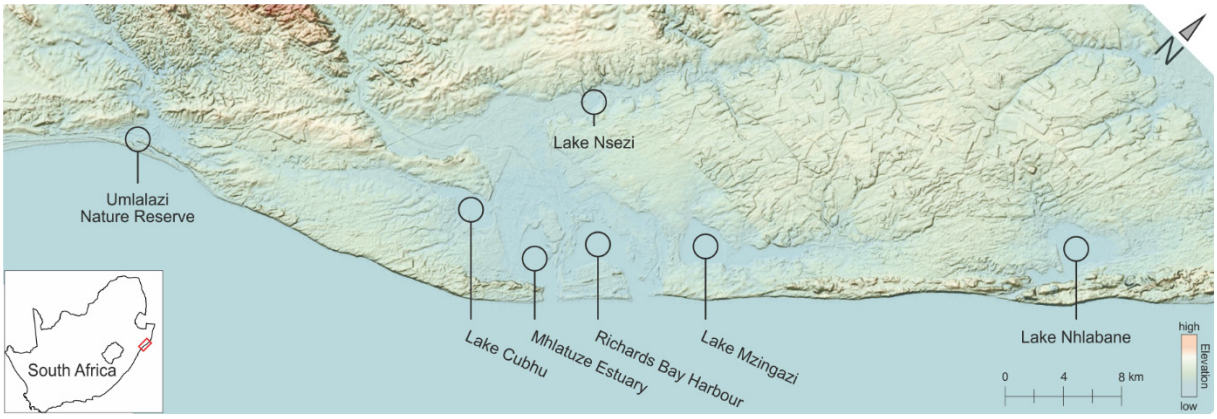


Fig. 6.3: Map of the KwaZulu-Natal coastline of South Africa showing potential geoarchives as reference-locations for Richards Bay Harbour.

Nevertheless, the Richards Bay region has great potential for further investigations. Northwest of Richards Bay Harbour, the natural freshwater Lake Mzingazi shows great potential for further (paleo-) environmental analyses (Fig. 6.3). As presented in Chapter 5, investigations on Lake Mzingazi revealed the lake to be affected by organochlorine pesticides, especially of agricultural origin. Three qualification theses by Rohrbach (2020), Siggelkow (2020) and Feldmann (2021) based their paleoenvironmental reconstructions on different aspects of a sediment core from Lake Mzingazi. Prospectively, a fourth bachelor thesis is expected on surface sediment samples of Lake Mzingazi. At the current point of research, Lake Mzingazi indicates few signs of anthropogenic impact. Nevertheless, high concentrations of Cr in surface sediment resemble conditions as found in the port of Richards Bay. However, an in depth understanding on the chronological, geochemical and sedimentological processes of Lake Mzingazi is missing.

Two additional qualification theses focus on the Mhlatuze alluvial fan (Lübeck 2022) and Lake

Cubhu (Brüggeman 2022). These investigations also base on sediment cores that indicate a similar sedimentary record and dating results, compared to Lake Mzingazi. Other potential sites, as additional reference system in the direct vicinity of Richards Bay, include Lake Nsezi to the northwest or Lake Nhlabane northeast of Richards Bay (Fig. 6.3). Further, the Umlalazi River, south of Richards Bay, also provides a comparable environmental settings within the Umlalazi Nature Reserve.

## References

Brüggemann, A. 2022: Umweltrekonstruktion basierend auf sedimentologischen Untersuchungen eines Sedimentkerns aus dem Cubhu-See, Südafrika. Unpublished bachelor thesis, 62 pp. University of Greifswald.

Lübeck, E. 2022: Sedimentologische Untersuchungen an Bohrkernen aus dem Schwemmfächer des Mhlathuze-Flusses, KwaZulu-Natal, Südafrika. Unpublished bachelor thesis, 67 pp. University of Greifswald

Mehlhorn, P., Newman, B., Haberzettl, T. [accepted]: Comparison of different normalisers for identifying metal enrichment of sediment – a case study from Richards Bay Harbour, South Africa. In: von Maltitz, G., Midgley, G., Veitch, J., Brümmer, C., Viehberg, F., Rötter, R., Veste, M. (Eds). Sustainability of southern African ecosystems under global change: Science for management and policy interventions. Springer, Heidelberg.

Mehlhorn, P., Humphries, M., Gensel, J., Buah-Kwofie, A., Tyohemba, R. L., Haberzettl, T. [subm.]: Organochlorine pesticide contamination in sediments from Richards Bay, South Africa: spatial trends and ecotoxicological risks. Environmental Science and Pollution Research.

Mehlhorn, P., Viehberg, F., Kirsten, K., Newman, B., Frenzel, P., Gildeeva, O., Green, A., Hahn, A., Haberzettl, T. 2021: Spatial distribution and consequences of contaminants in harbour sediments – A case study from Richards Bay Harbour, South Africa. Marine Pollution Bulletin, 172, 112764. https://doi.org/10.1016/j.marpolbul.2021.112764.

Rohrbach, M. 2020: Paleoenvironmental Reconstructions Based on Sedimentological Investigations of a Sediment Core from Lake Mzingazi, South Africa. Unpublished state examination, 49 pp. University of Greifswald.

Siggelkow, C. 2020: Vergleichende Umweltrekonstruktion aus Seesedimenten am Beispiel des Mzingazi Sees und des Goedertrou Stausees in Südafrika. Unpublished bachelor thesis, 30 pp. University of Greifswald.

Schell, A. C. 2022: Makrofauna, Schalenchemie und Sedimentkomponenten als Indikatoren anthropogener Einflüsse im Hafengebiet von Richards Bay, Südafrika. Unpublished bachelor thesis, 66 pp. Friedrich Schiller University Jena.

# Eigenständigkeitserklärung

Hiermit erkläre ich, dass diese Arbeit bisher von mir weder an der Mathematisch-Naturwissenschaftlichen Fakultät der Universität Greifswald noch einer anderen wissenschaftlichen Einrichtung zum Zwecke der Promotion eingereicht wurde.

Ferner erkläre ich, dass ich diese Arbeit selbstständig verfasst und keine anderen als die darin angegebenen Hilfsmittel und Hilfen benutzt und keine Textabschnitte eines Dritten ohne Kennzeichnung übernommen habe.

Greifswald, den 16. Mai 2022

Paul Mehlhorn

# Curriculum Vitae

## Paul Mehlhorn

For data protection reasons, the curriculum vitae will not be published in the electronic version.

# List of publications

## Peer reviewed journals

Dladla, N. N., Green, A., Cooper, J. A. G., **Mehlhorn, P.**, Haberzettl, T. 2021: Bayhead delta evolution in the context of late Quaternary and Holocene sea-level change, Richards Bay, South Africa. *Marine Geology, 441*, 106608. https://doi.org/10.1016/j.margeo.2021.106608.

Hüneke, H., Gibb, M. A., Mayer, O., Kniest, J. F., **Mehlhorm, P.**, Gibb, L. M., Aboussalam, S., Becker, T., El Hassani, A., Baidder, L. [accepted]: Bioclastic bottom-current deposits of a Devonian contourite terrace: Facies variability and depositional architecture (Tafilalt Platform, Morocco). *Sedimentology.*

**Mehlhorn, P.**, Humphries, M., Gensel, J., Buah-Kwofie, A., Tyohemba, R. L., Haberzettl, T. [**subm.**]: Organochlorine pesticide contamination in sediments from Richards Bay, South Africa: spatial trends and ecotoxicological risks. *Environmental Science and Pollution Research.*

**Mehlhorn, P.**, Viehberg, F., Kirsten, K., Newman, B., Frenzel, P., Gildeeva, O., Green, A., Hahn, A., Haberzettl, T. 2021: Spatial distribution and consequences of contaminants in harbour sediments – A case study from Richards Bay Harbour, South Africa. *Marine Pollution Bulletin, 172*, 112764. https://doi.org/10.1016/j.marpolbul.2021.112764.

**Mehlhorn, P.**, Winkler, L., Grabbe, F.-C., Kenzler, M., Gehrmann, A., Hüneke, H., Rother, H. 2019: Coastal cliff at Lenzer Bach on Jasmund Peninsula, Rügen Island (Pleistocene Stripe 4): reconstructed history of glacitectonic deformation based on fold geometry and microstructural mapping, *DEUQUA Special Publications, 2*, 35–41, https://doi.org/10.5194/deuquasp-2-35-2019.

## Reviewed book sections

**Mehlhorn, P.**, Newman, B., Haberzettl, T. [accepted]: Comparison of different normalisers for identifying metal enrichment of sediment – a case study from Richards Bay Harbour, South Africa. *In:* von Maltitz, G., Midgley, G., Veitch, J., Brümmer, C., Viehberg, F., Rötter, R., Veste, M. (Eds). *Sustainability of southern African ecosystems under global change: Science for management and policy interventions*. Springer, Heidelberg.

## Unpublished thesis

**Mehlhorn, P.** 2018: Sediment accumulation, bypassing and erosion at a current-influenced palagic carbonate platform: Microfacies of the Devonian record at Jebel Amelane (Tafilalt Platform, Anti-Atlas, Morocco). Unpublished master thesis, 100 pp. University of Greifswald.

**Mehlhorn, P.** 2016: Makro- und mikrostrukturelle Analyse der Pleistozän-Sedimente am Streifen 4 von Jasmund (Rügen). Unpublished bachelor thesis, 64 pp. University of Greifswald.

## Conference contributions – orals

**Mehlhorn, P.**, Viehberg, F., Finch, J., Frenzel, P., Gildeeva, O., Green, A., Hill, T., Humphries, M., Haberzettl, T. 2019: Heavy metals in surface sediments of Richards Bay Harbour: anthropogenic impact on the former Mhlatuze estuary, South Africa. GeoMünster 2019, Münster, Germany.

## Conference contribution – poster

Viehberg, F., Cawthra, H.C., Finch, J., Frenzel, P., Green, A., Haberzettl, T., Hahn, A., Hill, T., Humphries, M., **Mehlhorn, P.**, Schefuss, E., Zabel, M. 2018: Tracing Human and Climate impacts in South Africa. 4$^{th}$ National Global Change Conference, Polokwane, South Africa.

**Mehlhorn, P.**, Finch, J., Frenzel, P., Green, A., Hill, T., Viehberg, F., Zabel, M., Haberzettl, T. 2018: A system divided – sanctuary vs harbour: anthropogenic and climate impact on the Mhlatuze and Mfule rivers catchment/estuary at Richards Bay Harbour, South Africa. 4$^{th}$ National Global Change Conference, Polokwane, South Africa.

**Mehlhorn, P.**, Humphries, M., Frenzel, P., Gildeeva, O., Hahn, A., Viehberg, F., and Haberzettl, T. 2019: Surface sediments of Richards Bay Harbour, South Africa – potential pollutants (heavy metals, persistent organic pollutants, microplastics) and grainsize distribution, EGU General Assembly 2020, Online, 4–8 May 2020, EGU2020-1623, https://doi.org/10.5194/egusphere-egu2020-1623.

# Acknowledgements

I am deeply grateful to Prof. Dr. Torsten Haberzettl and PD Dr. Finn Viehberg for their shared enthusiasm, guidance and patience. Torsten, thank you for the chance to take on this challenge, I honour your calm and thoughtful support. Finn, thank you for answering so many of my questions by creating additional challenges and sharing fantastic stories.

I thank all my co-authors, colleagues and friends who accompanied me from the University of KwaZulu-Natal, the University of the Witwatersrand, the University of Cape Town, Nelson Mandela University, Friedrich Schiller University Jena, the University of Bremen and of course the University of Greifswald. It was a joy visiting, working outdoors and learning together, it means a lot to me.

I would also like to acknowledge the German Federal Ministry of Education and Research (BMBF) for funding the research project “Tracing Human and climate impact in South Africa”, wherein this thesis is embedded.

To Marc, Archibold, Letitia, Raymond and Julia. It was such a pleasure working together at Wits. Thank you for your hospitality, shared motivation and view of life.

To Heiko Hüneke, thank you for your inspiration in the field of geology and beyond.

To my family and friends, thank you for supporting me and getting on with life as if a PhD did not exist; it was a much-needed reminder.

To Julia, Anton and Ruben, I love you.